

TECHNISCHE UNIVERSITÄT MÜNCHEN
Lehrstuhl für Biomolekulare NMR-Spektroskopie

Regulation of Mammalian Autophagy by Unc-51-Like Kinase 1

Hildegard Isolde Dietlinde Mack

Vollständiger Abdruck der von der Fakultät für Chemie der Technischen Universität München zur Erlangung des akademischen Grades eines

Doktors der Naturwissenschaften

genehmigten Dissertation.

Vorsitzender:

Univ.-Prof. Dr. Steffen J. Glaser

Prüfer der Dissertation:

1. Priv.-Doz. Dr. Gerd Gemmecker
2. apl. Prof. Dr. Karl-Friedrich Becker
3. Univ.-Prof. Dr. Michael Groll

Die Dissertation wurde am 10.01.2011 bei der Technischen Universität München eingereicht und durch die Fakultät für Chemie am 14.06.2011 angenommen.

Meiner Familie

Nemo nascitur sapiens, sed fit.

SENECA

Acknowledgement/Danksagung

An dieser Stelle meiner Dissertation möchte ich meinen tiefen Dank all denjenigen Menschen gegenüber zum Ausdruck bringen, die durch ihre fachliche, organisatorische oder moralische Unterstützung zum Fortschritt meiner Arbeit beigetragen bzw. es ermöglicht haben, diese überhaupt erst zu beginnen und angemessen zu vollenden.

Prof. Dr. Karl-Friedrich Becker danke ich für die wissenschaftliche Betreuung meines Dissertationsvorhabens an der Technischen Universität München, sein stets offenes Ohr für meine Anliegen und sein Interesse an meinem Projekt.

PD Dr. Gerd Gemmecker danke ich dafür, dass er die Betreuung meiner Promotion an der Chemiefakultät übernommen hat und mir dort stets als Ansprechpartner zur Verfügung stand.

Prof. Dr. Steffen Glaser danke ich für seine Bereitschaft, den Vorsitz meiner Prüfungskommission zu übernehmen.

Prof. Dr. Michael Groll danke ich für seine Bereitschaft, als zusätzlicher Prüfer meiner Dissertation zu fungieren.

Meiner gesamten Familie danke ich für die permanente moralische Unterstützung. Zudem danke ich meinen Eltern dafür, dass sie sich um all meine Angelegenheiten in Deutschland gekümmert haben, so dass ich mich in Boston vollständig auf meine Forschungsarbeit konzentrieren konnte. Bei meiner Schwester Elisabeth möchte ich mich für die hilfreichen Diskussionen bei der Planung und Auswertung von Experimenten bedanken.

I thank Dr. Karl Münger for providing the opportunity to complete my thesis project in his lab, for his interest in my work, his helpful advice and generous support, and for organizing the journal club which definitely enhanced my scientific training in Boston..

I thank my principal investigator Dr. Sheila Thomas for the opportunity to perform my thesis research on a challenging question and in an outstanding scientific environment in her lab. Thanks for the close supervision and the permanent availability for questions, the frequent eye-to-eye discussions, the occasional critic, the experimental support and the interest not just in the progress of my work but also in broadening my scientific education beyond the bench.

Thanks also to the members of the Münger Lab, the Thomas Lab and their neighbouring labs for the collaborative atmosphere and for sharing reagents and know how, which greatly accelerated the progress of my work. In particular I would like to thank Dr. Ken Swanson who was always ready to solve problems with/to provide training on virtually all equipment on our floor.

Finally, I would like to thank Dr. Bin Zheng, our department's AMPK-person, for the continuous collaboration from the beginning to the end of the AMPK-project, for providing constructs, reagents and experimental protocols, and for all his helpful comments and suggestions.

Table of Contents

Acknowledgement/Danksagung	iii
Table of Contents	iv
1 Summary/Zusammenfassung.....	1
1.1 Summary.....	1
1.2 Zusammenfassung.....	2
2 Introduction.....	3
2.1 Autophagy in yeast and mammalian cells.....	3
2.1.1 Overview of the process and physiological role	3
2.1.2 The autophagy machinery	5
2.1.2.1 The Atg1-complex.....	8
2.1.2.2 The class III PI3-Kinase complex	8
2.1.2.3 The two Ubiquitin-like conjugation systems	10
2.1.2.4 The membrane trafficking system.....	11
2.1.2.5 Components of selective autophagy pathways.....	12
2.1.3 Signaling pathways regulating autophagy.....	13
2.1.3.1 The mTOR-pathway.....	14
2.1.3.2 The Ras/PKA-pathway in yeast	15
2.1.3.3 The JNK-pathway in mammalian cells	16
2.2 The autophagy-regulating kinase ULK1	17
2.2.1 ULK-family kinases - Atg1-homologs in higher organisms.....	17
2.2.2 Cellular functions of Atg1/ULKs.....	17
2.2.3 Atg1- and ULK-complexes	18
2.2.4 Regulation and role of Atg1/ULK1 in autophagy.....	19
2.2.5 Similarities and differences between ULK1 and ULK2	21
2.3 The energy-sensing kinase AMPK.....	23
2.3.1 Structure and regulation of the AMPK holoenzyme.....	23
2.3.2 Metabolic and non-metabolic functions of AMPK.....	25
2.3.3 AMPK and autophagy	27
2.4 Specific aims	29
3 Materials and Methods	30
3.1 Materials.....	30
3.1.1 Chemicals, reagents and solvents.....	30
3.1.2 Buffers, solutions and bacterial growth media.....	32
3.1.3 Commercial kits, standards and ready-to-use solutions	33
3.1.4 Oligonucleotides.....	34
3.1.4.1 Oligonucleotides for mutagenesis	34
3.1.4.2 Oligodesoxynucleotides for PCR.....	34

Table of Contents

3.1.4.3	Oligonucleotides for sequencing.....	35
3.1.5	Enzymes.....	35
3.1.6	Antibodies.....	36
3.1.6.1	Primary antibodies.....	36
3.1.6.2	Secondary antibodies and isotype controls.....	36
3.1.7	Plasmids.....	37
3.1.7.1	Bacterial expression plasmids.....	37
3.1.7.2	Mammalian expression plasmids.....	37
3.1.7.3	Retro- and lentiviral expression vectors.....	38
3.1.8	Bacterial strains.....	38
3.1.9	Mammalian cells.....	38
3.1.9.1	Cell lines.....	38
3.1.9.2	Mouse embryonic fibroblasts.....	38
3.1.10	Media and reagents for tissue culture.....	39
3.1.11	Consumables.....	39
3.1.12	Equipment.....	40
3.1.13	Computer programs and data bases.....	41
3.1.14	List of manufacturers.....	42
3.2	Methods.....	43
3.2.1	Biological and radiation safety.....	43
3.2.2	Cell biological methods.....	43
3.2.2.1	Culturing and passaging of cells.....	43
3.2.2.2	Freezing and thawing of cells.....	43
3.2.2.3	Transfections.....	44
3.2.2.4	Production of recombinant retrovirus.....	44
3.2.2.5	Retroviral infections.....	45
3.2.2.6	Treatments.....	45
3.2.3	Molecular biological methods.....	45
3.2.3.1	Culturing of <i>E. coli</i> -strains.....	45
3.2.3.2	Cryoconservation of bacteria.....	45
3.2.3.3	Transformation of <i>E. coli</i> with plasmid DNA.....	45
3.2.3.4	Isolation of double-stranded plasmid DNA from <i>E. coli</i> (mini- and maxiprep).....	46
3.2.3.5	DNA amplification by polymerase chain reaction (PCR).....	46
3.2.3.6	Analytical agarose gel electrophoresis.....	47
3.2.3.7	Gel purification of DNA.....	47
3.2.3.8	Site-directed mutagenesis of DNA.....	47
3.2.3.9	Restriction digest of DNA.....	48
3.2.3.10	Ligation of DNA-fragments.....	49
3.2.3.11	Sequencing of DNA.....	49
3.2.3.12	Production of recombinant proteins in <i>E. coli</i>	49
3.2.4	Biochemical methods.....	50
3.2.4.1	Preparation of total cell lysates under denaturing conditions.....	50
3.2.4.2	Protein quantitation.....	51
3.2.4.3	Immuno- and co-immunoprecipitation experiments.....	51
3.2.4.3.1	Lysis of cells for immuno- and co-immunoprecipitation experiments.....	51

3.2.4.3.2	Immunoprecipitation of myc-tagged proteins	52
3.2.4.3.3	Immunoprecipitation of FLAG-tagged proteins	52
3.2.4.3.4	Immunoprecipitation of exogenous mSIN1	52
3.2.4.3.5	Immunoprecipitation of endogenous AMPK α	53
3.2.4.3.6	Immunoprecipitation of endogenous 14-3-3	53
3.2.4.3.7	Immunoprecipitation and coimmunoprecipitation of endogenous Raptor... 53	53
3.2.4.4	GST-14-3-3 pulldown experiments.....	53
3.2.4.5	<i>In vitro</i> kinase assays.....	54
3.2.4.5.1	ULK1 kinase assays on AMPK, INPP4B and mSIN1	54
3.2.4.5.2	AMPK kinase assays on ULK1.....	54
3.2.4.6	Dephosphorylation of proteins with shrimp alkaline phosphatase.....	55
3.2.4.7	SDS-polyacrylamide gel electrophoresis	55
3.2.4.8	Western blot	56
3.2.4.9	Cell viability assay	58
3.2.4.10	Mass spectrometry.....	58
3.2.5	Computational methods.....	59
3.2.5.1	Design of primers for site-directed mutagenesis, PCR and sequencing	59
3.2.5.2	Searching of protein sequences for defined motifs using Scansite	59
3.2.5.3	Sequence alignments	60
3.2.5.4	Image processing and analysis	60
3.2.5.5	Statistical analyses.....	60
4	Results	61
4.1	Bioinformatics and proteomics studies to predict candidate regulators and substrates of ULK1.....	61
4.1.1	Mass spectrometry reveals 30 phosphorylated sites in ULK1	61
4.1.2	Scansite search and high throughput proteomic screening predict autophagy-relevant proteins as ULK1-substrates	64
4.2	Experimental validation of ULK1-interactions with predicted substrates.....	66
4.2.1	N-terminally tagged mSIN1 does not associate with myc-ULK1.....	66
4.2.2	Exogenous InPP4B and ULK1 interact.....	67
4.2.3	AMPK associates with ULK1 and ULK2.....	69
4.3	Biochemical characterization of the ULK1-AMPK-complex	71
4.3.1	Complex-stability is independent of ULK1- and AMPK-kinase activity.....	71
4.3.2	Complex-formation is mediated by the AMPK α -subunit and the ULK1-spacer region.....	72
4.3.3	The AMPK-bound ULK-population is hyperphosphorylated.....	73
4.3.4	Regulation of the ULK1-AMPK association by nutrient- and energy-stress.....	74
4.3.4.1	AMPK is activated in very early and in late stages of starvation	74
4.3.4.2	Nutrient-sensitivity of the ULK1-AMPK-interaction is cell-line dependent.....	75
4.3.4.3	ULK1-AMPK-complex stability is largely independent of AMPK-activation ..	76
4.4	Phosphorylation of ULK1 by AMPK	77
4.4.1	AMPK and ULK1 as potential targets of each other	77
4.4.2	An AMPK motif antibody detects basal phosphorylation of ULK1	80
4.4.3	AMPK-regulation of 14-3-3-binding to ULK1	80

4.4.3.1	GST-14-3-3-pulldown assays on exogenous and endogenous ULK1	81
4.4.3.2	Myc-ULK1 coprecipitates with endogenous 14-3-3	82
4.4.4	Identification of AMPK-dependent 14-3-3 binding sites in ULK1	83
4.4.4.1	Mass spectrometry detects several AMPK-phosphorylation sites on ULK1	83
4.4.4.2	GST-14-3-3 pulldown identifies two AMPK-dependent 14-3-3-binding sites in ULK1	85
4.4.4.3	AMPK phosphorylates ULK1 <i>in vitro</i>	87
4.4.5	ULK1-overexpression induces hyperphosphorylation of AMPK	89
4.5	Regulation of ULK1 by AMPK	90
4.5.1	Destabilization of the ULK1-Raptor interaction is independent of AMPK activity	90
4.5.2	p62-degradation is normal in AMPK-deficient MEFs	91
4.5.3	AMPK-deficient MEFs have decreased ULK1 protein levels	91
4.5.4	ULK1-overexpression is not sufficient to substantially restore energy-stress tolerance in AMPK-deficient MEFs	93
5	Discussion.....	97
5.1	Potential substrates and novel functions of ULK1	97
5.1.1	Predicted substrates of ULK1 during autophagy and axon guidance	97
5.1.2	ULK1, INPP4B and phosphoinositide signaling	98
5.2	Regulation of ULK1 and autophagy by AMPK	99
5.2.1	General role of ULK1, ULK2 and AMPK	99
5.2.2	Effects of AMPK-phosphorylation and 14-3-3-binding to ULK1	101
5.2.3	Function of the ULK1-AMPK-complex	101
5.2.4	Overlap of the ULK1-AMPK-complex with known ULK1- and AMPK- complexes	102
5.2.5	Conservation of the AMPK-ULK1 signaling module	103
5.2.6	Feedback regulation of ULK1-, AMPK- and mTOR-signaling	105
5.3	Future directions	107
6	References	109
7	Appendix	130
7.1	Abbreviations	130
7.2	Supplementary data	134
7.2.1	Sequence alignment of ULK1-homologs from various species	134
7.2.2	ULK1-phosphorylation pattern and predicted upstream kinases	136
7.2.3	Full names of predicted ULK1-substrates	139
7.2.4	Influence of AMPK-activation on ULK1-AMPK-complex stability	140
7.2.5	Determination of AMPK-dependent 14-3-3-binding sites in ULK1	141

1 Summary/Zusammenfassung

1.1 Summary

Autophagy is a lysosomal degradation pathway that physiologically facilitates turnover of long-lived cellular components and organelles. The process is upregulated in response to environmental or internal stress such as nutrient-deprivation or organelle damage in order for the cell to maintain homeostasis. Deregulation of autophagy has been implicated in a variety of human diseases, including cancer and neurodegenerative disorders. While many components of the autophagy-machinery have been characterized, primarily through studies in yeast, the signaling pathways that regulate this process are poorly defined. Yet, enhanced understanding of these signaling cascades is a central prerequisite when designing novel therapeutic strategies that are based on interference in the autophagy-pathway. Thus, the aim of this thesis was to elucidate regulation and function of the kinase ULK1, the mammalian ortholog of the Atg1-protein, a known key initiator of autophagy in yeast. Using a combination of bioinformatics, proteomics and biochemical approaches, we identified the cellular energy sensor AMPK as a novel kinase targeting ULK1. AMPK and ULK1 form a constitutive complex and AMPK-activation leads to increased binding of regulatory 14-3-3-proteins to ULK1. We show that AMPK-dependent 14-3-3-binding sites in ULK1 map to residues S555 and T659 and that AMPK phosphorylates ULK1 *in vitro* at these two sites, and at a third site, S637. Furthermore, we provide evidence that ULK1-protein levels are regulated by AMPK and that AMPK is subject to feedback regulation by ULK1. Taken together, our data reveal a novel and direct connection of the major cellular energy sensing pathway to the autophagy machinery and suggest mechanistic explanations of how AMPK and ULK1 are able to regulate autophagy.

1.2 Zusammenfassung

Bei Autophagie handelt es sich um einen Mechanismus zum lysosomalen Abbau intrazellulärer Strukturen. Dieser Prozess ermöglicht unter physiologischen Bedingungen den Umsatz von langlebigen Substraten und von Zellorganellen und kann in Anpassung an intra- oder extrazelluläre Stressfaktoren wie Nährstoffentzug oder Schädigung von Organellen verstärkt werden um das Überleben der Zelle zu gewährleisten. Deregulierung von Autophagie trägt zur Entstehung oder dem Fortschreiten zahlreicher menschlicher Erkrankungen bei, einschließlich von Krebs und neurodegenerativen Erkrankungen. Durch Studien in Modellorganismen, in erster Linie in Hefe, wurden bereits zahlreiche Gene bzw. Proteine identifiziert, die auf molekularer Ebene Autophagie ausführen; die Signaltransduktionswege zur Steuerung dieses Prozesses allerdings sind bislang weitestgehend unbekannt. Ein genaues Verständnis dieser regulatorischen Zusammenhänge ist jedoch eine entscheidende Voraussetzung für die Entwicklung neuartiger Behandlungsstrategien, die auf der Beeinflussung von Autophagie beruhen. Dementsprechend bestand das Ziel der vorliegenden Arbeit darin, Regulation und Funktion der Kinase ULK1 in menschlichen Zellen zu klären. Eine grundsätzliche Bedeutung von ULK1 in Autophagie wurde angenommen aufgrund der Homologie dieser Kinase mit dem Atg1-Protein der Hefe, dessen zentrale Rolle im Autophagieprozess umfassend experimentell gesichert ist. Durch eine breite Kombination von bioinformatischen, biochemischen und proteomweiten Analysemethoden konnten wir eine weitere Kinase, AMPK, die als Energiesensor der Zelle fungiert, als Regulator von ULK1 identifizieren. ULK1 und AMPK liegen in einem gemeinsamen Komplex vor, und Aktivierung von AMPK führt zu erhöhter Bindung von regulatorischen Proteinen der 14-3-3-Familie an ULK1. Wir konnten zeigen, dass AMPK-abhängige 14-3-3-Bindung über die Serinreste S555 und T659 in ULK1 erfolgt und dass AMPK diese Serinreste, sowie einen weiteren Serinrest, S637, *in vitro* phosphoryliert. Ferner lieferten unsere Untersuchungen Hinweise darauf, dass AMPK die Menge des ULK1-Proteins in der Zelle beeinflusst und dass umgekehrt ULK1 AMPK reguliert. Insgesamt zeigen unsere Ergebnisse eine bislang unbekannt direkte Verbindung zwischen einem zentralen zellulären Energiesensor, AMPK, und der Autophagiemaschinerie auf und stellen damit eine entscheidende Erweiterung unseres gegenwärtigen Verständnisses der Regulation von Autophagie unter Stressbedingungen dar.

2 Introduction

2.1 Autophagy in yeast and mammalian cells

2.1.1 Overview of the process and physiological role

Autophagy (greek for “self-eating”) is an evolutionary conserved mechanism for lysosomal degradation and recycling of long-lived cellular components. This pathway is constitutively active in every cell, although at varying levels depending on internal or environmental stresses, to maintain homeostasis. According to the specific mechanism, three different subtypes can be distinguished: The first, macroautophagy (referred to as autophagy hereafter) is characterized by the formation of double-membraned vesicles, so called autophagosomes, that sequester bulk portions of cytoplasm and subsequently fuse with lysosomes to form autolysosomes where the cargo is degraded by lysosomal enzymes. In the second subtype, microautophagy, cytoplasmic components are taken up directly by lysosomes, and in the third subtype, chaperone-mediated autophagy, chaperones select substrates and mediate their translocation across the lysosomal membrane (Mizushima et al., 2008). Under physiologic conditions, autophagy occurs at low, basal levels in every cell since this pathway in principle constitutes a second intracellular degradation system, functioning in parallel to the ubiquitin-proteasome pathway. Whereas the latter specifically targets short-lived proteins, autophagy is not restricted to a particular class of macromolecules but facilitates turnover of all types of long-lived substrates. Furthermore, autophagy is the only mechanism with the capacity to degrade entire organelles (Levine and Klionsky, 2004). Although (macro)autophagy is generally considered to be non-selective, selective forms that target, for example only certain types of organelles, exist as well. In particular, mitophagy (Ashford and Porter, 1962; Lemasters, 2005), pexophagy (Bormann and Sahn, 1978), ribophagy (Kraft et al., 2008) and reticulophagy or ER-phagy (Bernales et al., 2006; Tasdemir et al., 2007) have been described to selectively mediate autophagic degradation of mitochondria, peroxisomes, ribosomes and the endoplasmic reticulum, respectively.

Autophagy is upregulated in response to a variety of environmental and endogenous stressors, such as nutrient- and growth factor deprivation, hypoxia, high temperature or organelle damage. This suggests that autophagy may have initially evolved as a survival strategy. Indeed, the function of autophagy to allow adaptation to nutrient deprivation is evolutionary conserved from yeast to mammals (Levine and Klionsky, 2004). Conversely, excessive self digestion will negatively affect cell viability, and thus, autophagy may also be considered as a type of programmed cell death, which becomes of particular importance when apoptosis is blocked (Yu et al., 2004). Yet, so far, a role for autophagy in mediating cell death

has only been described in *Drosophila melanogaster* and in mammalian cells (Berry and Baehrecke, 2007; Mizushima, 2005).

Through stimulation of cell survival or cell death, autophagy contributes to a variety of additional important biological processes besides from homeostasis, such as development, differentiation and ageing (Bjedov et al., 2010; Hansen et al., 2008; Toth et al., 2008). These roles of autophagy have been primarily studied in model organisms, including *Saccharomyces cerevisiae*, *Caenorhabditis elegans* and *Arabidopsis thaliana* (Deutschbauer et al., 2002; Doelling et al., 2002; Hanaoka et al., 2002; Melendez et al., 2003). In certain cases, autophagy-mediated developmental and differentiation processes constitute stress-responses, for example sporulation in yeast, fruit body-formation in *Dictyostelium discoideum* or entering the dauer-stage in *C. elegans* (Levine and Klionsky, 2004). In addition, autophagy plays an essential role in normal development, as indicated by the fact that knockdown or knockout of certain autophagy-genes results in larval lethality in *D. melanogaster* and *C. elegans*, embryonic lethality in mice and in enhanced chlorosis and premature leaf senescence in *A. thaliana* (Levine and Klionsky, 2004).

In mammals, autophagy occurs in different contexts at all stages of life: it contributes to tissue morphogenesis, in particular to the formation of hollow structures like the acini of glands (Mills et al., 2004). Starvation-induced autophagy is also of special importance for survival of neonates after disruption of the placental nutrient supply at birth (Kuma et al., 2004). Furthermore, autophagy functions in the immune defense. On the one hand, this pathway can serve as a first step in the processing of viral and of self-antigens for presentation on MHC class II molecules by professional antigen presenting cells (Nimmerjahn et al., 2003). On the other hand, the autophagy machinery (in a process termed xenophagy, i.e. eating of foreign matter) can mediate degradation of invading bacteria in phagocytic and non-phagocytic cells (Gutierrez et al., 2004; Levine, 2005; Nakagawa et al., 2004; Ogawa et al., 2005). Moreover, autophagy is assumed to be a central mechanism in the onset and progression of a great variety of human diseases, including heart and liver diseases, myopathies, neurodegenerative diseases and cancer (Mizushima et al., 2008). The special importance of autophagy in the development of malignant tumors is underscored by the fact that alterations in numerous well-established oncoproteins such as receptor protein tyrosine kinases, Phosphatidylinositol-3 (PI3)-kinase and AKT/protein kinase B, or in tumor suppressors like p53, Phosphatase and tensin homolog deleted on chromosome 10 (PTEN) and tuberous sclerosis complex protein (TSC) 2, affect autophagy (Maiuri et al., 2009b); cf. section 2.1.3). Moreover, several core autophagy genes have been shown to be lost in certain

types of cancer. For example, monoallelic deletion of the essential autophagy gene Beclin 1 (cf. section 2.1.2.1) is frequently observed in breast- and ovarian cancers (Aita et al., 1999); furthermore, the UV irradiation resistance associated gene (UVRAG), whose product interacts with Beclin 1 (Liang et al., 2006) is monoallelically mutated in colon cancers (Ionov et al., 2004), and the gene for the UVRAG interaction partner Bax-interacting factor (Bif) 1 (Takahashi et al., 2007) shows decreased expression in gastric cancers and homozygous deletion in mantle cell lymphomas (Balakrishnan et al., 2006). Although these data stress the role of autophagy as a tumor suppressor mechanism, autophagy may also promote tumor growth, in that it may allow malignant cells to survive in a hypoxic and nutrient-deprived environment as it is typically found in a emerging tumor (Mizushima et al., 2008) Thus, the beneficial or detrimental effect of autophagy is determined by the global state of the cell or the organism.

2.1.2 The autophagy machinery

Autophagy is mediated by the so-called *Autophagy-related* (Atg)-genes, thirty-four of which so far have been identified, predominantly in the yeast *S. cerevisiae* (Harding et al., 1995; Tsukada and Ohsumi, 1993). However, not all Atg-genes are required for bulk autophagy; rather, some are specific to specialized forms, i.e. mitophagy or pexophagy, or for the Cvt (Cytoplasm to vacuole *targeting*)-pathway (Table 2.1). This latter pathway, which is unique to yeast, facilitates transport of certain enzymes to vacuoles for biosynthetic purposes, but is nevertheless considered a model for selective autophagy (Noda et al., 2010).

The Atg-genes that are required for non-selective macroautophagy are grouped into four functional modules that control the major steps of the process (Fig. 2.1; Yang and Klionsky, 2010):

1. The Atg1-kinase complex important for autophagy initiation (Atg1, 13, 17)
2. The class III PI3-kinase complex mediating autophagosome nucleation (Atg6, 14)
3. Two interconnected ubiquitin-like conjugation systems involved in autophagosome maturation and cargo recruitment (Atg3, 4, 5, 7, 8, 10, 12, 16) and
4. A membrane trafficking and recycling system (Atg2, 9, 18)

The components of these four modules comprise the core autophagy machinery and are largely conserved from yeast to mammals, whereas Atg-proteins that are required only for selective forms of autophagy or for the Cvt-pathway, are not (Meijer et al., 2007).

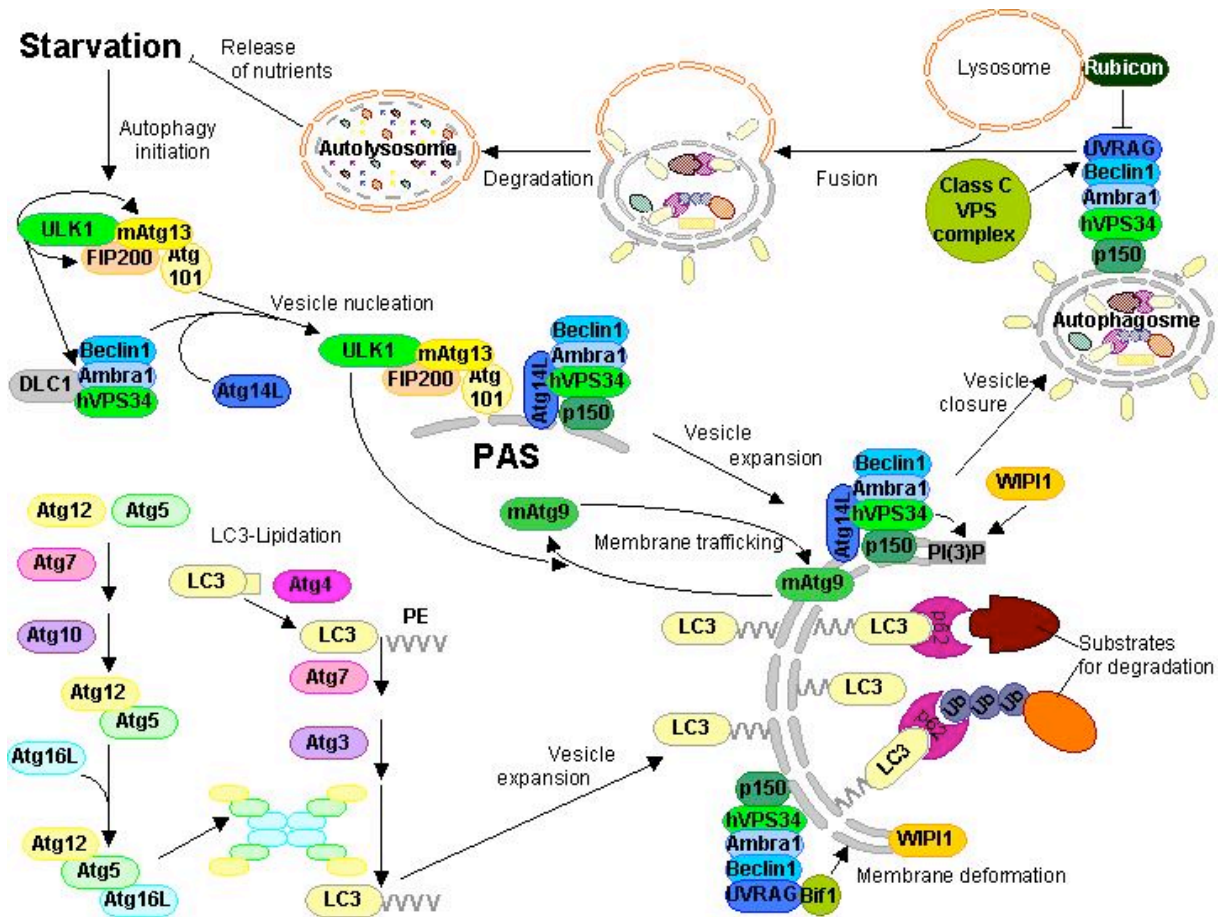


Figure 2.1. Molecular machinery and steps of autophagy. Depicted is the set of autophagy-related proteins in mammalian cells. Mammalian orthologs of yeast-Atg-proteins whose role in autophagy is not established yet (Atg2, WIP1/2/3) have been omitted. Autophagy is induced by starvation and other stresses and the stress signal is transferred to the ULK1-kinase-complex that initiates autophagy by phosphorylation of other Atg-proteins, including mAtg13, FIP200, and Ambra 1 in the hVPS34-complex, which thereby is released from microtubule-associated DLC1. The hVPS34-complex associates with Atg14L and initiates formation of the preautophagosomal structure (PAS) and vesicle nucleation by synthesizing PI(3)P, which is required for recruitment of other Atg-proteins, including the PI(3)P binding protein WIP1, to the PAS and to the expanding vesicle. The ULK1-complex also translocates to the PAS. Vesicle expansion includes incorporation of Phosphatidylethanolamine (PE)-conjugated LC3 into inner and outer vesicle membrane. LC3-lipidation is mediated by the protease Atg4, E1- and E2-like enzymes Atg7 and Atg10/Atg3, and the E3-ligase, the tetrameric Atg5-Atg12-Atg16L-complex. Membranes are thought to be delivered to the expanding vesicle by mAtg9, which shuttles between the PAS and the trans-Golgi-network (not shown) in an ULK1-dependent manner. Membrane deformation is mediated by Bif1, which is bound to UVRAG in a second hVPS34-complex. Cargo, including ubiquitylated and non-ubiquitylated proteins and organelles (not shown) is recruited in part by binding to the adapter protein p62, which also binds to LC3 in the inner membrane. After closure, the autophagosome fuses with a lysosome; this process is facilitated by interaction of UVRAG with the class C Vps-complex and inhibited by interaction of UVRAG with the Rubicon-protein present at the lysosome. Autophagosomal cargo is degraded by lysosomal enzymes in the autolysosome and breakdown products are released into the cytoplasm. ▶: activation; ⊣: inhibition. Adapted from Yang and Klionsky, 2010. For additional details, see main text.

Table 2.1. Role of *S. cerevisiae* Atg-proteins during autophagy and related processes. Atg-genes are grouped based on their requirement for non-selective autophagy, the cytoplasm to vacuole targeting (Cvt)-pathway, or selective autophagy of mitochondria (mitophagy) or peroxisomes (pexophagy). Their molecular function or structural features and mammalian homologs, if known, are listed as well. For references, see main text. PAS: preautophagosomal structure; PE: phosphatidylethanolamine; PI3K: phosphatidylinositol 3-kinase; PI(3)P: phosphatidylinositol-3-phosphate; PI(3,5)P₂: phosphatidylinositol-(3,5)-bisphosphate.

NAME	MOLECULAR FUNCTION	ROLE IN AUTOPHAGY	HUMAN HOMOLOG
AUTOPHAGY AND CVT			
Atg1	Ser/Thr kinase,	Initiation of vesicle formation	ULK1/2
Atg2	Peripheral membrane protein	Vesicle formation	ATG2A/B
Atg3	E2-like enzyme	Conjugation of Atg8 to PE	ATG3
Atg4	cysteine protease	Processing of Atg8	ATG4A/B/C/D
Atg5	E3-like enzyme when conjugated to Atg12	Conjugation of Atg8 to PE	ATG5
Atg6	Regulatory class III PI3-K complex subunit	Regulation of vesicle formation	Beclin 1
Atg7	E1-like enzyme	Activation of Atg8 and Atg12	ATG7
Atg8	Ubiquitin-like protein	Vesicle elongation, membrane fusion	LC3
Atg9	Transmembrane protein	Potentially: membrane delivery for vesicle expansion	mATG9
Atg10	E2-like enzyme	Conjugation of Atg12 to Atg5	ATG10
Atg12	Ubiquitin-like protein	Conjugation of Atg8 to PE	ATG12
Atg13	Regulatory Atg1-complex subunit	Increase of Atg1-kinase activity	mAtg13
Atg14	Regulatory class III PI3K-complex subunit	PAS-localization of additional Atg-proteins and the PI3K-complex	ATG14L1, Barkor
Atg15 ¹	Lipase	Intravacuolar lysis of autophagy/Cvt vesicles	---
Atg16	Scaffold	Multimerization and proper localization of the Atg12-Atg5 conjugate	ATG16L1
Atg18	WD-40 repeat protein	PI(3,5)P ₂ and PI(3)P-binding, vesicle formation	WIPI1/2
Atg27 ¹	Transmembrane protein	Potentially: membrane delivery for vesicle expansion	---
AUTOPHAGY-SPECIFIC			
Atg17	Scaffold in the Atg1-complex	Increase of Atg1-kinase activity, recruitment of other Atg-proteins to the PAS	FIP200
Atg22 ¹	Amino acid permease	Release of breakdown products	---
Atg29	Adapter	Recruitment of other Atg-proteins to the PAS	---
Atg31	Adapter	Recruitment of other Atg-proteins to the PAS	---
CVT-SPECIFIC			
Atg11	Scaffold in the Atg1-complex	Cargo loading, recruitment of other proteins to the PAS, Atg9 and Atg27 anterograde transport	---
Atg19	Receptor	Cargo selection/delivery in Cvt under physiological growth conditions	---
Atg20	Sorting nexin	Membrane protein sorting	---
Atg21	WD-40 repeat protein	PI(3,5)P ₂ and PI(3)P-binding, vesicle formation	WIPI3
Atg23 ³	Peripheral membrane protein	Atg9 and Atg27 anterograde transport	---
Atg24	Sorting nexin	Membrane protein sorting	SNX4, SNX30
Atg34	Receptor	Cargo selection/delivery in Cvt during starvation	---
MITOPHAGY			
Atg32	Mitochondrial receptor	Cargo recruitment	---
Atg33	Mitochondrial transmembrane protein	Unknown	---
PEXOPHAGY			
Atg25 ⁴	Coiled-coil-protein	Potentially: pexophagosome-vacuole fusion	---
Atg26 ⁵	UDP-glucose:sterol glucosyltransferase	Vesicle expansion	---
Atg28 ⁶	Coiled-coil protein	Formation of vacuolar sequestering membrane	---
Atg30 ⁷	Peroxisome receptor	Cargo recruitment	---

- ¹ other authors (Nakatogawa et al., 2009) do not list these proteins among the components of the core autophagy machinery (Atg15, Atg23, Atg27) or the autophagy-specific factors (Atg22), yet the defects in autophagy and/or the Cvt-pathway observed in the respective knockout yeast strains suggest that their assignment to functional groups as in this table is appropriate. (cf. entries for these proteins in the *Saccharomyces* Genome Database (SGDTM), www.yeastgenome.org).
- ² Atg11 is also required for pexophagy and mitophagy (Yorimitsu and Klionsky, 2005), but not for non-selective autophagy.
- ³ Atg23 is not essential for autophagy but increases efficiency of the process (Meiling-Wesse et al., 2004b; Tucker et al., 2003).
- ⁴ identified in *Hansenula polymorpha* (Monastyrska et al., 2005), not present in *S. cerevisiae*.
- ⁵ identified in *Pichia pastoris*, present in *S. cerevisiae* but not required for autophagy-related pathways (Warnecke et al., 1999).
- ⁶ identified in *Pichia pastoris* (Stasyk et al., 2006), not present in *S. cerevisiae*.
- ⁷ in Δ atg20 and Δ atg24 strains, mitophagy is decreased and pexophagy absent (Kanki et al., 2009; Nice et al., 2002).

2.1.2.1 The Atg1-complex

Autophagosomes are generated by expansion and finally closure of a precursor structure termed the isolation membrane or phagophore. This isolation membrane originates from a specialized site, the pre-autophagosomal structure (PAS), which in yeast is first marked by the autophagy-specific scaffold protein Atg17 and its constitutive interaction partners Atg29 and Atg31 (Itakura and Mizushima, 2010; Kabeya et al., 2007; Kawamata et al., 2005). Upon autophagy-induction, additional Atg-proteins are recruited to the PAS in a hierarchical fashion, beginning with the Atg1-Atg13 complex (Funakoshi et al., 1997; Kabeya et al., 2009; Matsuura et al., 1997; Straub et al., 1997). Regulation and function of Atg1-complexes in yeast and mammalian cells will be discussed in more detail in section 2.2.

In the Cvt-pathway and in mitophagy and pexophagy, Atg11 replaces Atg17 as the scaffold of the Atg1-complex and recruits additional Atg-proteins to the PAS, including the Cvt-specific sorting nexins Atg20 and Atg24 (Hettema et al., 2003; Nice et al., 2002; Yorimitsu and Klionsky, 2005). Atg24 is so far the only Cvt-specific yeast protein that is conserved up to humans, reflecting the fact that it also functions in other endosomal trafficking processes (Meijer et al., 2007).

2.1.2.2 The class III PI3-Kinase complex

Nucleation and expansion of autophagosomes in yeast depend on the class III PI3-kinase, vacuolar protein sorting defective (Vps) 34 (Odorizzi et al., 2000). Class III PI3-kinases synthesize phosphatidylinositol-3-phosphate (PI(3)P) from phosphatidylinositol (PI) to mark membranes for trafficking events (Engelman et al., 2006). Upon induction of autophagy, PI(3)P is required for the recruitment of additional Atg-proteins to the PAS. Vps34/hVPS34 (the human Vps34-ortholog) forms several complexes with different function but a common

core, consisting of the enzyme itself and two regulatory proteins, Vps15/p150 and Atg6 (Vps30)/Beclin 1 (Kihara et al., 2001).

In yeast, Vps34 participates in two complexes; complex I contains, in addition to the core, Atg14, and regulates autophagosome formation, while complex II with its accessory protein Vps38 mediates sorting of carboxypeptidase Y to the vacuole (Kametaka et al., 1998; Kihara et al., 2001). In contrast, mammalian/human VPS34 is a component of at least three distinct complexes, all of which regulate different steps of autophagy (cf. Fig. 2.1). The first of these complexes contains an Atg14-like protein (Atg14L or Barkor, Beclin 1-associated autophagy-related key regulator; Sun et al., 2008), thus resembling the yeast complex I. Atg14L is required for autophagosome biogenesis and responsible for increasing hVPS34-kinase activity and for localizing the entire hVPS34-complex to the PAS. In the second complex, Beclin 1 interacts with UVRAG, which shares some similarity with Vps38 and also regulates additional membrane trafficking processes besides from autophagy (Liang et al., 2008).

A role for the hVPS34-p150-Beclin 1-UVRAG complex in autophagosome nucleation is controversial at present. Early studies suggested that UVRAG mediates this process by contributing to hVPS34-activation (Liang et al., 2006). More recent work, however demonstrated that UVRAG is dispensable for autophagosome formation and competes with the positive regulator, Atg14L, for binding to Beclin 1 (Itakura et al., 2008; Matsunaga et al., 2009; Sun et al., 2008). Independent of its ability to bind to Beclin 1, UVRAG promotes autophagosome maturation via interaction with additional proteins that either are capable of deforming membranes (Bif 1), or mediate endosomal fusion (Vps11, 16, 18 and 33, which together form the class C Vps-complex; Liang et al., 2008; Peterson and Emr, 2001; Takahashi et al., 2007).

The third hVPS34-complex contains in addition to the core, UVRAG and RUN domain and cysteine-rich domain containing Beclin 1-interacting protein (Rubicon) and suppresses autophagosome maturation at late endosomes/lysosomes where Rubicon, an inhibitor of hVPS34 kinase activity, is localized (Matsunaga et al., 2009; Zhong et al., 2009). Another important Beclin 1-interacting protein, Activating molecule in Beclin 1 mediated autophagy (Ambra) 1, has not yet been assigned to any of these three complexes and might be part of the core complex (Fimia et al., 2007; He and Levine, 2010). Of note, Ambra 1 recently has been identified as the first autophagy-regulating protein outside the ULK1-complex that it phosphorylated by ULK1. Under physiologic conditions, Ambra 1 - and thus the hVPS34-core complex - is bound to the microtubule-associated Dynein motor protein complex via the

Dynein light chains (DLC) 1 and 2, and phosphorylation of Ambra 1 by ULK1 disrupts this interaction (Di Bartolomeo et al., 2010). Thus, the class III PI3-kinase complex appears to function downstream of the ULK1-complex in stress/starvation-induced autophagy.

2.1.2.3 The two Ubiquitin-like conjugation systems

Autophagic vesicle expansion includes incorporation of the lipidated form of Atg8 (mammalian homolog: microtubule-associated protein 1 light chain 3, LC3) into inner and outer layer of the autophagosomal double membrane. There, Atg8/LC3, an ubiquitin-like protein, is involved in membrane fusion and cargo recruitment (Ichimura et al., 2000; Nakatogawa et al., 2007). Lipidation of Atg8/LC3 with phosphatidylethanolamine (PE) requires the cysteine protease Atg4 for initial processing, and two ubiquitin-like conjugation systems. (Ichimura et al., 2000; Kirisako et al., 2000). The first of these consists of another Ubiquitin-like protein, Atg12, which is conjugated to Atg5 in a reaction that requires the activating enzyme (E1) Atg7 and the conjugating enzyme (E2) Atg10, but apparently no E3-like ligase (Hanada et al., 2007; Nakatogawa et al., 2009; Shintani et al., 1999; Tanida et al., 1999). This Atg5-Atg12 conjugate associates with Atg16 (mammalian homolog: Atg16-like protein, Atg16L), which mediates oligomerization and localization of the entire complex to the isolation membrane (Kuma et al., 2002; Matsushita et al., 2007; Mizushima et al., 1999). There, Atg5-Atg12 serves as the E3-ligase in the second conjugation system that links Atg8/LC3 to PE; the activating enzyme in this system is also and the the conjugating enzyme is Atg3 (Schlumpberger et al., 1997).

Although the two ubiquitin-like conjugation systems were originally thought to be essential for autophagy, a more recent study demonstrated formation of autophagosomes in Atg5^{-/-} and Atg7^{-/-}-MEFs and proposed an alternative, Atg5/Atg7-independent pathway of macroautophagy in mammalian cells. This pathway does not require other components of the ubiquitin-like conjugation systems (Atg12, 16) or of the membrane trafficking system (Atg9, cf. section 2.1.2.4), but is dependent on the ULK1-ination-complex (cf. section 2.2) and the class III PI3K-complex (cf. section 2.1.2.2). Autophagosome maturation occurs by fusion of isolation membranes with trans-Golgi-derived vesicles and late endosomes. The authors further show that *in vivo*, this alternative pathway predominantly mediates organelle clearance during embryogenesis while the conventional, Atg5/Atg7-dependent pathway is responsible for basal and starvation-induced autophagy. This suggests that the precise mechanism of macroautophagy utilized might depend on cell type and nature of the stimulus (Nishida et al., 2009).

2.1.2.4 The membrane trafficking system

In yeast, nucleation and expansion of autophagosomes, as well as recycling of autophagosomal components, is mediated by a set of additional Atg-proteins that transfer membranes to and from the PAS. The putative membrane carriers are the two transmembrane proteins Atg9 and Atg27, which shuttle between the PAS and the mitochondria (Atg9) or between PAS, mitochondria and Golgi-complex (Atg27; Noda et al., 2000; Yen and Klionsky, 2007). Atg9 and Atg27 depend on each other in trafficking to the PAS (Reggiori et al., 2004; Yen et al., 2007), while their retrieval from the PAS requires the Atg1-kinase complex (cf. section 2.2) and a small Atg-protein complex, consisting of Atg2 and Atg18, that is localized at the expanding membrane. Atg18 binds to PI(3)P, a phospholipid essential for autophagosome formation that is generated by the class III-PI3-kinase Vps34 and contributes to vesicle formation (Guan et al., 2001; Shintani et al., 2001). Atg18 is the only PI(3)P-binding Atg-protein conserved up to humans. Of the two transmembrane proteins, Atg9 and -27, only Atg9 is present in mammalian cells (Meijer et al., 2007), but in contrast to yeast Atg9, mammalian Atg9 shuttles between the trans-Golgi-network and late endosomes (Young et al., 2006). While peripheral redistribution of mAtg9 also requires the Atg1-homolog ULK1 (Young et al., 2006), the roles of the mammalian counterparts of Atg18 and Atg2, WD-repeat protein interacting with Phosphoinositides (WIPI)-1/2 and mAtg2A/B in mAtg9-trafficking have not been examined yet (Polson et al., 2010; Proikas-Cezanne et al., 2004).

Additional factors are required for membrane trafficking in the Cvt-pathway. These include a second PI(3)P-binding protein closely related to Atg18 (and therefore also to the mammalian Atg18-homologs of the WIPI-family), Atg21/Mai1, and Atg23. Atg23 is necessary for Atg9 and Atg27 trafficking under Cvt-conditions, whereas during autophagy, it just enhances efficiency of the process (Barth et al., 2002; Meiling-Wesse et al., 2004a; Meiling-Wesse et al., 2004b; Stromhaug et al., 2004; Tucker et al., 2003).

The source of the autophagosomal membranes is not entirely clear. Shuttling of Atg9 from the mitochondria and of Atg27 from mitochondria and Golgi-complex lead to the hypothesis that these two organelles supply lipids for autophagosome formation (Yen et al., 2007). In mammalian cells, autophagosomes have been suggested to be derived from a variety of sources, most recently from the ER, the plasma membrane and the outer mitochondrial membrane, with the latter being involved specifically in formation of autophagosomes during starvation (Axe et al., 2008; Hailey et al., 2010; Hayashi-Nishino et al., 2009; Ravikumar et al., 2010; Yla-Anttila et al., 2009). Thus, it is possible that the membrane source for autophagosomes differs with the autophagy-inducing stimulus (McEwan and Dikic, 2010).

Two of the yeast Atg-proteins, Atg15 and Atg22, fulfill unique functions in the final stages of autophagy and cannot be assigned to one of the four modules described above. Atg15 is a lipase required for intravacuolar degradation of autophagosomes and Cvt-vesicles, and Atg22 functions as an amino acid permease for the release of breakdown products from the vacuole into the cytosol (Epple et al., 2001; Teter et al., 2001; Yang et al., 2006b). Mammalian homologs of these two Atg-proteins are unknown at present.

2.1.2.5 Components of selective autophagy pathways

Although macroautophagy, appears to be a non-selective process because the expanding autophagosomal membranes sequester cytoplasm in bulk, this pathway can also be used for targeted elimination of protein aggregates or particular organelles. Furthermore, general starvation-induced autophagy seems to degrade cellular components in an ordered fashion, ordered in terms of localization and size of the substrates (from free proteins to protein complexes to organelles), as well as ordered in terms of their function (from the components of amino acid biosynthesis to metabolic enzymes to proteins involved in vesicular transport; Kristensen et al., 2008). Such selectivity results in part from the utilization of autophagy subtype-specific proteins that function as cargo receptors, for example Atg19 and Atg34 in the Cvt-pathway, Atg30 in pexophagy in *P. pastoris*, and Atg32 in mitophagy in *S. cerevisiae* (Farre et al., 2008; Leber et al., 2001; Noda et al., 2010; Okamoto et al., 2009; Scott et al., 2001; Suzuki et al., 2010). Mammalian cells also possess a mitophagy-specific receptor, the protein NIX, which does not share sequence homology with Atg32, and two more general adapter proteins, p62/sequestosome (SQSTM) 1 and neighbor of BRCA1 (NBR) 1 (Kirkin et al., 2009; Novak et al., 2010). Although these proteins for selective autophagy are not conserved, they all (except for PpAtg30, which has not been examined in this respect) share the ability to connect substrates for degradation to the inner autophagosomal membrane by interacting with Atg8 (or Atg8-homologs like LC3). In all cases, the interaction with Atg8/the Atg8-homolog occurs via a common motif matching the consensus sequence WXXL, which therefore has been termed LC3-interacting region (LIR) or Atg8 family interacting motif (AIM; Noda et al., 2008; Noda et al., 2010; Pankiv et al., 2007).

Misfolded, aggregated proteins and mitochondria are marked for autophagosomal degradation by ubiquitin, the same tag that marks substrates for proteasomal degradation. p62 and NBR1 can bind to ubiquitin via their ubiquitin associated (UBA)-domains. Although not fully established yet, K63-linked polyubiquitin chains might be of particular importance in autophagy since these are preferentially bound by p62 (Seibenhener et al., 2004; Tan et al., 2008). However, p62 can also recruit substrates independent of ubiquitin (Gal et al., 2009).

The ubiquitin conjugation systems that tag substrates for autophagic degradation are not known, except in the case of depolarized mitochondria. These are marked for elimination by ubiquitination of the voltage-dependent anion channel (VDAC) in the outer membrane by the E3-ligase Parkin, mutations of which are associated with Parkinson's disease (Geisler et al., 2010).

2.1.3 Signaling pathways regulating autophagy

A central question in the field is how stress signals are transmitted to the autophagy machinery. So far, three different stress-sensitive signal transduction pathways have been shown to target certain Atg-proteins in various organisms, namely the mTOR-pathway, the PKA-pathway and the JNK-pathway (Fig. 2.2)

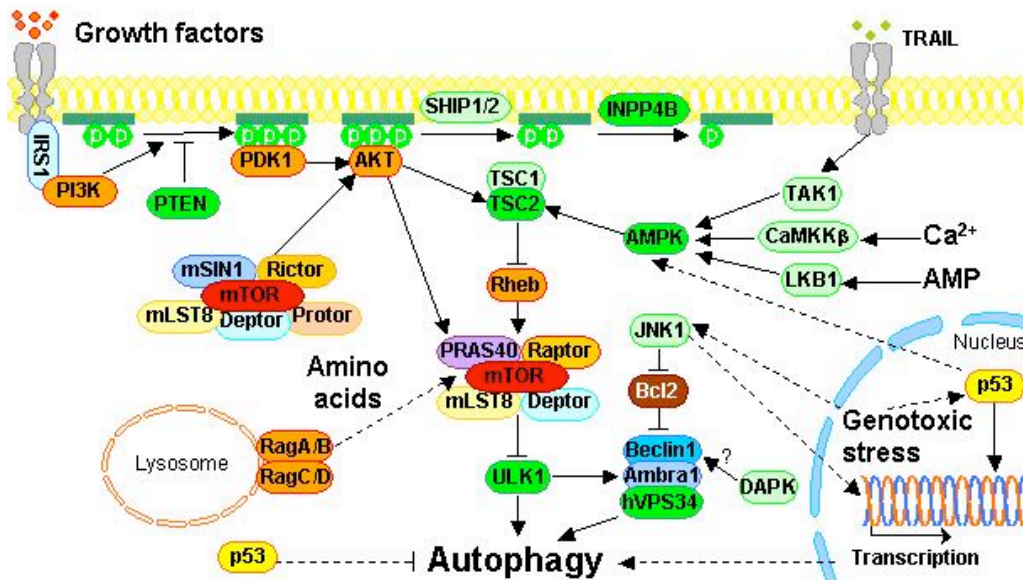


Figure 2.2. Important signaling pathways regulating autophagy in mammalian cells. The PI3K-AKT-pathway transmits growth factor signals and inhibits autophagy. After binding to intracellular domains of activated receptor protein tyrosine kinases via adapter proteins such as IRS1, PI3K generates membrane binding sites for PDK1 and AKT. The PI3K-reaction is reverted by the phosphatase PTEN, and membrane binding sites can also be destroyed by the phosphatases SHIP1/2 and INPP4B. At the membrane, AKT is activated by phosphorylation by PDK1 and mTORC2 (mTOR-Rictor-complex) and subsequently inhibits TSC2 (a GAP for the mTOR-activating small GTPase Rheb) and PRAS40 (an inhibitory subunit of the mTOR-Raptor-complex, mTORC1). Amino acids also inhibit autophagy and activate mTORC1. This includes mTORC1 translocation and docking to lysosomes via Rag-GTPases. mTORC1 directly inhibits autophagy by phosphorylation of ULK1 and its interacting protein mAtg13 (not shown), which are part of the autophagy core machinery. Conversely, certain cytokines, high cytosolic Calcium-concentrations or low energy levels activate autophagy via the kinases TAK1, CaMKK β and LKB1, respectively, which activate AMPK. AMPK in turn phosphorylates TSC2 and Raptor to suppress mTORC1. Genotoxic stress activates autophagy via p53 and the JNK-pathway, which induce transcription of stress- and autophagy-related genes. Nuclear p53 promotes AMPK-signaling and autophagy, whereas cytoplasmic p53 inhibits autophagy. JNK1 phosphorylates Bcl-2 to relieve its inhibitory interaction with the key autophagy protein and hVPS34-complex-subunit Beclin 1, and potential phosphorylation of Beclin 1 by DAP-kinase might have the same effect. The hVPS34-complex is also activated by phosphorylation of Ambra 1 by ULK1 and initiates autophagosome formation. ►: activation; ⊥: inhibition; —: direct regulation; - - -: indirect effect/precise mechanism not defined. Adapted from Yang and Klionsky, 2010. For additional details, see main text.

2.1.3.1 The mTOR-pathway

Reflecting the fundamental role of autophagy as a starvation response, one of the most important pathways regulating this process in all eukaryotes from yeast to mammals, is the TOR-pathway, whose basic function is to control cell growth (Wullschleger et al., 2006). TOR (target of rapamycin, called mTOR in mammals) is an evolutionary conserved serine/threonine kinase that forms two distinct complexes with different functions and sensitivities to the antibiotic Rapamycin. In mammalian cells, the Rapamycin-sensitive mTOR-complex 1 (mTORC1), where mTOR is associated with the regulatory proteins Raptor (regulatory associated protein of mTOR), G protein β subunit-like/mammalian lethal with SEC13 protein 8 (G β L/mLST8), DEP-domain containing mTOR-interacting protein (Deptor) and the proline-rich AKT substrate of 40 kDa (PRAS40), promotes cell growth and proliferation by activating translation and ribosome biogenesis and by suppressing autophagy (Kim et al., 2002; Kim et al., 2003; Peterson et al., 2009; Sancak et al., 2007). The mTOR-complex 2 (mTORC2) is defined by the protein Rictor (Rapamycin insensitive companion of mTOR) and is not inhibited by Rapamycin. mTORC2 further contains G β L, Deptor, mammalian stress-activated MAP kinase-interacting protein 1 (mSIN1) and protein observed with Rictor/proline-rich protein 5 (Protor/PRR5) and its best studied cellular function is reorganization of the actin cytoskeleton (Jacinto et al., 2006; Jacinto et al., 2004; Pearce et al., 2007; Sarbassov et al., 2004; Woo et al., 2007; Yang et al., 2006a). Although general composition and features of the TOR-complexes are similar between all species, the only mTOR-associated proteins that actually are conserved back to yeast are G β L (LST8), Raptor (Kog1), Rictor (Avo3) and mSIN1 (Avo1; Diaz-Troya et al., 2008).

mTORC1 integrates signals from various nutrient-, growth factor- and energy-sensing pathways, e.g. the (class I) PI3K-AKT-pathway that is coupled to receptor protein tyrosine kinases such as insulin-like growth factor receptor (IGFR) and epidermal growth factor receptor (EGFR), and the AMPK-pathway (Fig. 2.2; cf. also section 2.3; Sarbassov et al., 2005). Both signal transduction cascades target TSC2, which functions as a GTPase activating protein (GAP) and thus, as negative regulator of mTOR's direct activator, the small GTPase Ras homolog enriched in brain (Rheb; Garami et al., 2003; Long et al., 2005; Tee et al., 2003; Zhang et al., 2003). Whereas phosphorylation of TSC2 by AKT inhibits TSC2's GAP-activity and allows Rheb and mTOR to be active, TSC2 phosphorylation by AMPK increases its GAP-function and inhibits mTOR activity (Inoki et al., 2002; Inoki et al., 2003; Manning et al., 2002; Potter et al., 2002). Additionally, AKT phosphorylates the mTORC1-component PRAS40 to increase mTOR-kinase activity, whereas AMPK achieves the opposite by

phosphorylating another mTORC1-subunit, i.e. Raptor (Gwinn et al., 2008; Vander Haar et al., 2007).

Amino acid activation of mTORC1 comprises two aspects. First, amino acids induce translocation of mTORC1 to the lysosomes, and second, they also promote docking of mTORC1 to the lysosomal surface. This occurs via binding to the small GTPases of the Rag family, RagA/B/C/D (Sancak et al., 2010; Sancak et al., 2008).

mTORC1 is the major negative regulator of autophagy, and all signaling cascades that activate mTORC1 are expected to inhibit this process. Thus, mTORC2 is connected to autophagy as well, since it is required for full activation of AKT. AKT subsequently not only activates mTORC1 but also inhibits the FOXO3-transcription factor that induces expression of several Atg-genes, including LC3 and Atg12 (Mammucari et al., 2007; Zhao et al., 2007).

2.1.3.2 The Ras/PKA-pathway in yeast

In contrast to the mTORC1-pathway, whose involvement in autophagy has been demonstrated in multiple model systems, including yeast, *Drosophila*, and mammalian cell lines, regulation of autophagy by protein kinase A (PKA) has only been studied in yeast (Neufeld, 2010). PKA (Tpk1/2/3 in yeast; Toda et al., 1987) is activated by cyclic adenosine monophosphate (cAMP). In yeast, synthesis of cAMP by the enzyme adenylate cyclase is stimulated by two glucose-responsive G-protein systems: the first is defined by the small GTPases Ras1/2, but how it is activated by glucose is not fully understood at present (Colombo et al., 2004); the second consists of the G α protein Gpa2 and its G-protein-coupled receptor (GPCR) Gpr1, which functions as a sensor for fermentable sugars (Casperson et al., 1985; Kataoka et al., 1985; Lorenz et al., 2000; Matsumoto et al., 1982; Nakafuku et al., 1988). Maximum rates of cAMP-synthesis require both systems to be active (Colombo et al., 2004).

Autophagy can be induced independently of TOR-inhibition when the PKA-pathway is suppressed; yet, it is controversial whether this alone is sufficient or whether another protein kinase, Sch9, which is homologous to the mammalian kinase AKT, has to be inactivated in parallel (Stephan et al., 2009; Yorimitsu et al., 2007). Although PKA and TOR have the same target among the Atg-proteins, namely the Atg1-Atg13 complex (cf. section 2.2), autophagy induced by inactivation of PKA and Sch9 depends on additional factors that are not involved in TOR-mediated autophagy. The precise role of these additional factors, i.e. the zinc-finger transcription factors Msn2 and Msn4, and the protein kinase Rim15 (Yorimitsu et al., 2007) in autophagy have not been characterized and their mammalian homologs have not been identified yet.

2.1.3.3 The JNK-pathway in mammalian cells

In mammalian cells, autophagy can also be regulated by the JNK (c-Jun amino terminal kinase) pathway (Li et al., 2009; Lorin et al., 2009; Ogata et al., 2006; Puissant et al., 2010). The three mammalian JNKs, JNK1/2/3, are mitogen activated protein kinases (MAPKs) and responsive to diverse environmental stress stimuli, e.g. heat shock, UV irradiation and growth factor deprivation. Certain proinflammatory cytokines such as tumor necrosis factor α (TNF α) can also activate JNKs. JNKs act downstream of receptor protein tyrosine kinases, G-protein coupled receptors or the small GTPases Rac, Rho and Cdc42. The MAP-kinase-kinases (MAPKK) for the JNKs are MKK4/7, and their MAP-kinase-kinase-kinase-kinases (MAPKKK) are most commonly MEKK1-4. JNKs control a variety of cellular processes, including growth, differentiation, survival and apoptosis via phosphorylation of target proteins, mostly transcription factors like c-Jun or STAT3 (Kyriakis and Avruch, 2001; Roux and Blenis, 2004). JNKs are also activated by poorly defined mechanisms by DNA-damaging agents and by some anticancer drugs, e.g. Resveratrol, 2-Methoxyestradiol and Topotecan, in a variety of cell lines, and several studies demonstrated a JNK-dependent increase in the expression of certain autophagy-genes upon such treatments (Li et al., 2009; Lorin et al., 2009; Puissant et al., 2010). Furthermore, JNK-activity is essential for autophagy-induction in response to ER-stress (Ogata et al., 2006). However, direct JNK-targets mediating the observed effects remained to be identified in these studies.

JNK1 can also regulate autophagy at the level of the class III PI3-kinase complex important for autophagosome nucleation. Under nutrient-rich conditions, assembly of this complex is inhibited by antiapoptotic proteins of the Bcl-2-family, such as Bcl-2 and Bcl-X_L. These two proteins bind to Beclin 1, thereby preventing its interaction with hVPS34 (Pattingre et al., 2005). When autophagy is induced by starvation, Bcl-2 is phosphorylated by JNK1, which leads to disruption of its association with Beclin 1 (Wei et al., 2008). There is also evidence that phosphorylation of Beclin 1 by death receptor associated-kinase (DAPK) can antagonize its interaction with Bcl-X_L (Zalckvar et al., 2009). One caveat to this study is that the experiments were conducted in the context of overexpression of DAPK and did not examine whether endogenous DAPK in response to a physiologic autophagy-activating stimulus had the same effect.

2.2 The autophagy-regulating kinase ULK1

2.2.1 ULK-family kinases - Atg1-homologs in higher organisms

Atg1 is a serine/threonine kinase originally identified in genetic screens for autophagy genes in *S. cerevisiae* (Matsuura et al., 1997). Orthologs for this gene have been found in all higher eukaryotes; based on the Atg1-relative in *C. elegans*, Unc-51, they are referred to as Unc-51 like kinases (ULKs). In mammalian cells, two clear Atg1-orthologs are present, the kinases ULK1 and ULK2 (Kuroyanagi et al., 1998; Yan et al., 1998; Yan et al., 1999). Both genes are ubiquitously expressed, although their relative abundance differs among various tissues. Like Atg1, ULK1/2 are composed of three modular regions (Fig. 2.3): an N-terminal kinase domain, followed by a serine/proline rich spacer region, and a C-terminal region. Alignment of Atg1 and its mammalian and *Drosophila* orthologs shows a high degree of homology for the kinase domain with some conservation at the C-terminus. ULK1 and ULK2 share 55 % overall identity on the protein level and 78 % identity in their kinase domains, including residues in the conserved T-loop activation domain. ULK1/2 form a unique family in the human kinome, together with three more distantly related kinases, ULK3, ULK4 and Fused/STK (serine/threonine kinase)³⁶. Sequence conservation between these three kinases and ULK1/2 is limited to the kinase domain and excludes the regulatory spacer- and C-terminal regions which are important for ULK1/2-function, suggesting that the cellular role of ULK3/4/Fused differs from that of ULK1/2 (Mizushima, 2010).



Figure 2.3. Domain structure of the mammalian kinases ULK1 and ULK2. Mammalian Unc-51 like kinases 1 and -2 are both orthologous to the autophagy-related kinase Atg1 in yeast and share a high degree of identity or similarity with each other across all three functional regions of the protein, which are an N-terminal kinase domain, a serine and proline rich spacer region and a C-terminal domain. The figure is drawn to scale and the relative proportions of the three domains are correct.

2.2.2 Cellular functions of Atg1/ULKs

Atg1 was first described in yeast as a critical regulator of autophagy induction, whereas its *C. elegans* ortholog, Unc-51 (uncoordinated-51) was originally identified as an axonal guidance mutant (Hedgecock et al., 1985; Ogura et al., 1994); only later, it was also shown to be required for dauer-formation, a specialized autophagy-related developmental stage entered in response to an unfavorable environment (Melendez et al., 2003). Both, the role in autophagy and that in neuronal processes are conserved up to mammals, and ULK1 as well as ULK2 have been shown to function in either context, although ULK1 has been studied to a greater extent. ULK1 and ULK2 are required for fiber formation in cerebellar granular neurons and

regulate filopodia extension and axon-branching of sensory neurons by non-clathrin-coated endocytosis (Tomoda et al., 1999; Zhou et al., 2007). A role in autophagy has been clearly determined for ULK1, yet, in the case of ULK2, contradictory findings were reported (cf section 2.2.5; Chan et al., 2007; Hara et al., 2008). Another member of the mammalian ULK-family, ULK3, recently also has been reported to be involved in autophagy, specifically in the context of the mitotic senescence transition. In contrast, other studies identified ULK3 as a positive regulator of Sonic Hedgehog (Shh)-signaling (Maloverjan et al., 2010a; Maloverjan et al., 2010b; Young et al., 2009). This is in line with its similarity to the kinase Fused, a known and essential component of the Hedgehog (Hh)-pathway and thus, of embryonic development, in *Drosophila*. Mammalian Fused however, despite its possible involvement in the Shh-pathway, is not absolutely required for development, suggesting the presence of redundant kinases, possibly ULK3 (Maloverjan et al., 2007). With regard to ULK4, several single nucleotide polymorphisms (SNPs) in the gene (and in the ULK3-gene) have been identified for their association with variations in diastolic blood pressure in a genome wide association study, however, there currently is no report on the biological function of this member of the ULK-kinase family (Levy et al., 2009).

2.2.3 Atg1- and ULK-complexes

In all organisms, the ability of the Atg1-ortholog to participate in multiple distinct processes relies on its interaction with pathway-specific proteins. In yeast, Atg1 functions at the earliest steps of the Cvt-pathway as part of a complex containing the scaffolding protein Atg11 and two sorting nexins, Atg20 and Atg24 (Hetteema et al., 2003; Nice et al., 2002; Yorimitsu and Klionsky, 2005). The switch to autophagy occurs when Atg1 dissociates from Atg11 and binds to Atg17, which forms a constitutive subcomplex with Atg29 and Atg31. (Kabeya et al., 2007; Kabeya et al., 2009; Kawamata et al., 2005). The only Atg1-interacting protein required for autophagy and the Cvt-pathway is the regulatory protein Atg13, although it only binds to Atg1 during autophagy (Mizushima et al., 2010). As the entire Cvt-pathway, homologs of Atg11 and the other Cvt-specific Atg1-interacting proteins are absent in mammalian cells, which, however, also do not contain components with detectable sequence conservation to Atg13 and Atg17 (Meijer et al., 2007). Instead, functional counterparts of Atg13 and Atg17 have only recently been identified, based on their ability to bind to ULK1 and to positively regulate autophagy in complex with this kinase. These functional homologs are a novel protein called mammalian Atg13 (mAtg13) and the previously characterized Focal Adhesion Kinase family interacting protein of 200 kDa, FIP200 (Chan et al., 2009; Ganley et al., 2009; Hara et al., 2008; Jung et al., 2009; Meijer et al., 2007). Similarly, in *C. elegans*, *epg-1* has

been suggested to be a (highly divergent) homolog of Atg13 based on its ability to interact with Unc-51 and to regulate autophagy (Tian et al., 2009). Homologs for yeast Atg29 and Atg31 in higher eukaryotes are currently not known (Meijer et al., 2007). On the other hand, mammalian ULK-complexes contain an Atg13-binding protein, Atg101, which is absent in yeast (Hosokawa et al., 2009b; Mercer et al., 2009).

Regulation of axon outgrowth by Unc-51 and Unc-51-like kinases in higher eukaryotes also requires certain interaction partners, e.g. the adaptor protein Unc-14 and the kinesin-like protein Vab-8 in *C. elegans*, a kinesin heavy chain homolog, Unc-76, in *Drosophila* and the scaffold protein Syntenin and the Ras-GAP Syngap in mammalian neurons (Lai and Garriga, 2004; Ogura et al., 1997; Toda et al., 2008; Tomoda et al., 2004). So far, none of these proteins has been examined for a potential role in autophagy, and vice versa, the autophagy-specific factors functionally homologous to Atg13 or Atg17 have not been studied for their requirement in axonal development.

2.2.4 Regulation and role of Atg1/ULK1 in autophagy

With regard to their function during autophagy, yeast Atg1 and mammalian ULK1, together with their complex partners (m)Atg13 and Atg17/FIP200 display common features but also major differences (Fig. 2.4).

First, both proteins are thought to be the most upstream component of the autophagy machinery and to receive inputs from multiple regulatory signaling pathways, i.e. the (m)TOR- and the PKA-pathway, at least in yeast. In either case, the signal transferred to Atg1/ULK1 is inhibitory (Mizushima, 2010). When (m)TOR or PKA are suppressed, Atg1/ULK1 is derepressed and initiates autophagy. Yet, the mechanism of autophagy-induction by Atg1/ULK1 is not well understood. To date, only two substrates have been described for ULK1, besides from its associated proteins mAtg13 and FIP200 (Chan et al., 2009; Ganley et al., 2009; Hara et al., 2008; Hosokawa et al., 2009a), namely the focal adhesion protein Paxillin (Chen et al., 2008) and the class III PI3-kinase complex subunit Ambra 1 (cf. section 2.1.2.2; Di Bartolomeo et al., 2010). However, the mechanism by which Paxillin regulates autophagy remains to be elucidated, and Ambra 1 is not conserved in yeast, suggesting that Atg1/ULK1 phosphorylate additional Atg-proteins. It should be noted that the requirement for Atg1/ULK1 for autophagy induction seems to be general and independent from the inducing stimulus (Mizushima, 2010)

Second, Atg1 and ULK1 regulate the trafficking of (m)Atg9 to peripheral compartments (cf. section 2.1.2.4). Yet, the precise mechanism for this has not been elucidated up to now (Reggiori et al., 2004; Young et al., 2006).

Third, full activation of Atg1 and ULK1 requires their binding partners (m)Atg13 and Atg17/FIP200 and kinase activities increase (although only moderately in mammalian cells) upon starvation (Hara et al., 2008; Kamada et al., 2000). Furthermore, (m)Atg13 enhances the interaction of Atg1/ULK1 with Atg17/FIP200 (Ganley et al., 2009; Hosokawa et al., 2009a; Jung et al., 2009; Suzuki et al., 2007).

On the other hand, regulatory and functional differences between Atg1 and ULK1 have been reported, indicating that certain findings in one organism are not readily transferable to others.

First, in yeast, hyperphosphorylation of Atg13 by TOR under nutrient-rich conditions prevents its binding to Atg1, which occurs only with nutrient deprivation and dephosphorylation of Atg13 (Kamada et al., 2010). A direct interaction between TOR and the Atg1-complex has not been demonstrated. Mammalian ULK1 however, is constitutively associated with mAtg13, Atg101 and FIP200. Under nutrient rich conditions, mTORC1, via Raptor, also binds to ULK1 and directly phosphorylates not only mAtg13 but also ULK1 itself (Hara et al., 2008; Hosokawa et al., 2009a). Upon starvation, mTORC1 dissociates from the ULK1-mAtg13-Atg101-FIP200-complex and ULK1 phosphorylates mAtg13 and FIP200 (Chan et al., 2009; Hosokawa et al., 2009a; Jung et al., 2009).

Second, kinase activity of yeast Atg1, although increased with starvation, is not required for initial recruitment of other Atg-proteins, including Atg8, to the PAS but only for subsequent membrane extension and dissociation of these Atg-proteins from the PAS. This suggests that Atg1 itself acts as a scaffold (Cheong et al., 2008; Kabeya et al., 2005; Kamada et al., 2000; Sekito et al., 2009). One exception is Atg2, which localizes to the PAS in an Atg1-kinase-activity-dependent manner (Kawamata et al., 2008). In contrast, ULK1-kinase activity is also required for localization of the Atg8-homolog LC3 to isolation membranes (Chan et al., 2009; Hara et al., 2008). The regulation of mammalian Atg2 has not been examined.

Third, in yeast, the interaction of Atg1 and Atg17 seems to be completely dependent on Atg13, whereas ULK1 also directly binds to FIP200, although this association is enhanced by mAtg13 (Hara et al., 2008; Hosokawa et al., 2009a; Jung et al., 2009; Kabeya et al., 2005).

Besides from that, studies in yeast demonstrated additional regulatory influences on the Atg1-complex that have not yet been examined in mammalian cells. In particular, Atg1 and Atg13 can be phosphorylated by PKA, which prevents localization of these proteins to the PAS (Budovskaya et al., 2005; Stephan et al., 2009). Moreover, Atg1 has been shown to

phosphorylate its own activation loop upon exposure to pro-autophagic stimuli, and this event requires Atg13 and Atg17 and is essential for initiation of autophagy (Yeh et al., 2010).

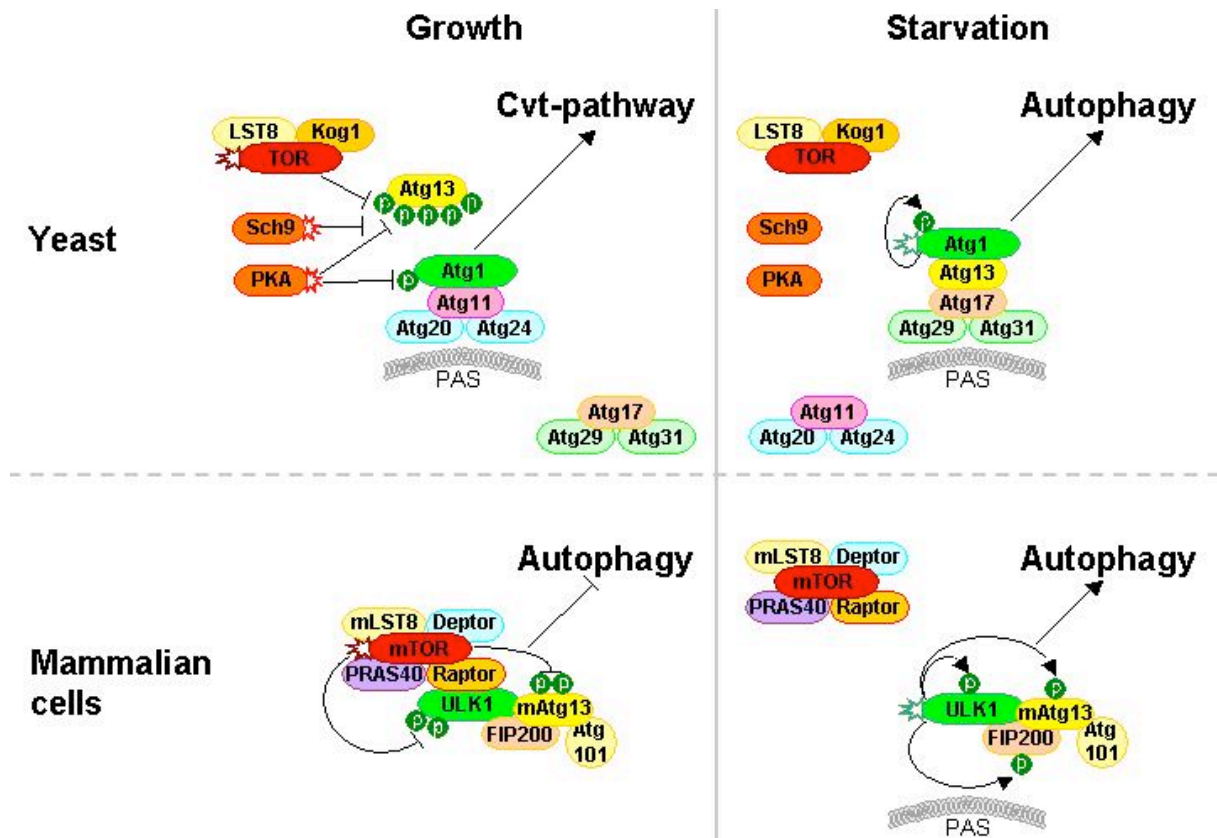


Figure 2.4. Subunit composition and regulation of Atg1-complexes in yeast and of the ULK1-complex in mammalian cells. The Ser/Thr-kinases Atg1 in yeast and ULK1 in mammalian cells are orthologs of each other and function in autophagy, however, the sets of interacting proteins and mechanisms of regulation differ. Under physiological growth conditions, Atg1 in yeast associates with Atg11, Atg20 and Atg24 at the preautophagosomal structure (PAS) and regulates the Cytoplasm-to-vacuole-targeting (Cvt)-pathway. TOR and PKA phosphorylate Atg13 and inhibit its binding to Atg1. The kinase Sch9 also inhibits autophagy under these conditions. Upon starvation, Atg13 is dephosphorylated and binds to Atg1, which then allows association with the Atg14-Atg29-Atg-31-complex and an increase in Atg1-kinase activity, which leads to the activation of autophagy. In mammalian cells, ULK1 is constitutively associated with the homologs of Atg13 and Atg17, mAtg13 and FIP200, respectively, and the mammalian-specific mAtg13-binding protein Atg101. Under physiological growth conditions, the ULK1-complex interacts with mTORC1 (mTOR-Raptor-complex). mTORC1 phosphorylates ULK1 and Atg13 and autophagy is suppressed. Starvation induces dissociation of mTORC1 from the ULK1-complex and allows ULK1-kinase activity to increase. Subsequently, ULK1 phosphorylates mAtg13 and FIP200 and other Atg-proteins (not shown) to initiate autophagy. Note that in mammalian cells, which lack the Cvt-pathway, a PAS is only formed under starvation conditions. ►: activation; ⊣: inhibition. Adapted from Mizushima et al., 2010.

2.2.5 Similarities and differences between ULK1 and ULK2

Whereas ULK1 clearly is involved in autophagy, the role of ULK2 in this process is controversial (Chan et al., 2007; Hara et al., 2008). While, for example, siRNA-knockdown of ULK2 in HEK293T cells did not affect autophagy, studies of ULK1-knockout mice provided evidence for functional redundancy of ULK1 and ULK2 (Chan et al., 2007; Kundu et al., 2008). These animals display only mild phenotypic abnormalities, consisting in delayed

erythrocyte maturation, whereas knockout of other Atg-genes in mice, in particular of Beclin 1, Atg5 or Atg7, results in embryonic or perinatal lethality (Hara et al., 2006; Komatsu et al., 2006; Yue et al., 2003). Consistent with this notion, ULK2-knockout mice are also viable, yet, no defects in erythrocyte development have been described. Instead, these mice are characterized by abnormal anxiety behavior, which in turn has not been reported for ULK1-knockout mice (www.informatics.jax.org). This suggests that ULK1 and ULK2 have common as well as unique functions. The effect of ULK1-ULK2-double knockout in mice, which, if similar to that of knockout of other Atg-genes, would proof that ULK1/2 are essential for autophagy, has not been examined yet.

On the molecular and cellular level, ULK2 shares many of the above listed features with ULK1, including phosphorylation by mTOR, interaction with mAtg13 and FIP200 and phosphorylation of mAtg13. Yet, in contrast to the ULK1-mAtg13-interaction, binding of ULK2 to mAtg13 is not direct but mediated by FIP200 (Jung et al., 2009). As ULK1, ULK2 localizes to the isolation membrane upon starvation in NIH3T3 murine fibroblasts, and overexpression of its kinase dead mutant inhibits autophagy (Hara et al., 2008).

Notably, and unexpectedly, given their putative roles as positive regulators of autophagy and previous results in *Drosophila* showing that ULK-overexpression accelerated the process, overexpression of wild type ULK1 and ULK2 in mammalian cells was found to block starvation-induced autophagy in a dose-dependent manner, with high levels of overexpression causing apoptosis, as also seen in *Drosophila* (Chan et al., 2007; Hara et al., 2008; Scott et al., 2007). The potential mechanism of autophagy-suppression by overexpressed wild type and by kinase-inactive ULKs has been investigated using ULK1. These studies suggested that autophagy is inhibited due to sequestration of two different, thus far unidentified, pro-autophagic factors by ULKs, one that interacts with the beginning of the ULK-spacer region and one that associates with the end of the C-terminal domain. This hypothesis further states that sequestration of the C-terminally interacting factor occurs only with kinase-inactive ULKs which are defective in autophosphorylation and thus adopt a conformation in which the binding site for this factor is exposed (Chan et al., 2007; Chan et al., 2009; Hara et al., 2008; Scott et al., 2007).

Yet, there also are biochemical differences between ULK1 and ULK2. In HEK293 cells, ULK2 was found to enter into different protein complexes than ULK1 and to increase its association with membranes upon starvation, whereas the membrane-bound fraction of ULK1 remained constant under all nutrient-conditions. These observations further strengthen

the view that the functions of ULK1 and ULK2 might not be completely identical (Chan et al., 2009).

2.3 The energy-sensing kinase AMPK

2.3.1 Structure and regulation of the AMPK holoenzyme

Adenosine-5'-monophosphate activated protein kinase, AMPK, is an evolutionary conserved central regulator of energy balance on the cellular and organismal level (Hardie, 2007). Mammalian AMPKs and their orthologs in yeast and plants, SNF1 (sucrose non fermenting) and SNF1-related kinases, function as heterotrimers composed of a catalytic α -subunit and two regulatory subunits, β and γ (Celenza and Carlson, 1986; Mitchelhill et al., 1994). While the β -subunit serves as a scaffold and potentially as a sensor for long-term energy reserves via its glycogen binding domain, the γ -subunit allows the AMPK-complex to monitor the current energy state of the cell because of its ability to bind AMP or ATP in a mutually exclusive manner (Hudson et al., 2003; Polekhina et al., 2003; Scott et al., 2004). Binding of AMP and ATP to the γ -subunit occurs via its four cystathionine β -synthase (CBS)-motifs, two of which function together to form a Bateman domain, i.e. a specialized domain for binding of adenosine-derivatives (Scott et al., 2004). Full activation of AMPK is achieved by the interplay of various mechanisms. The key event is phosphorylation of a particular threonine residue in the activation loop in the α -subunit (Thr172 in human AMPK α 2) by an upstream kinase, which allows an approximately 100-fold increase in catalytic activity (Suter et al., 2006). A second aspect is binding of AMP to the γ -subunit, which causes allosteric changes and has at least three different positive effects on AMPK activity. First, AMP stimulates phosphorylation of the activation loop threonine; however, an essential prerequisite for this is myristoylation of an N-terminal glycine residue in the β -subunit, and the precise mechanism is still elusive (Oakhill et al., 2010). Second, these allosteric changes per se lead to an approximately tenfold increase in catalytic activity (Suter et al., 2006), and third, the activation loop threonine is protected from dephosphorylation by protein phosphatases 2A and 2C (Fig. 2.5; Davies et al., 1995; Sanders et al., 2007).

Up to now, four kinases that can phosphorylate AMPK at its activation-loop under various conditions have been identified. When energy levels are low, the AMPK-activation loop is phosphorylated by liver kinase B1 (LKB1; Hawley et al., 2003; Woods et al., 2003), which appears to be constitutively active (Lizcano et al., 2004; Sakamoto et al., 2004), but the presence of AMP allows this phosphorylation to become stabilized. In addition, Calcium-calmodulin-dependent protein kinase β (CaMKK β), and to a lesser extent, CaMKK α , also

have been reported to activate AMPK when cytosolic levels of Ca^{2+} increase (Hawley et al., 2005; Hurley et al., 2005; Woods et al., 2005); and lastly, there is evidence that transforming growth factor (TGF) β -activated kinase 1 (TAK1) is also able to phosphorylate the AMPK-activation loop threonine (Herrero-Martin et al., 2009; Momcilovic et al., 2006).

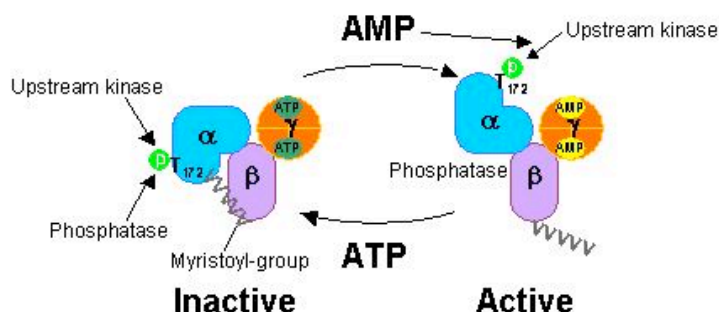


Figure 2.5. Structure and activation of the AMPK-holoenzyme. AMPK functions as a heterotrimer, composed of a catalytic subunit (α), a scaffolding subunit (β) and a regulatory subunit (γ). When energy levels are high, AMPK is inactive because ATP is bound to the γ -subunit and the activation loop threonine (Thr172 in human AMPK α 2), which is phosphorylated by an upstream kinase such as constitutively active LKB1, is rapidly dephosphorylated by protein phosphatases 2A and 2C. A myristoyl-group attached to the β -subunit interacts with the α -subunit and contributes to stabilization of the inactive conformation. When energy levels drop, AMP further triggers phosphorylation of the activation loop threonine in the α -subunit, displaces ATP from the nucleotide binding sites in the γ -subunit and induces conformational changes which also protect the activation loop threonine from dephosphorylation. The combination of these three effects of AMP results in a strong increase in the catalytic activity of the α -subunit.

AMPK α -, β - and γ -subunits each exist in several isoforms encoded by distinct genes. Mammals possess two genes each for the α - and β -subunits and three for the γ -subunit with differential expression in various tissues (Hardie, 2007). *In vitro* and *in vivo* studies of various AMPK transgenic and conditional-, tissue specific- and whole body- knockout mice revealed common features as well as distinct characteristics and/or physiological roles for all isoforms of all subunits (Viollet et al., 2009). For example, single knockout of either AMPK α 1 or AMPK α 2 (the double knockout is embryonically lethal) has no influence on important physiologic and metabolic parameters such as body weight, energy expenditure and 24 h respiratory quotient despite predominant high-level expression of AMPK α 2 only in heart and skeletal muscle and certain regions of the brain (Stapleton et al., 1996; Turnley et al., 1999; Viollet et al., 2009). High expression of AMPK α 2 in the hypothalamus is thought to account for the phenotypic abnormalities that are seen exclusively in AMPK α 2-deficient mice, which include mild insulin resistance and glucose intolerance. This indicates that AMPK α 1 can only complement some, but not all, functions of AMPK α 2 (Viollet et al., 2003).

The different expression patterns and characteristics of all isoforms of all subunits allow assembly of AMPK-heterotrimers with different capability for activation by a particular

upstream kinase (depending on the α -subunit), different intracellular localization (depending on the β -subunit) and different sensitivity to AMP and ATP (depending on the γ -subunit; Cheung et al., 2000; Sakamoto et al., 2005; Sakamoto et al., 2006; Warden et al., 2001). This ultimately results in AMPK-complexes with different modes of regulation and function, including different substrate preference, and provides a way to adjust AMPK-activity to the special conditions and requirements of a particular cell- or tissue type (Viollet et al., 2009).

2.3.2 Metabolic and non-metabolic functions of AMPK

AMPK catalytic activity is sensitive to the ATP:AMP-ratio and increases when ATP-levels drop, e.g. in response to metabolic stresses like hypoxia or glucose starvation (Laderoute et al., 2006). Certain hormones, such as leptin, also can modulate cellular AMPK-activity. AMPK activates ATP-generating pathways, including glycolysis and glucose uptake, and inhibits ATP-consuming processes like fatty acid-, glycogen- and protein biosynthesis (Fig. 2.6; Kahn et al., 2005). Important substrates among metabolic enzymes include cytosolic Acetyl-CoA-Carboxylase 1 (ACC) and the peripheral mitochondrial membrane protein ACC2. ACC1 and ACC2 synthesize malonyl-CoA either for use in fatty acid biosynthesis (ACC1) or as an inhibitor of fatty acid transport into mitochondria for β -oxidation (ACC2), and both enzymes are inhibited by AMPK (Munday et al., 1988; Wakil and Abu-Elheiga, 2009; Winder et al., 1997). Glycogen synthase, and thus glycogen synthesis, is also negatively regulated by AMPK-phosphorylation, whereas inducible and cardiac isoforms of Phosphofructokinase 2 (PFK2), a key glycolytic enzyme, are activated by AMPK (Carling and Hardie, 1989; Jorgensen et al., 2004a; Marsin et al., 2000; Marsin et al., 2002). Furthermore, AMPK stimulates glucose uptake by phosphorylating the AKT substrate of 160 kDa (AS160), which subsequently allows translocation of the glucose transporter GLUT4 to the plasma membrane (Sano et al., 2003).

AMPK also is a negative regulator of protein biosynthesis and thus, of cell growth. On the one hand, AMPK inhibits translation initiation at the level of mTORC1 by phosphorylation of TSC2 and Raptor (cf. section 2.1.3.1). On the other hand, AMPK suppresses translation at the elongation step by activating eukaryotic elongation factor 2-kinase (eEF2K), an inhibitor of this process (Browne et al., 2004; Horman et al., 2003).

Furthermore, AMPK mediates long-term metabolic adaption by inducing expression of glycolytic and mitochondrial genes, and by downregulation of genes required for gluconeogenesis or lipid synthesis; however, the primary substrates of AMPK in this context are largely unknown (Kahn et al., 2005). One recently identified mechanism through which AMPK activates transcription in response to various stresses consists in direct association

with chromatin and phosphorylation of histone H2B in promoter- and coding regions of p53-target genes that promote cell survival, such as p21 (Burgard et al., 2010). Some effects of AMPK on mitochondrial gene expression are mediated by the NAD⁺-dependent deacetylase SIRT1. Thereby, activation of SIRT1 by AMPK appears to be indirect and to result from an AMPK-dependent increase in β -oxidation, which is accompanied by an increase in NAD⁺, i.e. the co-factor required for SIRT1-activity (Canto et al., 2009).

Another aspect of AMPK's metabolic function consists in connecting nutrient- and energy sensing to the peripheral circadian clock in the liver. The circadian clock functions based on a negative feedback loop in which the CLOCK-BMAL1-transcription factor complex activates expression of its antagonists, e.g. the Cryptochrome 1-protein (Cry1). Cry1 is phosphorylated by AMPK, and this destabilizes Cry1, interrupts the negative feedback loop and resets the clock (Lamia et al., 2009).

In mammalian epithelial cells, AMPK has acquired one additional function, unrelated to its original role in the metabolic stress response, namely in the maintenance of tight junctions and cell polarity. Stabilization of tight junctions provides an independent mechanism, besides from suppression of protein biosynthesis, for AMPK to limit cell proliferation, and thus generalizes its role as a negative regulator of this process (Zhang et al., 2006; Zheng and Cantley, 2007). Studies in *Drosophila* suggest that failure to establish cell polarity account for the fact that AMPK knockout animals are not viable (Lee et al., 2007a). Direct substrates of AMPK that have been found to mediate its positive effect on cell polarity include non-muscle myosin regulatory light chain (MRLC; Lee et al., 2007a) and the Cytoplasmic linker protein of 170 kDa (CLIP-170), that binds to microtubule plus ends (Nakano et al., 2010).

Given its central role in cellular and organismal metabolism, AMPK emerged as an attractive drug target, originally for treatment of type 2 diabetes or the metabolic syndrome, but also for cancer (Gonzalez-Angulo and Meric-Bernstam, 2010; Winder and Hardie, 1999). Intriguingly, patients treated for diabetes with Metformin, which indirectly activates AMPK, have a significantly reduced risk of cancer compared to diabetic subjects not treated with this drug (Libby et al., 2009; Owen et al., 2000).

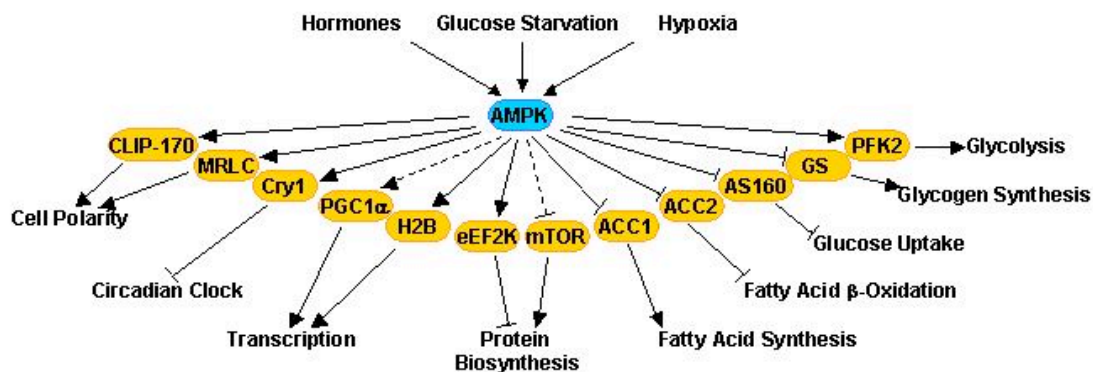


Figure 2.6. Cellular processes regulated by AMPK. The diagram summarizes central cellular processes regulated by AMPK. Important mediators of AMPK-signaling in each context are shown. ►: activating signal; ⊥: inhibitory signal; —: direct AMPK-substrate; - - -: indirect regulation. Adapted from Hardie, 2007. For details, see main text.

2.3.3 AMPK and autophagy

Due to its primary function as a master regulator of energy status, a role for AMPK in the regulation of autophagy has been inferred, but remains controversial. A screen in yeast originally designed to identify multicopy suppressors of the glycogen storage defect caused by loss of the AMPK-ortholog SNF1 revealed Atg1 and Atg13 as candidates. This provided the first evidence of SNF1 being as a positive regulator of autophagy, presumably upstream of the Atg1-Atg13 initiation complex (Wang et al., 2001). Data supporting a pro-autophagic function of AMPK in mammalian cells come from a study that utilized overexpression of dominant negative kinase inactive or constitutively active mutants of AMPK. While the dominant negative mutant inhibited starvation-induced autophagic proteolysis in two human cancer cell lines, constitutively active AMPK under nutrient-deprived conditions did not cause an additional increase in autophagy and was not able to initiate the process in complete medium. This led the authors to conclude that only a low, basal level of AMPK-activity is required to activate autophagy (Meley et al., 2006).

AMPK is an important mediator of the effects of p53, the probably most important tumor suppressor known today, on autophagy (Lane, 1992). Thereby, regulation of AMPK by p53 is reciprocal and complex. Induction of autophagy by the AMPK-activating drug Metformin occurs only in AMPK-positive cells that are also positive for p53 (Buzzai et al., 2007). p53 can activate autophagy in response to treatment with the cytotoxic drug Etoposide by signaling to mTOR via an AMPK- and TSC2-dependent pathway (Jin, 2005). Although the respective study could not clarify the mechanistic basis for this observation, it appears likely that it depends on two particular p53 target genes, Sestrin 1 and -2, which connect AMPK to its substrate TSC2 (Budanov and Karin, 2008). Additionally, p53 can

upregulate expression of TSC2 and AMPK β 1 (Feng et al., 2007). In contrast to the pro-autophagic function of nuclear p53, cytoplasmic p53 suppresses autophagy, and this also involves inhibition of AMPK and mTOR, although the mechanism for this is not known (Tasdemir et al., 2008).

In addition, three of the four possible upstream kinases of AMPK, i.e. LKB1, CaMKK β and TAK1, have been shown to mediate autophagy in response to glucose deprivation, cytosolic Ca²⁺-increase or TRAIL-treatment, and AMPK was found to be important in these settings as well (Herrero-Martin et al., 2009; Hoyer-Hansen et al., 2007; Liang et al., 2007). Interestingly, all these experiments involved comparatively long treatments (24 h) with glucose-free media, the Ca²⁺-ionophore Ionomycin and the cytokine TRAIL, respectively. On the other hand, in a recent study demonstrating AMPK-independent induction of autophagy by cytosolic Ca²⁺-increase, a much shorter time frame (6 h) has been examined (Grote-meier et al., 2010). Similarly, absence of AMPK only caused a significant block in hypoxia-induced autophagy when cells were exposed to low oxygen for a long time (20 h), but not with short-term (6 h) treatment (Papandreou et al., 2008).

The view of AMPK being an universal regulator of autophagy (Herrero-Martin et al., 2009) is further challenged by a report on the autophagy properties of AMPK α 1/ α 2-double-knockout mouse embryonic fibroblasts (MEFs; Williams et al., 2009). In these cells, autophagy can still be induced as a stress response to chronic glucose deprivation, although a similar upregulation is not seen in wild type MEFs. Additionally, AMPK α 1/ α 2-double knockout-MEFs were found to be much more susceptible to apoptotic cell death under prolonged and/or exacerbated energy stress. A mechanistic explanation for this is provided by previous work that demonstrated that AMPK-dependent phosphorylation of the cyclin-dependent kinase inhibitor p27^{Kip1} is important for entering autophagy instead of apoptosis (Liang et al., 2007). In summary, currently available data suggest that AMPK is not essential for induction of autophagy, but for long-term maintenance or additional upregulation of the process at later stages.

2.4 Specific aims

Autophagy is a cellular self-eating process with the capacity to prevent or to promote pathological states or cell death; this implies that autophagy has to be tightly regulated in order to be beneficial to the cell and/or the organism. Yet, the precise signal transduction mechanisms that facilitate this tight regulation are poorly understood at present. Furthermore, defining the pathways that regulate autophagy is complicated by the fact that certain findings in one model organism are not readily transferable to others, because the set of genes mediating autophagy diverged during evolution. Thus, the goal of this dissertation project was to elucidate regulation and function of the kinase ULK1, a homolog of the autophagy-related yeast kinase Atg1 and potential key initiator of this process in mammalian cells. In particular, we aimed to

1. Identify upstream kinases phosphorylating ULK1
2. Identify ULK1-substrates

These objectives first required identifying candidate regulators and substrates of ULK1 for experimental validation by bioinformatic analyses and proteomic studies. Integration of these data strongly suggested a functional relationship between ULK1 and the energy sensing kinase AMPK. We further strengthened this hypothesis by demonstrating that both kinases are recruited to a common complex. Thus, the second part of the thesis work focused on:

1. Biochemical characterization of the ULK1-AMPK-complex
2. Validation of ULK1 as an AMPK-substrate
3. Identification of AMPK-dependent phosphorylation sites in ULK1
4. Determining the biological function of the ULK1-AMPK-complex and of AMPK-dependent phosphorylation of ULK1.

These questions were addressed by a combination of biochemical, proteomic and cell biological approaches to study genetically and/or pharmacologically manipulated mammalian cells in culture.

3 Materials and Methods

3.1 Materials

3.1.1 Chemicals, reagents and solvents

2-Deoxy-D-glucose, grade III	Sigma
2-Mercaptoethanol	Sigma
3-[(3-Cholamidopropyl)dimethylammonio] -1-propanesulfonate (CHAPS)	Sigma
3X FLAG® peptide	Sigma
4-(2-hydroxyethyl)-1-piperazineethanesulfonic acid (HEPES)	Sigma
5-aminoimidazole-4-carboxamide-1-β-D-ribofuranoside (AICAR)	Toronto Research Chemicals
A-769662	Tocris
Acetic acid, glacial	Sigma
Adenosine 5'-triphosphate, disodium salt hydrate	Sigma
Adenosine 5'-triphosphate, ³² P labeled	Perkin Elmer
Agar	Fisher Scientific
Agarose, molecular biology grade	Sigma
Ammonium persulfate (APS)	Sigma
Ampicillin, sodium salt	Sigma
Aprotinin, bovine lung, solution	Calbiochem
Boric acid	Sigma
Bovine serum albumin	Roche
Brilliant blue R	Sigma
Bromphenol blue	Sigma
Calcium chloride	Sigma
Crystal violet	Sigma
Deoxycholate, sodium salt	Sigma.
Dimethyl sulfoxide (DMSO)	Sigma
DL-Dithiothreitol	Sigma
Ethanol	Pharmco
Ethylenediamine tetraacetic acid (EDTA)	Sigma.
Ethidium bromide	Sigma
Fibronectin, 0.1 % solution from bovine plasma	Sigma
Glutathione Sepharose™ 4B	GE Healthcare
Glycerol	Fisher Scientific

Glycerol-2-phosphate disodium salt hydrate	Sigma
Glycine	Sigma
Hexadimethrine bromide (Polybrene)	Sigma
Hank's buffered salt solution (HBSS)	Gibco/Invitrogen
IGEPAL® CA-630	Sigma
Isopropanol, absolute	Fisher Scientific
Isopropyl β -D-1-thiogalactopyranoside (IPTG)	Sigma
Kanamycin sulfate	Sigma
Leupeptin	Sigma
Magnesium acetate	Sigma
Magnesium chloride	Sigma
Methanol	Fisher Scientific
Milk powder	Albertsons
Mineral oil for PCR	Sigma
N, N, N', N'-tetramethylethylenediamine (TEMED)	Bio-Rad
Pansorbin® Cells, standardized	Calbiochem
Paraformaldehyde	Sigma
Phenformin hydrochloride	Sigma
Phenylmethanesulfonylfluoride (PMSF)	Sigma
Polyethyleneimine (PEI), linear, MW~25,000	Polysciences
Poly-L-lysine	Sigma
Potassium acetate	Sigma
Potassium chloride	Sigma
Potassium phosphate, monobasic	Sigma
rProtein A agarose	Repligen
Rec-Protein G-Sepahrose® 4B conjugate	Invitrogen
Sodium chloride	Sigma
Sodium fluoride	Sigma
Sodium dodecyl sulfate (SDS)	Sigma
Sodium hydroxide	Sigma
Sodium orthovanadate	Sigma
Sodium phosphate, dibasic	Sigma
Sodium pyrophosphate, decahydrate	Sigma
Sterile H ₂ O (for injection)	American Pharmaceutical Partners
Trizma® (Tris(hydroxymethyl)aminomethane)	Sigma

Tris·Cl	Sigma
Triton® X-100	Sigma
Tryptone	Sigma
TWEEN®-20	Sigma
Xylene cyanol FF	EM Science
Yeast extract	Fisher Scientific

3.1.2 Buffers, solutions and bacterial growth media

Buffers for agarose gel electrophoresis

Loading Buffer (6X) 0.27 % w/v bromphenol blue; 0.27 % w/v xylene cyanol FF; 30 % v/v glycerol

Running Buffer (TBE): 89 mM Tris; 89 mM boric acid; 10 mM EDTA, pH 8.0

Buffers for cell lysis

Protease/phosphatase inhibitors: 7.7U/ml Aprotinin; 1 µM Leupeptin, 1 mM PMSF, 2.5 mM β-Glycerophosphate; 2.5mM sodium fluoride; 1 mM sodium pyrophosphate; 200 µM pervanadate

Inhibitors were added to all lysis buffers except SDS lysis buffer immediately before use

CHAPS lysis buffer A (Sarbasov et al., 2004):

40 mM HEPES, pH 7.5; 120 mM NaCl; 1 mM EDTA; 0.3 % w/v CHAPS

CHAPS lysis buffer B (Sancak et al., 2007):

40 mM HEPES, pH 7.5; 1 mM; 1 mM EDTA; 0.3 % w/v CHAPS

Modified RIPA: 10 mM Tris, pH 7.2; 158 mM NaCl; 0.5 mM EDTA, pH 8.0; 1 % v/v Triton X-100; 1 % w/v deoxycholate

NP-40 lysis buffer (DeYoung et al., 2008):

0.75 % v/v IGEPAL® CA-630 in PBS; 1 mM DTT

SDS lysis buffer: 60 mM Tris, pH 7.4; 1 % w/v SDS

Triton lysis buffer: 20 mM Tris, pH 7.4; 100 mM NaCl; 1 mM EDTA; 1 % v/v Triton X-100

Buffers for SDS-polyacrylamide gel electrophoresis and gel staining solutions

Coomassie staining solution: 45 % v/v methanol; 10 % v/v acetic acid; 0.1 % w/v Coomassie brilliant blue

Destaining solution: 45 % v/v methanol; 10% v/v acetic acid

Running buffer: 25 mM Tris; 192 mM glycine; 0.1 % w/v SDS; pH 8.3

Sample buffer (5X): 250 mM Tris, pH 6.8 ; 50 % v/v glycerol; 10 % w/v SDS; 0.5 % w/v bromphenol blue; 4.77 M β-mercaptoethanol

Separation gel buffer: 1.5 M Tris; 0.4% w/v SDS; pH 8.8
Stacking gel buffer: 0.5 M Tris; 0.4 % w/v SDS; pH 6.8

Buffers for Western blotting

Blocking Buffer: 5% w/v non-fat milk powder or BSA in wash buffer
Stripping Buffer: 4 N NaOH
Transfer buffer: 20 mM Tris; 154 mM glycine; 20 % v/v methanol; 0.08 % w/v SDS; pH 8.3
Wash buffer (TBST): 20 mM Tris, pH 7.4; 137 mM NaCl; 0.1% v/v Tween
Alternative Wash Buffer (TBSTX): 20 mM Tris, pH 7.4; 137 mM NaCl; 0.1%v/v

Common Solutions

Phosphate buffered saline (PBS): 137 mM NaCl; 2.7 mM KCl; 4.3 mM Na₂HPO₄; 1.47 mM KH₂PO₄; pH 7.4
Tris buffered saline (TBS): 100 mM NaCl; 20 mM Tris; pH 7.4

Bacterial growth media

Luri-Bertani (LB) Media: 10 g/l NaCl; 10 g/l tryptone; 5 g/l yeast extract
LB^{Amp}, LB^{Kan}: 50-100 µg/ml Ampicillin or 50 µg/ml Kanamycin
LB agar plates: LB, 15 g/l agar
LB^{Amp}, LB^{Kan} agar plates: LB, 15 g/l agar, 50µg/ml Ampicillin or Kanamycin

All Media were autoclaved immediately after preparation and stored at RT until use. After addition of antibiotics, media were stored at 4 °C and used within 2 weeks.

3.1.3 Commercial kits, standards and ready-to-use solutions

Chemiluminescent HRP substrate	Millipore
DNA-ladder, 1 kb	New England Biolabs
Protein assay, detergent compatible (Dc)	Bio-Rad
Protein standards (Precision Plus, Kaleidoscope and all blue)	Bio-Rad
ProtoBlue TM safe colloidal Coomassie blue G-250 stain	National Diagnostics
ProtoGel® (30 % acrylamide-bisacrylamide stock solution, 37.5:1)	National Diagnostics
QIAGEN® plasmid maxi kit	Qiagen
QIAprep® spin miniprep kit	Qiagen
QIAquick® gel extraction kit	Qiagen
QIAquick® PCR purification kit	Qiagen
QuickChange® XL site-directed mutagenesis kit	Stratagene

3.1.4 Oligonucleotides

3.1.4.1 Oligonucleotides for mutagenesis

*All primers were synthesized and purified via polyacrylamide gel electrophoresis by Invitrogen. Primers marked with * were provided by colleagues in the Thomas Lab.*

K46AF(127-147)*	5'-gtg gcc gtc gct tgc att aac-3'
K46AR(147-127)*	5'-ggt aat gca agc gac ggc cac-3'
S248A(730-754)F	5'-ccc cgg gag aca gca gct ccc ctg c-3'
S248(754-730)R	5'-gca ggg gag ctg ctg tct ccc ggg g-3'
S467A(1386-1413)F	5'-ccg aag gtc agg ggc cac cag ccc cct g-3'
S467A(1413-1386)R	5'-cag ggg gct ggt ggc ccc tga cct tgc g-3'
S467D(1386-1413)F	5'-ccg aag gtc agg gga cac cag ccc cct g-3'
S467D(1413-1386)R	5'-cag ggg gct ggt gtc ccc tg cct tgc g-3'
S494A(1467-1493)F	5'-ggc cag gaa gct ggc act tgg agg tgg-3'
S494A(1493-1467)R	5'-cca cct cca agt gcc agc ttc ctg gcc-3'
S555A(1650-1677)F	5'-ctg ccg cct gca cgc tgc ccc taa cct g-3'
S555A(1677-1650)R	5'-cag gtt agg ggc agc gtg cag gcg gca g-3'
T574A(1707-1733)F	5'-gcc taa gcc ccc agc aga ccc act ggg-3'
T574A (1733-1707)R	5'-ccc agt ggg tct gct ggg ggc tta ggc-3'
S637A(1892-1928)F	5'-act tcc cca aaa ccc ccg cct ctc aga att tgc tga c-3'
S637A(1928-1892)R	5'-gtc agc aaa ttc tga gag gcg ggg gtt ttg ggg aag t-3'
T659A(1961-1989)F	5'-cac ctc gga acc gtg cac tgc ctg acc tc-3'
T659A(1989-1961)R	5'-gag gtc agg cag tgc acg gtt ccg agg tg-3'
S774D(2302-2340)F	5'-acc cgt acc aga atg ttc gat gtg ggc tct tcc agc tcc-3'
S774D(2340-2302)R	5'-gga gct gga aga gcc cac atc gaa cat tct ggt acg ggt-3'
S774A(2304-2336)F	5'-ccg tac cag aat gtt cgc agt ggg ctc ttc cag-3'
S774A(2336-2304)R	5'-ctg gaa gag ccc act gcg aac att ctg gta cgg-3'
S777D(2313-2346)F	5'-aat gtt ctc agt ggg cga ttc cag ctc cct ggg c-3'
S777D(2346-2313)R	5'-gcc cag gga gct gga atc gcc cac tga gaa cat t-3'
S777A(2315-2343)F	5'-tgt tct cag tgg gcg ctt cca gct ccc tg-3'
S777A(2343-2315)R	5'-cag gga gct gga agc gcc cac tga gaa ca-3'
S1043A(3114-3140)F	5'-tga gag gag act cgc ggc cct gct gag-3'
S1043A(3140-3114)R	5'-ctc agc agg gcc gcg agt ctc ctc tca-3'

3.1.4.2 Oligodesoxynucleotides for PCR

All Primers were ordered in desalted purity from Invitrogen.

Sin1FEcoR1	5'-ccg gaa ttc gcc ttc ttg gac aat cca ac-3'
Sin1RXhoI	5'-ata ctc gag cca gtg tca ctg ctg ccc tg-3'

3.1.4.3 Oligonucleotides for sequencing

All Primers were ordered in desalted purity from Invitrogen. Primers marked with * were provided by colleagues in the Thomas Lab.

M-Ulk1F(266-285)*	5'-acc tgg tca tgg agt att gt-3'
M-Ulk1R(297-274)*	5'-gtc tcc acc att aca ata ctc cat-3'
mu-ULK1 (425-444)F	5'-aaa aca tcc tgc tgt cca ac-3'
M-Ulk1R(832-813)*	5'- aga aag ggt ggt gga aaa at-3'
mmULK1(1041-1061)F	5'-cag caa aga ctc ctg tga cac-3'
mmULK1(1619-1640)F	5'-ctg agc act ctc caa gaa cca c-3'
M-Ulk1F(1876-1894)*	5'-gcc ggg ccc tcc ttt gac t-3'
mmULK1(2798-2824)F	5'-tga agc agg tgg tac gca gac taa atg-3'
M-Ulk1R(2475-2455)II*	5'-ggt cac agc ccc ctc caa gtt-3'
pcDNA3(772-789)F	5'-aaa tgg gcg gta ggc gtg-3'
pcDNA3(1073-1054)R	5'-aac aac aga tgg ctg gca ac-3'
Sin1(678-700)F	5'-tgt tgg cag tac acg agt gaa gg-3'
Sin1(947-923)R	5'-ggt gac ctt tgt gtt gtc tac ttg g-3'

3.1.5 Enzymes

AMPK, active, heterotrimeric. Partially purified from rat liver	Upstate/Millipore
Lysozyme	Sigma
<i>PfuUltra</i> TM high-fidelity DNA polymerase	Stratagene
Quick Ligation TM kit	New England Biolabs
Restriction enzymes (BamH1, EcoRI, HindIII, NcoI, NotI, Sall, SpeI, XbaI, XhoI)	New England Biolabs
Shrimp alkaline phosphatase	Affymetrix

3.1.6 Antibodies

Antibodies are listed as in the manufacturers' catalogs.

3.1.6.1 Primary antibodies

Name (clone)	Host	Catalog#, Manufacturer
α -14-3-3, pan Ab-4 (CG-15)	mouse	MS-1504-PABX, Thermo Fisher Scientific
α -14-3-3 (K-19), pan	rabbit	sc-629, Santa Cruz Biotechnology
α -Acetyl-CoA Carboxylase 1	mouse	#437100, Invitrogen
α -Acetyl-CoA Carboxylase (C83B10)	rabbit	#3676, Cell Signaling Technology
α - β -Actin (AC-15)	mouse	A1978, Sigma
α -AMPK α (23A3)	rabbit	#2603, Cell Signaling Technology
α -AMPK α (F6)	mouse	#2793, Cell Signaling Technology
α -AMPK α 1, rabbit monoclonal	rabbit	#04-323, Upstate/Millipore
α -AMPK α 2	rabbit	#2757, Cell Signaling Technology
α -AMPK α 2	rabbit	#07-363, Upstate/Millipore
α -AMPK β 1/2 (57C12)	rabbit	#4150, Cell Signaling Technology.
α -Atg1/ULK1	rabbit	A7481, Sigma
α -DDDDK-tag	rabbit	PM020, MBL
α -FLAG $\text{\textcircled{R}}$ -tag (M2)	mouse	F3165, Sigma
α -FLAG $\text{\textcircled{R}}$ M2 affinity gel	mouse	A2220, Sigma
α -GFP	mouse	#8362-1, Clontech
α -myc-tag (9E10)	mouse	Thomas Lab, BIDMC/Harvard Medical School, Boston, MA/USA
α -p62/SQSTM1	rabbit	P0067, Sigma
α -Phospho-Acetyl-CoA Carboxylase (Ser79)	rabbit	#3661, Cell Signaling Technology
α -Phospho-AMPK α (Thr172) (40H9)	rabbit	#2535, Cell Signaling Technology
α -Phospho-(Ser/Thr) PKD motif*	rabbit	#4381, Cell Signaling Technology
α -Raptor (24C12)	rabbit	#2280, Cell Signaling Technology
α -Sin1	rabbit	A300-910A, Bethyl Laboratories

* This antibody was used as an AMPK motif antibody since the motifs of both kinases are similar

3.1.6.2 Secondary antibodies and isotype controls

Name (clone)	Host	Catalog#, Manufacturer
α -Mouse-IgG (H+L) Alexa Flour 488-conjugate	goat	A11001, Invitrogen
α -Mouse-IgG (H+L) Alexa Flour 555-conjugate	goat	A21425, Invitrogen
α -Mouse-IgG (H+L) Alexa Flour 680 conjugate	goat	A21057, Invitrogen
α -Mouse-IgG (H&L), HRP conjugate	goat	172-1011, Bio-Rad
α -Rabbit-IgG (H+L) Alexa Flour 488-conjugate	goat	A11008, Molecular Probes
α -Rabbit-IgG (H+L) Alexa Flour 555-conjugate	goat	A21428, Invitrogen
α -Rabbit-IgG(H+L), HRP conjugate	goat	#7074, Cell Signaling Technology
α -Rabbit-IgG (H&L), IRDye $\text{\textcircled{R}}$ 800 conjugate	goat	#611-132-122, Rockland
Mouse IgG1 negative control	mouse	MABC002, Millipore
Rabbit anti-mouse-IgG (H+L)	rabbit	#315-005-045, Jackson Immunoresearch

3.1.7 Plasmids

3.1.7.1 Bacterial expression plasmids

pGEX-4T1: GE Healthcare; Amp^r

pGEX-4T1-14-3-3 zeta GST: pGEX-4T1-derived expression plasmid for *Bos taurus* 14-3-3 ζ fused to an N-terminal GST-tag (Yaffe et al., 1997); The plasmid was provided by Dr. Bin Zheng (Cantley laboratory, BIDMC/Harvard Medical School, Boston, MA/USA)

3.1.7.2 Mammalian expression plasmids

p3xFLAG-CMV-14: Sigma; Amp^r; Neo^r

p3xFLAG-CMV-14-ULK1: p3X-FLAG-CMV-14 with insertion of full length ULK1 from *mus musculus* (aa 1-1051) into the EcoRI-site of the multiple cloning site; plasmids for expression of the ULK1-truncation mutants listed below were generated analogously (Hosokawa et al., 2009a). All constructs were provided by Dr. Noboru Mizushima (Tokyo Medical and Dental University, Japan).

p3xFLAG-CMV-14-ULK1- Δ C: mmULK1(1-828), i.e. deletion of the C-terminal domain

p3xFLAG-CMV-14-ULK1- Δ K: mmULK1(279-1051), i.e. deletion of the kinase domain

p3xFLAG-CMV-14-ULK1-S: mmULK1(279-828), i.e. the spacer region only

p3xFLAG-CMV-14-ULK1-K: mmULK1(1-278), i.e. the kinase domain only

p3xFLAG-CMV-14-ULK1-C: mmULK1(829-1051), i.e. the C-terminal domain only

pcDNA3-FLAG: parental plasmid for N-terminally tagged FLAG-fusion proteins; the FLAG-sequence was inserted upstream of the BamHI-site in the multiple cloning site of pcDNA3.1 (Invitrogen); Amp^r; Neo^r. The plasmid was obtained from the Cantley lab.

pcDNA3-FLAG-AMPK α 1-wt: pcDNA3-FLAG with insertion of the human AMPK α 1 cDNA between the EcoRI- and XhoI-sites in the multiple cloning site. The plasmid was constructed by Dr. Reuben Shaw (Cantley lab) and provided by Dr. Bin Zheng.

pcDNA3-FLAG-AMPK α 1-kd: encodes kinase defective AMPK α 1 (K45R), derived from pcDNA3-FLAG-AMPK α 1-wt by site-directed mutagenesis. The plasmid was constructed by Dr. Reuben Shaw (Cantley lab) and provided by Dr. Bin Zheng.

pcDNA3-FLAG-AMPK α 1-ca: encodes constitutively active AMPK α 1 (T174E, truncated at aa 312, i.e. L313Stop-mutation), derived from pcDNA3-FLAG-AMPK α 1-wt by site-directed mutagenesis. The plasmid was constructed and provided by Dr. Bin Zheng.

pcDNA3-FLAG-mSIN1: expression construct for full-length murine mSIN1 fused to a N-terminal FLAG-tag. mSIN1 was amplified from an IMAGE cDNA-clone (ID: 30629263; Open Biosystems) using the primers Sin1FEcoR1 and Sin1RxhoI and the PCR-product was digested with EcoRI and XhoI and ligated to a pcDNA3-FLAG vector fragment cut with the same enzymes.

pcDNA3-myc-AMPK α 2-wt: Addgene plasmid 15991; rat AMPK α 2 fused to a N-terminal myc-tag and inserted into the EcoRI-site of pcDNA3 (Mu et al., 2001). The plasmid was provided by Dr. Bin Zheng.

pcDNA3-myc-AMPK α 2-kd: Addgene plasmid 15992; encodes kinase defective (K45R) AMPK α 2; derived from pcDNA3-myc-AMPK α 2-wt by site-directed mutagenesis (Mu et al., 2001). The plasmid was provided by Dr. Bin Zheng.

pCS2+MT: parental vector for N-terminally 6X myc-tagged fusion proteins; Amp^r; Neo^r; (Roth et al., 1991).

pEAK-FLAG-INPP4B: Addgene plasmid 24324; expression plasmid for full length human INPPB fused to N-terminal HA- and FLAG-tags; Amp^r, Puro^r. The plasmid was provided by Dr. Christina Gewinner (Cantley lab).

pEX-EF1-YFP-ULK2: ATCC #1037973; encodes N-terminally YFP-tagged murine ULK1; Kan^r, Neo^r

pDS-EF1-YFP-XB: ATCC #10326351; control vector for N-terminally YFP-tagged fusion proteins; Kan^r, Neo^r

3.1.7.3 Retro- and lentiviral expression vectors

pCX-myc-ULK1: encodes N-terminally 6X-myc-tagged murine ULK1; Amp^r; the construct was a gift from Dr. Mary Hatten, Rockefeller University, New York, NY/USA (Tomoda et al., 2004).

pLPCX: Clontech; Amp^r, Puro^r

pLPCX-mSIN1: contains the full length murine mSIN1-cDNA excised from the IMAGE clone (ID: 30629263; Open Biosystems) with EcoRI and NotI and ligated to a pLPCX vector-fragment obtained by digestion with the same enzymes.

Packaging plasmids to generate VSVG-pseudotyped retroviral particles (Bartz and Vodicka, 1997): pVSV-G; pCMV-Tat2; pJK3

3.1.8 Bacterial strains

E. coli B strain BL-21(DE3): F⁻ ompT gal dcm lon hsdSB(rB- mB-) λ(DE3 [lacI lacUV5-T7 gene 1 ind1 sam7 nin5]) (Studier and Moffatt, 1986)

E. coli K12 strain XL1-Blue: recA1 endA1 gyrA96 thi-1 hsdR17 supE44 relA1 lac [F' proAB lacIqZΔM15 Tn10 (Tetr)] (Bullock et al., 1987)

3.1.9 Mammalian cells

3.1.9.1 Cell lines

COS7: African green monkey kidney fibroblast cell line, derived from CV-1 cells by transformation with an origin-defective mutant of SV40 coding for wild-type large T antigen (Gluzman, 1981).

HEK293T: Human embryonic kidney cells of epithelial morphology, transformed by adenovirus 5 DNA and SV40 large T antigen (Graham et al., 1977).

3.1.9.2 Mouse embryonic fibroblasts

ampka1^{-/-}: Jorgensen et al., 2004b; referred to as α1-KO

ampka2^{-/-}: Viollet et al., 2003; referred to as α2-KO

ampka1^{-/-}; ampka2^{-/-}: Laderoute et al., 2006; referred to as DKO

pxl^{-/-}, myc-Pxl-infected: Hagel et al., 2002; MEFs carrying a deletion of the gene for the focal adhesion protein Paxillin (Pxl), infected with myc-Pxl-retrovirus (Thomas et al., 1999), referred to as Pxl-rescue MEFs

wt: wild type MEFs corresponding to the α 1-KO-, α 2-KO- and DKO-MEFs. All MEFs of this set (referred to as AMPK-MEFs) were provided by Dr. Bin Zheng (Cantley Lab) with permission of Dr. Benoit Viollet (INSERM U567; Paris, France)

3.1.10 Media and reagents for tissue culture

Calf serum	Atlanta Biologicals
Dulbecco's modification of Eagle's medium (DMEM), with 4.5 g/l glucose, L-glutamine and sodium pyruvate	Cellgro/Mediatech
Earle's balanced salt solution (EBSS)	Sigma
Fetal bovine serum	Atlanta Biologicals
Penicillin/Streptomycin	Gibco/Invitrogen
Trypsin-EDTA (0.25 %)	Gibco/Invitrogen

3.1.11 Consumables

6 well plates, tissue culture treated	Becton Dickinson Labware
12 well plates	Becton Dickinson Labware
12 well plates, tissue culture treated	Corning
96 well plates	Fisher Scientific
Conical tubes, 15 ml and 50 ml	Becton Dickinson Labware
Cell scrapers	Fisher Scientific, Sarstedt
Cryovials, 1.8 ml (for bacterial glycerol stocks)	Wheaton Scientific Products
Cryovials, 1.8 ml (for mammalian cells)	Nalge Nunc
Cover slips for microscopy	Fisher Scientific
Culture tubes, gamma irradiated, 14 ml	USA Scientific
Disposable cuvettes	Fisher Scientific
Petri dishes	Fisher Scientific
Pipet tips, standard and filtered, 2 μ l, 20 μ l, 200 μ l and 1000 μ l	Denville Scientific
Pipet tips for gel loading	Fisher Scientific
PVDF membrane, 0.45 μ m	Bio-Rad
PVDF membrane "Immobilon FL" for fluorescent immunodetection	Millipore
Microcentrifuge tubes, 1.7 ml and 2.0 ml	Denville Scientific
Round-bottom tubes, polystyrene, 14 ml	Becton Dickinson Labware
PCR reaction tubes	Fisher Scientific
Serological pipets, sterile, 5 ml and 10 ml	Becton Dickinson Labware

Serological pipets, sterile, 25 ml	Corning
Slides for microscopy	Fisher Scientific
Tissue culture dishes, 6 cm, 10 cm and 15 cm	Becton Dickinson Labware
Tissue culture dishes, 10 cm	Sarstedt
Vacuum filter systems, 150 ml	Corning
Vacuum filter systems, 150 ml	Millipore
Whatman paper	Fisher Scientific
X-ray film <i>Hyblot CLTM</i>	Denville Scientific
3.1.12 Equipment	
Agarose gel electrophoresis system	Owl Separation Systems
Automated cell counter <i>Cellometer[®] Auto T4</i>	Nexcelcom Bioscience
CO ₂ Incubators for tissue culture	Thermo Fisher Scientific
Centrifuge <i>Avanti[®] J-E</i>	Beckman Instruments
Fluorescence Microscope <i>AxioVert 200M</i> including CCD camera <i>AxioCam HRm</i>	Carl Zeiss
Gel documentation system <i>Gel DocTM 1000</i>	Bio-Rad
Heat block	Thermo Fisher Scientific
Hemocytometer	Hausser Scientific
Incubator	Boekel Scientific
Incubator shaker	New Brunswick
Infrared imaging system <i>Odyssey[®]</i>	LI-COR [®] Biosciences
Inverted microscope <i>Eclipse TS100</i> and digital camera <i>SPOTTM RT-KE</i>	Nikon, SPOT Imaging Solutions/Diagnostic Instruments
Magnetic stirrers	Corning
Microcentrifuges	Denville Scientific, Eppendorf, Heraeus
Microplate reader <i>Victor-3</i>	Perkin Elmer
Oak Ridge centrifuge tubes, 50 ml	Nalge Nunc
pH meter	Corning
Pipets	Gilson, Denville Scientific
Power supply units	Bio-Rad
Rotator	Labindustries
Scanner <i>hp Scanjet 3770</i>	Hewlett-Packard
SDS-Polyacrylamide gel electrophoresis system	C.B.S. Scientific
Shakers (orbital and rocking)	Bellco Glass, Reliable Scientific, Thermo Fisher Scientific

Spectrophotometer <i>DU® 800</i>	Beckman Instruments
Table top centrifuge <i>Allegra™ 6R</i>	Beckman Instruments
Tank blotting system	Hoefler
Thermal cycler <i>MyCycler™</i>	Bio-Rad
Vortex mixer	Thermo Fisher Scientific
Water baths	Polyscience, Thermo Fisher Scientific
X-ray film processor <i>X-omat 2000A</i>	Eastman Kodak

3.1.13 Computer programs and data bases

4Peaks, 2006	A. Griekspoor and Tom Groothuis, mekentosj.com.
Adobe Photoshop 5.0.2	Adobe Systems
<i>AxioVision</i> digital imaging software	Carl Zeiss
BLAST	http://blast.ncbi.nlm.nih.gov
Entrez Gene	http://www.ncbi.nlm.nih.gov/sites/entrez
GraphPad Prism®, Version 5.00	GraphPad Software
ImageJ	http://rsb.info.nih.gov/ij .
Lasergene® Software, 5th ed; 10/2006	DNASTAR
Mouse Genome Informatics (MGI)	http://www.informatics.jax.org/mgi_home/homepages
Odyssey® Application Software v3	LI-COR® Biosciences
Phosphosite	http://www.phosphosite.org
QuickChange® Primer Design Program	http://www.stratagene.com/sdmdesigner/default.aspx
<i>Saccharomyces cerevisiae</i> phosphorylome database	http://networks.gersteinlab.org/phosphorylome
Saccharomyces Genome Database (SGD™)	http://www.yeastgenome.org
Scansite (Obenauer et al., 2003)	http://scansite.mit.edu
SPOT™ imaging software version 4.0.4	Diagnostic Instruments
Swissprot/Uniprot	http://ca.expasy.org

3.1.14 List of manufacturers

Adobe Systems Inc., San José, CA/USA
Affymetrix Inc., Santa Clara, CA/USA
Albertsons, Inc., Boise, ID
American Pharmaceutical Partners Inc,
Schaumburg, IL/USA
Atlanta Biologicals, Lawrenceville,
GA/USA
Beckman Instruments, Inc., Fullerton,
CA/USA
Becton Dickinson Labware, Franklin
Lakes, NJ/USA
Bellco Glass Inc., Vineland, NJ/USA
Bethyl Laboratories, Inc, Montgomery,
TX/USA
Bio-Rad Laboratories, Hercules, CA/USA
Boekel Scientific, Feasterville, PA/USA
C.B.S. Scientific Co., Del Mar, CA/USA
Calbiochem/EMD Biosciences, Inc., La
Jolla, CA/USA
Carl Zeiss Jena GmbH, Jena, Germany
Cell Signaling Technology, Inc., Danvers,
MA/USA
Cellgro/Mediatech, Inc., Manassas,
VA/USA
Clontech Laboratories, Inc., Mountain
View, CA/USA
Corning, Inc., Corning, NY/USA
Denville Scientific, Inc., South Plainfield,
NJ/USA
Diagnostic Instruments, Inc., Sterling
Heights, MI
DNASTAR Inc., Madison, WI/USA
Eastman Kodak Co., Rochester, NY/USA
EM Science, Cherry Hill, NJ/USA
Eppendorf, Hamburg/Germany
Fisher Scientific, Fair Lawn, NJ/USA
GE Healthcare Bi-Sciences AB, Uppsala,
Sweden
Gilson Inc., Middleton, WI/USA
GraphPad Software, Inc., San Diego,
CA/USA
Hausser Scientific, Horsham, PA/USA
Heraeus Instruments, Hanau, Germany
Hewlett-Packard, Wilmington, DE/USA
Hofer, Inc., Holliston, MA/USA
Invitrogen Corp., Carlsbad, CA/USA
Jackson Immunoresearch Laboratories,
Inc., West Grove, PA/USA
Labindustries, Inc., Berkeley, CA/USA
LI-COR® Biosciences, Lincoln, NR/USA
MBL Medical & Biological Laboratories
Co., Ltd, Nagoya, Japan
Millipore Corp., Billerica, MA/USA
Nalge Nunc International Co., Rochester,
NY/USA
National Diagnostics, Inc., Atlanta,
GA/USA
New Brunswick Scientific, Edison,
NJ/USA
New England Biolabs, Inc., Ipswich,
MA/USA
Nexcelcom Bioscience, Lawrence,
MA/USA
Nikon Inc., Melville, NY/USA
Nuaire, Inc., Plymouth, MN/USA
Open Biosystems, Huntsville, AL/USA
Owl Separation Systems Inc., Portsmouth,
NH/USA
Perkin Elmer, Inc., Waltham, MA/USA
Pharmco Products, Inc., Brookfield,
CT/USA
Polyscience, Niles, IL/USA
Thermo Fisher Scientific
Polysciences, Inc., Warrington, PA/USA
Qiagen GmbH, Hilden/Germany
Reliable Scientific, Nesbit, MS
Thermo Fisher Scientific
Repligen Corp., Waltham, MA/USA
Roche Diagnostics Corp., Indianapolis,
IN/USA
Rockland, Inc., Gilbertsville, PA/USA
Santa Cruz Biotechnology, Inc., Santa
Cruz, CA/USA
Sarstedt, Inc., Newton, NC/USA
Sigma-Aldrich, Inc., St. Louis, MO/USA
Stratagene, La Jolla, CA/USA
Thermo Fisher Scientific, Anatomical
Pathology, Fremont, CA/USA
Thermo Fisher Scientific, Waltham,
MA/USA
Tocris Bioscience, Ellisville, MO/USA
Toronto Research Chemicals, North York,
ON/Canada
Upstate/Millipore Corp., Temecula,
CA/USA
USA Scientific, Enfield, CT/USA
Wheaton Scientific Products, Millville,
NJ/USA

3.2 Methods

3.2.1 Biological and radiation safety

Laboratory work, including work with mammalian cells, recombinant retroviruses and radioactive substances was performed according to the organizational standards at Harvard Medical School and Beth Israel Deaconess Medical Center (BIDMC) as communicated by these institutions' Environmental Health and Safety offices; guidelines for biological safety, chemical handling, -hygiene, -transport and -storage, exposure control, fire safety, radiation safety, radioactive materials handling, -storage and -disposal, safety equipment and procedures, waste management and disposal including biological waste comply with requirements and regulations set by the Occupational Safety and Health Administration (OSHA) Lab Standard (29CFR 1910.1450) and of other federal, state and local agencies, including the National Institutes of Health (NIH), National Institute of Occupational Safety and Health (NIOSH), Center for Disease Control (CDC), Environmental Protection Agency (EPA), Commonwealth of Massachusetts Radiation Control Program (RCP), Massachusetts Departments of Environmental Protection (DEP) and Fire Services, Massachusetts Water Resource Authority and City of Boston Department of Health and Hospitals.

3.2.2 Cell biological methods

3.2.2.1 Culturing and passaging of cells

All work on living cells was performed in class II, type 2A or type 2B biological safety cabinets (Thermo Fisher Scientific, Nuaire) in a separate tissue culture room (biosafety level 2+) using sterile single-use materials or materials sterilized by autoclaving. All cells were grown in cell culture dishes at 37 °C and 10 % CO₂. The culture media was DMEM containing 100 U/ml Penicillin/Streptomycin and supplemented with 10 % heat inactivated fetal bovine serum in case of COS7-cells, HEK293T-cells and AMPK-MEFs and with 15 % heat inactivated calf serum in case of Pxl-rescue MEFs. When confluent, cells were washed once with PBS, trypsinized, resuspended in media and the desired fraction of the cell suspension was transferred to new dishes containing fresh culture media. When desired, cells were counted prior to plating using a hemacytometer or an automated cell counter.

3.2.2.2 Freezing and thawing of cells

For long-term storage, cells were grown to confluency on 10 cm-dishes, trypsinized and resuspended, transferred to a 15 ml conical tube and centrifuged at 1,500 rpm, 4 °C for 5 min. The cell pellet was resuspended in 3-5 ml of freeze media (growth media containing 10 % DMSO) and the cell suspension was distributed to cryovials in 1 ml aliquots and immediately frozen at -80 °C and 24 h later transferred to liquid nitrogen.

To thaw cells, the cryovial was placed into a 37 °C water bath until the content was completely thawed. Then, the cell suspension was transferred to a 15 ml conical tube containing 10 ml of serum free media and centrifuged at 1,500 rpm, 4 °C for 5 min. Cells were resuspended in 10 ml growth media and plated on a 10 cm dish. In case of COS7- and HEK293T-cells, the cell suspension from the cryovial was directly transferred to a 10 cm tissue culture dish containing 10 ml of growth media and the media was changed after 8-16 h.

3.2.2.3 Transfections

HEK293T- and COS7-cells were transfected using PEI (polyethyleneimine, 1 µg/µl in H₂O, pH 7.2). Cells were plated 24 h in advance to achieve 70–80 % confluency by the time of transfection. For cells grown on 10 cm dishes, a transfection mix was prepared by diluting 5–10 µg DNA in 500 µl serum free media (2–4 µg DNA in 200 µl serum free media in case of 6-well plates), adding the appropriate amount of PEI (see below), vortexing immediately for 20 sec and incubating at room temperature (RT) for 20 min. In the meantime, cells were washed 3 x with PBS and changed to 7 ml (2 ml for 6-well plates) fresh growth media. After completion of incubation, the transfection mix was distributed drop wise and evenly over the cells and mixed with the media by gently swirling the plate. 16 h post transfection, cells were changed to fresh media, cultured for an additional 24 h and then subjected to treatment and lysis. The PEI:DNA-ratios used for transfection of particular cell lines were:

COS7 PEI:DNA = 5:1

HEK293T PEI:DNA = 3:1

3.2.2.4 Production of recombinant retrovirus

Recombinant retrovirus for stable expression of a target protein in infected mammalian cells was produced by cotransfecting HEK293T-cells with the appropriate retroviral plasmid and a set of three packaging plasmids, pJK3, pVSV-G and pCMV-TAT2. Cells were plated on 10 cm tissue culture dishes to achieve 60 % confluency by the time of transfection and a transfection mix was prepared as described above, consisting of 10 µg target DNA, 4 µg of each of the three packaging plasmids and 800 µl of serum free media. Cells were washed 3 x with PBS before addition of the transfection mix. Media was replaced by 7 ml of fresh media 16 h and 24 h post transfection. 40 h, 48 h and 72 h post transfection, virus-containing supernatant was collected from the culture and 7 ml of fresh media were added back to the cells. Supernatants of all three collections were pooled, centrifuged at 2000 rpm and 4 °C for 10 min and frozen at –80 °C in 1 ml aliquots.

3.2.2.5 Retroviral infections

For infections with recombinant retroviruses, cells were plated on 6-well plates at 10–30 % confluency 12-16 h prior to infection. Then, the media was replaced by 2 ml of viral supernatant supplemented with 8 µg/ml polybrene. After 24 h of incubation, the virus was removed and cells were cultured in regular growth media.

3.2.2.6 Treatments

Cells were subjected to various treatments to induce autophagy or to activate AMPK. In time course experiments where treatment duration varied between culture dishes, treatment was started staggered and cells of all dishes were lysed at the same time. For induction of autophagy with EBSS, cells were washed twice with PBS before adding fresh culture media (“0 h EBSS”) or EBSS. In long-term starvation experiments for 48 h, all cells were changed to fresh media or fresh EBSS 12 h before lysis. When treating with 2-Deoxyglucose, A-769662, AICAR or Phenformin, cells were changed to fresh media 2 h before addition of the compound to the dish of cells designated for the longest treatment. The following stock solutions of these substances were used:

2-Deoxyglucose	1	M	in sterile H ₂ O
A-769662	100	mM	in DMSO
AICAR	100	mM	in sterile H ₂ O
Phenformin	400	mM	in sterile H ₂ O

3.2.3 Molecular biological methods

3.2.3.1 Culturing of *E. coli*-strains

Liquid cultures of bacteria were grown in LB media supplied with 50-100 µg/ml of the appropriate antibiotic (Ampicillin or Kanamycin) at 37 °C, 225 rpm for 12-16 h. Small cultures (2-4 ml in sterile disposable 15 ml culture tubes) were directly inoculated with a single colony picked from a selection plate or from the glycerol stock. For large cultures (400 ml in 2 l sterile Erlenmeyer flasks), 2 ml starter cultures were inoculated first and grown for 8-16 h and then diluted 1/200 – 1/1000 with the appropriate selection media.

3.2.3.2 Cryoconservation of bacteria

For long-term storage of bacteria, 800 µl of a 3 ml over night culture were mixed with 200 µl 80 % glycerol under sterile conditions and glycerol stocks were frozen in cryotubes at -80 °C.

3.2.3.3 Transformation of *E. coli* with plasmid DNA

Chemically competent *E. coli* XL1-Blue cells (available in the Thomas lab) were thawed on ice and 50 µl of the bacterial suspension was transferred to a pre-chilled polypropylene round

bottom tube that already contained the desired amount of plasmid DNA for transformation. Bacterial cells and DNA were mixed by gentle stirring, incubated on ice for 30 min and subjected to a heat shock at 42 °C for 45 sec. After cooling on ice for 2 min, 500 µl of LB media (preheated to 42 °C) were added and bacteria were grown at 37 °C, 225 rpm for 1 h. 250 µl of transformed cells were plated on LB agar plates containing the appropriate selection antibiotic, and plates were incubated at 37 °C for 16 h. Transformation efficiency was assessed by counting colonies on the plates. Plates were stored at 4 °C and used for inoculation of liquid cultures for a maximum of two weeks.

3.2.3.4 Isolation of double-stranded plasmid DNA from *E. coli* (mini- and maxiprep)

Plasmid DNA was isolated from *E. coli* using the QIAprep[®] spin miniprep- and Qiagen[®] plasmid maxi kits according to the manufacturer's instructions. Minipreps were performed from 3 ml liquid cultures and elution was done with 30 µl of injection quality H₂O. The culture volume for maxipreps was 400 ml and the resuspension volume 50-250 µl of injection quality H₂O, depending on the size of the DNA pellet. DNA yield and quality were determined spectrophotometrically by reading absorptions at 260 and 280 nm. Plasmid DNA was stored at -20 °C.

3.2.3.5 DNA amplification by polymerase chain reaction (PCR)

Polymerase chain reaction was used to selectively amplify defined DNA sequences and to add restriction sites to fragments for cloning into plasmid vectors. Reaction mixes were prepared in thin walled 8-strip PCR tubes, overlaid with 40 µl PCR oil and subjected to thermal cycling as specified in table 3.1.

Table 3.1. Assay composition and cycling parameters for PCR amplification of DNA fragments. Sequences of primers are given in section 3.1.4.2.

assay composition		cycling parameters		
Component	V [µl]	Step	Temperature - Time	Cycles
10X reaction buffer	5	Initialization	95 °C - 2 min	1
dNTPs, 25 mM each	0.5	Denaturation	95 °C - 30 sec	25
Primer F, 10 mM	2	Annealing	55 °C - 30 sec	
Primer R, 10 mM	2	Elongation	72 °C - 1 min/kb	
DNA (~ 10 ng/µl)	10	Final extension	72 °C - 5 min	1
Sterile H ₂ O	29.5			
<i>PfuUltra</i> (2.5 U/µl)	1			
Total	50			

3.2.3.6 Analytical agarose gel electrophoresis

To separate DNA fragments according to size, samples were subjected to electrophoresis on 0.8 or 1 % agarose gels, depending on the length of the fragments of interest. Gels contained 1/100,000 volume of a 10 mg/ml Ethidium bromide solution to stain DNA. Prior to loading, samples were mixed with 1/5 volume of 6X loading dye. Gels were run at 50-100 V, depending on their size, until the dye front had migrated about $\frac{3}{4}$ of the gel length. DNA fragments were visualized under 312 nm UV light. Preparative gels were poured using low melting point agarose, run at 10 V for 12-16 h and analyzed under 365 nm UV light to prevent damage to the DNA.

3.2.3.7 Gel purification of DNA

DNA products of PCR reactions or restriction digests were purified from primers, nucleotides, polymerases and salts and from salts and restriction endonucleases, respectively, directly after the reaction using the QIAquick® PCR purification kit (Qiagen) according to the manufacturers protocol. The final elution was performed with 30 µl injection quality H₂O.

To purify vector fragments after restriction digest from enzymes and salts as well as from uncut DNA, the entire 50 µl reaction assay was subjected to preparative agarose gel electrophoresis and the piece of gel containing the fragment of interest was excised under 365 nm UV light. DNA was isolated from the gel with the QIAquick® gel extraction kit as recommended in the instruction manual. The volume of injection quality H₂O for the final elution was 30 µl.

3.2.3.8 Site-directed mutagenesis of DNA

In order to generate targeted single amino acid substitutions in proteins, site-directed mutagenesis of the encoding gene was performed using the QuickChange® XL Site-directed mutagenesis kit (Stratagene) with some modifications of the recommended protocol. Double-stranded plasmid DNA to be mutated was isolated from *E. coli* XL1-blue as described in section 3.2.3.4. A pair of mutagenic primers hybridizing to the target sequence on opposite strands of the template was designed as outlined in section 3.2.5.1.

For synthesis of the mutant strand, 50 µl reaction mixes were prepared on ice in 8-strip PCR tubes according to table 3.2. Then, 2.5 U (1 µl) of *PfuUltra*TM DNA polymerase were added to each tube and the reaction mixes were immediately overlaid with 40 µl PCR oil, placed in the thermal cycler and subjected to temperature cycling as outlined in table 3.2.

Table 3.2. Assay composition and cycling parameters for site directed mutagenesis/synthesis of the mutant strand. Primers used for generation of the various mutants are listed in section 3.1.4.1.

assay composition		cycling parameters		
Component	V [μ l]	Step	Temperature - Time	Cycles
10X reaction buffer	5	Initialization	95 °C - 1 min	1
dNTP mix	1	Denaturation	95 °C - 50 sec	18
QuikSolution	3	Annealing	55 °C - 50 sec	
Primer F, 125 ng	1.25	Elongation	68 °C - 10 min	
Primer R, 125 ng	1.25	Final extension	68 °C - 7 min	1
dsDNA template	50 ng			
<i>PfuUltra</i> (2.5 U/ μ l)	1			
ddH ₂ O [μ l]	to 50 μ l			

After temperature cycling, and cooling to 37 °C, the mineral oil overlay was removed and 10 U (1 μ l) of DpnI restriction enzyme for digestion of methylated, non-mutated template DNA was added to each tube, mixed with the reaction solution and incubated at 37 °C for 2 h. Subsequently, 5 μ l of the DpnI-treated synthesis product were used for transformation of *E. coli* XL1-Blue competent cells (section 3.2.3.3). The entire transformation reaction was plated on two selection plates and colonies were counted after 16 h of incubation at 37 °C. Finally, several colonies per plate were picked, transferred to 3 ml LB^{Amp} (100 μ g/ml) media and cultured for miniprep. Isolated plasmid DNA was analyzed by restriction digest and –if the correct pattern was obtained– sequenced to verify successful mutagenesis.

3.2.3.9 Restriction digest of DNA

Restriction digests of DNA, including double digests with two different restriction enzymes (RE) in parallel, were performed for analytical and preparative purposes under the buffer and temperature conditions recommended by the enzyme manufacturer. Reaction time was 2 h. For analytical scale digests, 2 μ l of plasmid DNA isolated by miniprep were treated with 0.25-0.5 μ l, corresponding to 5-10 U, of each restriction endonuclease. The total reaction volume was 25 μ l. For analyzing the digest products, 12.5 μ l of the reaction assay were subjected to agarose gel electrophoresis. For preparative digests, 1 μ l, i.e. 10-20 U, of each restriction enzyme in an overall reaction volume of 50 μ l was used. The amount of DNA to be digested was either 5 μ g of vector DNA or an entire purified PCR reaction.

Routinely performed restriction digests included:

<i>Plasmid</i>	<i>RE 1</i>	<i>RE 2</i>	<i>Buffer</i>
p3xFLAG-CMV-14	SpeI	XbaI	NEB2+BSA
p3xFLAG-CMV-14-ULK1-variants	EcoRI	- - -	NEB2
pCS2+MT	BamHI	Sall	NEB3+BSA
pCX-myc-ULK1 wild type and mutants	EcoRI	HindIII	NEB2
pcDNA3-FLAG	BamHI	BglII	NEB3+BSA
pcDNA3-FLAG-AMPK α 1-variants	EcoRI	XhoI	NEB2+BSA
pcDNA3-FLAG-mSIN1	EcoRI	XhoI	NEB2+BSA
pcDNA3-myc-AMPK α 2-variants	EcoRI	- - -	NEB2
pDS-EF1-YFP-XB	NcoI	- - -	NEB3
pEAK-FLAG-INPP4B	NotI	- - -	NEB3+BSA
pEX-EF1-YFP-ULK2	NcoI	- - -	NEB3
pLPCX	EcoRI	HindIII	NEB2
pLPCX-mSIN1	EcoRI	NotI	NEB3+BSA

3.2.3.10 Ligation of DNA-fragments

Following restriction digest and purification, DNA fragments with compatible ends were ligated by Quick T4 DNA ligase (New England Biolabs) according to the recommended protocol. To determine background from uncut vector, a control reaction was set up containing only the vector fragment without insert DNA. After the ligation reaction, 5 μ l of sample and control were directly transformed into competent *E. coli* XL1-Blue cells (section 3.2.3.3). The entire transformation reactions, i.e. 2 x 250 μ l, were plated on selection media and incubated at 37 °C for 16 h.

3.2.3.11 Sequencing of DNA

To verify the correct sequence of a mutated plasmid, DNA sequencing was performed at the BIDMC DNA sequencing core on an ABI Prism 377XL automated DNA sequencer. Samples for sequencing contained 800-1500 ng of plasmid DNA, isolated by miniprep (section 3.2.3.4) and 3.2–5 pmoles of the sequencing primer in sterile H₂O in a total volume of 12 μ l.

3.2.3.12 Production of recombinant proteins in *E. coli*

Recombinant GST-14-3-3 fusion protein for pulldown experiments and a control protein comprising only the GST-tag were produced in *E. coli* BL21 transformed with the appropriate plasmid. 1 l liquid cultures in LB^{AMP}-media were inoculated from 2 ml over night starter cultures, evenly distributed to two 2 l Erlenmeyer flasks and grown at 37 °C, 225 rpm until OD₆₀₀ ~1. Then, expression of the GST fusion protein was induced by addition of 100 μ l of a 1 M IPTG stock solution to each flask to achieve a final IPTG concentration of 0.2 mM.

Bacteria were cultured for an additional 5 h at 30 °C, 225 rpm, harvested by centrifugation at 6,000 rpm, 4 °C, 15 min, and either frozen at -80 °C or lysed immediately.

Bacterial pellets from the same 1 l culture were combined by resuspension in 40 ml cold, sterile PBS containing 1 mM PMSF and, after adjusting the final volume to 50 ml, the bacterial suspension was equally redistributed to two 50 ml conical tubes. After incubation on ice for 5 min, 125 µl of 100 mg/ml lysozyme were added, mixed with the bacterial suspension and incubated on ice for 5 min. Then, 62.5 µl of 1 M DTT per tube were added and incubation was continued for an additional 5 min. Subsequently, cells were sonicated at 4 °C for 3 x 30 sec, with 30 sec of cooling on ice between the sonication steps. Lysates in each tube were mixed with 1.25 ml of a 20 % Triton-X100 solution in PBS, incubated under rotation at 4 °C for 30 min, transferred to oak ridge tubes and centrifuged at 14,000 rpm and 4 °C for 20 min. Supernatants were pooled in one 50 ml conical tube and incubated with 900 µl of washed glutathione sepharose beads over night at 4 °C under rotation. The next day, beads were precipitated by centrifugation, resuspended in 5 ml sterile PBS containing 1 mM PMSF and transferred to a 15 ml conical tube. Beads were washed 3 x by resuspension in 10 ml of PBS+PMSF, rotation at 4 °C for 20 min and centrifugation at 1,500 rpm, 4 °C for 5 min. One additional brief wash was performed with 5 ml 0.1 % Triton in TBST. Then, beads were resuspended in 3 ml sterile PBS+PMSF, equally distributed to three 1.7 ml microcentrifuge tubes, washed 2 x with 1 ml sterile PBS+PMSF and finally resuspended in 300 µl sterile PBS+PMSF, yielding a 50 % slurry. Beads were stored at 4 °C and used for experiments within two months of preparation. To quantify the amount of GST-14-3-3 and GST bound to beads, dilution series of the slurries and of a BSA standard solution were subjected to SDS-PAGE and the coomassie-stained gel was scanned on the LI-COR® Odyssey® system.

3.2.4 Biochemical methods

3.2.4.1 Preparation of total cell lysates under denaturing conditions

For preparation of total cell lysates under denaturing conditions, cells grown on 6-well plates were washed twice with ice cold PBS and covered with 50–150 µl of SDS lysis buffer (section 3.1.2), depending on confluency. Then, cells were further processed at RT and scraped off the growth surface with a cell scraper. The viscous lysates were transferred to 1.7 ml microcentrifuge tubes, vortexed, boiled at 95 °C for 15 min and centrifuged at 13,000 rpm for 15 min. Cleared lysates were transferred to fresh microcentrifuge tubes and quantitated. (Cf. also section 3.2.4.3.1 for critical parameters when lysing cells for subsequent analysis of AMPK-phosphorylation)

3.2.4.2 Protein quantitation

Protein concentration in total cell lysates was determined using a commercial detergent compatible (Dc) protein assay kit (Bio-Rad). Absorptions were read either at 750 nm in disposable plastic cuvettes in a spectrophotometer or at 630 nm in 96-well plates in a microplate reader.

3.2.4.3 Immuno- and co-immunoprecipitation experiments

Immunoprecipitation (IP) protocols varied with target protein, antibodies and purpose of the experiment. In general, cells from one confluent 10 cm tissue culture dish were used per IP. Lysates of cells of the same cell type that had been treated identically were pooled at the lysis step and divided again into the desired number of samples (usually one specific IP and one control-IP) after quantitation. protein A-, protein G- or antibody-bead-conjugates used to precipitate immune complexes were blocked with 0.1 % BSA in lysis buffer for at least 30 min before addition to the lysates. The following buffers were used to wash IP-reactions:

- High salt buffer: 10 mM Tris, pH 7.4; 500 mM NaCl
- Low salt buffer: 10 mM Tris, pH 7.4; 100 mM NaCl

3.2.4.3.1 Lysis of cells for immuno- and co-immunoprecipitation experiments

After treatment, cells were washed twice with ice cold PBS or HBSS, covered with lysis buffer, scraped off the growth surface and transferred to 1.7 ml microcentrifuge. The lysis buffers used were (cf. section 3.1.2):

- for general IP-experiments: modified RIPA
- for-co-IP-experiments: Triton lysis buffer or CHAPS lysis buffer A (primary target: affinity-tagged and endogenous AMPK α 1/ α 2, FLAG-INPP4B, FLAG-mSIN1) or CHAPS lysis buffer B (primary target: affinity-tagged and endogenous AMPK α 1/ α 2, Raptor, tagged ULK1) or
- for 14-3-3-co-IP experiments: NP-40 lysis buffer.

All lysis buffers were supplemented with protease- and phosphatase inhibitors immediately before use (section 3.1.2). If pooling of lysates was not required, the volume of lysis buffer was 1 ml per 10 cm dish and 1.5 ml per 15 cm dish. Lysates were incubated on a rocker at 4 °C for 15 min and centrifuged at 14,000 rpm, 4 °C for 15 min. To reduce non-specific binding in experiments in which protein A-agarose beads were used, 50 μ l of washed Pansorbin® cells were added to each tube (80 μ l in case of pooled lysates), incubated with the lysate at 4 °C under rotation for 15 min and removed again by centrifugation at 14.000 rpm and 4 °C for 2 min. After a second preclearing step with Pansorbin®, lysates were transferred to fresh 1.7 ml microcentrifuge tubes and quantitated using the Bio-Rad D_C protein assay.

It should be noted that in the course of the project, we found it critical to perform the cell lysis procedure extremely quickly and on ice in order to maintain a low level of AMPK-phosphorylation in untreated cells. Therefore, in experiments where AMPK-phosphorylation was to be analyzed, cells were grown on dishes no greater than 10 cm, and no more than two dishes (or one 6well plate, cf. section 3.2.4.1) were processed in parallel (i.e. washed 2 x with PBS/HBSS and covered with lysis buffer).

3.2.4.3.2 Immunoprecipitation of myc-tagged proteins

Myc-tagged proteins were immunoprecipitated using the α -myc-tag antibody 9E10. A non-specific mouse antibody of the same isotype, IgG1, raised against chicken IgG, served as a negative control. Lysates were incubated with 2 μ g of antibody on a rocker for 2 h at 4 °C. Then, samples were transferred to fresh 1.7 ml microcentrifuge tubes containing 15 μ l of blocked protein G-beads or of protein A-beads precoupled to 4 μ l rabbit anti-mouse-antibody and rocking was continued for 45 min. Subsequently, precipitates were washed 4 x with 1 ml lysis buffer and 1 x with 1 ml low salt buffer. When CHAPS-lysis buffer had been used, the low salt wash was replaced by a fifth wash with lysis buffer. Finally, immune complexes were eluted from the beads with 3X SDS-sample buffer, boiled at 95 °C for 10 min and centrifuged at 13,000 rpm for 2 min before loading the supernatants on a SDS-PAGE gel (section 3.2.4.7).

3.2.4.3.3 Immunoprecipitation of FLAG-tagged proteins

N- or C-terminally FLAG affinity tagged proteins were immunoprecipitated using α -FLAG M2 affinity gel. Lysates were incubated with 15 μ l blocked affinity gel for 2 h 45 min (45 min for IP of ULK1-FLAG proteins) at 4 °C on a rocker. Control-IP with non-specific mouse IgG1, washing, elution and SDS-PAGE were performed as described in section 3.2.4.3.2.

For immunoprecipitation of FLAG-INPP4B and FLAG-mSIN1, a different protocol was followed (Dr. Christina Gewinner, laboratory of Dr. Lewis Cantley): Lysates were incubated with 15 μ l α -FLAG M2 affinity gel for 30 min under rotation at 4 °C and washed 4 x with lysis buffer and once with low salt buffer by resuspension in the buffer, short vortexing, and rocking at 4 °C for 10 min. Subsequent steps were carried out as described above. In some experiments, FLAG-INPP4B was eluted from the affinity gel by resuspension in 100 μ l FLAG-elution buffer (50 mM Tris, pH 7.4; 150 mM NaCl, 300 ng/ μ l 3X FLAG-peptide) and incubation on a rocker for 1 h at RT.

3.2.4.3.4 Immunoprecipitation of exogenous mSIN1

Untagged exogenous mSIN1 encoded by the pLPCX-mSIN1-plasmid was immunoprecipitated from cell lysates by incubation with 2 μ l rabbit α -SIN1-antibody for 90 min at 4 °C

followed by incubation with 15 μ l blocked protein A-agarose for 30 min at 4 °C. Control-IP, washing and SDS-PAGE were performed as described in section 3.2.4.3.5.

3.2.4.3.5 Immunoprecipitation of endogenous AMPK α

Endogenous AMPK α 1 or α 2 were immunoprecipitated using isoform-specific mono (mAb)- and polyclonal rabbit-antibodies (pAb) respectively. Polyclonal rabbit antibodies against mouse-IgG (Rabbit-anti-mouse, R α M) were used as a negative control. Lysates were incubated with antibody (α -AMPK α 1 mAb: 1:50; α -AMPK α 2 pAb: 5 μ g, R α M: 5 μ g) for 12–16 h under rotation at 4 °C before addition to 15 μ l of blocked protein A-beads. Rocking was continued for 1.5–3 h, and precipitates were washed, eluted and analyzed by SDS-PAGE as outlined in section 3.4.3.2.

3.2.4.3.6 Immunoprecipitation of endogenous 14-3-3

Immunoprecipitation of endogenous 14-3-3 was performed as described (DeYoung et al., 2008). Cell lysates prepared with NP-40 lysis buffer were incubated with 2 μ g α -pan-14-3-3-antibody on a rocker for 2 h at 4 °C. Then, 15 μ l of blocked protein G-sepharose beads were added and rocking was continued for 45 min. A control IP with non-specific mouse IgG1 was performed analogously. Beads were washed 4 x with lysis buffer and elution and SDS-PAGE were performed as in section 3.2.4.3.2.

3.2.4.3.7 Immunoprecipitation and coimmunoprecipitation of endogenous Raptor

Immunoprecipitation of endogenous Raptor-protein with a Raptor-specific rabbit antibody, and coprecipitations of Raptor with myc- or FLAG-tagged ULK1-proteins were performed as described in sections 3.2.4.3.5, 3.2.4.3.2 and 3.2.4.3.3, respectively, with the following changes: cell lysates were prepared with CHAPS lysis buffer B (section 3.1.2) and bead-bound immune complexes were washed five times with lysis buffer.

3.2.4.4 GST-14-3-3 pulldown experiments

Recombinant GST-14-3-3 fusion protein used for pulldown experiments was expressed in *E. coli* and purified as described in section 3.2.3.12. Depending on cell type and density, cells were lysed in 600–1000 μ l of modified RIPA containing protease- and phosphatase inhibitors, and GST- and GST-14-3-3 coated glutathione sepharose beads were blocked as outlined in section 3.2.4.3. Following quantitation, equal amounts of cell lysates were incubated with GST- or GST-14-3-3-beads under rotation at 4 °C for 4 h. Then, beads were washed 3 x with lysis buffer and 1 x with low salt buffer and proteins were eluted with 30 μ l 3X SDS-sample buffer and analyzed by SDS-PAGE and Western Blot (sections 3.2.4.7/3.2.4.8).

3.2.4.5 *In vitro* kinase assays

3.2.4.5.1 ULK1 kinase assays on AMPK, INPP4B and mSIN1

To examine its kinase activity, myc-ULK1 was purified from HEK293T-cells after transient transfection. For use as substrates, FLAG-INPP4B, untagged exogenous mSIN1 or FLAG-mSIN1 were immunoprecipitated from transiently transfected HEK293T-cells. Immunoprecipitations, including control-IPs were performed as outlined in sections 3.2.4.3.2-3.2.4.3.4, with the following change: one high salt wash of the precipitate was included after four washes with lysis buffer and before the low salt wash. Lysates were prepared with modified RIPA. When the potential substrate was to be coprecipitated with myc-ULK1 (endogenous AMPK-subunits/INPP4B/mSIN1 or FLAG-INPP4B/pLPCX-mSIN1 cotransfected with myc-ULK1) cells were lysed with CHAPS lysis buffer A. In this case, a high salt wash was omitted.

At the low salt wash, samples were divided into two samples, one for analysis by Western blot (section 3.2.4.8) and one for the kinase assay. For the latter, bead-bound kinase and substrate were mixed by resuspension in 35 μ l 1X kinase buffer (10 mM HEPES, pH 7.5; 10 mM MgOAc; 1 mM DTT). If FLAG-INPP4B was used as the substrate and had been eluted from the beads, myc-ULK1-coated beads were resuspended in 31.5 μ l eluate + 3.5 μ l 10X kinase buffer. Then, 5 μ l of ATP-mix were added (8 μ M ATP, 80 μ Ci γ ^{32P}-ATP in kinase buffer to achieve final concentrations of 1 μ M and 10 μ Ci, respectively). Reactions were incubated at 30 °C for 20 min and stopped by addition of 10 μ l 5X SDS-sample buffer, boiled at 95 °C for 10 min and subjected to SDS-PAGE (section 3.2.4.7). Subsequently, the gel was dried in a gel dryer and incorporation of ³²P into proteins was detected by autoradiography on x-ray films.

3.2.4.5.2 AMPK kinase assays on ULK1

For use as substrates, myc- or FLAG-tagged ULK1-variants were overexpressed in HEK293T cells and immunoprecipitated from the lysates as described in sections 3.2.4.3.2 and 3.2.4.3.3, with addition of a high salt wash before the low salt wash of the precipitates. Lysis was performed using modified RIPA. At the final wash step, samples were split into three, with one sample being subjected to Western blot analysis and the two remaining to *in vitro* kinase assays. One sample was incubated in kinase buffer mix alone (1 μ M ATP and 10 μ Ci γ ^{32P}-ATP in 1X kinase buffer containing 20 mM HEPES, pH 7.0, 0.4 mM DTT, 0.01% Brij, and 10 mM MgCl₂), and the other in kinase buffer mix with partially purified AMPK and 300 μ M AMP. Reactions were performed at 30 °C for 15 min and stopped by addition of 2X SDS-sample buffer. Incorporation of ³²P into proteins was visualized by autoradiography as above.

3.2.4.6 Dephosphorylation of proteins with shrimp alkaline phosphatase

To investigate whether mobility shifts of proteins in SDS-PAGE were due to phosphorylation, these proteins were subjected to treatment with shrimp alkaline phosphatase (SAP) to remove phosphate groups. Proteins of interest were immunoprecipitated as described (section 3.2.4.3), and washed three additional times with low salt buffer containing protease inhibitors (cf. section 3.1.2) *only* to remove phosphatase inhibitors. Subsequently, beads were divided equally into two samples, one was resuspended in 40 μ l 1X SAP-buffer containing protease inhibitors and the other in 40 μ l 1X SAP-buffer with protease inhibitors and 5 U SAP. Reactions were incubated on a rocker at 37 °C for 1 h and stopped by addition of 10 μ l 5X SDS-sample buffer and boiling at 95 °C for 10 min. Samples were analyzed by SDS-PAGE and Western blot as described in sections 3.2.4.7 and 3.2.4.8.

3.2.4.7 SDS-polyacrylamide gel electrophoresis

Protein mixtures were separated into their components according to molecular size by discontinuous one-dimensional SDS-polyacrylamide gel electrophoresis (SDS-PAGE). Gel size and polyacrylamide percentage of the separation gel varied depending on the experiment. Samples from immunoprecipitation- or pulldown-experiments were analyzed on full-size gels (13 cm wide, 16 cm long and 1.5 mm thick); otherwise, minigels (8.5 cm wide, 6.5 cm long and 1.5 mm thick) were used. Composition of the gel-mixtures is given in table 3.3. If multiple proteins within a wide range of molecular weights had to be analyzed in the same sample in parallel, step gradient gels with the lower half of the separation gel containing 10 % polyacrylamide and the upper half containing 7.5 % polyacrylamide, were poured. Prior to loading, samples were mixed with 5X- SDS-loading buffer, boiled at 95 °C for 5-10 min and centrifuged at 13,000 rpm for 2 min. Electrophoresis was conducted at 20–40 mA for minigels and 10-50 mA for full-size gels until the blue dye front had just run out of the gel.

Table 3.3. Composition of polyacrylamide gels. Total volumes are sufficient for two minigels.

Component	Separation gel			Stacking gel 4%
	7.5 %	10 %	15 %	
30 % w/v acrylamide/bisacrylamide	5 ml	6.6 ml	10 ml	1.05 ml
Separation gel buffer	5 ml	5 ml	5 ml	
Stacking gel buffer				1.88 ml
Sterile H ₂ O	9.9 ml	8.3 ml	4.9 ml	4.5 ml
10 % w/v APS	100 μ l	100 μ l	100 μ l	88 μ l
TEMED	15 μ l	15 μ l	15 μ l	28 μ l
Total volume	20 ml	20 ml	20 ml	7.5 ml

3.2.4.8 Western blot

Immediately following SDS-PAGE, proteins in the gel were transferred („blotted“) to PVDF membrane for subsequent detection by specific antibodies. Transfers were performed by the wet method. A blotting sandwich was assembled in a special cassette in the following order from cathode to anode: sponge (wetted in transfer buffer)-2 Whatman paper (wetted in transfer buffer) – gel (equilibrated in transfer buffer)– PVDF membrane (activated with methanol, equilibrated in transfer buffer)– 2 Whatman paper and sponge (also wetted in transfer buffer). After removing air bubbles from in between the layers, the cassette was closed tightly and placed into the transfer tank. Transfer was performed at 750 mA, 4 °C for 2–3 h.

Following transfer, the membrane was washed briefly with deionized water and then consecutively incubated under gentle agitation first in blocking buffer for 1 h at RT to prevent non-specific binding to the membrane, second, with the appropriately diluted primary antibody under the conditions specified in table 3.4, and third, with the corresponding secondary antibody for 1 h at RT. Between incubations with primary and secondary antibodies and after incubation with the secondary antibody, the membrane was washed 2 x 10 min with TBST. Depending on the secondary antibody conjugate used, the signal was detected either by overlying the membrane with enhanced chemiluminescent detection reagent (ECL, for HRP-coupled secondary antibodies) and exposure to x-ray film in a dark room or, in case of fluorescent dye-conjugated secondary antibodies, by scanning the membrane on a LI-COR® Odyssey® Infrared scanner.

Table 3.4. Use of antibodies for Western blot.

Antibody	Dilution	Conditions
Primary antibodies		
α -14-3-3 (K-19), pan	1:1,000 in TBST + 5 % BSA	4 °C, 16 h
α -Acetyl CoA Carboxylase 1	1:250 in TBST + 5 % BSA	4 °C, 16 h
α -Acetyl-CoA Carboxylase (C83B10)	1:1,000 in TBST + 5 % BSA	4 °C, 16 h
α - β -Actin (AC-15)	1:5,000 in TBST + 5 % milk	4 °C, 16 h or RT, 1 h
α -AMPK α (23A3)	1:1,000 in TBST + 5 % BSA	4 °C, 16 h
α -AMPK α (F6)	1:1,000 in TBST + 5 % BSA	4 °C, 16 h
α -AMPK α 1	1:1,000 in TBST + 5 % BSA	4 °C, 16 h
α -AMPK α 2 (CST)	1:1,000 in TBST + 5 % BSA	4 °C, 16 h
α -AMPK α 2 (Upstate)	1:1,000 in TBST + 5 % BSA	4 °C, 16 h
α -AMPK β 1/2 (57C12)	1:1,000 in TBST + 5 % BSA	4 °C, 16 h
α -Atg1/ULK1	1:500 in TBST + 5 % BSA	4 °C, 16 h
α -DDDDK-tag	1:1,000 in TBST + 5 % BSA	4 °C, 16 h
α -FLAG (M2)	1:1,000 in TBST + 5 % milk	4 °C, 16 h or RT, 1 h

Table 3.4. continued.

Antibody	Dilution	Conditions
α -GFP	1:2,500 in TBST + 5 % milk	4 °C, 16 h or RT, 1 h
α -myc-tag (9E10)	1:1,000 in TBST + 5 % milk	4 °C, 16 h or RT, 1 h
α -p62/SQSTM1	1:1,000 in TBST + 5 % BSA	4 °C, 16 h
α -Phospho-Acetyl-CoA Carboxylase (Ser79)	1:1,000 in TBST + 5 % BSA	4 °C, 16 h
α -Phospho-AMPK α (Thr172) (40H9)	1:1,000 in TBST + 5 % BSA	4 °C, 16 h
α -Phospho-(Ser/Thr) PKD motif	1:1,000 in TBST + 5 % BSA	4 °C, 16 h
α -Raptor (24C12)	1:1,000 in TBST + 5 % BSA	4 °C, 16 h
α -Sin1	1:1,000 in TBST + 5 % BSA	4 °C, 16 h
Secondary antibodies		
α -Mouse-IgG (H+L) Alexa Flour 680 conjugate	1:10,000 in TBSTX + 5 % milk + 0.1 % SDS	RT, 1 h
α -Mouse-IgG (H&L), HRP conjugate	1:15,000 in TBSTX + 5 % milk	RT, 1 h
α -Rabbit-IgG(H+L), HRP conjugate	1:2,000 in TBSTX + 5 % milk	RT, 1 h
α -Rabbit-IgG (H&L), IRDye800 conjugate	1:5,000 in TBSTX + 5 % milk + 0.1 % SDS	RT, 1 h

In general, membranes were cut into horizontal stripes to allow parallel detection of multiple proteins of various molecular sizes in the same gel lane. Primary antibody dilutions were reused one additional time, except for the antibodies 9E10 (> 5 x), AC-15 (5 x) and M2 (4 x) and stored at 4 °C with addition of sodium azide to a final concentration of 0.02 % to dilutions prepared in 5 % milk.

When proteins of similar or identical molecular weight, in particular phosphorylated and total amount of a protein of interest, were to be detected by ECL, the phosphorylated form was analyzed first and the membrane was stripped before applying the antibody to the total protein. To strip a membrane, it was incubated in 4 N NaOH for 5 min at RT under gentle agitation, washed with TBST for 4 x 5 min and then blocked and incubated with primary and secondary antibodies as described above.

If fluorescent detection was chosen, primary antibody dilutions contained an antibody to the protein of interest as well as one against its phosphorylated form if the two antibodies were raised in different host species. The secondary antibody dilution also contained the antibodies against all host species coupled to different fluorescent dyes; in this work, the α -mouse-IgG Alexa Flour 680 conjugate and the α -rabbit-IgG IRDye 800 conjugate were used and 0.1 % SDS was added to the dilution buffer to overcome the hydrophobicity of the IRDye 800. Western blot signals detected on the LI-COR® Odyssey® infrared imager were quantitated using the software included in this system.

3.2.4.9 Cell viability assay

Cell numbers were determined by staining cells on culture dishes with crystal violet. 50,000 cells were seeded in triplicate for each cell type and time point on 12-well plates coated with 25 µg/ml poly-L-lysine in PBS at 4 °C for 8 h and treatment was started 24 h later. After the desired treatment time, cells were washed with PBS containing 0.1 mM CaCl₂ and 1 mM MgCl₂ (PBS+CM), fixed with 3.7 % Paraformaldehyde in PBS for 10 min at RT and stored at 4 °C in PBS+CM until the last set of cells had been fixed. Subsequently, cells were washed 3 x with PBS+CM and incubated with crystal violet staining solution (0.1 % w/v crystal violet in 20 % v/v methanol) for 1 h at RT under gentle agitation. Then, the staining solution was removed and the cells were washed with ddH₂O at least 5 x or until the water was clear. After the cells had dried, crystal violet was extracted by adding 500 µl 10 % v/v acetic acid per well and incubating at RT for 1 h under gentle agitation. 2 x 100 µl per well were transferred to a 96-well plate for duplicate reading of absorptions at 595 nm in a microplate reader.

3.2.4.10 Mass spectrometry

For analysis by mass spectrometry, myc-ULK1 was immunoprecipitated from lysates of COS7-cells or Pxl-rescue MEFs following appropriate treatment as described in section 3.2.4.3.2 with the following adjustments to the protocol: 8 15-cm dishes of COS7 cells or 12 15-cm dishes of MEFs per time point were used, and in the case of Pxl-rescue MEFs, IPs from three experiments were pooled prior to SDS-PAGE. Cells were lysed with 1.5 ml modified RIPA per dish and lysates from all dishes subjected to the same treatment were pooled in 15 ml conical tubes after preclearing with Pansorbin and before addition of α-myc-tag antibody to each pool (5 µl antibody per 15 cm dish). Lysates were incubated with the primary antibody for 2 h and after addition of 100 µl blocked protein G-sepharose beads for 1 h at 4 °C on a rocker. Beads were washed 5 x with lysis buffer, 1 x with high salt buffer and 1 x with low salt buffer and myc-ULK1 was eluted with 100 µl 5X SDS sample buffer. Following SDS-PAGE, staining of the gel with ProtoBlue SafeTM colloidal coomassie stain according to the manufacturer's protocol and destaining with five changes of ultra pure water, the myc-ULK1-bands were excised and submitted for analysis by reversed-phase microcapillary/tandem mass spectrometry (LC/MS/MS) to the BIDMC core facility equipped with an EASY-nLC nanoflow HPLC (Thermo Fisher Scientific) and a hybrid LTQ-Orbitrap XL mass spectrometer (Thermo Fisher Scientific).

3.2.5 Computational methods

3.2.5.1 Design of primers for site-directed mutagenesis, PCR and sequencing

Oligodesoxynucleotides for site-directed mutagenesis were designed with the QuickChange Primer Design Program provided on the Stratagene web page. Primers for PCR and sequencing were designed using the *PrimerSelect* module of the Lasergene software package.

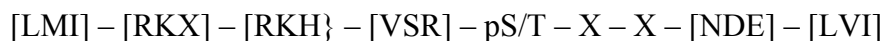
3.2.5.2 Searching of protein sequences for defined motifs using Scansite

The program Scansite provides a variety of tools to detect defined sequence motifs in proteins. In order to predict kinase regulators of ULK1, the sequence of the mouse protein was scanned for all known kinase phosphorylation motifs and protein binding motifs with the function “scan a protein by input sequence” at all three stringency levels (low, medium, high).

To identify potential substrates of ULK1, a kinase for which no target motif is available in Scansite, the function “search using an input motif” was chosen. The motif used in these analyses had been determined for the ULK1-homolog in yeast, Atg1 by Dr. Benjamin Turk, Yale University, and was provided to us prior to publication:



Similarly, murine ULK1 was scanned for AMPK-sites using the motif given by Gwinn et al. (Gwinn et al., 2008):



These two motifs were translated into Scansite matrices, as follows:

Table 3.5. Scansite matrix of the Atg1 phosphorylation motif.

A	C	D	E	F	G	H	I	K	L	M	N	P	Q	R	S	T	V	W	Y
1	1	1	1	1	1	1	1	1	1	1	1	1	1	1	1	1	1	1	1
1	1	1	1	1	1	1	1	1	1	1	1	1	1	1	1	1	1	1	1
1	1	1	1	1	1	1	1	1	1	1	1	1	1	1	1	1	1	1	1
1	1	1	1	1	1	1	1	1	1	1	1	1	1	1	1	1	1	1	1
1	1	1	1	1	1	1	1	1	1	1	1	1	1	1	1	1	1	1	1
4	0	0	0	0	4	0	4	0	4	4	0	0	0	0	0	0	0	0	0
1	1	1	1	1	1	1	1	1	1	1	1	1	1	1	1	1	1	1	1
1	1	1	1	1	1	1	1	1	1	1	1	1	1	1	1	1	1	1	1
0	0	0	0	0	0	0	0	0	0	0	0	0	0	0	21	21	0	0	0
3	3	0	0	3	3	0	3	0	3	3	0	0	0	0	0	0	3	3	0
3	3	0	0	3	3	0	3	0	3	3	0	0	0	0	0	0	3	3	0
1	1	1	1	1	1	1	1	1	1	1	1	1	1	1	1	1	1	1	1
1	1	1	1	1	1	1	1	1	1	1	1	1	1	1	1	1	1	1	1
1	1	1	1	1	1	1	1	1	1	1	1	1	1	1	1	1	1	1	1
1	1	1	1	1	1	1	1	1	1	1	1	1	1	1	1	1	1	1	1
1	1	1	1	1	1	1	1	1	1	1	1	1	1	1	1	1	1	1	1
1	1	1	1	1	1	1	1	1	1	1	1	1	1	1	1	1	1	1	1

Table 3.6. Scansite matrix of the AMPK phosphorylation motif.

A	C	D	E	F	G	H	I	K	L	M	N	P	Q	R	S	T	V	W	Y
1	1	1	1	1	1	1	1	1	1	1	1	1	1	1	1	1	1	1	1
1	1	1	1	1	1	1	1	1	1	1	1	1	1	1	1	1	1	1	1
1	1	1	1	1	1	1	1	1	1	1	1	1	1	1	1	1	1	1	1
0	0	0	0	0	0	0	5	0	9	7	0	0	0	0	0	0	0	0	0
1	1	1	1	1	1	1	1	7	1	1	1	1	9	1	1	1	1	1	1
0	0	0	0	0	0	5	0	7	0	0	0	0	9	0	0	0	0	0	0
0	0	0	0	0	0	0	0	0	0	0	0	0	5	7	0	9	0	0	0
1	1	1	1	1	1	1	1	1	1	1	1	1	1	1	1	1	1	1	1
0	0	0	0	0	0	0	0	0	0	0	0	0	0	0	21	21	0	0	0
1	1	1	1	1	1	1	1	1	1	1	1	1	1	1	1	1	1	1	1
1	1	1	1	1	1	1	1	1	1	1	1	1	1	1	1	1	1	1	1
0	0	7	5	0	0	0	0	0	0	9	0	0	0	0	0	0	0	0	0
0	0	0	0	0	0	0	5	0	9	0	0	0	0	0	0	0	9	0	0
1	1	1	1	1	1	1	1	1	1	1	1	1	1	1	1	1	1	1	1
1	1	1	1	1	1	1	1	1	1	1	1	1	1	1	1	1	1	1	1
1	1	1	1	1	1	1	1	1	1	1	1	1	1	1	1	1	1	1	1
1	1	1	1	1	1	1	1	1	1	1	1	1	1	1	1	1	1	1	1

3.2.5.3 Sequence alignments

Pair wise and multiple alignments of protein sequences obtained from the Swissprot database were generated with the module *MegAlign* of the Lasergene software package. In all cases, the alignment method ClustalW set to “slow-accurate” was chosen.

3.2.5.4 Image processing and analysis

In the interest of clarity, images of scanned Western blot films or of membranes scanned on the LI-COR® Odyssey® system were adjusted for brightness and contrast in Adobe Photoshop. If desired, Western blot- or kinase assay signals detected on films were quantitated on the scanned images with ImageJ, and fluorescent Western blot signals were quantitated with the LI-COR® Odyssey® software.

3.2.5.5 Statistical analyses

Statistical parameters including mean, standard deviation and standard error of the mean (SEM) were calculated using the appropriate functions of Microsoft Excel or the GraphPad Prism software. T-tests and Spearman rank correlation analyses were performed using GraphPad Prism.

4 Results

4.1 Bioinformatics and proteomics studies to predict candidate regulators and substrates of ULK1

4.1.1 Mass spectrometry reveals 30 phosphorylated sites in ULK1

Protein kinases phosphorylate particular amino acids residues (depending on specificity, either serine and threonine, tyrosine, or - less commonly in mammalian cells - histidine or aspartate) within defined sequence patterns. Thus, kinase-substrate-relationships can be predicted by searching protein sequences for such preferred target motifs using bioinformatics tools such as Scansite (scansit.mit.edu; Obenaus et al., 2003). In order to identify protein kinases that might regulate ULK1 function by phosphorylation during autophagy, we first determined the particular serine and threonine residues in this protein that are phosphorylated under various nutrient conditions. Mouse embryonic fibroblasts (MEFs) with stable ectopic expression of myc-tagged murine ULK1 were cultured in regular growth media or subjected to starvation in Earle's Balanced Salt Solution (EBSS) for 30 min or 2 h to induce autophagy. After immunoprecipitation of myc-ULK1 with anti-myc-antibody, SDS-PAGE, Coomassie blue staining, excision of the band of interest and in-gel digestion with trypsin, phosphopeptide analysis was performed by microcapillary liquid chromatography/tandem mass spectrometry (LC/MS/MS). All in all, 30 serine- and threonine residues were detected to be phosphorylated under at least one of the conditions tested, with six residues being constitutively phosphorylated and 24 residues changing their phosphorylation status during starvation. Subsequently, we compared the sequences surrounding each phosphorylated serine or threonine residue with known kinase target motifs using Scansite. This analysis revealed sites that are candidates for phosphorylation by several kinases involved in growth factor signaling and cellular metabolism, e.g. AKT, GSK3 β , ERK and PKA. We therefore hypothesized that these kinases may be potential regulators of ULK1. The most sites (six residues) were found to conform to the consensus phosphorylation motif of CDK5, a kinase with known function during neuronal development (Jessberger et al., 2009). This is interesting since in mammalian cells, ULK1 has been described to play a role in axon outgrowth (Tomoda et al., 1999). In addition, five potential binding sites for regulatory proteins of the 14-3-3-family were identified. A summary of all the phosphorylation sites detected in ULK1 under nutrient-rich and starvation conditions, including information on potential kinases phosphorylating them and on evolutionary conservation of these sites, is given in table 4.1.

Table 4.1. Phosphorylation sites on ULK1 identified by LC/MS/MS in this study under nutrient-rich and starvation conditions.

Site	Phosphorylated at			Sequence	Kinase	Conservation	Reference
	0 h	0.5 h	2 h				
S317	x		x	SHLASPPsLGEMPQL	PKC μ	ULK2, Ce	
S403		x		ESHGRTPsPSPTCSS	GSK3β		
S411			x	PSPTCSSsPSPSGRP	GSK3β ERK1	(Dm)	
S450		x	x	RIEQNLQsPTQQQTA	p38	(ULK2)	Brill <i>et al.</i> , Daub <i>et al.</i> , Dephoure <i>et al.</i> , Dorsey <i>et al.</i> , Oppermann <i>et al.</i> , (CS 3882; CS 2333)
S477	x	x		PLGFGRAsPsPPsHT	ERK1	(Ce)	Daub <i>et al.</i>
S479		x		GFGRASPsPPSHTDG	CDC2 CDK5	Ce	Daub <i>et al.</i> ; Dorsey <i>et al.</i>
S494		x		AMLARKLsLGGGRPY	AKT PKA PKCμ PKCδ (14-3-3)	ULK2	
S521	x	x	x	PSWSRVPsPQGADVR			Dorsey <i>et al.</i>
S532	x			ADVVRGRsPRPGSSV	CDK5	(ULK2)	
S543	x	x		GSSVPEHsPRTTGLG	CDC2 CDK5		
S555	x	x		GLGCRLHsAPNLSDF	(14-3-3)	ULK2	Dephoure <i>et al.</i> , Pan <i>et al.</i>
S614	x	x	x	LPDFLQRsPLPPILGS		ULK2, (Dm)	
S622	x	x	x	PLPPILGSPTKAGPS	CDC2 CDK5	ULK2, (Dm)	Brill <i>et al.</i> , Chen <i>et al.</i> , Daub <i>et al.</i> , Dephoure <i>et al.</i> , Dorsey <i>et al.</i> , Trinidad <i>et al.</i> , (CS 3885);
T624	x			PPILGSPtKAGPSFD		ULK2, (Dm)	Brill <i>et al.</i>
T635			x	PSFDFPKtPSSQNLL	CDK5	Sc, (ULK2, Ce)	
S637	x	x	x	FDFPKTPsSQNLLTL		Ce, (ULK2)	Cantin <i>et al.</i> , Chen <i>et al.</i> , Dephoure <i>et al.</i> , Pan <i>et al.</i>
T659			x	MTPPRNRtLPDLSEA	AKT (14-3-3)		
S693		x	x	GPFGRSFSsTSRITDL	AKT (14-3-3)	ULK2, (Dm)	
T694		x	x	PFGRSFSsTSRITDLL		ULK2, (Dm, Ce)	
S695	x			FGRSFSsTSRITDLLL			
S715	x	x	x	SDSGSTDsLQKPM EI	CK1	ULK2	
S718		x	x	SDSGSTDsLQEKPM E	CK1	ULK2, (Dm, Ce, Sc)	
S747	x			ARGGGASsPAPVVFT		(ULK2)	Beausoleil <i>et al.</i>
T754	x					ULK2, (Dm)	
S757	x		x	PVVFTVGsPPSGATP		ULK2, Dm, (Sc)	Beausoleil <i>et al.</i> , Dorsey <i>et al.</i> ,
T763	x			GSPPSGAtpPQSTRT	CDK5 GSK3 β	(ULK2, Ce)	
S774			x	STRTRMFsVGSSSSL	AKT CamK2 PKCδ (14-3-3)	ULK2, Dm, Sc	
S777		x		TRMFsvGsSSSLGST		ULK2, Dm, Sc	
S780	x	x	x	FSVgSSsLGSTGSS	PKC δ	ULK2, (Dm)	
S1043	x		x	LCIERRLsALLSGVY	PKA	ULK2, (Dm)	Dorsey <i>et al.</i>

Tandem mass spectrometry analyses were performed on myc-ULK1 stably overexpressed in MEFs and immunoprecipitated from the cell lysates after 0 h, 0.5 h or 2 h of EBSS-starvation. Conditions under which a site was detected are marked with “x”. The sequences surrounding the detected sites are shown, with the phosphorylated serine or threonine highlighted in bold font and lower case. Kinases potentially phosphorylating ULK1 were predicted by searching the protein sequence of murine ULK1 with Scansite using the function “Search protein by input sequence” at low stringency. Sites also detected at medium or high stringency are highlighted in bold or bold italic font, respectively. The regulatory protein 14-3-3 is put in brackets since it is not a kinase. Conservation of the sites in ULK1-homologs of other species was determined by ClustalW-alignment of the protein sequences (supplementary Fig. S1). If only the S/T-residue is conserved, but the surrounding residues between the -5 and +5 positions do not resemble the particular kinase’s target motif, the organism is listed in brackets. Ce – *Caenorhabditis elegans*; Dm – *Drosophila melanogaster*; Sc – *Saccharomyces cerevisiae*. CS 2333, CS 3882 and CS 3885 refer to studies performed at Cell Signaling Technology; the results are available in the Phosphosite database (www.phosphosite.org).

Of note, all the sites listed in table 4.1 map to the spacer- and C-terminal regions of ULK1 (amino acids 279-828 and amino acids 829-1051, respectively). However, we cannot exclude that we missed phosphorylated sites, especially in the kinase domain (amino acids 1-278), because the protein sequence was not completely covered by the peptides detected by mass spectrometry. While Scansite predicted additional target sites (table S1), some of which lay in regions that lacked peptide coverage, only one site in a non-covered region matched the motif of a kinase for which we had not found another site in a region that was covered. This kinase, possessing a single target site in these Scansite-analyses was AMPK, which therefore was also considered a candidate regulator of ULK1. All kinases predicted to phosphorylate ULK1 are summarized in table 4.2.

Table 4.2. Kinases predicted to phosphorylate ULK1.

Kinase	Number of target sites		
	predicted+detected	predicted only	total
(14-3-3)	5	3	8
AMPK		1	1
AKT	4		4
CamK2	1	1	2
CDC2	3	7	10
CDK5	6	7	13
CK1	2	11	13
ERK1	2	6	8
GSK3 β	3	13	16
p38	1	1	2
PKA	2		2
PKC $\alpha/\beta/\gamma$		1	1
PKC δ	3	5	8
PKC ϵ		3	3
PKC μ	2	2	4

Kinases were predicted by searching the protein sequence of murine ULK1 using the Scansite function “Search protein by input sequence” at low stringency. For each kinase, the number of predicted sites found to be phosphorylated by LC/MS/MS, the number of predicted sites that were not detected by LC/MS/MS, and the total number of predicted target sites in ULK1, are listed.

4.1.2 Scansite search and high throughput proteomic screening predict autophagy-relevant proteins as ULK1-substrates

To identify candidate substrates of ULK1, we used Scansite to search protein databases for the target motif of Atg1, the ULK1-homolog in yeast (B. Turk, personal communication and Mok et al., 2010). Atg1 exhibits selectivity for the large subsets of aliphatic and hydrophobic residues at position -3 and positions +1 and +2 relative to the phosphorylated serine or threonine residue (cf. Fig. 4.1B). Since this results in low specificity and a high number of Scansite hits, we defined the following criteria for good candidate substrates of ULK1:

1. Identification as an Atg1-substrate in a proteomics screen (Ptacek et al., 2005)
2. Presence of the target motif for phosphorylation by Atg1
3. Gene ontology annotation with relevance to autophagy, which included
 - a) Autophagy
 - b) Kinases and other signal transduction proteins, since ULK1 itself is a kinase
 - c) Chaperones, since one autophagy-subtype is chaperone-mediated autophagy
 - d) Cytoskeleton, since our lab previously had identified a role for the cytoskeletal protein Paxillin in autophagosome formation (Chen et al., 2008)
 - e) Energy homeostasis, since autophagy contributes to maintenance of energy levels during starvation
 - f) Vesicular trafficking, since autophagy is a vesicular process and potentially could employ components of related pathways
4. Evolutionary conservation of predicted phosphorylation sites

The high throughput proteomics screen of Ptacek *et al.* was conducted in the yeast *S. cerevisiae* on 87 of the 122 yeast kinases and involved approximately 4,400 proteins and predicted proteins (~ 2/3 of the yeast proteome) as substrates. This analysis identified 188 open reading frames, 140 of which correspond to annotated proteins as potential phosphorylation targets of Atg1. This is the third highest number of substrates detected for any of the investigated kinases, and this high number is consistent with the broad consensus of the Atg1 phosphorylation motif (Mok et al., 2010). Importantly, we found this motif in 88.5 % (124/140) of Atg1-substrates suggested by the proteomics screen, which to a certain degree indicates predictive power. Out of the 140 potential Atg1-substrates, 30 proteins (table 4.3) fell into one of the six functional groups defined above. We identified their mammalian homologs by BLAST-search and scanned these for the presence of the Atg1-target motif by Scansite. For four of these proteins, Srp40, App1, Pde1 and Sip2, no human homolog was detected. Of the remaining 26, 24 proteins contained consensus Atg1-phosphorylation sites in the human and in the yeast homolog. Only in seven proteins, however, these sites were evolutionary conserved. These seven proteins, Bmh2/14-3-3, Crn1/CORO6, Mss4/PIP5K1,

Vip1/VIP, Apm2/AP1M1, Glo3/ ARFGAP2 and Sec2/ Rabin-3 thus, emerged as the primary candidates for experimental validation.

Table 4.3. Candidate substrates of Atg1.

YEAST PROTEIN		HUMAN HOMOLOG	
Name	Atg1-Sites	Name	Atg1-Sites
Autophagy			
Aut7/Atg8	T56, T87, S92, T114	LC3	T100
Aut10/Atg18	S142, S173, S220, T238, T393	WIPI3	S15, T134, T143
Mai1/Atg21	0	WIPI2	T180
Kinases/Signal Transduction			
Avo1	T123, S144, S273, T904	mSIN1	S140, T194, T261
Bmh2	S180	14-3-3 ϵ	S148, S178
Elm1 ¹	T9, S93, T587	CamKK β	S51, T347, T489, S553
		CamKK α	T310, S452
Pde1 ²	S93, T219, S359	---	
Rio1	S177, S294, S354, S376	RIOK1	T245, S278, S372
		RIOK3	S34, S247, S263, S360
		RIOK2	S40
YDL025C	S317	CHK1	T14, T153, T199, T476
Chaperones			
Cns1	S229	TTC4	T345
Srp40	T361	---	
Cytoskeleton			
Abp140	T122, T447, T489	METL2B	T336
App1 ²	T289	---	
Cdc55	T432, T470	PP2A-B δ	S265, S361, T428
		PP2A-B β	S195, S291, T358
		PP2A-B α	S259, S355, T422
		PP2A-B γ	S13, S106, S351, T418
Crn1	T243 , T346, T585	CORO6	T236
		CRN2B	S59, S150, T235, S328
Mss4	S33, S352, S638 , T678	PIP5K1 γ	S27, T90, S175, T189, S318 , T356, T442, T472, S605
		PIP5K1 α	T96, S118, S176, S181, S324 ,
		PIP5K1 β	T362, T448 T40, S62, S125, S268 , T297, T306
Vip1	S45, T511 , S568, S674, S862, S1004	VIP1	T356 , S484, S516, S1017, S1127, S1359
Energy homeostasis			
Mig2	S91, T95, S150, S233, S282	EGR3	0
Pfk26	S272, S580, S607, S656	PFKFB1	S274
		PFKFB3	S26, S269, S487, S492
Sip2	S161	AMPK β 2	T79, S249
		AMPK β 1	T80
Sip5	T414	---	

Table 4.3. continued.

YEAST PROTEIN		HUMAN HOMOLOG	
Name	Atg1-Sites	Name	Atg1-Sites
Vesicular trafficking			
Apm2	S4 , T253	AP1M1	S4 , S78, S82
Ent5	0	EPN2	T397, S587, S622
Glo3	S55	ARFGAP2	S50 , T89, S211, S269, S368, S479, S498
Osh3	S113, S131, T203, S288, T312	OSBL3	S386, T738, S766
Prc1	T16, S181, S311, S6	PPGB	S21, T469
Sec2	S107 , S335	Rabin-3	S215 , T257
Vps55	S16, T53, S88, S106, S120	VPS8	S131, S136, T158, S164, S194, S203, T223, T408, T1123, S1159, S1188, S1239, S1279, S1286, S1409
Ypt11	S9, T22, T80, T167	Rab12	S57, T98, S220

Listed are yeast proteins that were identified as *in vitro* substrates of Atg1 in the high throughput screen by Ptacek *et al.* (Ptacek et al., 2005) and that have a cellular function relevant to autophagy. Their human homologs were identified by BLAST-search. No human homolog was listed when the BLAST-hits were proteins of completely unrelated function. Where considered appropriate, several isoforms or closely related family members of the best BLAST-hit were included. Proteins were scanned for the Atg1 consensus phosphorylation motif using the Scansite-function "Scan input sequence by input motif" and the Scansite-matrix given in Materials and Methods, table 3.5. Conserved sites are highlighted in bold font. If a cellular function or process for a particular protein was given by Ptacek *et al.*, assignment to a functional group was done accordingly. Full names for all proteins are given in supplementary table S4.

¹ The kinase ELM1 is considered to be unique to yeast (Hunter and Plowman, 1997) but was included in the list due to its similarity to CaMKK β , a known regulator of autophagy (Hoyer-Hansen et al., 2007).

² The human protein that by BLAST-search was found to be most similar to Pde1, a low affinity cAMP-phosphodiesterase, was hSNM1A (DNA cross-link repair 1A protein), i.e. a protein with unrelated function. However, a human Calcium/calmodulin-dependent 3', 5'-cyclic nucleotide phosphodiesterase, Cam-PDE-1C was detected as the human protein most similar to another *in vitro* Atg1-substrate identified by Ptacek *et al.*, namely the Actin patch protein App1.

4.2 Experimental validation of ULK1-interactions with predicted substrates

The prediction that ULK1 may phosphorylate a particular substrate also includes the possibility that the two proteins interact. Thus, we first investigated whether selected candidate substrates stably associated with ULK1 under regular growth conditions.

4.2.1 N-terminally tagged mSIN1 does not associate with myc-ULK1

MSin1 (mammalian stress-activated MAP-kinase-interacting protein 1, also known as MAPKAP1, i.e. mitogen-activated protein kinase 2-associated protein1) is the homolog of the yeast protein Avo1 that had been identified as an Atg1-substrate in the global analysis of protein phosphorylation in yeast (Ptacek et al., 2005). Avo1/mSIN1 is a unique component of the mTOR-complex 2, mTORC2, whose function in autophagy is not well defined (Diaz-Troya et al., 2008); thus, Avo1/mSIN1 may provide an entry point into elucidating the role of

mTORC2 in this process. Furthermore, Avo1 and mSIN1 both contain several Atg1 consensus phosphorylation sites (cf. table 4.3), although none of these sites is conserved. This can at least partially be explained by the overall very low degree of sequence similarity between the two proteins.

To examine whether mSIN1 may associate with and/or be phosphorylated by ULK1, myc-ULK1 was transiently overexpressed in HEK293T cells and immunoprecipitated from the cell lysates and association of mSIN1 was analyzed by Western blot. In these experiments, neither endogenous nor cotransfected N-terminally FLAG-tagged mSIN1 was found to coprecipitate with myc-ULK1. Similarly, in *in vitro* kinase assays on myc-ULK1, in which separately isolated endogenous mSIN1 or FLAG-mSIN1 proteins were used as substrates, no evidence for mSIN1 phosphorylation was obtained (data not shown). At this point, experimental validation of mSIN1 as an ULK1-substrate was not further pursued.

4.2.2 Exogenous INPP4B and ULK1 interact

INPP4B (inositol polyphosphate 4-phosphatase type II) is a recently discovered candidate tumor suppressor and negative regulator of the PI3K-AKT-signaling pathway (Gewinner et al., 2009). Notably, an INPP4B-ortholog is not present in yeast, and thus could not be identified as an Atg1-substrate in the screen for global analysis of protein phosphorylation in yeast (Ptacek et al., 2005). However, INPP4B may be expected to promote autophagy due to its suppressive effect on mTORC1-activity. (Fig. 4.1A). To address the question of whether INPP4B is involved in autophagy, we searched its protein sequence for the Atg1-phosphorylation motif using Scansite and detected nine potential target sites in the human protein, seven of which are conserved in the mouse and rat homologs (Fig. 4.1B). Notably, five of the conserved sites are unique to INPP4B and absent in the related enzyme INPP4A, including one site in the phospholipid-binding C2-domain (T94) and one close to the catalytic core (T840; Davletov and Sudhof, 1993; Norris et al., 1997).

To test the ability of INPP4B to interact with ULK1, FLAG-INPP4B was coexpressed with myc-ULK1 in HEK293T cells and immunoprecipitated from the lysates. Myc-ULK1 coprecipitated with FLAG-INPP4B, however, in subsequent *in vitro* kinase assays using separately purified proteins, we did not detect phosphorylation of FLAG-INPP4B by myc-ULK1 (Fig. 4.1C and data not shown). Whether ULK1 is able to phosphorylate INPP4B under different conditions, in particular starvation, remained to be investigated.

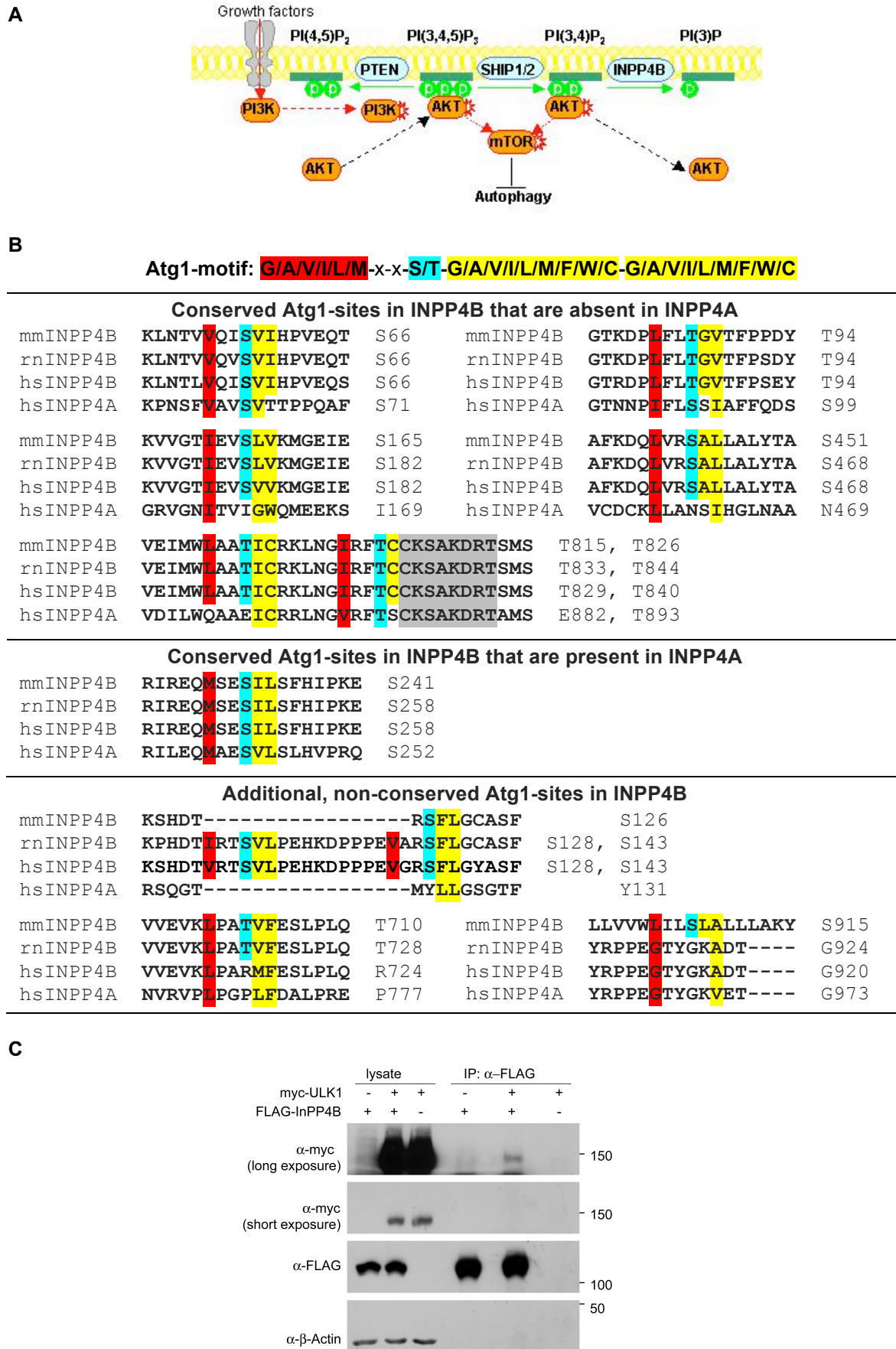


Figure 4.1. Exogenous INPP4B interacts with ULK1. See next page for figure legend.

Figure 4.1. Exogenous INPP4B interacts with ULK1. (A) Simplified signaling pathway regulated by INPP4B. AKT is activated when bound to the plasma membrane and in turn activates mTORC1-signaling to inhibit autophagy. Binding sites for AKT are the membrane phospholipids PI(3,4,5)P₃, which is generated from PI(4,5)P₂ in the PI3K-reaction in response to growth factor signaling, and PI(3,4)P₂. Membrane binding sites are destroyed by the phosphatases PTEN, SHIP1/2 and INPP4B. SHIP1/2 and INPP4B have to act sequentially in order to deactivate AKT. Adapted from Gewinner et al., 2009. (B) Predicted ULK1-phosphorylation sites in INPP4B. Shown are parts of the ClustalW-alignment of the INPP4B protein sequences of *Homo sapiens* (hs), *Rattus norvegicus* (rn) and *Mus musculus* (mm) surrounding predicted Atg1/ULK1-sites. The sequence of human INPP4A was included as well. Atg1-sites were detected using the Quick matrix method of Scansite and the motif given in this figure (B. Turk, personal communication). Residues specified by the Atg1-motif are color-coded, the catalytic core following T840 in human INPP4B is highlighted in grey. Numbers indicate the sequence position of the phosphorylated Ser/Thr-residue or the residue aligning to it (C) FLAG-INPP4B coprecipitates with myc-ULK1. HEK293T cells were cotransfected with FLAG-INPP4B and myc-ULK1 or corresponding empty vectors and lysed in CHAPS-buffer. FLAG-INPP4B was immunoprecipitated using anti-FLAG antibodies coupled to agarose beads. Cell lysates and immunoprecipitates were analyzed by Western blot with the antibodies indicated.

4.2.3 AMPK associates with ULK1 and ULK2

Heterotrimeric AMPK is a central sensor of cellular energy levels and has been suggested to regulate autophagy (Meley et al., 2006). Our bioinformatics analyses predicted ULK1 and AMPK as substrates of each other and global analysis of protein phosphorylation in yeast (Ptacek et al., 2005) had identified the β -subunit of the AMPK-complex, Sip2, as an *in vitro* substrate of Atg1. Thus, we began to investigate a regulatory relationship between the two kinases by testing for stable association in coimmunoprecipitation experiments. We found that a small fraction of myc-ULK1, when coexpressed in HEK293T cells with FLAG-AMPK α 1, but not with an empty vector, was precipitated by anti-FLAG antibodies coupled to agarose beads, indicating that the two kinases participate in a common complex (Fig. 4.2A). To confirm this result, we probed anti-myc-immunoprecipitates from lysates of COS7 cells infected with myc-ULK1 or an empty vector, for endogenous AMPK α and detected this protein only when myc-ULK1 was expressed (Fig. 4.2B). Furthermore, myc-ULK1 stably overexpressed in HEK293T cells could be precipitated by AMPK α 1- or AMPK α 2-specific rabbit antibodies, but not by a non-specific rabbit anti-mouse-antibody (Fig. 4.2C). Finally, when examining the interaction of endogenous AMPK and endogenous ULK1 in MEFs, which were used in this experiment since at this stage of the project, only antibodies against endogenous murine ULK1 were available, a small amount of endogenous ULK1 could be precipitated from the cell lysates with antibodies against endogenous AMPK α 1, but not with non-specific control antibodies (Fig. 4.2D). Taken together, these results indicated an association of endogenous ULK1 and AMPK.

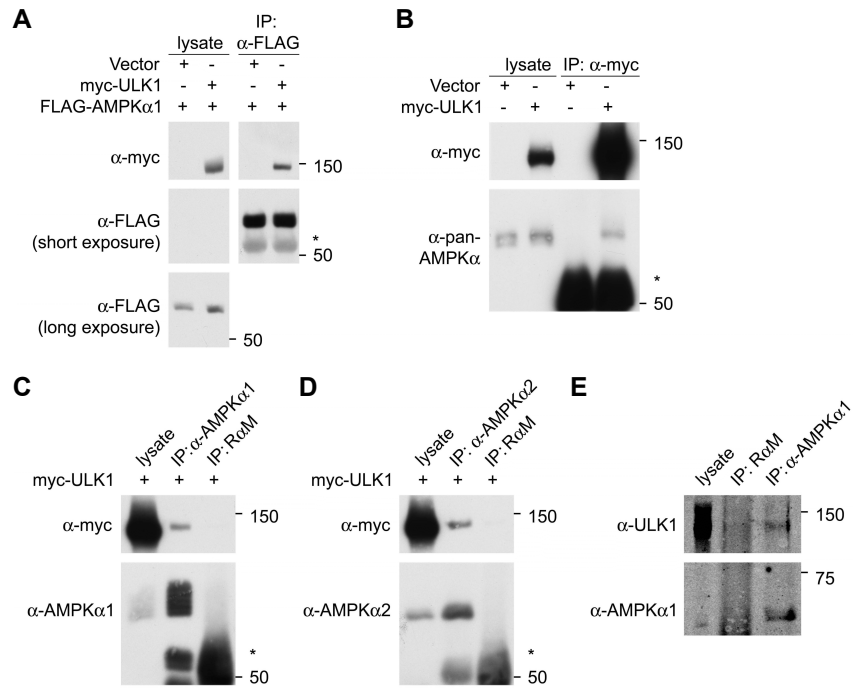


Figure 4.2. ULK1 and AMPK associate. (A) Exogenous AMPK α and ULK1 coprecipitate. HEK293T cells were cotransfected with FLAG-AMPK α 1 and myc-ULK1 or an empty vector and FLAG-AMPK α 1 was immunoprecipitated from the cell lysates using anti-FLAG antibodies coupled to agarose beads. Cell lysates and immunoprecipitates were analyzed by Western blot with the antibodies indicated. (B) Endogenous AMPK α coprecipitates with exogenous ULK1. COS7 cells infected with myc-ULK1 or an empty vector were lysed and myc-ULK1 was immunoprecipitated using myc-tag specific antibodies. Cell lysates and immunoprecipitates were analyzed by Western blot with the antibodies indicated. (C, D) Exogenous myc-ULK1 coprecipitates with both isoforms of endogenous AMPK α . Myc-ULK1-infected HEK293T cells were lysed and subjected to immunoprecipitation using rabbit antibodies against (C) AMPK α 1 or (D) AMPK α 2 or non-specific rabbit-anti-mouse IgG (R α M) as a control. Cell lysates and immunoprecipitates were analyzed by Western blot with the antibodies indicated. (E) Endogenous ULK1 coprecipitates with endogenous AMPK α . MEFs were lysed and endogenous AMPK α 1 was immunoprecipitated as in (C). Cell lysates and immunoprecipitates were analyzed by Western blot with the antibodies indicated. The asterisk in (A)-(D) denotes IgG.

To investigate whether ULK2, a kinase closely related to ULK1, can also interact with AMPK, we performed similar coimmunoprecipitation experiments on FLAG-AMPK α 1 and YFP-ULK2 coexpressed in HEK293T cells. As myc-ULK1, YFP-tagged ULK2 coprecipitated with FLAG-AMPK α 1, demonstrating that both ULK family kinases can bind to AMPK (Fig. 4.3).

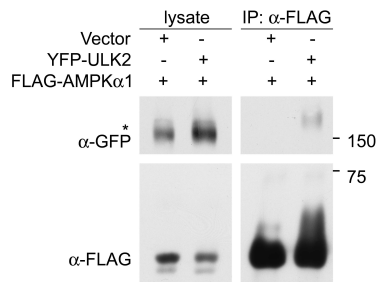


Figure 4.3. ULK2 and AMPK associate. HEK293T cells were cotransfected with FLAG-AMPK α 1 and YFP-ULK2 or an empty vector and FLAG-AMPK α 1 was immunoprecipitated from the cell lysates as in Fig. 4.2A. Lysates and precipitates were analyzed by Western blot with the antibodies indicated. An α -GFP-antibody was used to detect the YFP-tag on ULK2. The asterisk denotes a non-specific band recognized by this antibody in total cell lysates at a molecular weight similar to that of YFP-ULK2.

Having identified two novel interaction partners of ULK1 - INPP4B and AMPK - I subsequently focussed my efforts on characterizing and investigating the function of the interaction between ULK1 and AMPK because of the phosphoproteomics and bioinformatics data that suggested a kinase-substrate relationship being more comprehensive for ULK1 and AMPK than for ULK1 and INPP4B.

4.3 Biochemical characterization of the ULK1-AMPK-complex

4.3.1 Complex-stability is independent of ULK1- and AMPK-kinase activity

Having established an association of ULK1 and AMPK under physiological growth conditions, we sought to define the factors regulating this interaction more closely. First, we examined whether the catalytic activities of these kinases may be necessary for the association. To determine the influence of intact ULK1 kinase activity, we performed immunoprecipitation of endogenous AMPK α 1 and - α 2 in lysates of COS7 cells stably overexpressing the wild type form of myc-tagged ULK1 or a kinase defective mutant (K46A). Both myc-ULK1 proteins coprecipitated with endogenous AMPK α 1 and - α 2 (Fig. 4.4A, B), demonstrating that the ULK1-AMPK-association does not require ULK1 catalytic activity.

To determine whether the interaction with ULK1 depended on AMPK kinase activity, HEK293T cells were cotransfected with wild type, kinase defective (K45A) or constitutively active (T174E, residues 1-312) versions of FLAG-tagged AMPK α 1, and FLAG-AMPK α 1 variants were immunoprecipitated from the cell lysates. In all cases, myc-ULK1 coprecipitated with the FLAG-AMPK α 1-protein, implying that the interaction of ULK1 with AMPK is independent of AMPK-kinase activity (Fig. 4.4C).

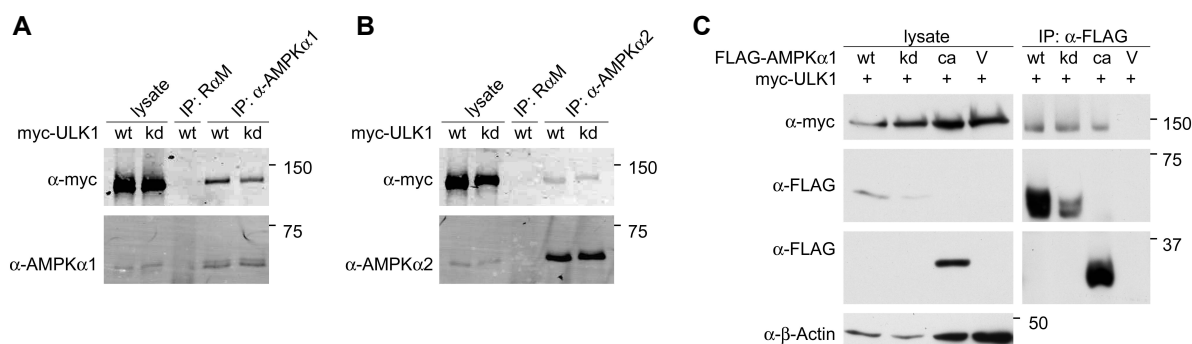


Figure 4.4. Association of ULK1 and AMPK is independent of their kinase activities. (A, B) ULK1 binds to AMPK independently of its catalytic activity. Lysates of COS7 cells infected with wild type (wt) or kinase defective (kd) myc-ULK1 were subjected to immunoprecipitation using (A) AMPK α 1- or (B) AMPK α 2-specific rabbit antibodies or non-specific rabbit-anti-mouse IgG (R α M) as a control. Lysates and immunoprecipitates were analyzed by Western blot with the antibodies indicated. **(C)** AMPK's interaction with ULK1 is independent of its kinase activity. HEK293T cells were cotransfected with myc-ULK1 and wild type (wt), kinase defective (kd) or constitutively active (ca) FLAG-AMPK α 1 or an empty vector. Following lysis, FLAG-AMPK α 1-variants were immunoprecipitated using anti-FLAG antibodies coupled to agarose beads. Western blot analysis was performed with the antibodies indicated.

4.3.2 Complex-formation is mediated by the AMPK α -subunit and the ULK1-spacer region

The coimmunoprecipitation experiment described above on myc-ULK1 and FLAG-tagged wild type, kinase defective and constitutively active AMPK α 1-variants (cf. Fig. 4.4C) also revealed the AMPK-domain important for the association with ULK1; AMPK α binds to the regulatory β - and γ -subunits of the AMPK-complex via its C-terminus, which is deleted in the constitutively active mutant. Thus, the observation of myc-ULK1 coprecipitating not just with full length wild type and kinase defective, but also with the C-terminally truncated constitutively active form of FLAG-AMPK α 1 indicated that the association is mediated by the kinase domain comprising amino acids 1-312 of the catalytic α -subunit.

We also determined which of the three ULK1-domains – N-terminal kinase domain, Ser/Pro-rich spacer region or C-terminal domain – is required for its association with AMPK. Various FLAG-tagged ULK1-fragments were transiently expressed in HEK293T cells, immunoprecipitated from the cell lysates with anti-FLAG antibodies coupled to agarose beads and analyzed for coprecipitation of endogenous AMPK α by Western blot. Deletion of the kinase- or of the C-terminal domain did not abolish the basic ability of the ULK1-fragment to interact with AMPK α . Rather, deletion of the kinase domain resulted in an increase in the amount of coprecipitated AMPK α , suggesting that this domain may play an autoinhibitory role for the association with AMPK α . Consistent with this hypothesis, the relative amount of AMPK α coprecipitating with the isolated spacer region was also higher than for full length ULK1 or the C-terminal truncation mutant. Finally, the isolated kinase- and C-terminal domains were not able to efficiently coprecipitate endogenous AMPK α . These results indicated that the spacer region of ULK1 is the major determinant for the interaction with AMPK (Fig. 4.5).

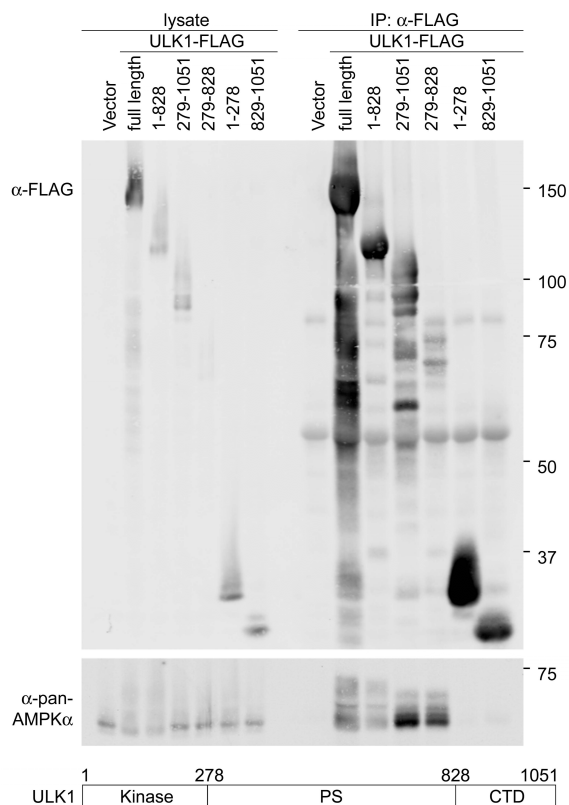


Figure 4.5. ULK1 interacts with AMPK via its Ser/Pro-rich spacer region. HEK293T cells were transfected with empty vector or FLAG-tagged ULK1-fragments containing various combinations of the three ULK1-domains depicted in the schematic drawing. Following lysis, ULK1-FLAG-proteins were immunoprecipitated using anti-FLAG antibodies coupled to agarose beads and cell lysates and immunoprecipitates were analyzed by Western blot with the antibodies indicated.

4.3.3 The AMPK-bound ULK-population is hyperphosphorylated

In our coimmunoprecipitation studies (section 4.2.3), we noticed that the subpopulation of ULK1, and even more dramatically, that of ULK2, associating with AMPK ran at a higher molecular size in SDS-PAGE than the majority of the cellular ULK1/2-pool, suggesting differential posttranslational modification of the AMPK-interacting population (cf. Fig. 4.3). To examine whether phosphorylation accounted for this upward shift, we treated myc-AMPK α 2-immunoprecipitates from lysates of HEK293T cells cotransfected with myc-AMPK α 2 and ULK1-FLAG or YFP-ULK2 or an empty vector, with shrimp alkaline phosphatase. This resulted in a downshift of the signal for coprecipitated ULK1-FLAG and YFP-ULK2 from above to below of the 150 kDa marker band. Of note, in total cell lysates, ULK1-FLAG and YFP-ULK2 run at the lower molecular size observed for phosphatase-treated immunoprecipitated proteins (Fig. 4.6). This result demonstrated that under normal growth conditions at which the experiment was performed, the (minor) populations of ULK-family kinases that interact with AMPK are hyperphosphorylated, and also suggested that this hyperphosphorylation might be required for the association.

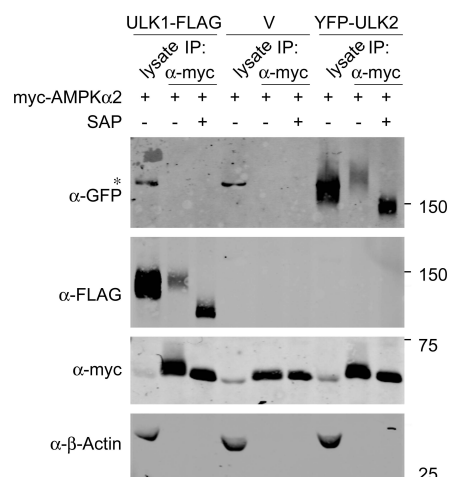


Figure 4.6. The AMPK-interacting ULK-population is hyperphosphorylated. HEK293T cells were cotransfected with myc-AMPK α 2 and either ULK1-FLAG, an empty vector (V) or YFP-ULK2, and myc-AMPK α 2 was immunoprecipitated from the cell lysates using myc-tag specific antibodies. Following IP, precipitates were split into two samples and one was treated with shrimp alkaline phosphatase (SAP) while the other was mock-treated. Lysates and precipitates were analyzed by Western blot with the antibodies indicated. An α -GFP-antibody was used to detect the YFP-tag on ULK2. The asterisk denotes a non-specific band recognized by this antibody in total cell lysates at a molecular weight similar to that of YFP-ULK2.

4.3.4 Regulation of the ULK1-AMPK association by nutrient- and energy-stress

4.3.4.1 AMPK is activated in very early and in late stages of starvation

ULK1 plays a role in autophagy, a process that AMPK has also been connected to (Chan et al., 2007; Meley et al., 2006). To address the question of whether nutrient-stress may regulate the ULK1-AMPK-interaction, we first determined the effect of starvation on AMPK-activity in COS7 cells. We chose this cell line since it has no known defects in the AMPK-signaling pathway and responds well to AMPK-activating compounds (Bin Zheng, personal communication). The readouts for AMPK-activation used throughout this study were phosphorylation of the AMPK activation loop threonine (Thr172) or phosphorylation of the AMPK-substrate ACC at Ser 79.

When subjecting COS7 cells to complete nutrient- and growth-factor deprivation by incubation in EBSS, we reproducibly found AMPK to be strongly active only after very short (less than 5 min) or very long (more than 12-24 h) treatment times (Fig. 4.7A, B). This first, rapid, transient wave of AMPK-activation was also observed in MEFs (Fig. 4.7C). In MEFs, reactivation of AMPK occurred earlier, however, substantial cell death in response to starvation was already observed at 24 h, whereas COS7 cells largely survived even when starved for 48 hours. This implies that high AMPK activity is not required for starvation-induced autophagy in early to intermediate stages of the process.

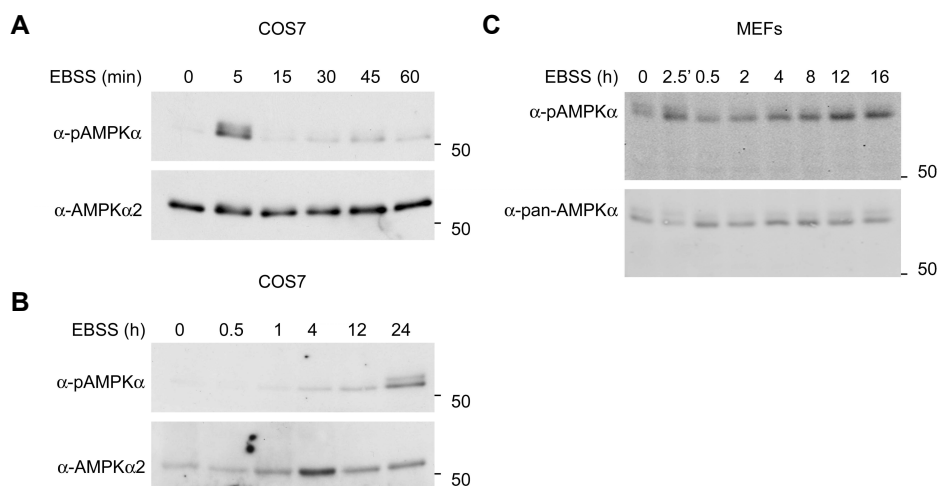


Figure 4.7. AMPK is activated in very early and in late stages of starvation. (A, B) COS7 cells or (C) MEFs were subjected to complete starvation with EBSS for the times indicated. Note that the shortest starvation time in (C) is 2.5 min. AMPK-activation was assessed by Western blot for phosphorylation of Thr172 (pAMPK). In panels (A) and (C), the unstarved control cells were subjected to a mock-treatment with fresh media for the shortest starvation time.

4.3.4.2 Nutrient-sensitivity of the ULK1-AMPK-interaction is cell-line dependent

To investigate the influence of nutrients on ULK1-AMPK-complex stability, endogenous AMPK α 2 was immunoprecipitated from lysates of myc-ULK1-infected HEK293T cells after 30 min or 120 min of EBSS-treatment. Western blot analysis revealed that the amount of myc-ULK1 associated with AMPK α was decreased at the early, and even further, at the late starvation time point, indicating destabilization of the complex upon nutrient deprivation (Fig. 4.8). The same result was obtained when myc-ULK1 was coprecipitated with endogenous AMPK α 1 (data not shown).

In COS7 cells however, we did not consistently observe a marked decrease in the amount of myc-ULK1 coprecipitating with endogenous AMPK α 2 during the course of time from 0 to 4 h of EBSS-treatment. Upon prolonged starvation of up to 48 h, clearly less myc-ULK1 was associated with AMPK α 2 than in untreated cells, however, myc-ULK1-levels were also reduced. Quantification of the Western blot data suggested that ULK1-expression cycles during starvation and is minimal at 24 h and in part restored at 48 h after starvation. Similarly, the percentage of the ULK1-population bound to AMPK cycles, with a minimum reached between 6 h and 12 h and a maximum occurring at 12 to 24 h of starvation (data not shown). This implies that ULK1-AMPK-complexes can be formed regardless of nutrient-availability and that additional factors or signaling pathways determine whether they are assembled or disassembled.

Experiments conducted in MEFs to examine the effect of starvation on the association of myc-ULK1 with endogenous AMPK α 1, the predominant isoform in this cell type (Bin

Zheng, personal communication), failed, since a non-specific band of comparable intensity to that of coprecipitated myc-ULK1 was detected in R α M-control-immunoprecipitates.

Given the different results obtained in HEK293T- and COS7 cells, we concluded that regulation of the ULK1-AMPK-interaction by nutrients is cell line dependent.

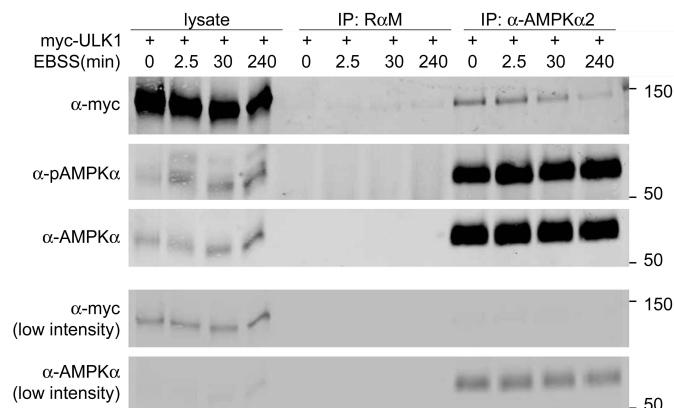


Figure 4.8. Starvation induces dissociation of the ULK1-AMPK-complex in HEK293T cells. HEK293T cells were starved with EBSS for the times indicated and endogenous AMPK α 2 was immunoprecipitated from the lysates using AMPK α 2-specific rabbit antibodies. Non-specific rabbit-anti-mouse IgG (R α M) served as a control. Lysates and immunoprecipitates were analyzed by Western blot with the antibodies indicated. Additional images of the LI-COR scanned Western blot membranes of myc-ULK1 and AMPK α , adjusted to low intensity are shown at the bottom of the figure.

4.3.4.3 ULK1-AMPK-complex stability is largely independent of AMPK-activation

We also examined whether activation of AMPK *per se* changed its ability to interact with ULK1. Endogenous AMPK α -isoforms and myc-ULK1 stably overexpressed in COS7 cells were precipitated with AMPK α 1- or - α 2-specific rabbit antibodies after treatment with a variety of compounds that activate AMPK via different mechanisms. Western blot signals were quantified and successful treatment, i.e. AMPK activation was verified by Western blot for phospho-AMPK Thr172 or phospho-ACC Ser 79. When treating with the AMP-mimetic 5-aminoimidazole-4-carboxamide-1- β -D-ribofuranoside (AICAR) for up to 4 h, we did not consistently observe either an increase or a decrease in the amount of myc-ULK1 coprecipitating with endogenous AMPK α 1/ α 2. The same was the case for myc-ULK1 coprecipitated with endogenous AMPK α 2 after treatment with 2-Deoxyglucose (2DG, a glycolytic inhibitor) for 15-60 min, or with Phenformin (a respiratory chain inhibitor) for up to 4 h, or with EBSS for 2.5 min. Yet, there was a trend towards destabilization with 2DG- and towards stabilization with short Phenformin- and EBSS-treatment (supplementary table S5). Only 2 h-treatment with a novel AMPK-activator, A-769662 (Cool et al., 2006) consistently caused a slight decrease in the amount of myc-ULK1 bound to AMPK α 2 (Fig. 4.9).

In summary, these experiments did not result in a uniform picture of how AMPK-activity influences its interaction with ULK1. Considering the results obtained with A-769662, the most specific AMPK-activator currently available (Bin Zheng, personal communication), the effect of AMPK-activity appears to be minor and thus easily could have been overridden by off-target effects of the other compounds, the primary target of which (except for AICAR) is not AMPK. Therefore, the results presented here imply that AMPK-activity is not a major determinant of ULK1-AMPK-complex stability, at least in COS7 cells.

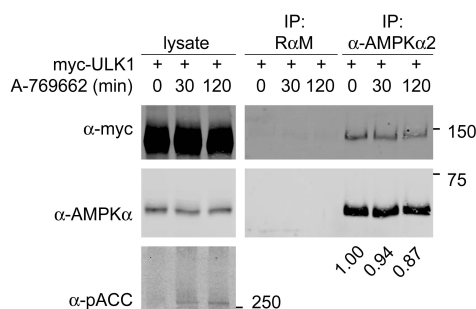


Figure 4.9. Stability of the ULK1-AMPK-complex is largely independent of AMPK-activity. Myc-ULK1-infected COS7 cells were treated with 100 μ M A-769662 for the times indicated to activate AMPK, as reflected in phosphorylation of its substrate Acetyl-CoA carboxylase (pACC). Cell lysates were subjected to immunoprecipitation with AMPK α 2-specific rabbit antibodies or non-specific rabbit anti-mouse antibodies (R α M) as a control. Western blot analysis was performed with the antibodies indicated. Western blot signals were quantitated and numbers below the IP-panel indicate the relative amount of ULK1 bound to AMPK, calculated as $(\text{myc-ULK1}^{\text{IP}}/\text{myc-ULK1}^{\text{TCL}})/(\text{AMPK}^{\text{IP}}/\text{AMPK}^{\text{TCL}})$. The result shown is representative for three independent experiments.

4.4 Phosphorylation of ULK1 by AMPK

4.4.1 AMPK and ULK1 as potential targets of each other

Our previous experiments demonstrated an interaction between ULK1 and AMPK, further strengthening the hypothesis that at least one of these kinases phosphorylates the other. Since the scaffolding subunit of the AMPK-heterotrimer, Sip2/AMPK β 2, that had been identified as an *in vitro* Atg1-substrate (Ptacek et al., 2005) did not meet our most stringent requirements for experimental validation because the predicted Atg1-sites were not evolutionary conserved (cf. section 4.1.2), we searched the yeast and the human catalytic Snf1/AMPK α - and regulatory Snf4/AMPK γ -subunits for Atg1-sites; Snf1 and Snf4 were not included as substrates in the screen of Ptacek *et al.* Scansite-analysis revealed, among other sites, one conserved site each in AMPK α and AMPK γ . The site in AMPK α , corresponding to Ser173 in the human α 2-isoform immediately follows the critical activation loop threonine and is present in all AMPK α -subunits of all organisms examined. The site in AMPK γ , Ser416 in human AMPK γ 3 (the longest isoform), lies just adjacent to the end of the third CBS-domain that is important for AMP- and ATP-binding. At this site, at least one AMPK γ -isoform of

each organism examined completely or closely matches the Atg1 consensus phosphorylation motif. In summary, this bioinformatic analysis predicts AMPK α and AMPK γ , rather than AMPK β , as candidate substrates for Atg1/ULK1 (Fig. 4.10).

Atg1-motif: G/A/V/I/L/M-x-x-S/T-G/A/V/I/L/M/F/W/C-G/A/V/I/L/M/F/W/C

		Conserved sites			
AMPKα	hsAMPKa1	159	DFGLSNMMSDGEFLRTS	CGSPNYAAPE	185 S175
	hsAMPKa2	157	DFGLSNMMSDGEFLRTS	CGSPNYAAPE	183 S173
	dmSNF1A	169	DFGLSNMMLDGEFLRTS	CGSPNYAAPE	195 S185
	ceAAK1	165	DFGLSNYMTDGDLLSTAC	GSPNYAAPE	191 A181
	ceAAK2	228	DFGLSNIMTDGDFLRTS	CGSPNYAAPE	254 S244
	spSSP2	174	DFGLSNIMTDGNFLKTS	CGSPNYAAPE	200 S190
	scSNF1	191	DFGLSNIMTDGNFLKTS	CGSPNYAAPE	221 S211
Additional sites					
AMPKγ	hsAMPKg3	408	QTYNHLDMSVGEALRQR		424 S416
	hsAMPKg1	253	KTYNNLDVSVTKALQHR		269 S261
	hsAMPKg2	485	KTYNNLDITVTQALQHR		501 T493
	dmSNF4A	394	KTYNDLDVSLRKANEHR		410 S402
ceAMPKg5	370	HQGGNFHDMLKEPVKIL		386 M378	
ceAMPKg4	381	N-FIEPKRWLQETKVS		396 W388	
ceAMPKg3	280	N-RLDITVKEALAFKSQ		295 K287	
ceAMPKg2	335	D-HIDLSVSVTRAIQER		350 S342	
ceAMPKg1	434	SSYDKLDCTVQEALQHR		450 T442	
spYL28	244	GDYSNLDLSVGEALLKR		260 S252	
scSNF4	248	GIYNDLSLSVGEALMRR		264 S256	

hsAMPKα1 T23, T28, S202, S242	hsAMPKβ1 T80	hsAMPKγ1 S144, T325
hsAMPKα2 T21, T26, S240, S355, S545, T549	hsAMPKβ2 T79, S249	hsAMPKγ2 S124, S376, T519
scSNF1 T60, S65, T355	scSIP2 S161	hsAMPKγ3 T87, T208, T299, S336
		scSNF4 S47, S61, S163

Figure 4.10. Conservation of predicted Atg1-sites in AMPK α and γ of various model organisms. Shown are parts of the ClustalW-alignments of the protein sequences of all AMPK α and γ isoforms present in *Saccharomyces cerevisiae* (sc), *Schizosaccharomyces pombe* (sp), *Caenorhabditis elegans* (ce), *Drosophila melanogaster* (dm) and *Homo sapiens* (hs) surrounding conserved predicted Atg1-sites. Atg1-sites were detected using the Scansite-function “Search input sequence by input motif” and the Scansite-matrix given in Materials and Methods, table 3.5. Sequences are ordered according to increasing divergence from the *S. cerevisiae* protein. Residues specified by the Atg1-motif are color-coded. Residues identical with the residue in the *S. cerevisiae*-protein are shaded in light gray, chemically similar amino acids are shaded in dark gray. Numbers indicate the first and the last sequence position shown in the alignment and the sequence position of the phosphorylated Ser/Thr-residue or the residue aligning to it. For the AMPK α -homologs, the entire activation loop sequences are shown. Additional, non-conserved Atg1-sites in all human and yeast AMPK-subunits are listed as well. Note: The Atg1-consensus phosphorylation motif specified here and used for all analyses was communicated by B. Turk, the subsequently published paper by Mok *et al.* provides a slightly different version: [LM(GISTCVD)]XXS/T[VIMFCLWYST][YIFMWVLHCST].

On the other hand, we investigated the possibility that Atg1 may be an AMPK-substrate by Scansite-analysis. Although Atg1 was included as a substrate in the screen of Ptacek *et al.*, Snf1 was not among the kinases tested. AMPK is a highly selective kinase,

exhibiting preference for particular residues at six out of the nine amino acid positions flanking the phosphorylated serine or threonine (Gwinn et al., 2008). Refined Scansite-search revealed ten potential AMPK-sites in ULK1 matching the target motif at three to five of the six selected positions (Fig. 4.12). Although none of these sites is absolutely conserved across all species, at eight of the ten sites, the motif is shared between ULK1 and ULK2, the closely related kinase in mammalian cells. Furthermore, seven sites, S494, S555, S637, T659, S693, S774 and S1043, were found to be phosphorylated in our phosphoproteomic mass spectrometry studies (cf. table 4.1).

	Optimal AMPK-motif	LRRVxS/TxxNL		14-3-3 mode 1 binding motif
	Secondary selections	MKKSxS/TxxDV		R(K)S(X)xS/TxP(S/G)
	Additional selections	IxxRxxS/TxxEI		
mmULK1	SAI RR SG ST TP L	S467	mmULK1	PP R NR T LP-D L T659
mmULK2	AV V RRS-NTSPM T441		mmULK2	QSKDGNDPREC N637
dmULK	GG Q R P QQQQ N QS Q423			
ceUNC51	SA V SAQH Q H Q H Q 429		mmULK1	F G RS F ST S R I S693
spATG1	H P TI S ST Q LSNE Q449		mmULK2	F G RS V ST G KL S679
scATG1	I K H P T S T Q N Q NV Q463			
			mmULK1	I E RR L S A LLS S1043
mmULK1	I P R-ET S AP L R S248		mmULK2	I E RR L S A LCC S1028
mmULK2	I P R-ET S PY L A S241		dmULK	VE K RL S IL Q Q S840
dmULK	I P S-G V SP D LR S244		ceUNC51	VE K RL R IL E R R843
ceUNC51	I P E-W C SP N LR S245			
spATG1	PE E AFI H PD I K H277		mmULK1	I A R K LS L GGG S494
scATG1	PS Y C N IE P EL K E295		mmULK2	G G RR L ST G SS S467
			dmULK	P A RR Q VA R PG V451
mmULK1	L G C R L H S A P N L S555		ceUNC51	Q L PR R T L Q D T457
mmULK2	L G A R L Q S A P T L S528		spATG1	-----V F Q G S V472
dmULK	P P TR M RS A SGG S512		scATG1	EN P RL L R A T S L491
ceUNC51	D Q ML S N L D P TT L518			
spATG1	E Q A T A H V P Q S G V531		mmULK1	I P K P P T D E L-----G A T T574
scATG1	Q Q IT S SP P Y S Q P553		mmULK2	L R K Q H S D P V C PS H A G A G S547
			dmULK	T P PP H A P -----S T A526
mmULK1	F P K T PS S Q N L S637		ceUNC51	I P K S A T T-----A N S530
mmULK2	I P K T Q A SS N L A615		spATG1	S A L E R A L N V A N A R L N E V A547
dmULK	L G S I G S A G S G S579		scATG1	L F H E L T E N I I -L R I D H L T569
ceUNC51	I K N Q T T C S T S T589			
spATG1	L E S I A M K S N S M605		mmULK1	R T R M F S V G S S S774
scATG1	E N RR S M D S N A M636		mmULK2	R T R T T S V G S S S751

Figure 4.11. Conservation of predicted AMPK-sites in ULK1-homologs of various model organisms. Shown are parts of the ClustalW-alignment of the protein sequences of the Atg1-homologs from *Saccharomyces cerevisiae* (sc), *Schizosaccharomyces pombe* (sp) *Caenorhabditis elegans* (ce), *Drosophila melanogaster* (dm) and *Mus musculus* (mm) surrounding predicted AMPK-sites in murine ULK1. To detect these sites, the sequence of murine ULK1 was searched for the AMPK-motif using the Scansite-function “Search input sequence for input motif” and the matrix given in Materials and Methods, table 3.6. Sites are sorted in the order of increasing divergence from the ideal AMPK-motif. Residues specified by the AMPK-motif are color-coded. Numbers depict the sequence position of the phosphorylated Ser/Thr-residue or the residue aligning to it. Also shown is the 14-3-3 mode 1 binding motif that overlaps with the AMPK-motif at the positions -3 and -2 (cf. section 4.4.3).

4.4.2 An AMPK motif antibody detects basal phosphorylation of ULK1

To address the question of whether AMPK phosphorylates ULK1, we first tested whether the latter reacted with a phosphospecific antibody raised against the sequence L/I-x-R-x-x-pS/T, which conforms to the AMPK motif (cf. Fig. 4.11; Doppler et al., 2005). Five of the predicted AMPK-sites in ULK1 (S248, S467, S494, T574 and S1043) match this sequence. Myc-ULK1 was stably overexpressed in COS7 cells and immunoprecipitated from the cell lysates with anti-myc-antibodies after various AMPK-activating treatments, i.e. AICAR, EBSS and A-769662. The AMPK motif antibody recognized myc-ULK1 isolated from untreated myc-ULK1 COS7 cells where AMPK activation was low, but detectable, and there was no apparent difference in reactivity towards myc-ULK1 isolated from cells where AMPK was strongly activated by AICAR, 2DG or EBSS (Fig. 4.12 and data not shown). Similarly, no change in reactivity with the AMPK motif antibody was seen for myc-ULK1 immunoprecipitated from wild type or AMPK α 1/ α 2-deficient MEFs (data not shown). These data suggest that the sites detected by the motif antibody under basal conditions are not regulated by AMPK but by a different kinase such as PKD, that phosphorylates a similar motif (Doppler et al., 2005).

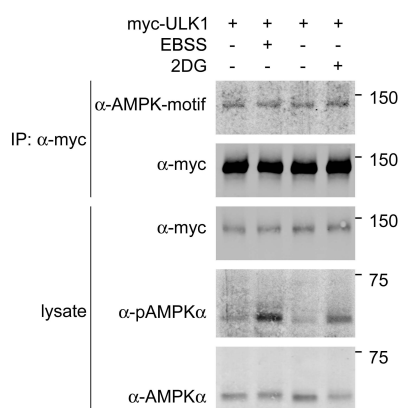


Figure 4.12. An AMPK motif antibody recognizes basal, but not inducible phosphorylation of ULK1 by AMPK or a kinase with similar specificity. COS7 cells infected with myc-ULK1 were treated with EBSS for 2.5 min or with 25 mM 2DG for 15 min to activate AMPK and myc-ULK1 was immunoprecipitated from the lysates with anti-myc-antibodies. Western blot analysis of cell lysates and immunoprecipitates was performed with the antibodies indicated.

4.4.3 AMPK-regulation of 14-3-3-binding to ULK1

The optimal sequence motif targeted by AMPK conforms in one of its versions to mode 1 of the 14-3-3-binding motif, R-S-x-pS/T-x-P (Yaffe et al., 1997). Scansite search for this motif in the sequence of murine ULK1 revealed up to 14 potential 14-3-3 binding sites, depending on the search method and stringency criteria chosen (data not shown). Eight of these sites were also found to be AMPK-sites (S248, S467, S494, S555, T659, S693, S774, 1043), including six sites (i.e. all except for S248 and S467) that we had detected to be

phosphorylated by mass spectrometry (cf. table 4.1). Thus, we hypothesized that phosphorylation of ULK1 by AMPK may lead to generation of 14-3-3-binding sites, as shown previously for other AMPK substrates (Gwinn et al., 2008).

4.4.3.1 GST-14-3-3-pulldown assays on exogenous and endogenous ULK1

To investigate the possibility of AMPK phosphorylating ULK1 to generate 14-3-3-binding sites, we employed a pulldown approach using GST-tagged bovine 14-3-3 ζ (Yaffe et al., 1997) as a bait. Lysates of COS7 cells stably overexpressing myc-ULK1 and subjected to AMPK-activating treatment with AICAR, 2DG, EBSS or A-769662, were incubated with plain or GST-14-3-3-coated glutathione sepharose beads, and binding of myc-ULK1 was analyzed by Western blot. Myc-ULK1 could be pulled down with GST-14-3-3, but not with glutathione beads alone, and the amounts of GST-14-3-3-bound myc-ULK1 increased upon AMPK-activation with any treatment applied. This indicated the presence of AMPK-dependent 14-3-3 binding sites in ULK1 (Fig. 4.13).

To determine if 14-3-3 binding was dependent on AMPK, we performed the GST-14-3-3 pulldown assay in lysates prepared from untreated or 2DG-treated wild type MEFs and from MEFs deficient for either one (α 1-KO, α 2-KO) or both isoforms (DKO) of the catalytic AMPK α -subunit. Whereas the amount of endogenous ULK1 pulled down with GST-14-3-3 increased with treatment-induced AMPK-activity in wild type cells, no change was seen in AMPK-DKO-MEFs. In addition, these cells displayed lower ULK1-expression levels, which at least in part may account for the reduction in 14-3-3-binding seen under basal conditions (cf. also section 4.5.3). Analysis of single knockout cells indicated that AMPK α 1 loss was sufficient for this decrease in ULK1-expression and baseline-association with 14-3-3. This is consistent with the observation that AMPK α 1 is the predominant isoform in fibroblasts (Bin Zheng, personal communication). Upon AMPK-activation, the amount of ULK1 pulled down by GST-14-3-3 still increased in AMPK α 1- and in AMPK α 2-KO cells (Fig. 4.14). Taken together, these results suggested that ULK1 may be phosphorylated by either AMPK α -isoform, and confirmed that increased 14-3-3-binding to ULK1 induced by 2DG-treatment was dependent on AMPK.

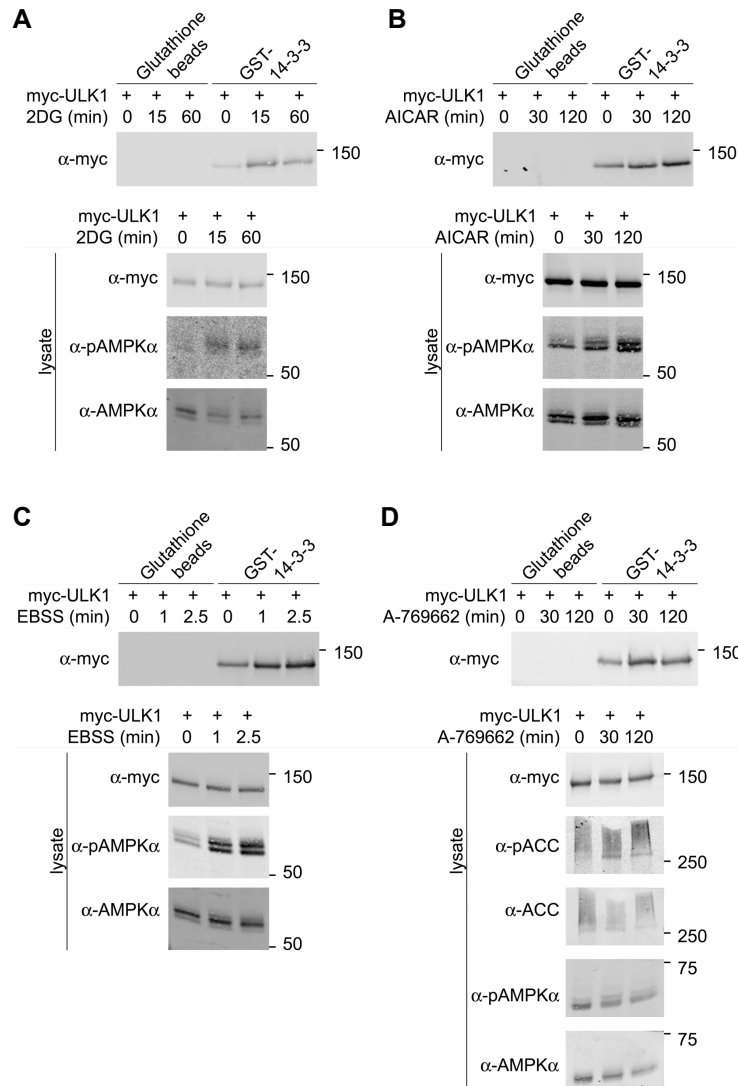


Figure 4.13. AMPK activation leads to increased 14-3-3 binding to myc-ULK1. COS7 cells infected with myc-ULK1 were treated with (A) 25 mM 2DG, (B) 1 mM AICAR, (C) EBSS or (D) 100 μ M A-769662 for the times indicated. Cell lysates were incubated with plain glutathione sepharose beads or with GST-14-3-3-coated glutathione sepharose beads, and pull-down of myc-ULK1 was analyzed by Western blot with the antibodies indicated.

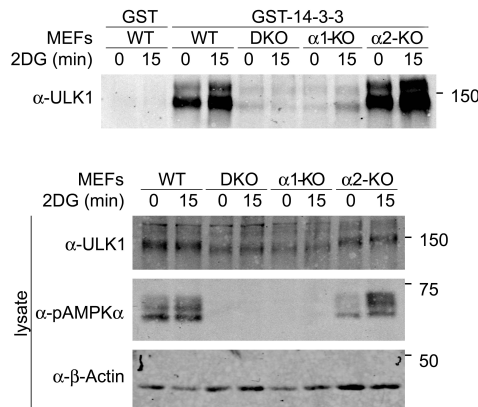


Figure 4.14. 14-3-3 binding to endogenous ULK1 is regulated by AMPK. Wild type (WT) MEFs and MEFs lacking the genes for both (DKO) or one of the AMPK α -isoforms (α 1-KO, α 2-KO) were treated with 25 mM 2DG for 0 or 15 min and endogenous ULK1 was pulled down with GST-14-3-3. The GST-tag alone served as a negative control. Western blot analysis was performed with the antibodies indicated.

4.4.3.2 Myc-ULK1 coprecipitates with endogenous 14-3-3

To confirm the interaction of ULK1 with 14-3-3 and its regulation by AMPK by an alternative method, we immunoprecipitated endogenous 14-3-3 from lysates of untreated and 2DG-treated wild type MEFs stably overexpressing myc-ULK1. As expected, the amount of myc-ULK1 coprecipitating with endogenous 14-3-3 increased with AMPK-activation, further demonstrating that AMPK regulates 14-3-3-binding to ULK1 (Fig. 4.15).

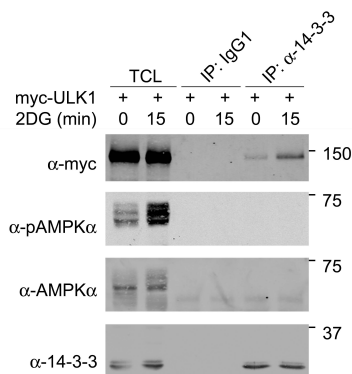


Figure 4.15. Myc-ULK1 coprecipitates with endogenous 14-3-3. Mouse embryonic fibroblasts stably overexpressing myc-ULK were treated with 25 mM 2DG for 0 or 15 min and endogenous 14-3-3 was immunoprecipitated using pan-14-3-3-antibodies or non-specific mouse IgG1 as a negative control. Western blot analysis was performed with the antibodies indicated.

4.4.4 Identification of AMPK-dependent 14-3-3 binding sites in ULK1

4.4.4.1 Mass spectrometry detects several AMPK-phosphorylation sites on ULK1

After establishing AMPK-dependent phosphorylation of ULK1 in the GST-14-3-3-pulldown assay, we aimed to identify the exact sites targeted by AMPK. Thus, we performed a second set of LC/MS/MS experiments using myc-ULK1 stably overexpressed in COS7 cells. Prior to lysis, cells had been subjected to AMPK-activating treatments with EBSS for 2.5 min or 2DG for 15 min. Only very few sites were detected under conditions of EBSS-treatment due to only 50 % of the protein sequence being covered by peptides. One of these sites, S537, had not been identified in the first experiment (cf. tables 4.1 and S3). Under 2DG-treated conditions, peptide coverage was higher (67 %) and two sites not identified previously were detected, S460 under basal conditions only, and S638 under both conditions (supplementary table S3). Yet none of these three novel sites corresponded to a predicted AMPK-site.

Three sites, S543, S494 (a potential AMPK-site) and T757, were detected in all three mass spectrometry experiments, although the treatment conditions under which these sites were detected (untreated vs. treated) varied. However, this was not considered an issue given the rapid induction and immediate inactivation of AMPK that we observed when subjecting cells to nutrient stress (cf. Fig. 4.7). This suggests that the stress cells experience when lysed under non-optimal conditions (cf. section 3.2.4.3.1) may also cause AMPK activation and

may explain why we and other groups detected phosphorylation of putative AMPK-sites even under nutrient-rich conditions. Alternatively, other kinases than AMPK may phosphorylate these sites. Additional predicted AMPK-sites that we repeatedly detected in at least two experiments were S637 and T659 (Fig. 4.16B). Quantitation of S637-phosphorylation revealed an approximately four-fold increase with 2DG-treatment and confirmed this site as a genuine AMPK-phosphorylation site (Fig. 4.16C). With regard to AMPK-dependent 14-3-3-binding sites in ULK1, S494 and T659 appeared to be the best candidates.

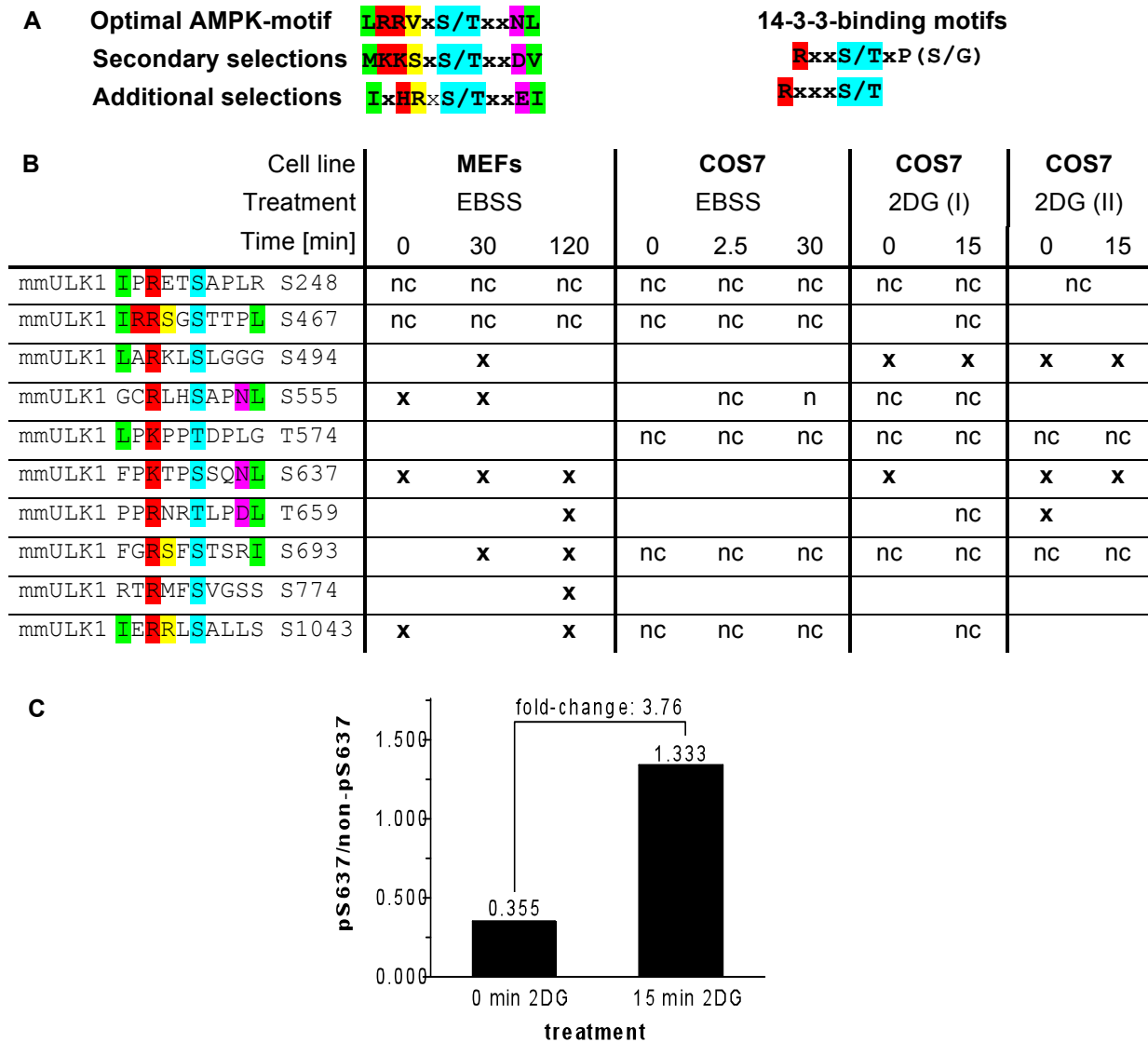


Figure 4.16. Identification of AMPK-phosphorylation sites in ULK1 by LC/MS/MS. (A) Optimal AMPK-phosphorylation- and 14-3-3-binding motifs (Gardino et al., 2006; Gwinn et al., 2008; Yaffe et al., 1997). Phosphorylated Ser/Thr residues or residues towards which AMPK and/or 14-3-3 exhibit selectivity, are highlighted. (B) Predicted AMPK- and 14-3-3-binding sites in ULK1 identified in this study by LC/MS/MS. Myc-ULK1 was stably overexpressed in MEFs or COS7 cells and cells were subjected to treatment with EBSS or 25 mM 2-Deoxyglucose (2DG) for the times indicated. Myc-ULK1 was immunoprecipitated using myc-tag specific antibodies. Conditions under which a site was detected are marked with “x”; “nc” denotes that the site was not covered by peptides. The phosphorylated Ser/Thr and residues specified by the AMPK- and 14-3-3-binding motifs are color-coded as in A. (C) Quantitation of ULK1 S637-phosphorylation in COS7 cells treated for 0 or 15 min with 25 mM 2DG.

4.4.4.2 GST-14-3-3 pulldown identifies two AMPK-dependent 14-3-3-binding sites in ULK1

Subsequently, we sought to identify AMPK-dependent 14-3-3 binding sites in ULK1. Therefore, we screened a series of ULK1-mutants in which a single serine residue within one of the potential AMPK- and/or 14-3-3-binding sites had been replaced by non-phosphorylatable alanine (S248A, S467A, S494A, S555A, T574A, S637A, T659A, S1043A) in the GST-14-3-3-pulldown assay. COS7 cells infected with wild type myc-ULK1 or one of the SA-mutants were treated with 2DG for 0 min or 15 min and GST-14-3-3 pulldown was performed with the lysates as described in section 4.4.3.1. For one of these mutants, S555A, we consistently observed lower baseline association with 14-3-3 in untreated cells. Furthermore, the treatment-induced increase in 14-3-3-binding was less pronounced in the S555A-mutant than in the wild type or in other mutants analyzed in parallel (Fig. 4.17A and data not shown). The remaining increase in 14-3-3-binding was blocked when in addition to S555, T659 was mutated to alanine. Single mutation of T659 to alanine however had only very little to no detectable effect on 14-3-3-binding relative to the wild type.

In an alternative approach, we examined a set of ULK1-mutants in which the confirmed AMPK-site S637 and three out of the four strong candidate AMPK/14-3-3-binding-sites, S467A, S494A, S555A and T659A, were mutated to alanines, leaving only one site available for phosphorylation. Quantitative Western blotting revealed that increased 14-3-3-binding to ULK1 upon AMPK-activation consistently occurred only in the mutants with intact S555 or T659. In summary, these data implied that S555 is the major and T659 a minor AMPK-dependent 14-3-3-binding site in ULK1 (Fig. 4.17B, C).

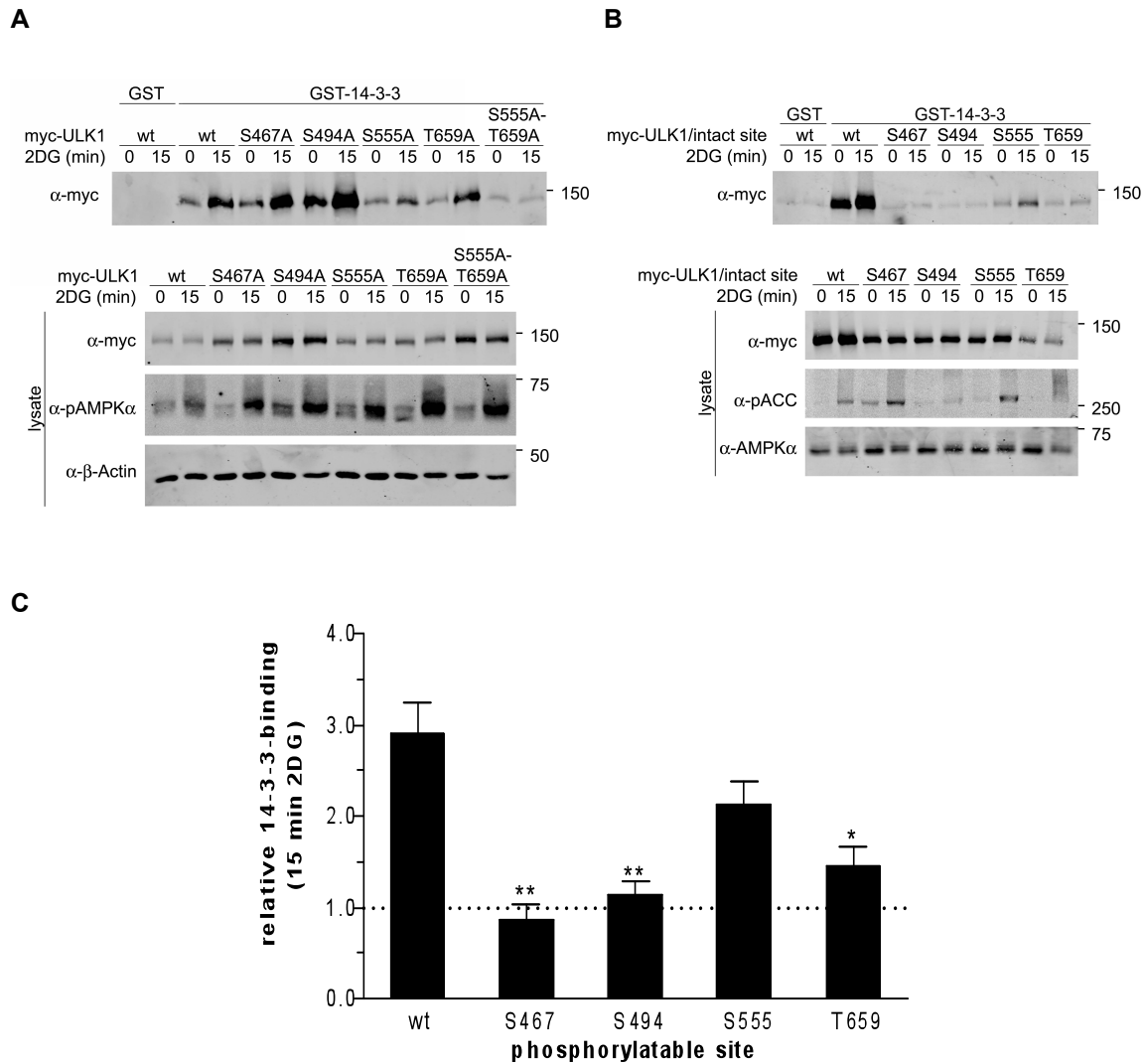


Figure 4.17. S555 and T659 are AMPK-dependent 14-3-3 binding sites in ULK1. (A) Wild type (wt) or non-phosphorylatable serine-to-alanine mutants of myc-ULK1 at potential AMPK- and/or 14-3-3-binding sites (S467A, S494A, S555A, T659A and the S555A-T659A-double mutant) were stably overexpressed in COS7 cells. Following treatment with 25 mM 2-Deoxyglucose (2DG) for 0 or 15 min, myc-tagged ULK1-variants were pulled down from the cell lysates with GST-14-3-3. The GST-tag alone served as a negative control. Precipitates and lysates were analyzed by Western blot with the antibodies indicated. (B) 2DG-treatment and GST-14-3-3-pulldown as described in (A) were performed on COS7 cells stably overexpressing myc-tagged ULK1-quadruple-mutants in which the AMPK-site S637 and three out of the four potential 14-3-3-binding sites examined in (A) were mutated to alanine, leaving only one site available for potential phosphorylation and 14-3-3-binding. (C) Quantitative Western blot analysis of the experiment described in (B). Western blot-signals were quantified and 14-3-3-binding was calculated for each myc-ULK1-construct and condition as $[\text{ULK1}^{\text{GST-14-3-3}} / (\text{ULK1}^{\text{TCL}} / \text{AMPK}^{\text{TCL}})]$, to account for differences in expression of the ULK1-mutants and in loading. Relative 14-3-3-binding was calculated as 14-3-3-binding at 15 min 2DG divided by 14-3-3-binding at 0 min 2DG of the same ULK1-construct. The bar graph shows the average values of relative 14-3-3-binding obtained in five independent experiments. Error bars indicate standard errors of the mean, the dotted line indicates the baseline association at 0 min 2DG, which was set to “1” for each ULK1-construct. Statistical significance was calculated using unpaired T-tests. Two asterisks indicate statistical significant differences in relative 14-3-3-binding (nominal P-value < 0.05) compared to wt and S555, one asterisk indicates a statistical significant difference (nominal P-value < 0.05) to wt only. A complete data table is given in supplementary table S6.

4.4.4.3 AMPK phosphorylates ULK1 *in vitro*

Our mass spectrometry and biochemical analyses strongly suggested that ULK1 may be a novel AMPK-substrate and identified ULK1-residues S555, S637 and T659 as the AMPK-phosphorylation sites. To further confirm this, we conducted *in vitro* kinase assays on purified heterotrimeric AMPK. As substrates, various affinity-tagged ULK1-proteins isolated from HEK293T cells were used.

In one type of experiment, we aimed to determine whether AMPK is able to phosphorylate sites in the kinase domain and/or in the C-terminal domain, which we had not identified by mass spectrometry and/or the GST-14-3-3-pulldown assay. In these experiments, AMPK was found to phosphorylate full length kinase defective ULK1, the isolated spacer region and the C- or N-terminally truncated ULK1-fragments, but not the isolated kinase- or C-terminal domains. Furthermore, we observed ULK1-autophosphorylation only for the fragment lacking the C-terminal domain, but not for the isolated kinase domain (Fig. 4.18A). These data indicated that the ULK1-spacer region is required for ULK1-autophosphorylation and confirmed that the spacer region is the only ULK1-domain that contains AMPK phosphorylation sites.

A second type of experiment was conducted to validate ULK1-residues S555, S637 and T659 that we had identified as AMPK-phosphorylation-sites by mass spectrometry or GST-14-3-3-pulldown assay, by an alternative method. To avoid ULK1-autophosphorylation in these experiments, kinase defective versions (K46A-substitution) of all mutants to be examined were generated. These mutants were S637A, S555A-T659A and S555A-S637A-T659A, in which either the major AMPK-site *in vivo* (S637) or the two AMPK-dependent 14-3-3-binding sites (S555, T659) or all three AMPK-phosphorylation sites had been replaced by non-phosphorylatable alanine residues. Furthermore, a 6A-mutant was generated, in which three other predicted AMPK-sites (S467, S494, T574) were substituted by alanines in addition to the three sites of interest (S555, S637, T659). As shown in Figure 4.18B, alanine-substitution of S637 alone resulted in an approximately 50 % decrease in ULK1-phosphorylation, whereas mutation of S555 and T659 together only reduced ULK1-phosphorylation by approximately 30 %. The effects of the S637A-, S555A- and T659A-mutations on AMPK-dependent ULK1-phosphorylation were additive and were not further enhanced by introduction of three additional point mutations on candidate AMPK-sites, i.e. S467A, S494A and T574A. Taken together, these studies confirmed S555A, S637A and T659A as AMPK-sites, with S637A as the major site *in vitro* and *in vivo*, and did not provide evidence for additional AMPK phosphorylation sites in ULK1.

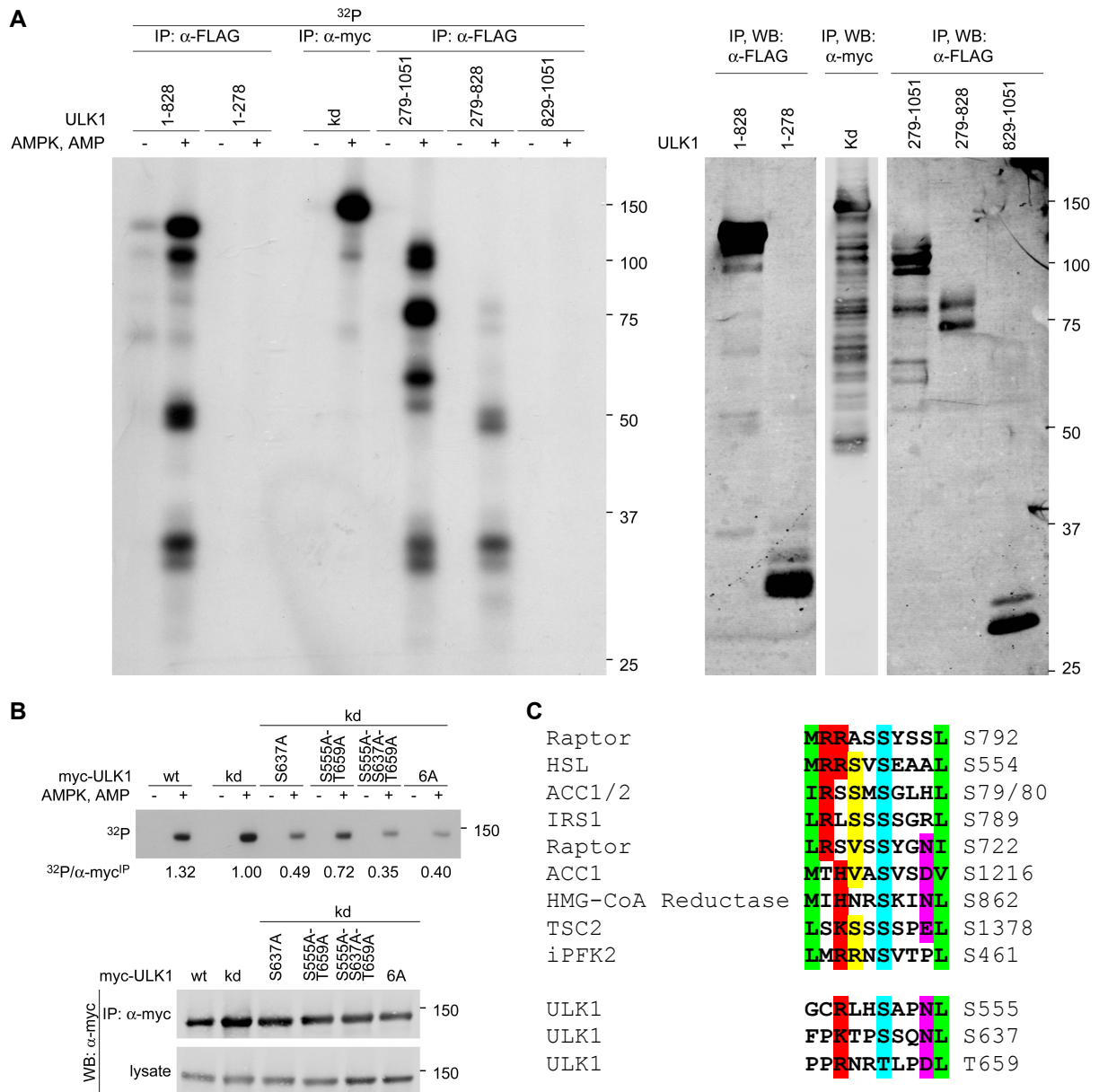


Figure 4.18. AMPK phosphorylates ULK1 *in vitro*. (A) AMPK phosphorylates ULK1 in the Ser/Pro-rich spacer region. Kinase defective (kd) myc-ULK1 or FLAG-tagged ULK1-fragments comprising kinase domain and spacer region (1-828), kinase domain alone (1-278), spacer region and C-terminal domain (279-1051), spacer region alone (279-828) or C-terminal domain alone (829-1051) were transiently overexpressed in HEK293T cells, immunoprecipitated from the cell lysates with antibodies against the affinity tag and used as substrates in *in vitro* kinase assays on purified AMPK. For each substrate, one reaction was performed without AMPK and AMP to control for phosphorylation by coprecipitating kinases and ULK1-autophosphorylation where applicable. Phosphorylation of the substrates was determined by incorporation of ³²P and autoradiography. Successful immunoprecipitation of the ULK1-fragments was verified by subjecting 1/3 of the precipitates to Western blot analysis with the antibodies indicated. (B) S637 is the major site in ULK1 phosphorylated by AMPK *in vitro*. Myc-tagged wild type and kinase defective ULK1, and the kinase defective mutants indicated (6A: S467A-S494A-S555A-T574A-S637A-T659A) were transiently expressed in HEK293T cells and immunopurified and used as substrates in *in vitro* kinase assays as in (A). Efficient precipitation and expression of the ULK1-constructs was monitored by Western blot. ³²P- and Western blot signals were quantified and phosphorylation efficiency was calculated as the ratio of the ³²P-signal divided by the Western blot signal in the IP of the same ULK1-fragment. (C) Comparison of the experimentally validated AMPK-dependent 14-3-3 binding sites in ULK1, S555 and T659, and the AMPK-phosphorylation site identified by mass spectrometry, S637, with known AMPK-sites in other proteins (adapted from Gwinn et al., 2008). Sequence positions towards which AMPK/14-3-3 are selective are highlighted as in Fig. 4.11 and 4.16. For evolutionary conservation of the sites in ULK1, see Fig. 4.11.

4.4.5 ULK1-overexpression induces hyperphosphorylation of AMPK

In our previous coimmunoprecipitation experiments to validate the interaction between ULK1/2 and AMPK, we repeatedly noted broadening of the Western blot band for immunoprecipitated or coprecipitated AMPK α when wild type, full length ULK1/2 were overexpressed, but not with overexpression of a control vector or a mutant lacking the N-terminal kinase domain (cf. Fig. 4.3 and Fig. 4.5). Thus, and given our bioinformatics analyses that predicted all AMPK-subunits as potential ULK1-substrates (cf. section 4.4.1 and Fig. 4.10), we examined ULK-dependent AMPK phosphorylation more closely (Fig. 4.19).

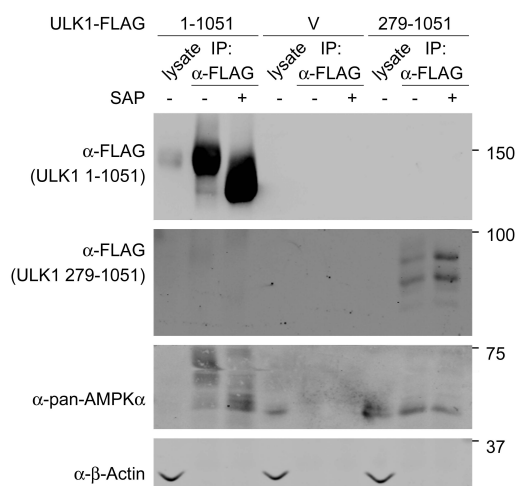


Figure 4.19. Hyperphosphorylation of AMPK α is induced by ULK1-overexpression and dependent on the ULK1-kinase domain. HEK293T cells were transfected with full length (1-1051) ULK1-FLAG or an empty vector (V) or an ULK1-FLAG-mutant deleted for the kinase domain (279-1051), and ULK1-FLAG-proteins were immunoprecipitated from the cell lysates using anti-FLAG antibodies coupled to agarose beads. Following IP, precipitates were split into two samples and one was treated with shrimp alkaline phosphatase (SAP) while the other was mock-treated. Lysates and precipitates were analyzed by Western blot with the antibodies indicated.

The experiments outlined in section 4.3.3, which were primarily conducted to verify hyperphosphorylation of the AMPK-associated ULK-population, already had revealed that myc-AMPK α 2 precipitated from ULK1/ULK2-overexpressing cells run as a sharper band when treated with shrimp alkaline phosphatase (SAP), and this band resembled the bands obtained for myc-AMPK α 2 from vector control transfected cells regardless of SAP-or mock-treatment (Fig. 4.6). To verify that this hyperphosphorylation required ULK-kinase activity, full length- or kinase-domain-deleted ULK1-FLAG were overexpressed in HEK293T cells and immunoprecipitated from the lysates with anti-FLAG-agarose, and precipitates were dephosphorylated by SAP-treatment and analyzed by Western blot. In ULK1-FLAG expressing cells, the signal for coprecipitated endogenous AMPK α was shifted to a higher molecular size in the mock-treated relative to the SAP-treated sample. Moreover, the molecular size observed in the SAP-treated sample corresponded to that observed for endogenous AMPK α coprecipitated with kinase-domain-deleted ULK1-FLAG irrespective of

mock- or SAP-treatment (Fig. 4.19). This implied that AMPK α hyperphosphorylation caused by ULK-overexpression requires their kinase activity, suggesting that ULKs either directly phosphorylate AMPK α or initiate a kinase-cascade that leads to phosphorylation of AMPK α .

4.5 Regulation of ULK1 by AMPK

4.5.1 Destabilization of the ULK1-Raptor interaction is independent of AMPK activity

Our previous studies had identified a direct biochemical link between autophagy and energy-sensing, consisting of the interaction between two major kinases in each pathway, ULK1 and AMPK, and of phosphorylation of ULK1 by AMPK. Subsequently, we aimed to elucidate the functional significance of this dual connection. Interestingly, ULK1 and mTORC1 have been reported to interact with each other under nutrient-rich conditions via the mTORC1-component Raptor, another AMPK-substrate (Gwinn et al., 2008; Hosokawa et al., 2009a). Since dissociation of mTORC1 from ULK1 is an early event in starvation-induced autophagy, and on the other hand, the role of AMPK in autophagy-induction is undefined at present, we investigated whether AMPK regulates induction of autophagy by regulating the interaction of ULK1 and mTORC1. HEK293T cells were transiently transfected with ULK1-FLAG and wild type or kinase defective (K45A-mutation) myc-AMPK α 2 and subjected to starvation with EBSS for 0 or 4 h. ULK1-FLAG was immunoprecipitated from the cell lysates and coprecipitation of the mTORC1-component Raptor was assessed by Western blot. The amount of Raptor associating with ULK1-FLAG was decreased in starved cells overexpressing either form of myc-AMPK α 2, indicating that AMPK-activity is not required to destabilize the ULK1-mTORC1-interaction (Fig. 4.20).

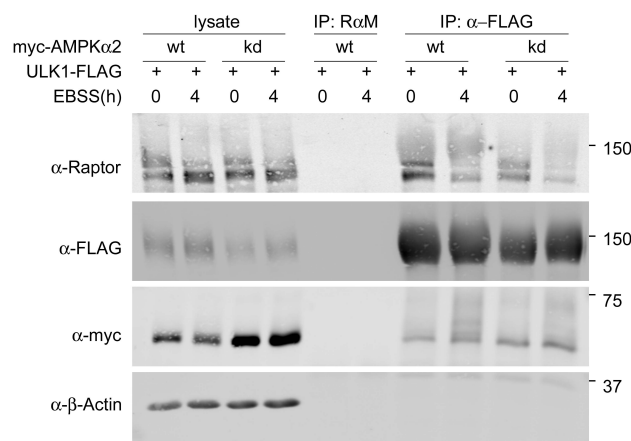


Figure 4.20. AMPK-activity is not required to destabilize the interaction of ULK1 with mTORC1. HEK293T cells were cotransfected with ULK1-FLAG and either wild type (wt) or kinase defective (kd) myc-AMPK α 2 and subjected to starvation with EBSS for the times indicated. ULK1-FLAG was immunoprecipitated from the cell lysates using anti-FLAG-agarose and lysates and precipitates were analyzed by Western blot with the antibodies indicated.

4.5.2 p62-degradation is normal in AMPK-deficient MEFs

Given its poorly characterized function in autophagy, we examined the basic requirement of AMPK in this process using a genetic approach. Wild type MEFs and MEFs deficient in the genes for both isoforms of the catalytic AMPK α -subunit (AMPK-DKO-MEFs) were subjected to starvation with EBSS for up to 12 h and activation of autophagy was monitored by quantitative Western blot analysis of p62-protein levels. p62/SQSTM1 is an autophagic cargo adaptor protein that is efficiently degraded during the process, and this degradation has been demonstrated to adequately reflect increased flux of substrates through the autophagy system in numerous studies (Mizushima et al., 2010). Our experiments revealed that p62-turnover upon complete nutrient- and growth factor deprivation was essentially normal in AMPK-DKO-MEFs (Fig. 4.21A, B). Furthermore, other starvation treatments, i.e. removal of growth factors alone, or treatment with 2DG (to mimic glucose deprivation) or a combination of both, also had the same effect on p62-levels in AMPK-DKO-MEFs than in wild type MEFs (Fig. 4.21C). These data implied that p62-turnover is not regulated by AMPK and suggested that this kinase is not required for autophagy under the conditions and within the time frame examined.

Despite normal p62-degradation upon EBSS-starvation, we noted a trend towards slightly elevated levels of p62-protein in AMPK-DKO-MEFs in the untreated state. Although this difference was not statistically significant, it may indicate inhibition of p62-degradation or conversely, transcriptional upregulation of p62-expression in these cells under physiological growth conditions, suggesting that basal autophagy is used differently in AMPK-DKO- than in wild type MEFs to maintain homeostasis (Fig. 4.21D).

4.5.3 AMPK-deficient MEFs have decreased ULK1 protein levels

In several experiments performed with AMPK-DKO-MEFs, ULK1-protein levels appeared to be reduced when compared to the ULK1-levels in wild type MEFs (cf. Fig. 4.14). To systematically confirm this observation, Western blot signals for endogenous ULK1 in wild type and AMPK-DKO-MEFs were quantified and normalized to a loading control (Actin or Tubulin) in 18 independent experiments. Indeed, ULK1-levels in DKO-MEFs were found to be decreased to approximately 70 % of the wild type level, and this reduction was statistically significant (Fig. 4.22A). This suggested that AMPK either regulates ULK1-expression at the transcriptional level or controls ULK1-protein stability, potentially by direct phosphorylation.

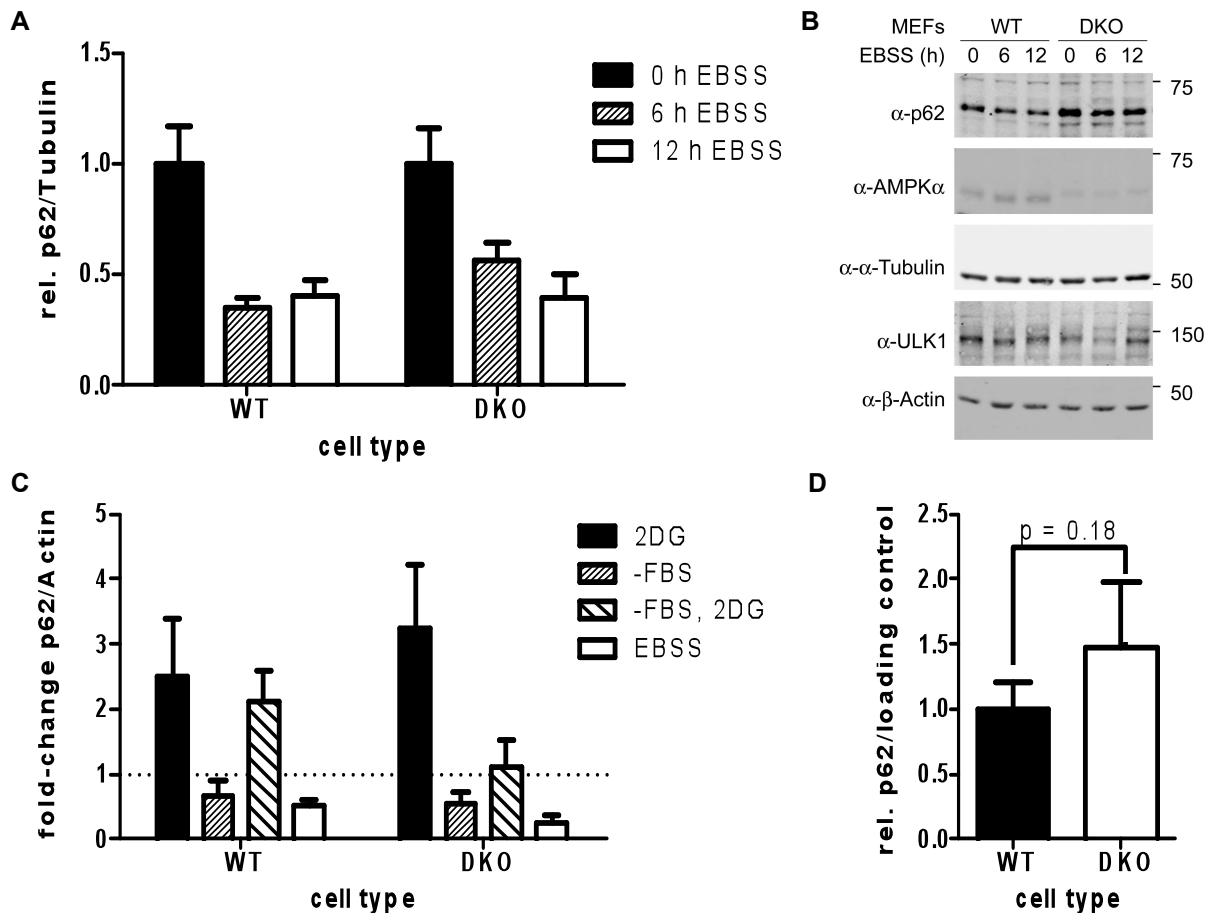


Figure 4.21. AMPK-deficient MEFs display normal starvation-induced turnover, but slightly elevated basal levels of p62. (A) Quantitative Western blot analysis of p62-levels in wild type (WT) MEFs and MEFs deficient in the genes for both AMPK α -subunits (DKO) in response to EBSS-starvation for 6 and 12 h. In each sample, the p62-signal was normalized to the signal of the loading control Tubulin. Plotted are mean values of the p62/Tubulin-ratios relative to the mean p62/Tubulin-ratio at 0 h in the same cell type obtained from 6 independent experiments. Error bars indicate standard errors of the mean. (B) One representative experiment for the quantitative analysis described in (A). In this particular experiment, ULK1-levels were also quantified (cf. Fig. 4.22A). (C) WT and DKO-MEFs were subjected to EBSS-starvation as in (A) and to various other starvation treatments (2DG: 25 mM 2-Deoxyglucose; -FBS: serum-free DMEM; -FBS, 2DG: 25 mM 2DG in serum-free DMEM) for 12 h, and levels of p62- and Actin (loading control) were analyzed by Western blot. Western blot signals were quantified and for each cell type and treatment, the fold-change in the p62/Actin-ratio relative to the p62/Actin-ratio in untreated cells (incubated in DMEM for 12 h) of the same cell type was determined. Plotted are the mean fold-changes in the p62/Actin-ratios \pm standard errors of the mean obtained from four independent experiments. The dotted line indicates the p62/Actin-ratios in untreated cells which were set to "1". (D) Quantitation of Western blot signals for p62 and a loading control-protein (Actin or Tubulin) in untreated WT- and DKO-MEFs from 11 independent experiments. In each sample, the p62-signal was normalized to the loading control-signal. Plotted are mean values of the p62/loading control-ratios relative to the mean p62/loading control-ratio in WT cells. Error bars indicate standard errors of the mean. To test statistical significance, a paired T-test was used.

We also examined changes of ULK1-protein levels in wild type and AMPK-DKO-MEFs upon treatment with EBSS and 2DG for up to 16 h. In both cell types, ULK1-levels oscillated, but we were unable to determine a precise timely pattern from the limited number of experiments performed ($n = 3$). Only at the late time points (12h and 16 h) of each treatment, ULK1-levels consistently were slightly reduced in wild type MEFs and elevated in

DKO-MEFs (data not shown). The same trend was observed in a second set of three independent experiments and in response to serum deprivation or combined serum- and glucose deprivation, with the latter mimicked by 2DG-treatment (Fig. 4.22B). Such late treatment-induced changes of ULK1-protein-levels into opposite directions in the presence and absence of AMPK would indicate that AMPK negatively affects ULK1-stability only with prolonged starvation, implying that these are the only conditions under which ULK1-regulation by AMPK occurs or is not/no longer antagonized by other factors.

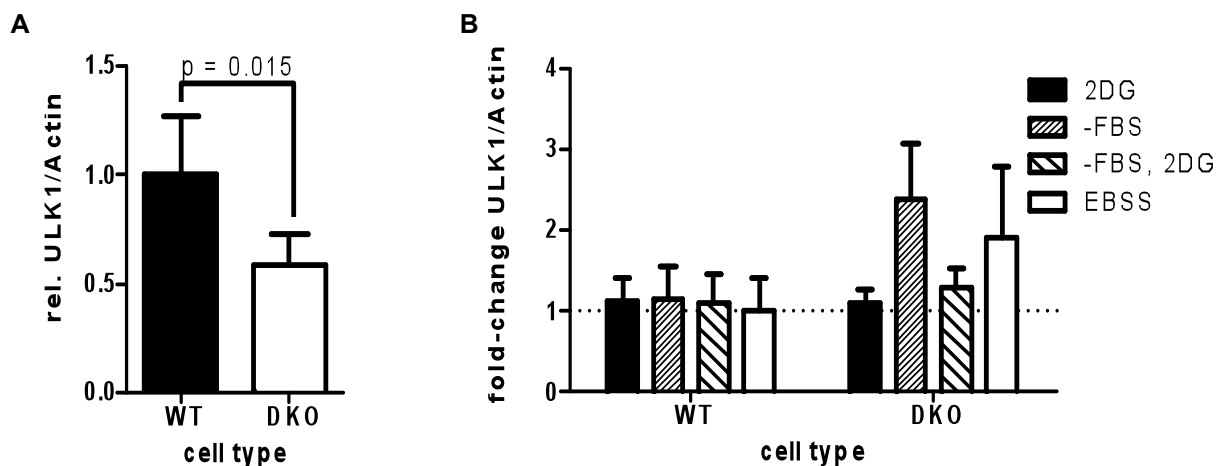


Figure 4.22. AMPK-deficient MEFs display reduced ULK1-protein levels. (A) Quantitation of Western blot signals for endogenous ULK1 and Actin (loading control) in 12 independent experiments. In each sample, the ULK1-signal was normalized to the Actin-signal. Plotted are mean values of the ULK1/Actin-ratios relative to the mean ULK1/Actin-ratio in WT cells. Error bars indicate standard errors of the mean. Statistical significance was determined by paired T-test. For one representative experiment, see Fig. 4.21.B. Statistical significant differences between ULK1-levels in WT and DKO MEFs were also obtained in a set of six independent experiments where Tubulin was used as the loading control (data not shown). (B) WT and DKO-MEFs were subjected to various starvation treatments as in Fig. 4.21B (2DG: 25 mM 2-Deoxyglucose; -FBS: serum-free DMEM; -FBS, 2DG: 25 mM 2DG in serum-free DMEM) for 12 h, and ULK1- and Actin-levels were analyzed by Western blot. Western blot signals were quantified and for each cell type and treatment, the fold-change in the ULK1/Actin-ratio relative to the ULK1/Actin-ratio in untreated cells (incubated in DMEM for 12 h) of the same cell type was determined. Plotted are the mean fold-changes in the ULK1/Actin-ratios +/- standard errors of the mean obtained from three independent experiments. The dotted line indicates the ULK1/Actin-ratios in untreated cells which were set to "1".

4.5.4 ULK1-overexpression is not sufficient to substantially restore energy-stress tolerance in AMPK-deficient MEFs

AMPK-deficient MEFs are less resistant to nutrient- and energy stress than wild type MEFs and more susceptible to cell death under these conditions (Williams et al., 2009). To address the question whether AMPK-dependent increased stress resistance also required ULK1, we compared the effect of long-term 2DG-treatment (30 h), which resembles glucose deprivation, on cell survival of wild type and AMPK-DKO-MEFs overexpressing wild type or kinase defective ULK1 or a control vector. While untreated cells (cultured in regular growth media) of all cell types continued to proliferate during the time of the experiment (data not shown),

2DG-treatment caused an arrest in cell growth in wild type cells and substantial cell death in DKO-cells (Fig. 4.23A). In the series of 13 repetitions of this experiment, overexpression of either form of ULK1 did not seem to improve or diminish stress resistance of wild type cells (Fig. 4.23B). In DKO-cells however, we consistently observed slightly higher cell survival with overexpression of wild type or kinase defective ULK1 than with overexpression of the control vector, and this increase in cell survival was statistically significant ($p < 0.0006$). Furthermore, the positive effect on survival of DKO-cells was not significantly different between overexpression of wild type and of kinase defective ULK1 (Fig. 4.23C). Nevertheless, wild-type ULK1-infected DKO-MEFs were still significantly less resistant to energy stress than wild-type ULK1-infected wild type MEFs, and the same was observed for kinase defective ULK1-infected wild type and DKO-MEFs (Fig. 4.23D, E). Therefore, we concluded that overexpression of ULK1 is not able to substantially rescue resistance to nutrient- and energy stress in DKO-MEFs, implying that a potential positive role of ULK1 in this context required its interaction with and/or phosphorylation by AMPK.

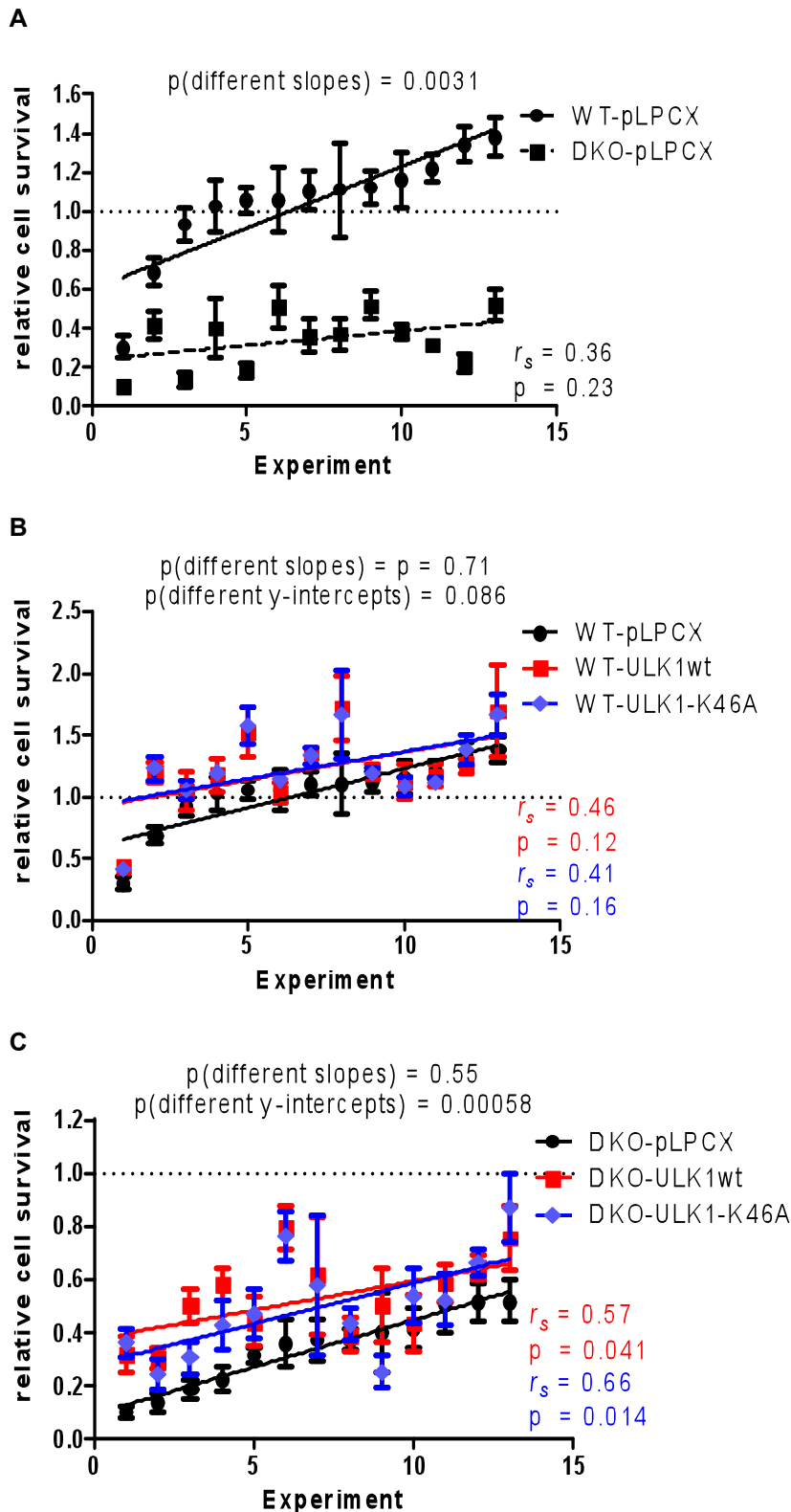
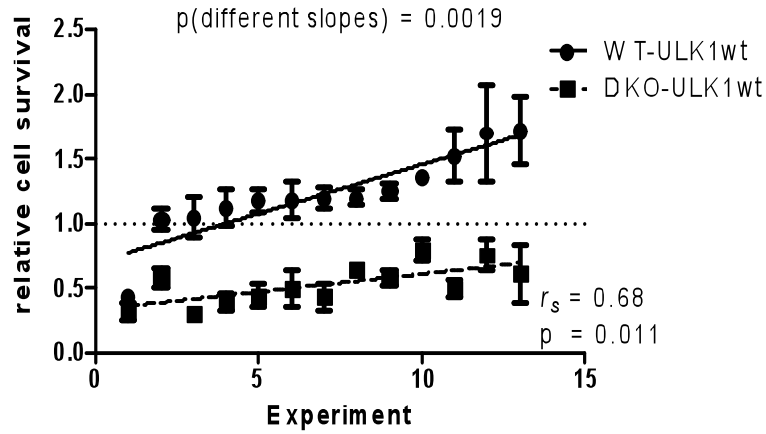


Figure 4.23. ULK1-over-expression is not able to substantially rescue resistance to nutrient- and energy stress caused by loss of AMPK. Wild type (WT) MEFs and MEFs deficient in the genes for both AMPK α -subunits (DKO) were infected with either a control vector (pLPCX) or with wild type ULK1 (ULK1wt) or a kinase defective ULK1-mutant (ULK1-K46A). Cells were seeded in triplicate on 12 well plates and either subjected to 30 h incubation in full media or in full media containing 25 mM 2DG, or fixed at the beginning of the treatment to obtain the cell numbers at 0 h. Cell numbers were determined by crystal violet staining and normalized to the cell number at 0 h of the same cell type. The following graphs show relative cell survival of the various cell types after 30 h of 2DG-treatment in 13 independent experiments. Each data point represents one independent experiment performed in triplicate, and error bars indicate standard deviations. The dotted line at $y = 1$ represents the cell numbers at 0 h. Data analysis was performed using Spearman rank correlation tests. P-values and Spearman rank correlation coefficients (r_s) are given in each graph. **(A)** 2DG-treatment causes cell death in DKO-MEFs but not in wild type MEFs. Experiments were sorted according to relative survival of WT-pLPCX-MEFs. Note the significant difference in the slopes of the straight (WT) and the dashed lines (DKO) in the graph. Due to these difference, statistical significance of the difference in the y-intercepts cannot be calculated.

(B) Overexpression of ULK1wt or -K46A does not alter stress resistance of wild type MEFs. Experiments were sorted according to relative survival of WT-pLPCX-MEFs. Note the non-significant differences in slopes and y-intercepts of the red (ULK1wt), blue (ULK1-K46A) and black line (pLPCX) in the graph. There is no significant difference in the slopes ($p = 0.9702$) or the y-intercepts ($p = 0.9455$) of the red and the blue line. **(C)** Overexpression of ULK1wt or -K46A increases cell survival of DKO-MEFs. Experiments were sorted according to relative survival of DKO-pLPCX-MEFs. Note the significant difference in the y-intercepts of the red (ULK1wt) and the blue (ULK1-K46A) line from the black line (pLPCX) in the graph. There is no significant difference in the slopes ($p = 0.5647$) or the y-intercepts ($p = 0.5455$) of the red and the blue line.

D



E

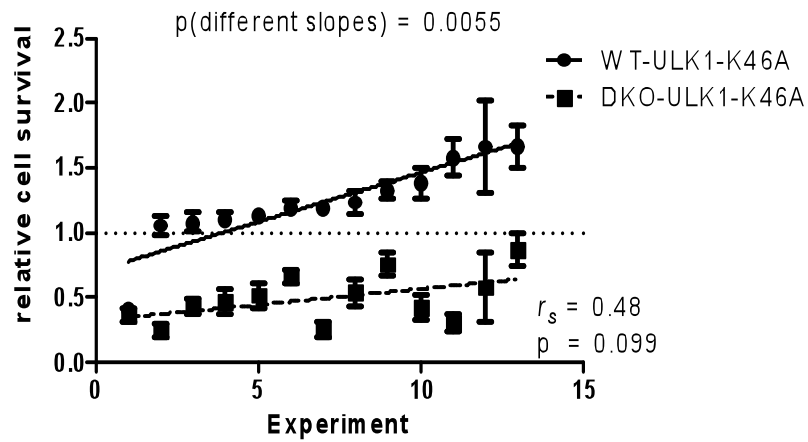


Figure 4.23. Continued. (D, E) Overexpression of (D) ULK1wt or (E) ULK1-K46A has different effects in WT- and DKO-MEFs. Experiments were sorted according to relative survival of WT-ULK1wt- and WT-ULK-K46A-MEFs, respectively. Note the significant differences in the slopes of the straight (WT) and the dashed lines (DKO) in the graphs. Due to these differences, statistical significance of the differences in the y-intercepts cannot be calculated.

5 Discussion

Upregulation of autophagy is a common cellular response to a variety of cellular stress conditions, however, the signaling networks regulating this process are only beginning to be elucidated. In this thesis work, we investigated regulation and function of the kinase ULK1, a putative key regulator of autophagy induction in mammalian cells. We discovered that ULK1 is differentially modified by phosphorylation depending on nutrient conditions, and predicted kinases targeting and potentially regulating ULK1. Based on our analysis of published proteomics data, we also suggested 30 candidate substrates of ULK1, and identified two novel ULK1-interacting proteins, INPP4B and AMPK. We comprehensively characterized the ULK1-AMPK-complex and validated ULK1 as a direct substrate of AMPK, thereby establishing a previously unknown direct connection of energy sensing and autophagy.

5.1 Potential substrates and novel functions of ULK1

5.1.1 Predicted substrates of ULK1 during autophagy and axon guidance

Our bioinformatics analysis of a published proteomics data set of *in vitro* substrates for the kinase Atg1 (Ptacek et al., 2005), the ULK1-homolog in yeast, revealed a subset of 30 proteins that, based on their known cellular function, may provide a mechanistic explanation of how Atg1/ULK1 regulates autophagy (cf. tables 4.3 and S4). While some candidates are obvious, such as Atg-proteins or kinases or proteins involved in vesicular trafficking, other predicted substrates point to novel links between autophagy and certain other cellular processes or structures. For example, potential phosphorylation of Phosphofructokinase 2 (PFK2) by Atg1/ULK1 may couple energy homeostasis to autophagy, either as part of the ULK1-AMPK-signaling axis we describe here, or as an additional or alternative mechanism (cf. section 5.2.3). Furthermore, our bioinformatics data contains hypothetical connections of Atg1/ULK1 to the actin cytoskeleton and associated structures such as focal adhesions. This is interesting with regard to the fact that ULK1 has been reported to localize to focal contacts (Hara et al., 2008). These results have several implications: (1) cytoskeletal and focal adhesion reorganization or proteins associated with these structures might be required for autophagy; this view is supported by the results of a study that demonstrated a requirement for the focal adhesion component Paxillin in autophagosome formation (Chen et al., 2008); (2) upon exposure to stresses like nutrient deprivation, disassembly of focal adhesions might not be required for autophagy but is induced in parallel- via Atg1/ULK1- to allow the cell to migrate to a more favorable environment; and (3) ULK1 might regulate actin dynamics completely independent from its role in autophagy. In general it appears likely that autophagy is not the only process regulated by ULK1, considering that this kinase is constitutively active

(although at a higher level during starvation) and exists in several distinct complexes within the cell (Chan et al., 2009; Hara et al., 2008; Hosokawa et al., 2009b). Importantly, regulation of cytoskeletal rearrangements and of vesicular trafficking processes other than autophagy may also account for ULK1's function in axonal development, based on which it was originally identified in nematodes and mammalian cells (Tomoda et al., 1999; Tomoda et al., 2004). Indeed, in *C. elegans*, axon formation seems to be independent of autophagy, since silencing of Atg-genes, except for the Atg1-homolog Unc-51, did not cause abnormalities. Instead, correct axon outgrowth requires Unc-51-mediated relocalization of Unc-6, a receptor for guidance molecules, from the cell body to the axon, presumably by a specialized form of vesicular transport (Ogura and Goshima, 2006). Of note, several predicted Atg1/ULK1-substrates already have been shown by themselves to participate in neuronal processes, e.g. PIP5K β (Halstead et al., 2010), PIP5K γ (Di Paolo et al., 2002) and CRN2B (Nakamura et al., 1999). Yet, it is also possible that ULK1-phosphorylation of a given substrate might be important for both, autophagy and axon guidance. In particular, a recent study demonstrated physical association of PP2A with Unc-51 and thus suggested a role for PP2A in axon development in *C. elegans*, while PP2A in yeast has been shown to regulate autophagy (Ogura et al., 2010; Yorimitsu et al., 2009). In conclusion, it appears very promising to experimentally validate the Atg1/ULK1-substrates we propose here in the context of autophagy and of axon guidance, to more precisely characterize known functions of Atg1/Unc-51/ULK1 or to uncover novel regulatory roles of these kinases.

5.1.2 ULK1, INPP4B and phosphoinositide signaling

The type II Inositol-polyphosphate 4-phosphatase, INPP4B, is a candidate substrate of ULK1 that we discovered based on its ability to coprecipitate with this kinase. Even though we were unable to detect phosphorylation of INPP4B by ULK1 *in vitro* under physiological growth conditions, the only condition we examined, it is possible that phosphorylation occurs, yet only under specialized conditions, e.g. upon starvation. Alternatively, lack of INPP4B-phosphorylation by ULK might have been due to technical issues, e.g. the use of N-terminally instead of C-terminally tagged INPP4B- and ULK1-constructs (cf. also section 5.2.6). Lastly, it is possible that INPP4B-regulation by ULK1 is independent of ULK1 catalytic activity. Of note, it has been reported previously that the catalytic activity of the ULK1-homolog in yeast, Atg1, is dispensable for some of its functions during autophagy (Abeliovich et al., 2003).

A possible link of INPP4B to autophagy comes from its ability to hydrolyze PI(3,4)P₂ to generate PI(3)P, the phospholipid that is central to autophagosome nucleation. However, it is unlikely that this pathway constitutes a novel important, alternative or additional, source for

PI(3)P because the cellular levels of the substrate for this reaction, PI(3,4)P₂ are much lower than those of PI, which is converted into PI(3)P by the class III PI3-Kinase, hVps34 (Gewinner et al., 2009). Although INPP4B is absent in lower eukaryotes, other regulators of phosphoinositide signaling have been identified as *in vitro*-Atg1-substrates in yeast (cf. tables 4.3 and S4), including the PI(3)P-binding Atg-proteins Atg18 and Atg21, the inositol hexakisphosphate and diphosphoinositol-pentakisphosphate (IP₆/PP-IP₅)-kinase Vip1, and the phosphatidylinositol 4-phosphate 5-kinase (PIP5K) Mss4 (Barth et al., 2002; Desrivieres et al., 1998; Guan et al., 2001; Mulugu et al., 2007). This suggests that ULK1 may exert some of its regulatory activity during autophagy by altering the levels of certain phosphoinositides, and that INPP4B's role in yeast is taken over by different lipid-phosphatases. INPP4B in higher organisms is expected to be inhibited by inositol hexakisphosphate, the substrate for VIP1, and to be able to hydrolyze not just PI(3,4)P₂, but also PI(4,5)P₂, the product of PIP5Ks α , β and γ , although experimental evidence confirming or disproving these potential connections is still missing (Uniprot-entry O15327 on human INPP4B).

The predicted INPP4B-substrate, PI(4,5)P₂, affects actin cytoskeleton rearrangements and cell motility, focal adhesion turnover, cell-cell-contacts and clathrin-mediated endocytosis (van den Bout and Divecha, 2009). Therefore, it is tempting to speculate that the reported cellular effects of INPP4B-depletion by RNAi, i.e. increased anchorage independent growth and cell motility, and a potential role for INPP4B in autophagy, are not solely related to its ability to decrease PI(3,4)P₂-levels and thus, PI3K-AKT-mTOR-signaling. Indeed, modulation of the cellular PI(4,5)P₂-pools by INPP4B may be predicted to have the same effects. Taken together, further studies are required to clarify the complex picture arising from currently available *in silico*, *in vitro* and *in vivo* data on physical and functional interactions of ULK1 and multiple players in phosphoinositide signaling pathways.

5.2 Regulation of ULK1 and autophagy by AMPK

5.2.1 General role of ULK1, ULK2 and AMPK

Studies from several groups published in the past three years have confirmed ULK1 as a regulator of autophagy (as was expected from its homology to the autophagy-initiating kinase Atg1 in yeast) and began to elucidate how its biological activity is controlled. The work presented here uncovers ULK1 as a direct substrate and interaction partner of AMPK and thus establishes a previously unknown direct connection of energy sensing and autophagy. Given that ULK1 is also targeted by mTORC1 and potentially PKA, as suggested by studies in yeast demonstrating PKA-phosphorylation of Atg1 and Atg13 (Stephan et al., 2009), our data

confirm the view of ULK1/Atg1 constituting a central node in the autophagy signaling network.

In addition, we showed that ULK2, a second Atg1-homolog in mammalian cells and close relative of ULK1, could also interact with AMPK, and our bioinformatics analyses indicate that it may also be subject to phosphorylation by AMPK. Of note, only one out of three validated AMPK phosphorylation sites in ULK1 is present in ULK2, namely S528, corresponding to the major 14-3-3-binding site in ULK1, S555. This suggests that ULKs may be important effectors of AMPK, and that ULK2 may only be able to compensate for some, but not for all of ULK1's AMPK-dependent functions.

The fact that AMPK phosphorylates the important Atg-protein ULK1 strengthens the view that this kinase itself may play an important role in autophagy regulation. Although AMPK has been reported to be involved in this process under numerous conditions and in different organisms, its precise function remains controversial (Grotemeier et al., 2010; Herrero-Martin et al., 2009; Hoyer-Hansen et al., 2007; Liang et al., 2007; Meley et al., 2006; Papandreou et al., 2008; Wang et al., 2001; Williams et al., 2009). The picture emerging from the currently available literature suggests that AMPK-regulation of autophagy may be dependent on the cell type and the nature and/or duration of the autophagy-inducing stimulus. Moreover, our observation that AMPK is strongly active only after long-term starvation indicates that this kinase may be required for maintenance and further upregulation of the process upon prolonged stress, but not for its induction. Although our finding that AMPK is only weakly active in cells subjected to complete nutrient withdrawal is surprising at the first glance, this might simply reflect the fact that a cell may be able to quickly adapt to this condition and to reprogram its metabolism to become independent from external nutrients to produce ATP, which then might inhibit AMPK again. It will be interesting in the future to perform metabolomic studies on cells undergoing autophagy to precisely characterize this adaptation.

It is important to emphasize that the signaling-pathways that so far have been reported to converge on ULK1, including the AMPK-pathway as described in this thesis, are stress-sensitive; thus, our work further highlights the importance of ULK1 in stress-induced autophagy. It does not imply, however, that this kinase (or its related kinase ULK2) is required for all types of autophagy, in particular not for basal autophagy which physiologically facilitates turnover of cellular components.

5.2.2 Effects of AMPK-phosphorylation and 14-3-3-binding to ULK1

Although there is evidence that AMPK is required at late stages of autophagy, considering that AMPK-knockout-MEFs die earlier than wild type cells when deprived of glucose (cf. Fig. 4.23), it is unlikely that AMPK on its own is necessary and/or sufficient to induce autophagy (Williams et al., 2009). Given this observation, it appears counterintuitive that AMPK phosphorylates ULK1, a potential key modulator in autophagy-induction as is shown in this thesis. However, we demonstrated that a short initial wave of AMPK-activity immediately after withdrawal of all nutrients is sufficient to induce increased 14-3-3-binding to ULK1. This may constitute a switch to irrevocably enter the autophagy pathway. Binding of 14-3-3 may serve to regulate ULK1's catalytic activity, its interaction with other proteins including its substrates, or its intracellular localization. Our preliminary data from immunofluorescence studies in MEFs stably overexpressing the S555A-T659A double mutant defective in AMPK-dependent 14-3-3-binding suggest that the latter may be the case. Moreover, the interaction of 14-3-3 with ULK1 raises the possibility that 14-3-3 itself may be an important autophagy-regulator in its own right. Yet, since the major AMPK-phosphorylation site of ULK1, S637, is not a 14-3-3-binding site, AMPK may also regulate activity, stability or interactions of ULK1 directly and independently of 14-3-3.

5.2.3 Function of the ULK1-AMPK-complex

While the association of ULK1 and AMPK might reflect a simple kinase-substrate complex, bioinformatics analysis suggests an additional possibility: Several Atg-proteins, including Beclin-1, Atg9, Atg12, and Atg18 contain potential AMPK-sites, implying that AMPK may regulate autophagy at multiple steps of the pathway, not just at the level of ULK1. Interestingly, these proteins also contain Atg1 phosphorylation sites. Therefore, it is attractive to speculate that AMPK and ULK1 regulate autophagy in concert by phosphorylating common substrates including the Atg-proteins mentioned above. The fact that at least in certain cell lines the ULK1-AMPK-complex can persist upon exposure to nutrient- and energy-stress would greatly facilitate such coordinated action. Dual phosphorylation of substrates by AMPK and ULK1 may increase efficiency and/or selectivity of autophagy-initiation or -stimulation. Furthermore, ULK1 with its capacity to serve as a scaffolding protein, may mediate precise localization of AMPK to autophagy-related substrates. In this case, only basal AMPK activity, which is necessary for autophagy (Meley et al., 2006) would be required. Indeed, our findings indicate, that there is no general activation of the entire cellular AMPK-pool during short periods of starvation.

Of note, common AMPK- and Atg1/ULK1-substrates are not only predicted among Atg1-proteins but also include cytoskeletal and cytoskeleton-associated proteins such as Paxillin, metabolic enzymes such as PFK2, and regulators of phosphoinositide signaling such as INPP4B and PIP5K α . To test the hypothesis of concerted action of ULK1 and AMPK, one will need to map the AMPK-binding site in ULK1 more precisely and examine the AMPK-dependent aspect of ULK1 activity by reexpressing an AMPK-binding defective ULK1 mutant in ULK1^{-/-}-MEFs. In addition, it will be interesting in the future to investigate whether AMPK-dependent resistance to nutrient- and energy stress is mediated by ULK1. This would require overexpression of phosphomimetic ULK1-mutants at the AMPK-phosphorylation sites in AMPK α 1/ α 2-double-knockout-MEFs. However, given the vastly different phenotypes of AMPK α 1/ α 2-double- and of ULK1-single-knockout-mice (embryonically lethal vs. viable; Kundu et al., 2008; Viollet et al., 2009), it is highly unlikely that the two kinases absolutely require each other under all conditions to fulfill their regulatory roles, whatever the precise function of their interaction and of AMPK-phosphorylation of ULK1 may be.

5.2.4 Overlap of the ULK1-AMPK-complex with known ULK1- and AMPK-complexes

Previous studies have demonstrated that the majority of cellular ULK1, together with its constitutively associated regulatory proteins FIP200, mAtg13 and the mAtg13-binding protein Atg101, is incorporated into a large multiprotein complex of approximately 3 MDa. Under nutrient rich conditions this complex also contains mTORC1. Within this complex, ULK1 binds to Raptor, and mTOR suppresses ULK1-dependent autophagy initiation by phosphorylating ULK1 and mAtg13. Interestingly, the interactions of ULK1 with AMPK and of ULK1 with Raptor both are stable under nutrient rich conditions, and Raptor is another AMPK-substrate, phosphorylation of which inhibits mTORC1-activity. Thus, it is attractive to speculate that mTORC1, ULK1 and AMPK are all assembled into a common complex and that one aspect of ULK1 function in autophagy-initiation consists in placing AMPK in close proximity to the autophagy-suppressor mTORC1. This would allow immediate phosphorylation of Raptor and derepression of autophagy when energy levels drop. Yet, several of our experimental observations do not support such a model. (1) We found that in the absence of AMPK activity, which prevents phosphorylation of Raptor, the ULK1-Raptor-interaction is still destabilized upon nutrient withdrawal, implying that phosphorylation of Raptor is not required for disruption of the ULK1-mTORC1-complex and for subsequent induction of autophagy; (2) we were not able to detect coprecipitation of Raptor and AMPK,

although we cannot exclude that this is due to technical limitations, and (3) only a small fraction of ULK1 is bound to AMPK, whereas the major ULK1-population is recruited to the mTORC1-complex. These last two findings indicate that the ULK1-AMPK- and the ULK1-mTORC1-complexes are distinct. Of note, other groups have reported the presence of a second, less abundant, smaller (300-500 kDa) and up to now uncharacterized ULK1-complex, which might account for the ULK1 pool that is associated with AMPK (Fig. 5.1; (Chan et al., 2009; Hosokawa et al., 2009a).

Another possibility is that the ULK1-AMPK-complex overlaps with a previously described AMPK-complex. In particular, AMPK has been reported to associate with its substrate TSC2 in a manner that is dependent on the p53 target genes Sestrin1 and Sestrin2, which also play a role in autophagy (Budanov and Karin, 2008; Maiuri et al., 2009a). We did not observe TSC2 coprecipitating with ULK1 in COS7 cells under physiological growth conditions or after 4 h of starvation, i.e. conditions under which we readily detected interaction of AMPK and ULK1 (data not shown). However, it is unclear whether this starvation treatment was able to induce Sestrin-expression, which would have been required for connecting TSC2 to AMPK and ULK1. Thus, we cannot exclude that under conditions different from physiological growth conditions, the ULK1-AMPK-complex, which based on our studies is likely to be constitutively assembled (at least in certain cell lines), is identical to other known AMPK-complexes that only form upon exposure to particular stresses.

5.2.5 Conservation of the AMPK-ULK1 signaling module

In the first study proposing a role for the yeast AMPK homolog SNF1 in autophagy, this kinase intriguingly seemed to function upstream of Atg1 (Wang et al., 2001). Subsequent work in mammalian cells that still requires full confirmation in yeast, nevertheless provides an explanation for this observation by dissecting a multi-step, two-branched signaling pathway from AMPK to mTOR and ULK1: either via TSC2 or via Raptor (Corradetti et al., 2004; Gwinn et al., 2008; Inoki et al., 2003). The work presented in this thesis demonstrates that ULK1 is also subject to direct regulation by AMPK. Such multiple connections of AMPK and ULK1 (and potentially ULK2) raise the question of why in higher organisms, that many signaling axes were established between the same proteins. Lower eukaryotes from yeast to *C. elegans* lack a TSC2-ortholog, eliminating one possibility for AMPK to signal to Atg1. In contrast, one validated AMPK-phosphorylation site in human and murine Raptor is well conserved in the orthologous proteins of *S. cerevisiae*, *S. pombe*, *C. elegans* and *D. melanogaster* (Gwinn et al., 2008). Moreover, the ULK1-homologs of all species contain serine or threonine residues that at least to a certain extent match the AMPK consensus

phosphorylation motif and/or the 14-3-3 binding motif. Yet, none of the predicted or confirmed AMPK/14-3-3 sites is absolutely conserved (cf. Fig. 4.11 and data not shown), implying that the direct regulation of ULK1 by AMPK may be evolutionary conserved but that the precise mechanism might differ between species. This would not be unprecedented, considering that mTORC1-regulation of the ULK1-Atg13-FIP200-complex also has diverged during evolution (Mizushima, 2010). Taken together, the dual connection of AMPK to ULK1, the direct one and the indirect one via Raptor, might represent an ancient mechanism to tightly couple energy sensing to autophagy (Fig. 5.1). In theory, this provides a way for fine-tuning the autophagy response to the precise intensity and duration of the stress stimulus, and ensures that a backup mechanism is available when one pathway is blocked. Furthermore, it suggests that AMPK and ULK1 and their respective homologs in other species might be of central reciprocal importance to each other in the regulation of autophagy.

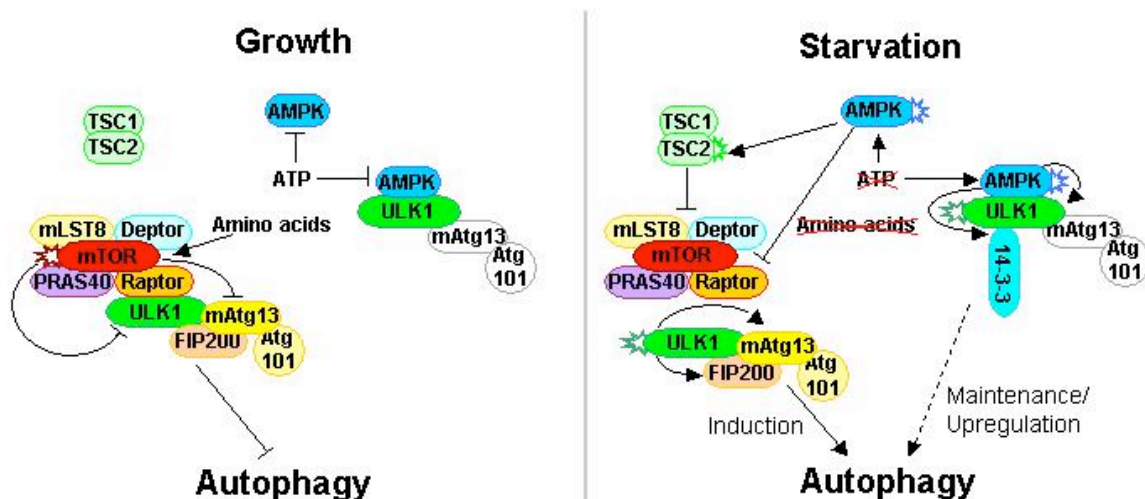


Figure 5.1. Extended model of autophagy regulation by ULK1 in mammalian cells. Under physiological growth conditions, the major ULK1-population forms a complex with the regulatory proteins FIP200, mAtg13 and the mAtg13-associated protein Atg101. This ULK1-mAtg13-Atg101-FIP200-complex enters into a higher order complex that also contains the mTOR-Raptor-PRAS40-mLST8-Deptor-complex (mTORC1). mTOR is activated by amino acids and suppresses autophagy under these conditions by inhibitory phosphorylation of ULK1 and mAtg13. Minor ULK1 populations have been reported to be bound in a smaller complex, which might contain mAtg13 and Atg101, but not FIP200. We propose that the ULK1-AMPK-complex we describe here accounts for such a minor ULK1-complex. Consequently only a minor fraction of the cellular AMPK-pool is recruited into this complex, too. Whether mAtg13/Atg101 is present in the ULK1/AMPK complex has not been examined yet. AMPK-activation is inhibited under nutrient-rich conditions by high levels of ATP. Upon starvation, ATP-levels decrease a AMPK is transiently activated and may contribute to mTORC1 inhibition by activating phosphorylation of TSC2 and inhibitory phosphorylation of Raptor. mTORC1 is also no longer activated by amino acids and dissociates from the ULK1-mAtg13-Atg101-FIP200-complex, and ULK1 kinase activity increases. ULK1 phosphorylates mAtg13 and FIP200 and potentially other Atg proteins to induce autophagy. In parallel, AMPK directly phosphorylates ULK1, which allows binding of regulatory 14-3-3-proteins. Whether or not the ULK1-AMPK-complex remains assembled under this conditions may be cell-type dependent. Our data suggest that AMPK is essential at late stages of autophagy for maintenance or stimulation of the process and that this may be mediated by ULK1. Yet, it is still possible that the mTOR-dependent and the direct branch of AMPK signaling to ULK1 are equally important when AMPK is active and participates in modulation of autophagy.

5.2.6 Feedback regulation of ULK1-, AMPK- and mTOR-signaling

The work presented in this thesis, as well as previously published reports (Corradetti et al., 2004; Ganley et al., 2009; Gwinn et al., 2008; Hosokawa et al., 2009a; Inoki et al., 2002; Inoki et al., 2003; Jung et al., 2009; Manning et al., 2002; Potter et al., 2002; Vander Haar et al., 2007), reveal a complex triangular relationship between two central stress-sensitive kinases, mTORC1 and AMPK, and the autophagy-related kinase ULK1. The multiple interconnections between these three include interactions between ULK1 and mTORC1 and between ULK1 and AMPK, presumably in distinct complexes. Our results suggest that AMPK does not influence the interaction of mTORC1 and ULK1, however, it is unclear at present whether mTORC1 regulates the interaction of ULK1 with AMPK. Furthermore, AMPK phosphorylates mTORC1 and ULK1 (Gwinn et al., 2008), and mTORC1 phosphorylates ULK1 (Hosokawa et al., 2009a), placing ULK1 at the bottom of this signaling cascade. However, several experimental results indicate that mTORC1 and AMPK are also subject to feedback regulation by ULK1. This comprises two aspects: First, ULK1-dependent autophagy will generate nutrients and energy, which will restore mTORC1 activity and AMPK inhibition, and a recent study suggested that this is indeed important for self-limitation of autophagy (Yu et al., 2010). Second, ULK1 may initiate signal transduction cascades targeting AMPK and/or mTORC1. Previous work in *Drosophila* demonstrated that Atg1 signals to TORC1, as indicated by the finding that Atg1 is able to interfere with phosphorylation of S6-kinase by TOR (Lee et al., 2007b). On the other hand, our work provides evidence for ULK signaling to AMPK, since AMPK α is hyperphosphorylated when full length ULK1 or ULK2, but not an ULK1-mutant lacking the kinase domain, is overexpressed. Of note, signaling to AMPK would be sufficient for ULK1 to modulate the function of both, mTORC1 and AMPK, since AMPK tightly regulates mTORC1 activity.

Multiple putative mechanisms of how ULK1 may positively or negatively regulate mTORC1 and/or AMPK emerge from the current literature and from bioinformatics and proteomics analyses. In particular, the ULK1-binding partner FIP200 can antagonize AMPK function at the level of the TSC1/2-complex, thus being a potential mediator of a negative feedback loop influencing AMPK and mTORC1 (Gan et al., 2005). A potential signaling cascade from ULK1 to mTORC1 that does not involve AMPK originates from mTORC2, whose component Avo1 (mSIN1 in mammals) is an *in vitro*-Atg1-substrate. This hypothesis is still valid, even though we could not formally show mSIN1 to be a substrate or an interaction partner of ULK1. However, this might have been caused by the fact that we utilized an N-terminally tagged mSIN1-construct in our experiments. N-terminally tagged

mSIN1 is unable to participate in mTORC2 (Frias et al., 2006), implying that mSIN1 function is severely disturbed, including possible interactions with other proteins such as ULK1.

Alternative hypothetical routes for ULK1 to signal to AMPK include direct phosphorylation of AMPK-subunits, all of which contain putative Atg1-phosphorylation sites, and a more indirect connection through the Elm1 kinase. Elm1 has been identified as an *in vitro* Atg1-substrate (Ptacek et al., 2005) Even though Elm1 is unique to yeast, its closest mammalian relative, CaMKK β , intriguingly is a known kinase upstream of AMPK (Fig. 5.2). It should be mentioned that in *in vitro* kinase assays involving kinase-active ULK1-fragments and heterotrimeric AMPK, no phosphorylation of any AMPK-subunit was detectable. However, this might be due to the reaction conditions, which included high concentrations of AMP. AMP induces AMPK to adopt its active conformation in which the Atg1-phosphorylation sites may be inaccessible. In conclusion, our bioinformatics predictions provide multiple entry points into studies to elucidate signaling pathways from ULK1 to mTORC1 and AMPK, as they are suggested by this work and by published results of others.

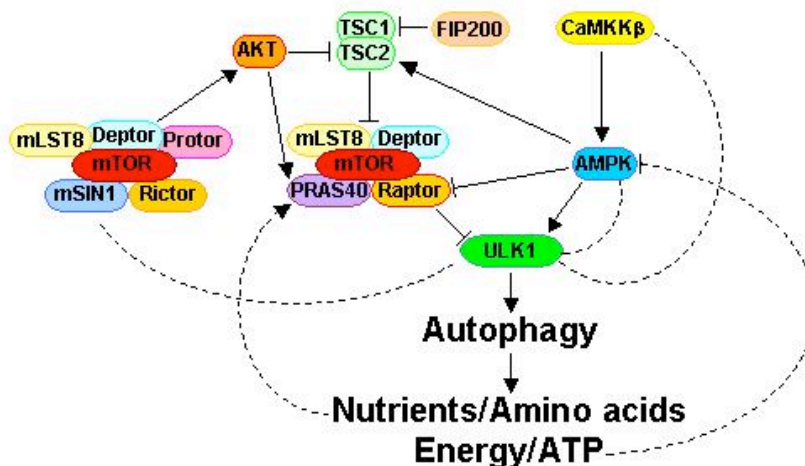


Figure 5.2. Hypothetical mechanisms or feedback regulation of autophagy. The mTOR-Raptor-PRAS40-mLST8-Deptor-complex (mTORC1) and AMPK regulate autophagy induction and/or maintenance/stimulation via ULK1 and its associated regulatory proteins FIP200, mAtg13 and Atg101 (not shown). Thereby, mTORC1 suppresses ULK1 under nutrient rich conditions, whereas AMPK activates ULK1 under conditions of nutrient- and energy stress by direct phosphorylation and by contributing to mTORC1 suppression via phosphorylation of TSC2 and Raptor. Autophagy can be self-limiting by generating nutrients (including amino acids) and energy, which will reactivate mTORC1 and restore AMP inhibition, respectively. In addition, ULK1 might initiate signal transduction cascades to modulate mTORC1 and/or AMPK activity. A hypothetical feedback loop from ULK1 to mTORC1 may originate from direct phosphorylation of mSIN1 in the mTOR-Rictor-mSIN1-mLST8-Deptor-Protector-complex (mTORC2) by ULK1. Subsequent alterations in mTORC2 and AKT activity may affect mTORC1. Alternatively, ULK1 may signal to AMPK by phosphorylating either one of the AMPK subunits (not shown) or the AMPK-kinase CaMKK β . Modulation of AMPK activity would also affect mTORC1 via changes in phosphorylation of TSC2 and Raptor. Furthermore, TSC2 activity is antagonized when its complex partner TSC1 is bound to FIP200, a protein that also participates in the ULK1-complex (not shown) targeted by mTORC1. ►: activating signal; ┘: inhibitory signal; —: established regulatory connection; — —: hypothetical regulatory connection. For reasons of simplicity, direct interactions between ULK1 and mTORC1 and ULK1 and AMPK as well as regulatory proteins associated with ULK1 and subunit-composition of AMPK have been omitted in this figure.

5.3 Future directions

The data presented in this thesis establish ULK1 as a novel phosphorylation substrate and interaction partner of AMPK and suggest that ULK1 is a critical signaling node connecting energy homeostasis, cell growth and autophagy. Moreover, it establishes a parallel pathway through which AMPK may modulate autophagy independently of its regulation of the mTORC1-pathway by phosphorylation of the mTORC1-suppressor TSC2 and of the mTORC1-subunit Raptor. Since the TSC2-branch of the pathway is not conserved throughout all eukaryotes, the Raptor-branch and the direct phosphorylation of ULK1 might represent the more ancestral mechanism through which AMPK controls autophagy during energy stress. To better understand how autophagy is regulated in response to various stress stimuli, it will be important to elucidate the functional significance of the dual connection of AMPK to one and the same component of the autophagy-machinery, ULK1, and to clarify the relative importance of direct and indirect, mTORC1-dependent, signals that ULK1 receives from AMPK. Particular questions to be answered include whether both pathways are utilized in parallel, whether each is activated only in response to certain stimuli or to mediate a specific subtype of autophagy such as mitophagy, whether one serves as a backup only when the other is blocked and whether there are positive and/or negative feedback loops from ULK1 to AMPK and/or mTORC1. Our work already paved the road for such functional studies by determining three precise sites in ULK1 that are phosphorylated by AMPK. Mutation of these sites may be predicted to alter ULK1-activities and -functions that are dependent on AMPK kinase activity.

A second aspect is the assembly of ULK1 and AMPK into a nutrient- and stress-resistant common complex; this raises the possibility that the two kinases regulate certain processes in concert. Both kinases might phosphorylate the same substrates, but alternatively, ULK1 might simply serve as a scaffold and help to precisely localize a small fraction of active AMPK to its substrates. Importantly, in such a model, high catalytic activity would not be required for the entire cellular AMPK population but just for a small fraction. Our bioinformatics analyses provide a rationale for a model of concerted and localized ULK1-AMPK-action and suggest several common substrates for these two kinases, whose function is not limited to autophagy, but also includes cellular processes such as cell adhesion and metabolism.

Lastly, we identified the candidate tumor suppressor, INPP4B, as an ULK1 interacting protein and putative substrate. At present, INPP4B has only been studied for its suppressive role in PI3K/AKT signaling, which has been connected to its ability to inhibit cell motility

and anchorage-independent growth. Our experimental result mentioned above and, intriguingly, our bioinformatics analysis of *in vitro* Atg1-substrates propose additional mechanisms through which INPP4B might exert its tumor-suppressive activities, independently of the PI3K-AKT-pathway: one, obviously, is autophagy, and the other is regulation of the actin cytoskeleton and related structures. Neither INPP4B nor ULK1 have so far been connected to the latter. Yet, there is experimental data suggesting that ULK1 also may influence focal adhesion dynamics, consisting in the genetic interaction between Atg1 and the focal adhesion component Paxillin in *Drosophila* (Chen et al., 2008) Moreover, we provide ample bioinformatic evidence on cytoskeletal proteins being candidate substrates of ULK1. This provides room for the speculation that ULK1 is not only central in the autophagy signaling network, but also in the regulation of other cellular pathways, including cytoskeletal organization.

In conclusion, this thesis substantially enhances our understanding of how autophagy is coupled to energy sensing on the molecular level by uncovering a physical interaction and kinase-substrate-relationship between AMPK and ULK1, and provides interesting novel perspectives towards additional and hitherto uncharacterized cellular activities for both kinases.

6 References

- Abeliovich, H., Zhang, C., Dunn, W. A., Jr., Shokat, K. M., and Klionsky, D. J. (2003). Chemical genetic analysis of Apg1 reveals a non-kinase role in the induction of autophagy. *Mol Biol Cell* 14, 477-490.
- Aita, V. M., Liang, X. H., Murty, V. V., Pincus, D. L., Yu, W., Cayanis, E., Kalachikov, S., Gilliam, T. C., and Levine, B. (1999). Cloning and genomic organization of beclin 1, a candidate tumor suppressor gene on chromosome 17q21. *Genomics* 59, 59-65.
- Ashford, T. P., and Porter, K. R. (1962). Cytoplasmic components in hepatic cell lysosomes. *J Cell Biol* 12, 198-202.
- Axe, E. L., Walker, S. A., Manifava, M., Chandra, P., Roderick, H. L., Habermann, A., Griffiths, G., and Ktistakis, N. T. (2008). Autophagosome formation from membrane compartments enriched in phosphatidylinositol 3-phosphate and dynamically connected to the endoplasmic reticulum. *J Cell Biol* 182, 685-701.
- Balakrishnan, A., von Neuhoff, N., Rudolph, C., Kamphues, K., Schraders, M., Groenen, P., van Krieken, J. H., Callet-Bauchu, E., Schlegelberger, B., and Steinemann, D. (2006). Quantitative microsatellite analysis to delineate the commonly deleted region 1p22.3 in mantle cell lymphomas. *Genes Chromosomes Cancer* 45, 883-892.
- Barth, H., Meiling-Wesse, K., Eppler, U. D., and Thumm, M. (2002). Maf1p is essential for maturation of proaminopeptidase I but not for autophagy. *FEBS Lett* 512, 173-179.
- Bartz, S. R., and Vodicka, M. A. (1997). Production of high-titer human immunodeficiency virus type 1 pseudotyped with vesicular stomatitis virus glycoprotein. *Methods* 12, 337-342.
- Bernales, S., McDonald, K. L., and Walter, P. (2006). Autophagy counterbalances endoplasmic reticulum expansion during the unfolded protein response. *PLoS Biol* 4, e423.
- Berry, D. L., and Baehrecke, E. H. (2007). Growth arrest and autophagy are required for salivary gland cell degradation in *Drosophila*. *Cell* 131, 1137-1148.
- Bjedov, I., Toivonen, J. M., Kerr, F., Slack, C., Jacobson, J., Foley, A., and Partridge, L. (2010). Mechanisms of life span extension by rapamycin in the fruit fly *Drosophila melanogaster*. *Cell Metab* 11, 35-46.
- Bormann, C., and Sahm, H. (1978). Degradation of microbodies in relation to activities of alcohol oxidase and catalase in *Candida boidinii*. *Arch Microbiol* 117, 67-72.
- Browne, G. J., Finn, S. G., and Proud, C. G. (2004). Stimulation of the AMP-activated protein kinase leads to activation of eukaryotic elongation factor 2 kinase and to its phosphorylation at a novel site, serine 398. *J Biol Chem* 279, 12220-12231.
- Budanov, A. V., and Karin, M. (2008). p53 target genes sestrin1 and sestrin2 connect genotoxic stress and mTOR signaling. *Cell* 134, 451-460.
- Budovskaya, Y. V., Stephan, J. S., Deminoff, S. J., and Herman, P. K. (2005). An evolutionary proteomics approach identifies substrates of the cAMP-dependent protein kinase. *Proc Natl Acad Sci U S A* 102, 13933-13938.
- Bullock, W.O., Fernandez, J.M., and Short, J.M. (1987). XL1-Blue: a high efficiency plasmid transforming *recA Escherichia coli* strain with β -galactosidase selection. *BioTechniques* 5, 376-378

- Bungard, D., Fuerth, B. J., Zeng, P. Y., Faubert, B., Maas, N. L., Viollet, B., Carling, D., Thompson, C. B., Jones, R. G., and Berger, S. L. (2010). Signaling kinase AMPK activates stress-promoted transcription via histone H2B phosphorylation. *Science* 329, 1201-1205.
- Buzzai, M., Jones, R. G., Amaravadi, R. K., Lum, J. J., DeBerardinis, R. J., Zhao, F., Viollet, B., and Thompson, C. B. (2007). Systemic treatment with the antidiabetic drug metformin selectively impairs p53-deficient tumor cell growth. *Cancer Res* 67, 6745-6752.
- Canto, C., Gerhart-Hines, Z., Feige, J. N., Lagouge, M., Noriega, L., Milne, J. C., Elliott, P. J., Puigserver, P., and Auwerx, J. (2009). AMPK regulates energy expenditure by modulating NAD⁺ metabolism and SIRT1 activity. *Nature* 458, 1056-1060.
- Carling, D., and Hardie, D. G. (1989). The substrate and sequence specificity of the AMP-activated protein kinase. Phosphorylation of glycogen synthase and phosphorylase kinase. *Biochim Biophys Acta* 1012, 81-86.
- Casperson, G. F., Walker, N., and Bourne, H. R. (1985). Isolation of the gene encoding adenylate cyclase in *Saccharomyces cerevisiae*. *Proc Natl Acad Sci U S A* 82, 5060-5063.
- Celenza, J. L., and Carlson, M. (1986). A yeast gene that is essential for release from glucose repression encodes a protein kinase. *Science* 233, 1175-1180.
- Chan, E. Y., Kir, S., and Tooze, S. A. (2007). siRNA screening of the kinome identifies ULK1 as a multidomain modulator of autophagy. *J Biol Chem* 282, 25464-25474.
- Chan, E. Y., Longatti, A., McKnight, N. C., and Tooze, S. A. (2009). Kinase-inactivated ULK proteins inhibit autophagy via their conserved C-terminal domains using an Atg13-independent mechanism. *Mol Cell Biol* 29, 157-171.
- Chen, G. C., Lee, J. Y., Tang, H. W., Debnath, J., Thomas, S. M., and Settleman, J. (2008). Genetic interactions between *Drosophila melanogaster* Atg1 and paxillin reveal a role for paxillin in autophagosome formation. *Autophagy* 4, 37-45.
- Cheong, H., Nair, U., Geng, J., and Klionsky, D. J. (2008). The Atg1 kinase complex is involved in the regulation of protein recruitment to initiate sequestering vesicle formation for nonspecific autophagy in *Saccharomyces cerevisiae*. *Mol Biol Cell* 19, 668-681.
- Cheung, P. C., Salt, I. P., Davies, S. P., Hardie, D. G., and Carling, D. (2000). Characterization of AMP-activated protein kinase gamma-subunit isoforms and their role in AMP binding. *Biochem J* 346 Pt 3, 659-669.
- Colombo, S., Ronchetti, D., Thevelein, J. M., Winderickx, J., and Martegani, E. (2004). Activation state of the Ras2 protein and glucose-induced signaling in *Saccharomyces cerevisiae*. *J Biol Chem* 279, 46715-46722.
- Cool, B., Zinker, B., Chiou, W., Kifle, L., Cao, N., Perham, M., Dickinson, R., Adler, A., Gagne, G., Iyengar, R., Zhao, G., Marsh, K., Kym, P., Jung, P., Camp, H. S., and Frevert, E. (2006). Identification and characterization of a small molecule AMPK activator that treats key components of type 2 diabetes and the metabolic syndrome. *Cell Metab* 3, 403-416.
- Corradetti, M. N., Inoki, K., Bardeesy, N., DePinho, R. A., and Guan, K. L. (2004). Regulation of the TSC pathway by LKB1: evidence of a molecular link between tuberous sclerosis complex and Peutz-Jeghers syndrome. *Genes Dev* 18, 1533-1538.
- Davies, S. P., Helps, N. R., Cohen, P. T., and Hardie, D. G. (1995). 5'-AMP inhibits dephosphorylation, as well as promoting phosphorylation, of the AMP-activated protein

- kinase. Studies using bacterially expressed human protein phosphatase-2C alpha and native bovine protein phosphatase-2AC. *FEBS Lett* 377, 421-425.
- Davletov, B. A., and Sudhof, T. C. (1993). A single C2 domain from synaptotagmin I is sufficient for high affinity Ca²⁺/phospholipid binding. *J Biol Chem* 268, 26386-26390.
- Desrivieres, S., Cooke, F. T., Parker, P. J., and Hall, M. N. (1998). MSS4, a phosphatidylinositol-4-phosphate 5-kinase required for organization of the actin cytoskeleton in *Saccharomyces cerevisiae*. *J Biol Chem* 273, 15787-15793.
- Deutschbauer, A. M., Williams, R. M., Chu, A. M., and Davis, R. W. (2002). Parallel phenotypic analysis of sporulation and postgermination growth in *Saccharomyces cerevisiae*. *Proc Natl Acad Sci U S A* 99, 15530-15535.
- DeYoung, M. P., Horak, P., Sofer, A., Sgroi, D., and Ellisen, L. W. (2008). Hypoxia regulates TSC1/2-mTOR signaling and tumor suppression through REDD1-mediated 14-3-3 shuttling. *Genes Dev* 22, 239-251.
- Di Bartolomeo, S., Corazzari, M., Nazio, F., Oliverio, S., Lisi, G., Antonioli, M., Pagliarini, V., Matteoni, S., Fuoco, C., Giunta, L., D'Amelio, M., Nardacci, R., Romagnoli, A., Piacentini, M., Cecconi, F., and Fimia, G. M. (2010). The dynamic interaction of AMBRA1 with the dynein motor complex regulates mammalian autophagy. *J Cell Biol* 191, 155-168.
- Di Paolo, G., Pellegrini, L., Letinic, K., Cestra, G., Zoncu, R., Voronov, S., Chang, S., Guo, J., Wenk, M. R., and De Camilli, P. (2002). Recruitment and regulation of phosphatidylinositol phosphate kinase type 1 gamma by the FERM domain of talin. *Nature* 420, 85-89.
- Diaz-Troya, S., Perez-Perez, M. E., Florencio, F. J., and Crespo, J. L. (2008). The role of TOR in autophagy regulation from yeast to plants and mammals. *Autophagy* 4, 851-865.
- Doelling, J. H., Walker, J. M., Friedman, E. M., Thompson, A. R., and Vierstra, R. D. (2002). The APG8/12-activating enzyme APG7 is required for proper nutrient recycling and senescence in *Arabidopsis thaliana*. *J Biol Chem* 277, 33105-33114.
- Doppler, H., Storz, P., Li, J., Comb, M. J., and Toker, A. (2005). A phosphorylation state-specific antibody recognizes Hsp27, a novel substrate of protein kinase D. *J Biol Chem* 280, 15013-15019.
- Engelman, J. A., Luo, J., and Cantley, L. C. (2006). The evolution of phosphatidylinositol 3-kinases as regulators of growth and metabolism. *Nat Rev Genet* 7, 606-619.
- Epple, U. D., Suriapranata, I., Eskelinen, E. L., and Thumm, M. (2001). Aut5/Cvt17p, a putative lipase essential for disintegration of autophagic bodies inside the vacuole. *J Bacteriol* 183, 5942-5955.
- Farre, J. C., Manjithaya, R., Mathewson, R. D., and Subramani, S. (2008). PpAtg30 tags peroxisomes for turnover by selective autophagy. *Dev Cell* 14, 365-376.
- Feng, Z., Hu, W., de Stanchina, E., Teresky, A. K., Jin, S., Lowe, S., and Levine, A. J. (2007). The regulation of AMPK beta1, TSC2, and PTEN expression by p53: stress, cell and tissue specificity, and the role of these gene products in modulating the IGF-1-AKT-mTOR pathways. *Cancer Res* 67, 3043-3053.
- Fimia, G. M., Stoykova, A., Romagnoli, A., Giunta, L., Di Bartolomeo, S., Nardacci, R., Corazzari, M., Fuoco, C., Ucar, A., Schwartz, P., Gruss, P., Piacentini, M., Chowdhury, K., and Cecconi, F. (2007). Ambra1 regulates autophagy and development of the nervous system. *Nature* 447, 1121-1125.

- Frias, M. A., Thoreen, C. C., Jaffe, J. D., Schroder, W., Sculley, T., Carr, S. A., and Sabatini, D. M. (2006). mSin1 is necessary for Akt/PKB phosphorylation, and its isoforms define three distinct mTORC2s. *Curr Biol* 16, 1865-1870.
- Funakoshi, T., Matsuura, A., Noda, T., and Ohsumi, Y. (1997). Analyses of APG13 gene involved in autophagy in yeast, *Saccharomyces cerevisiae*. *Gene* 192, 207-213.
- Gal, J., Strom, A. L., Kwinter, D. M., Kilty, R., Zhang, J., Shi, P., Fu, W., Wooten, M. W., and Zhu, H. (2009). Sequestosome 1/p62 links familial ALS mutant SOD1 to LC3 via an ubiquitin-independent mechanism. *J Neurochem* 111, 1062-1073.
- Gan, B., Melkounian, Z. K., Wu, X., Guan, K. L., and Guan, J. L. (2005). Identification of FIP200 interaction with the TSC1-TSC2 complex and its role in regulation of cell size control. *J Cell Biol* 170, 379-389.
- Ganley, I. G., Lam du, H., Wang, J., Ding, X., Chen, S., and Jiang, X. (2009). ULK1.ATG13.FIP200 complex mediates mTOR signaling and is essential for autophagy. *J Biol Chem* 284, 12297-12305.
- Garami, A., Zwartkruis, F. J., Nobukuni, T., Joaquin, M., Rocco, M., Stocker, H., Kozma, S. C., Hafen, E., Bos, J. L., and Thomas, G. (2003). Insulin activation of Rheb, a mediator of mTOR/S6K/4E-BP signaling, is inhibited by TSC1 and 2. *Mol Cell* 11, 1457-1466.
- Gardino, A. K., Smerdon, S. J., and Yaffe, M. B. (2006). Structural determinants of 14-3-3 binding specificities and regulation of subcellular localization of 14-3-3-ligand complexes: a comparison of the X-ray crystal structures of all human 14-3-3 isoforms. *Semin Cancer Biol* 16, 173-182.
- Geisler, S., Holmstrom, K. M., Skujat, D., Fiesel, F. C., Rothfuss, O. C., Kahle, P. J., and Springer, W. (2010). PINK1/Parkin-mediated mitophagy is dependent on VDAC1 and p62/SQSTM1. *Nat Cell Biol* 12, 119-131.
- Gewinner, C., Wang, Z. C., Richardson, A., Teruya-Feldstein, J., Etemadmoghadam, D., Bowtell, D., Barretina, J., Lin, W. M., Rameh, L., Salmena, L., Pandolfi, P. P., and Cantley, L. C. (2009). Evidence that inositol polyphosphate 4-phosphatase type II is a tumor suppressor that inhibits PI3K signaling. *Cancer Cell* 16, 115-125.
- Gluzman, Y. (1981). SV40-transformed simian cells support the replication of early SV40 mutants. *Cell* 23, 175-182.
- Gonzalez-Angulo, A. M., and Meric-Bernstam, F. (2010). Metformin: a therapeutic opportunity in breast cancer. *Clin Cancer Res* 16, 1695-1700.
- Graham, F. L., Smiley, J., Russell, W. C., and Nairn, R. (1977). Characteristics of a human cell line transformed by DNA from human adenovirus type 5. *J Gen Virol* 36, 59-74.
- Grote-meier, A., Alers, S., Pfisterer, S. G., Paasch, F., Daubrawa, M., Dieterle, A., Viollet, B., Wesselborg, S., Proikas-Cezanne, T., and Stork, B. (2010). AMPK-independent induction of autophagy by cytosolic Ca²⁺ increase. *Cell Signal* 22, 914-925.
- Guan, J., Stromhaug, P. E., George, M. D., Habibzadegah-Tari, P., Bevan, A., Dunn, W. A., Jr., and Klionsky, D. J. (2001). Cvt18/Gsa12 is required for cytoplasm-to-vacuole transport, pexophagy, and autophagy in *Saccharomyces cerevisiae* and *Pichia pastoris*. *Mol Biol Cell* 12, 3821-3838.
- Gutierrez, M. G., Master, S. S., Singh, S. B., Taylor, G. A., Colombo, M. I., and Deretic, V. (2004). Autophagy is a defense mechanism inhibiting BCG and Mycobacterium tuberculosis survival in infected macrophages. *Cell* 119, 753-766.

- Gwinn, D. M., Shackelford, D. B., Egan, D. F., Mihaylova, M. M., Mery, A., Vasquez, D. S., Turk, B. E., and Shaw, R. J. (2008). AMPK phosphorylation of raptor mediates a metabolic checkpoint. *Mol Cell* 30, 214-226.
- Hagel, M., George, E. L., Kim, A., Tamimi, R., Opitz, S. L., Turner, C. E., Imamoto, A., and Thomas, S. M. (2002). The adaptor protein paxillin is essential for normal development in the mouse and is a critical transducer of fibronectin signaling. *Mol Cell Biol* 22, 901-915.
- Hailey, D. W., Rambold, A. S., Satpute-Krishnan, P., Mitra, K., Sougrat, R., Kim, P. K., and Lippincott-Schwartz, J. (2010). Mitochondria supply membranes for autophagosome biogenesis during starvation. *Cell* 141, 656-667.
- Halstead, J. R., Savaskan, N. E., van den Bout, I., Van Horck, F., Hajdo-Milasinovic, A., Snell, M., Keune, W. J., Ten Klooster, J. P., Hordijk, P. L., and Divecha, N. (2010). Rac controls PIP5K localisation and PtdIns(4,5)P synthesis, which modulates vinculin localisation and neurite dynamics. *J Cell Sci* 123, 3535-3546.
- Hanada, T., Noda, N. N., Satomi, Y., Ichimura, Y., Fujioka, Y., Takao, T., Inagaki, F., and Ohsumi, Y. (2007). The Atg12-Atg5 conjugate has a novel E3-like activity for protein lipidation in autophagy. *J Biol Chem* 282, 37298-37302.
- Hanaoka, H., Noda, T., Shirano, Y., Kato, T., Hayashi, H., Shibata, D., Tabata, S., and Ohsumi, Y. (2002). Leaf senescence and starvation-induced chlorosis are accelerated by the disruption of an Arabidopsis autophagy gene. *Plant Physiol* 129, 1181-1193.
- Hansen, M., Chandra, A., Mitic, L. L., Onken, B., Driscoll, M., and Kenyon, C. (2008). A role for autophagy in the extension of lifespan by dietary restriction in *C. elegans*. *PLoS Genet* 4, e24.
- Hara, T., Nakamura, K., Matsui, M., Yamamoto, A., Nakahara, Y., Suzuki-Migishima, R., Yokoyama, M., Mishima, K., Saito, I., Okano, H., and Mizushima, N. (2006). Suppression of basal autophagy in neural cells causes neurodegenerative disease in mice. *Nature* 441, 885-889.
- Hara, T., Takamura, A., Kishi, C., Iemura, S., Natsume, T., Guan, J. L., and Mizushima, N. (2008). FIP200, a ULK-interacting protein, is required for autophagosome formation in mammalian cells. *J Cell Biol* 181, 497-510.
- Hardie, D. G. (2007). AMP-activated/SNF1 protein kinases: conserved guardians of cellular energy. *Nat Rev Mol Cell Biol* 8, 774-785.
- Harding, T. M., Morano, K. A., Scott, S. V., and Klionsky, D. J. (1995). Isolation and characterization of yeast mutants in the cytoplasm to vacuole protein targeting pathway. *J Cell Biol* 131, 591-602.
- Hawley, S. A., Boudeau, J., Reid, J. L., Mustard, K. J., Udd, L., Makela, T. P., Alessi, D. R., and Hardie, D. G. (2003). Complexes between the LKB1 tumor suppressor, STRAD alpha/beta and MO25 alpha/beta are upstream kinases in the AMP-activated protein kinase cascade. *J Biol* 2, 28.
- Hawley, S. A., Pan, D. A., Mustard, K. J., Ross, L., Bain, J., Edelman, A. M., Frenguelli, B. G., and Hardie, D. G. (2005). Calmodulin-dependent protein kinase kinase-beta is an alternative upstream kinase for AMP-activated protein kinase. *Cell Metab* 2, 9-19.
- Hayashi-Nishino, M., Fujita, N., Noda, T., Yamaguchi, A., Yoshimori, T., and Yamamoto, A. (2009). A subdomain of the endoplasmic reticulum forms a cradle for autophagosome formation. *Nat Cell Biol* 11, 1433-1437.
- He, C., and Levine, B. (2010). The Beclin 1 interactome. *Curr Opin Cell Biol* 22, 140-149.

- Hedgecock, E. M., Culotti, J. G., Thomson, J. N., and Perkins, L. A. (1985). Axonal guidance mutants of *Caenorhabditis elegans* identified by filling sensory neurons with fluorescein dyes. *Dev Biol* 111, 158-170.
- Herrero-Martin, G., Hoyer-Hansen, M., Garcia-Garcia, C., Fumarola, C., Farkas, T., Lopez-Rivas, A., and Jaattela, M. (2009). TAK1 activates AMPK-dependent cytoprotective autophagy in TRAIL-treated epithelial cells. *Embo J* 28, 677-685.
- Hettema, E. H., Lewis, M. J., Black, M. W., and Pelham, H. R. (2003). Retromer and the sorting nexins Snx4/41/42 mediate distinct retrieval pathways from yeast endosomes. *Embo J* 22, 548-557.
- Horman, S., Beauloye, C., Vertommen, D., Vanoverschelde, J. L., Hue, L., and Rider, M. H. (2003). Myocardial ischemia and increased heart work modulate the phosphorylation state of eukaryotic elongation factor-2. *J Biol Chem* 278, 41970-41976.
- Hosokawa, N., Hara, T., Kaizuka, T., Kishi, C., Takamura, A., Miura, Y., Iemura, S., Natsume, T., Takehana, K., Yamada, N., Guan, J. L., Oshiro, N., and Mizushima, N. (2009a). Nutrient-dependent mTORC1 association with the ULK1-Atg13-FIP200 complex required for autophagy. *Mol Biol Cell* 20, 1981-1991.
- Hosokawa, N., Sasaki, T., Iemura, S., Natsume, T., Hara, T., and Mizushima, N. (2009b). Atg101, a novel mammalian autophagy protein interacting with Atg13. *Autophagy* 5, 973-979.
- Hoyer-Hansen, M., Bastholm, L., Szyniarowski, P., Campanella, M., Szabadkai, G., Farkas, T., Bianchi, K., Fehrenbacher, N., Elling, F., Rizzuto, R., Mathiasen, I. S., and Jaattela, M. (2007). Control of macroautophagy by calcium, calmodulin-dependent kinase kinase-beta, and Bcl-2. *Mol Cell* 25, 193-205.
- Hudson, E. R., Pan, D. A., James, J., Lucocq, J. M., Hawley, S. A., Green, K. A., Baba, O., Terashima, T., and Hardie, D. G. (2003). A novel domain in AMP-activated protein kinase causes glycogen storage bodies similar to those seen in hereditary cardiac arrhythmias. *Curr Biol* 13, 861-866.
- Hunter, T., and Plowman, G. D. (1997). The protein kinases of budding yeast: six score and more. *Trends Biochem Sci* 22, 18-22.
- Hurley, R. L., Anderson, K. A., Franzone, J. M., Kemp, B. E., Means, A. R., and Witters, L. A. (2005). The Ca²⁺/calmodulin-dependent protein kinase kinases are AMP-activated protein kinase kinases. *J Biol Chem* 280, 29060-29066.
- Ichimura, Y., Kirisako, T., Takao, T., Satomi, Y., Shimonishi, Y., Ishihara, N., Mizushima, N., Tanida, I., Kominami, E., Ohsumi, M., Noda, T., and Ohsumi, Y. (2000). A ubiquitin-like system mediates protein lipidation. *Nature* 408, 488-492.
- Inoki, K., Li, Y., Zhu, T., Wu, J., and Guan, K. L. (2002). TSC2 is phosphorylated and inhibited by Akt and suppresses mTOR signalling. *Nat Cell Biol* 4, 648-657.
- Inoki, K., Zhu, T., and Guan, K. L. (2003). TSC2 mediates cellular energy response to control cell growth and survival. *Cell* 115, 577-590.
- Ionov, Y., Nowak, N., Perucho, M., Markowitz, S., and Cowell, J. K. (2004). Manipulation of nonsense mediated decay identifies gene mutations in colon cancer Cells with microsatellite instability. *Oncogene* 23, 639-645.
- Itakura, E., and Mizushima, N. (2010). Characterization of autophagosome formation site by a hierarchical analysis of mammalian Atg proteins. *Autophagy* 6, 764-776.

- Itakura, E., Kishi, C., Inoue, K., and Mizushima, N. (2008). Beclin 1 forms two distinct phosphatidylinositol 3-kinase complexes with mammalian Atg14 and UVRAG. *Mol Biol Cell* 19, 5360-5372.
- Jacinto, E., Facchinetti, V., Liu, D., Soto, N., Wei, S., Jung, S. Y., Huang, Q., Qin, J., and Su, B. (2006). SIN1/MIP1 maintains rictor-mTOR complex integrity and regulates Akt phosphorylation and substrate specificity. *Cell* 127, 125-137.
- Jacinto, E., Loewith, R., Schmidt, A., Lin, S., Ruegg, M. A., Hall, A., and Hall, M. N. (2004). Mammalian TOR complex 2 controls the actin cytoskeleton and is rapamycin insensitive. *Nat Cell Biol* 6, 1122-1128.
- Jessberger, S., Gage, F. H., Eisch, A. J., and Lagace, D. C. (2009). Making a neuron: Cdk5 in embryonic and adult neurogenesis. *Trends Neurosci* 32, 575-582.
- Jin, S. (2005). p53, Autophagy and tumor suppression. *Autophagy* 1, 171-173.
- Jorgensen, S. B., Nielsen, J. N., Birk, J. B., Olsen, G. S., Viollet, B., Andreelli, F., Schjerling, P., Vaulont, S., Hardie, D. G., Hansen, B. F., Richter, E. A., and Wojtaszewski, J. F. (2004a). The alpha2-5'AMP-activated protein kinase is a site 2 glycogen synthase kinase in skeletal muscle and is responsive to glucose loading. *Diabetes* 53, 3074-3081.
- Jorgensen, S. B., Viollet, B., Andreelli, F., Frosig, C., Birk, J. B., Schjerling, P., Vaulont, S., Richter, E. A., and Wojtaszewski, J. F. (2004b). Knockout of the alpha2 but not alpha1 5'-AMP-activated protein kinase isoform abolishes 5-aminoimidazole-4-carboxamide-1-beta-4-ribofuranosidebut not contraction-induced glucose uptake in skeletal muscle. *J Biol Chem* 279, 1070-1079.
- Jung, C. H., Jun, C. B., Ro, S. H., Kim, Y. M., Otto, N. M., Cao, J., Kundu, M., and Kim, D. H. (2009). ULK-Atg13-FIP200 complexes mediate mTOR signaling to the autophagy machinery. *Mol Biol Cell* 20, 1992-2003.
- Kabeya, Y., Kamada, Y., Baba, M., Takikawa, H., Sasaki, M., and Ohsumi, Y. (2005). Atg17 functions in cooperation with Atg1 and Atg13 in yeast autophagy. *Mol Biol Cell* 16, 2544-2553.
- Kabeya, Y., Kawamata, T., Suzuki, K., and Ohsumi, Y. (2007). Cis1/Atg31 is required for autophagosome formation in *Saccharomyces cerevisiae*. *Biochem Biophys Res Commun* 356, 405-410.
- Kabeya, Y., Noda, N. N., Fujioka, Y., Suzuki, K., Inagaki, F., and Ohsumi, Y. (2009). Characterization of the Atg17-Atg29-Atg31 complex specifically required for starvation-induced autophagy in *Saccharomyces cerevisiae*. *Biochem Biophys Res Commun* 389, 612-615.
- Kahn, B. B., Alquier, T., Carling, D., and Hardie, D. G. (2005). AMP-activated protein kinase: ancient energy gauge provides clues to modern understanding of metabolism. *Cell Metab* 1, 15-25.
- Kamada, Y., Funakoshi, T., Shintani, T., Nagano, K., Ohsumi, M., and Ohsumi, Y. (2000). Tor-mediated induction of autophagy via an Apg1 protein kinase complex. *J Cell Biol* 150, 1507-1513.
- Kamada, Y., Yoshino, K., Kondo, C., Kawamata, T., Oshiro, N., Yonezawa, K., and Ohsumi, Y. (2010). Tor directly controls the Atg1 kinase complex to regulate autophagy. *Mol Cell Biol* 30, 1049-1058.

- Kametaka, S., Okano, T., Ohsumi, M., and Ohsumi, Y. (1998). Apg14p and Apg6/Vps30p form a protein complex essential for autophagy in the yeast, *Saccharomyces cerevisiae*. *J Biol Chem* 273, 22284-22291.
- Kanki, T., Wang, K., Baba, M., Bartholomew, C. R., Lynch-Day, M. A., Du, Z., Geng, J., Mao, K., Yang, Z., Yen, W. L., and Klionsky, D. J. (2009). A genomic screen for yeast mutants defective in selective mitochondria autophagy. *Mol Biol Cell* 20, 4730-4738.
- Kataoka, T., Broek, D., and Wigler, M. (1985). DNA sequence and characterization of the *S. cerevisiae* gene encoding adenylate cyclase. *Cell* 43, 493-505.
- Kawamata, T., Kamada, Y., Kabeya, Y., Sekito, T., and Ohsumi, Y. (2008). Organization of the pre-autophagosomal structure responsible for autophagosome formation. *Mol Biol Cell* 19, 2039-2050.
- Kawamata, T., Kamada, Y., Suzuki, K., Kuboshima, N., Akimatsu, H., Ota, S., Ohsumi, M., and Ohsumi, Y. (2005). Characterization of a novel autophagy-specific gene, ATG29. *Biochem Biophys Res Commun* 338, 1884-1889.
- Kihara, A., Noda, T., Ishihara, N., and Ohsumi, Y. (2001). Two distinct Vps34 phosphatidylinositol 3-kinase complexes function in autophagy and carboxypeptidase Y sorting in *Saccharomyces cerevisiae*. *J Cell Biol* 152, 519-530.
- Kim, D. H., Sarbassov, D. D., Ali, S. M., King, J. E., Latek, R. R., Erdjument-Bromage, H., Tempst, P., and Sabatini, D. M. (2002). mTOR interacts with raptor to form a nutrient-sensitive complex that signals to the cell growth machinery. *Cell* 110, 163-175.
- Kim, D. H., Sarbassov, D. D., Ali, S. M., Latek, R. R., Guntur, K. V., Erdjument-Bromage, H., Tempst, P., and Sabatini, D. M. (2003). GbetaL, a positive regulator of the rapamycin-sensitive pathway required for the nutrient-sensitive interaction between raptor and mTOR. *Mol Cell* 11, 895-904.
- Kirisako, T., Ichimura, Y., Okada, H., Kabeya, Y., Mizushima, N., Yoshimori, T., Ohsumi, M., Takao, T., Noda, T., and Ohsumi, Y. (2000). The reversible modification regulates the membrane-binding state of Apg8/Aut7 essential for autophagy and the cytoplasm to vacuole targeting pathway. *J Cell Biol* 151, 263-276.
- Kirkin, V., Lamark, T., Johansen, T., and Dikic, I. (2009). NBR1 cooperates with p62 in selective autophagy of ubiquitinated targets. *Autophagy* 5, 732-733.
- Komatsu, M., Waguri, S., Chiba, T., Murata, S., Iwata, J., Tanida, I., Ueno, T., Koike, M., Uchiyama, Y., Kominami, E., and Tanaka, K. (2006). Loss of autophagy in the central nervous system causes neurodegeneration in mice. *Nature* 441, 880-884.
- Kraft, C., Deplazes, A., Sohrmann, M., and Peter, M. (2008). Mature ribosomes are selectively degraded upon starvation by an autophagy pathway requiring the Ubp3p/Bre5p ubiquitin protease. *Nat Cell Biol* 10, 602-610.
- Kristensen, A. R., Schandorff, S., Hoyer-Hansen, M., Nielsen, M. O., Jaattela, M., Dengjel, J., and Andersen, J. S. (2008). Ordered organelle degradation during starvation-induced autophagy. *Mol Cell Proteomics* 7, 2419-2428.
- Kuma, A., Hatano, M., Matsui, M., Yamamoto, A., Nakaya, H., Yoshimori, T., Ohsumi, Y., Tokuhiya, T., and Mizushima, N. (2004). The role of autophagy during the early neonatal starvation period. *Nature* 432, 1032-1036.
- Kuma, A., Mizushima, N., Ishihara, N., and Ohsumi, Y. (2002). Formation of the approximately 350-kDa Apg12-Apg5-Apg16 multimeric complex, mediated by Apg16 oligomerization, is essential for autophagy in yeast. *J Biol Chem* 277, 18619-18625.

- Kundu, M., Lindsten, T., Yang, C. Y., Wu, J., Zhao, F., Zhang, J., Selak, M. A., Ney, P. A., and Thompson, C. B. (2008). Ulk1 plays a critical role in the autophagic clearance of mitochondria and ribosomes during reticulocyte maturation. *Blood* 112, 1493-1502.
- Kuroyanagi, H., Yan, J., Seki, N., Yamanouchi, Y., Suzuki, Y., Takano, T., Muramatsu, M., and Shirasawa, T. (1998). Human ULK1, a novel serine/threonine kinase related to UNC-51 kinase of *Caenorhabditis elegans*: cDNA cloning, expression, and chromosomal assignment. *Genomics* 51, 76-85.
- Kyriakis, J. M., and Avruch, J. (2001). Mammalian mitogen-activated protein kinase signal transduction pathways activated by stress and inflammation. *Physiol Rev* 81, 807-869.
- Laderoute, K. R., Amin, K., Calaoagan, J. M., Knapp, M., Le, T., Orduna, J., Foretz, M., and Viollet, B. (2006). 5'-AMP-activated protein kinase (AMPK) is induced by low-oxygen and glucose deprivation conditions found in solid-tumor microenvironments. *Mol Cell Biol* 26, 5336-5347.
- Lai, T., and Garriga, G. (2004). The conserved kinase UNC-51 acts with VAB-8 and UNC-14 to regulate axon outgrowth in *C. elegans*. *Development* 131, 5991-6000.
- Lamia, K. A., Sachdeva, U. M., DiTacchio, L., Williams, E. C., Alvarez, J. G., Egan, D. F., Vasquez, D. S., Jugulon, H., Panda, S., Shaw, R. J., Thompson, C. B., and Evans, R. M. (2009). AMPK regulates the circadian clock by cryptochrome phosphorylation and degradation. *Science* 326, 437-440.
- Lane, D. P. (1992). Cancer. p53, guardian of the genome. *Nature* 358, 15-16.
- Leber, R., Silles, E., Sandoval, I. V., and Mazon, M. J. (2001). Yol082p, a novel CVT protein involved in the selective targeting of aminopeptidase I to the yeast vacuole. *J Biol Chem* 276, 29210-29217.
- Lee, J. H., Koh, H., Kim, M., Kim, Y., Lee, S. Y., Karess, R. E., Lee, S. H., Shong, M., Kim, J. M., Kim, J., and Chung, J. (2007). Energy-dependent regulation of cell structure by AMP-activated protein kinase. *Nature* 447, 1017-1020.
- Lee, S. B., Kim, S., Lee, J., Park, J., Lee, G., Kim, Y., Kim, J. M., and Chung, J. (2007). ATG1, an autophagy regulator, inhibits cell growth by negatively regulating S6 kinase. *EMBO Rep* 8, 360-365.
- Lemasters, J. J. (2005). Selective mitochondrial autophagy, or mitophagy, as a targeted defense against oxidative stress, mitochondrial dysfunction, and aging. *Rejuvenation Res* 8, 3-5.
- Levine, B. (2005). Eating oneself and uninvited guests: autophagy-related pathways in cellular defense. *Cell* 120, 159-162.
- Levine, B., and Klionsky, D. J. (2004). Development by self-digestion: molecular mechanisms and biological functions of autophagy. *Dev Cell* 6, 463-477.
- Levy, D., Ehret, G. B., Rice, K., Verwoert, G. C., Launer, L. J., Dehghan, A., Glazer, N. L., Morrison, A. C., Johnson, A. D., Aspelund, T., Aulchenko, Y., Lumley, T., Kottgen, A., Vasan, R. S., Rivadeneira, F., Eiriksdottir, G., Guo, X., Arking, D. E., Mitchell, G. F., Mattace-Raso, F. U., Smith, A. V., Taylor, K., Scharpf, R. B., Hwang, S. J., Sijbrands, E. J., Bis, J., Harris, T. B., Ganesh, S. K., O'Donnell, C. J., Hofman, A., Rotter, J. I., Coresh, J., Benjamin, E. J., Uitterlinden, A. G., Heiss, G., Fox, C. S., Witteman, J. C., Boerwinkle, E., Wang, T. J., Gudnason, V., Larson, M. G., Chakravarti, A., Psaty, B. M., and van Duijn, C. M. (2009). Genome-wide association study of blood pressure and hypertension. *Nat Genet* 41, 677-678.

- Li, D. D., Wang, L. L., Deng, R., Tang, J., Shen, Y., Guo, J. F., Wang, Y., Xia, L. P., Feng, G. K., Liu, Q. Q., Huang, W. L., Zeng, Y. X., and Zhu, X. F. (2009). The pivotal role of c-Jun NH2-terminal kinase-mediated Beclin 1 expression during anticancer agents-induced autophagy in cancer cells. *Oncogene* 28, 886-898.
- Liang, C., Feng, P., Ku, B., Dotan, I., Canaani, D., Oh, B. H., and Jung, J. U. (2006). Autophagic and tumour suppressor activity of a novel Beclin1-binding protein UVRAG. *Nat Cell Biol* 8, 688-699.
- Liang, C., Lee, J. S., Inn, K. S., Gack, M. U., Li, Q., Roberts, E. A., Vergne, I., Deretic, V., Feng, P., Akazawa, C., and Jung, J. U. (2008). Beclin1-binding UVRAG targets the class C Vps complex to coordinate autophagosome maturation and endocytic trafficking. *Nat Cell Biol* 10, 776-787.
- Liang, J., Shao, S. H., Xu, Z. X., Hennessy, B., Ding, Z., Larrea, M., Kondo, S., Dumont, D. J., Gutterman, J. U., Walker, C. L., Slingerland, J. M., and Mills, G. B. (2007). The energy sensing LKB1-AMPK pathway regulates p27(kip1) phosphorylation mediating the decision to enter autophagy or apoptosis. *Nat Cell Biol* 9, 218-224.
- Libby, G., Donnelly, L. A., Donnan, P. T., Alessi, D. R., Morris, A. D., and Evans, J. M. (2009). New users of metformin are at low risk of incident cancer: a cohort study among people with type 2 diabetes. *Diabetes Care* 32, 1620-1625.
- Lizcano, J. M., Goransson, O., Toth, R., Deak, M., Morrice, N. A., Boudeau, J., Hawley, S. A., Udd, L., Makela, T. P., Hardie, D. G., and Alessi, D. R. (2004). LKB1 is a master kinase that activates 13 kinases of the AMPK subfamily, including MARK/PAR-1. *Embo J* 23, 833-843.
- Long, X., Lin, Y., Ortiz-Vega, S., Yonezawa, K., and Avruch, J. (2005). Rheb binds and regulates the mTOR kinase. *Curr Biol* 15, 702-713.
- Lorenz, M. C., Pan, X., Harashima, T., Cardenas, M. E., Xue, Y., Hirsch, J. P., and Heitman, J. (2000). The G protein-coupled receptor gpr1 is a nutrient sensor that regulates pseudohyphal differentiation in *Saccharomyces cerevisiae*. *Genetics* 154, 609-622.
- Lorin, S., Borges, A., Ribeiro Dos Santos, L., Souquere, S., Pierron, G., Ryan, K. M., Codogno, P., and Djavaheri-Mergny, M. (2009). c-Jun NH2-terminal kinase activation is essential for DRAM-dependent induction of autophagy and apoptosis in 2-methoxyestradiol-treated Ewing sarcoma cells. *Cancer Res* 69, 6924-6931.
- Maiuri, M. C., Tasmimir, E., Criollo, A., Morselli, E., Vicencio, J. M., Carnuccio, R., and Kroemer, G. (2009a). Control of autophagy by oncogenes and tumor suppressor genes. *Cell Death Differ* 16, 87-93.
- Maiuri, M. C., Malik, S. A., Morselli, E., Kepp, O., Criollo, A., Mouchel, P. L., Carnuccio, R., and Kroemer, G. (2009b). Stimulation of autophagy by the p53 target gene Sestrin2. *Cell Cycle* 8, 1571-1576.
- Maloverjan, A., Piiroo, M., Kasak, L., Peil, L., Osterlund, T., and Kogerman, P. (2010a). Dual function of unc-51-like kinase 3 (Ulk3) in the sonic hedgehog signaling pathway. *J Biol Chem* 285, 30079-30090.
- Maloverjan, A., Piiroo, M., Michelson, P., Kogerman, P., and Osterlund, T. (2010b). Identification of a novel serine/threonine kinase ULK3 as a positive regulator of Hedgehog pathway. *Exp Cell Res* 316, 627-637.
- Maloveryan, A., Finta, C., Osterlund, T., and Kogerman, P. (2007). A possible role of mouse Fused (STK36) in Hedgehog signaling and Gli transcription factor regulation. *J Cell Commun Signal* 1, 165-173.

- Mammucari, C., Milan, G., Romanello, V., Masiere, E., Rudolf, R., Del Piccolo, P., Burden, S. J., Di Lisi, R., Sandri, C., Zhao, J., Goldberg, A. L., Schiaffino, S., and Sandri, M. (2007). FoxO3 controls autophagy in skeletal muscle in vivo. *Cell Metab* 6, 458-471.
- Manning, B. D., Tee, A. R., Logsdon, M. N., Blenis, J., and Cantley, L. C. (2002). Identification of the tuberous sclerosis complex-2 tumor suppressor gene product tuberlin as a target of the phosphoinositide 3-kinase/akt pathway. *Mol Cell* 10, 151-162.
- Marsin, A. S., Bertrand, L., Rider, M. H., Deprez, J., Beauloye, C., Vincent, M. F., Van den Berghe, G., Carling, D., and Hue, L. (2000). Phosphorylation and activation of heart PFK-2 by AMPK has a role in the stimulation of glycolysis during ischaemia. *Curr Biol* 10, 1247-1255.
- Marsin, A. S., Bouzin, C., Bertrand, L., and Hue, L. (2002). The stimulation of glycolysis by hypoxia in activated monocytes is mediated by AMP-activated protein kinase and inducible 6-phosphofructo-2-kinase. *J Biol Chem* 277, 30778-30783.
- Matsumoto, K., Uno, I., Oshima, Y., and Ishikawa, T. (1982). Isolation and characterization of yeast mutants deficient in adenylate cyclase and cAMP-dependent protein kinase. *Proc Natl Acad Sci U S A* 79, 2355-2359.
- Matsunaga, K., Saitoh, T., Tabata, K., Omori, H., Satoh, T., Kurotori, N., Maejima, I., Shirahama-Noda, K., Ichimura, T., Isobe, T., Akira, S., Noda, T., and Yoshimori, T. (2009). Two Beclin 1-binding proteins, Atg14L and Rubicon, reciprocally regulate autophagy at different stages. *Nat Cell Biol* 11, 385-396.
- Matsushita, M., Suzuki, N. N., Obara, K., Fujioka, Y., Ohsumi, Y., and Inagaki, F. (2007). Structure of Atg5-Atg16, a complex essential for autophagy. *J Biol Chem* 282, 6763-6772.
- Matsuura, A., Tsukada, M., Wada, Y., and Ohsumi, Y. (1997). Apg1p, a novel protein kinase required for the autophagic process in *Saccharomyces cerevisiae*. *Gene* 192, 245-250.
- McEwan, D. G., and Dikic, I. (2010). Not all autophagy membranes are created equal. *Cell* 141, 564-566.
- Meijer, W. H., van der Klei, I. J., Veenhuis, M., and Kiel, J. A. (2007). ATG genes involved in non-selective autophagy are conserved from yeast to man, but the selective Cvt and pexophagy pathways also require organism-specific genes. *Autophagy* 3, 106-116.
- Meiling-Wesse, K., Barth, H., Voss, C., Eskelinen, E. L., Epple, U. D., and Thumm, M. (2004a). Atg21 is required for effective recruitment of Atg8 to the preautophagosomal structure during the Cvt pathway. *J Biol Chem* 279, 37741-37750.
- Meiling-Wesse, K., Bratsika, F., and Thumm, M. (2004b). ATG23, a novel gene required for maturation of proaminopeptidase I, but not for autophagy. *FEMS Yeast Res* 4, 459-465.
- Melendez, A., Tallozy, Z., Seaman, M., Eskelinen, E. L., Hall, D. H., and Levine, B. (2003). Autophagy genes are essential for dauer development and life-span extension in *C. elegans*. *Science* 301, 1387-1391.
- Meley, D., Bauvy, C., Houben-Weerts, J. H., Dubbelhuis, P. F., Helmond, M. T., Codogno, P., and Meijer, A. J. (2006). AMP-activated protein kinase and the regulation of autophagic proteolysis. *J Biol Chem* 281, 34870-34879.
- Mercer, C. A., Kaliappan, A., and Dennis, P. B. (2009). A novel, human Atg13 binding protein, Atg101, interacts with ULK1 and is essential for macroautophagy. *Autophagy* 5, 649-662.

- Mills, K. R., Reginato, M., Debnath, J., Queenan, B., and Brugge, J. S. (2004). Tumor necrosis factor-related apoptosis-inducing ligand (TRAIL) is required for induction of autophagy during lumen formation in vitro. *Proc Natl Acad Sci U S A* 101, 3438-3443.
- Mitchell, K. I., Stapleton, D., Gao, G., House, C., Michell, B., Katsis, F., Witters, L. A., and Kemp, B. E. (1994). Mammalian AMP-activated protein kinase shares structural and functional homology with the catalytic domain of yeast Snf1 protein kinase. *J Biol Chem* 269, 2361-2364.
- Mizushima, N. (2005). The pleiotropic role of autophagy: from protein metabolism to bactericide. *Cell Death Differ* 12 Suppl 2, 1535-1541.
- Mizushima, N. (2010). The role of the Atg1/ULK1 complex in autophagy regulation. *Curr Opin Cell Biol* 22, 132-139.
- Mizushima, N., Levine, B., Cuervo, A. M., and Klionsky, D. J. (2008). Autophagy fights disease through cellular self-digestion. *Nature* 451, 1069-1075.
- Mizushima, N., Noda, T., and Ohsumi, Y. (1999). Apg16p is required for the function of the Apg12p-Apg5p conjugate in the yeast autophagy pathway. *Embo J* 18, 3888-3896.
- Mizushima, N., Yoshimori, T., and Levine, B. (2010). Methods in mammalian autophagy research. *Cell* 140, 313-326.
- Mok, J., Kim, P. M., Lam, H. Y., Piccirillo, S., Zhou, X., Jeschke, G. R., Sheridan, D. L., Parker, S. A., Desai, V., Jwa, M., Cameroni, E., Niu, H., Good, M., Remenyi, A., Ma, J. L., Sheu, Y. J., Sassi, H. E., Sopko, R., Chan, C. S., De Virgilio, C., Hollingsworth, N. M., Lim, W. A., Stern, D. F., Stillman, B., Andrews, B. J., Gerstein, M. B., Snyder, M., and Turk, B. E. (2010). Deciphering protein kinase specificity through large-scale analysis of yeast phosphorylation site motifs. *Sci Signal* 3, ra12.
- Momcilovic, M., Hong, S. P., and Carlson, M. (2006). Mammalian TAK1 activates Snf1 protein kinase in yeast and phosphorylates AMP-activated protein kinase in vitro. *J Biol Chem* 281, 25336-25343.
- Monastyrska, I., Kiel, J. A., Krikken, A. M., Komduur, J. A., Veenhuis, M., and van der Klei, I. J. (2005). The *Hansenula polymorpha* ATG25 gene encodes a novel coiled-coil protein that is required for macropexophagy. *Autophagy* 1, 92-100.
- Mu, J., Brozinick, J. T., Jr., Valladares, O., Bucan, M., and Birnbaum, M. J. (2001). A role for AMP-activated protein kinase in contraction- and hypoxia-regulated glucose transport in skeletal muscle. *Mol Cell* 7, 1085-1094.
- Mulugu, S., Bai, W., Fridy, P. C., Bastidas, R. J., Otto, J. C., Dollins, D. E., Haystead, T. A., Ribeiro, A. A., and York, J. D. (2007). A conserved family of enzymes that phosphorylate inositol hexakisphosphate. *Science* 316, 106-109.
- Munday, M. R., Campbell, D. G., Carling, D., and Hardie, D. G. (1988). Identification by amino acid sequencing of three major regulatory phosphorylation sites on rat acetyl-CoA carboxylase. *Eur J Biochem* 175, 331-338.
- Nakafuku, M., Obara, T., Kaibuchi, K., Miyajima, I., Miyajima, A., Itoh, H., Nakamura, S., Arai, K., Matsumoto, K., and Kaziro, Y. (1988). Isolation of a second yeast *Saccharomyces cerevisiae* gene (GPA2) coding for guanine nucleotide-binding regulatory protein: studies on its structure and possible functions. *Proc Natl Acad Sci U S A* 85, 1374-1378.
- Nakagawa, I., Amano, A., Mizushima, N., Yamamoto, A., Yamaguchi, H., Kamimoto, T., Nara, A., Funao, J., Nakata, M., Tsuda, K., Hamada, S., and Yoshimori, T. (2004).

- Autophagy defends cells against invading group A Streptococcus. *Science* 306, 1037-1040.
- Nakamura, T., Takeuchi, K., Muraoka, S., Takezoe, H., Takahashi, N., and Mori, N. (1999). A neurally enriched coronin-like protein, ClipinC, is a novel candidate for an actin cytoskeleton-cortical membrane-linking protein. *J Biol Chem* 274, 13322-13327.
- Nakano, A., Kato, H., Watanabe, T., Min, K. D., Yamazaki, S., Asano, Y., Seguchi, O., Higo, S., Shintani, Y., Asanuma, H., Asakura, M., Minamino, T., Kaibuchi, K., Mochizuki, N., Kitakaze, M., and Takashima, S. (2010). AMPK controls the speed of microtubule polymerization and directional cell migration through CLIP-170 phosphorylation. *Nat Cell Biol* 12, 583-590.
- Nakatogawa, H., Ichimura, Y., and Ohsumi, Y. (2007). Atg8, a ubiquitin-like protein required for autophagosome formation, mediates membrane tethering and hemifusion. *Cell* 130, 165-178.
- Nakatogawa, H., Suzuki, K., Kamada, Y., and Ohsumi, Y. (2009). Dynamics and diversity in autophagy mechanisms: lessons from yeast. *Nat Rev Mol Cell Biol* 10, 458-467.
- Neufeld, T. P. (2010). TOR-dependent control of autophagy: biting the hand that feeds. *Curr Opin Cell Biol* 22, 157-168.
- Nice, D. C., Sato, T. K., Stromhaug, P. E., Emr, S. D., and Klionsky, D. J. (2002). Cooperative binding of the cytoplasm to vacuole targeting pathway proteins, Cvt13 and Cvt20, to phosphatidylinositol 3-phosphate at the pre-autophagosomal structure is required for selective autophagy. *J Biol Chem* 277, 30198-30207.
- Nimmerjahn, F., Milosevic, S., Behrends, U., Jaffee, E. M., Pardoll, D. M., Bornkamm, G. W., and Mautner, J. (2003). Major histocompatibility complex class II-restricted presentation of a cytosolic antigen by autophagy. *Eur J Immunol* 33, 1250-1259.
- Nishida, Y., Arakawa, S., Fujitani, K., Yamaguchi, H., Mizuta, T., Kanaseki, T., Komatsu, M., Otsu, K., Tsujimoto, Y., and Shimizu, S. (2009). Discovery of Atg5/Atg7-independent alternative macroautophagy. *Nature* 461, 654-658.
- Noda, N. N., Kumeta, H., Nakatogawa, H., Satoo, K., Adachi, W., Ishii, J., Fujioka, Y., Ohsumi, Y., and Inagaki, F. (2008). Structural basis of target recognition by Atg8/LC3 during selective autophagy. *Genes Cells* 13, 1211-1218.
- Noda, N. N., Ohsumi, Y., and Inagaki, F. (2010). Atg8-family interacting motif crucial for selective autophagy. *FEBS Lett* 584, 1379-1385.
- Noda, T., Kim, J., Huang, W. P., Baba, M., Tokunaga, C., Ohsumi, Y., and Klionsky, D. J. (2000). Apg9p/Cvt7p is an integral membrane protein required for transport vesicle formation in the Cvt and autophagy pathways. *J Cell Biol* 148, 465-480.
- Norris, F. A., Atkins, R. C., and Majerus, P. W. (1997). The cDNA cloning and characterization of inositol polyphosphate 4-phosphatase type II. Evidence for conserved alternative splicing in the 4-phosphatase family. *J Biol Chem* 272, 23859-23864.
- Novak, I., Kirkin, V., McEwan, D. G., Zhang, J., Wild, P., Rozenknop, A., Rogov, V., Lohr, F., Popovic, D., Occhipinti, A., Reichert, A. S., Terzic, J., Dotsch, V., Ney, P. A., and Dikic, I. (2010). Nix is a selective autophagy receptor for mitochondrial clearance. *EMBO Rep* 11, 45-51.
- Oakhill, J. S., Chen, Z. P., Scott, J. W., Steel, R., Castelli, L. A., Ling, N., Macaulay, S. L., and Kemp, B. E. (2010). beta-Subunit myristoylation is the gatekeeper for initiating

- metabolic stress sensing by AMP-activated protein kinase (AMPK). *Proc Natl Acad Sci U S A* 107, 19237-19241.
- Obenaus, J. C., Cantley, L. C., and Yaffe, M. B. (2003). Scansite 2.0: Proteome-wide prediction of cell signaling interactions using short sequence motifs. *Nucleic Acids Res* 31, 3635-3641.
- Odorizzi, G., Babst, M., and Emr, S. D. (2000). Phosphoinositide signaling and the regulation of membrane trafficking in yeast. *Trends Biochem Sci* 25, 229-235.
- Ogata, M., Hino, S., Saito, A., Morikawa, K., Kondo, S., Kanemoto, S., Murakami, T., Taniguchi, M., Tanii, I., Yoshinaga, K., Shiosaka, S., Hammarback, J. A., Urano, F., and Imaizumi, K. (2006). Autophagy is activated for cell survival after endoplasmic reticulum stress. *Mol Cell Biol* 26, 9220-9231.
- Ogawa, M., Yoshimori, T., Suzuki, T., Sagara, H., Mizushima, N., and Sasakawa, C. (2005). Escape of intracellular *Shigella* from autophagy. *Science* 307, 727-731.
- Ogura, K., and Goshima, Y. (2006). The autophagy-related kinase UNC-51 and its binding partner UNC-14 regulate the subcellular localization of the Netrin receptor UNC-5 in *Caenorhabditis elegans*. *Development* 133, 3441-3450.
- Ogura, K., Okada, T., Mitani, S., Gengyo-Ando, K., Baillie, D. L., Kohara, Y., and Goshima, Y. (2010). Protein phosphatase 2A cooperates with the autophagy-related kinase UNC-51 to regulate axon guidance in *Caenorhabditis elegans*. *Development* 137, 1657-1667.
- Ogura, K., Shirakawa, M., Barnes, T. M., Hekimi, S., and Ohshima, Y. (1997). The UNC-14 protein required for axonal elongation and guidance in *Caenorhabditis elegans* interacts with the serine/threonine kinase UNC-51. *Genes Dev* 11, 1801-1811.
- Ogura, K., Wicky, C., Magnenat, L., Tobler, H., Mori, I., Muller, F., and Ohshima, Y. (1994). *Caenorhabditis elegans unc-51* gene required for axonal elongation encodes a novel serine/threonine kinase. *Genes Dev* 8, 2389-2400.
- Okamoto, K., Kondo-Okamoto, N., and Ohsumi, Y. (2009). Mitochondria-anchored receptor Atg32 mediates degradation of mitochondria via selective autophagy. *Dev Cell* 17, 87-97.
- Owen, M. R., Doran, E., and Halestrap, A. P. (2000). Evidence that metformin exerts its anti-diabetic effects through inhibition of complex 1 of the mitochondrial respiratory chain. *Biochem J* 348 Pt 3, 607-614.
- Pankiv, S., Clausen, T. H., Lamark, T., Brech, A., Bruun, J. A., Outzen, H., Overvatn, A., Bjorkoy, G., and Johansen, T. (2007). p62/SQSTM1 binds directly to Atg8/LC3 to facilitate degradation of ubiquitinated protein aggregates by autophagy. *J Biol Chem* 282, 24131-24145.
- Papandreou, I., Lim, A. L., Laderoute, K., and Denko, N. C. (2008). Hypoxia signals autophagy in tumor cells via AMPK activity, independent of HIF-1, BNIP3, and BNIP3L. *Cell Death Differ* 15, 1572-1581.
- Pattingre, S., Tassa, A., Qu, X., Garuti, R., Liang, X. H., Mizushima, N., Packer, M., Schneider, M. D., and Levine, B. (2005). Bcl-2 antiapoptotic proteins inhibit Beclin 1-dependent autophagy. *Cell* 122, 927-939.
- Pearce, L. R., Huang, X., Boudeau, J., Pawlowski, R., Wullschleger, S., Deak, M., Ibrahim, A. F., Gourlay, R., Magnuson, M. A., and Alessi, D. R. (2007). Identification of Protor as a novel Rictor-binding component of mTOR complex-2. *Biochem J* 405, 513-522.
- Peterson, M. R., and Emr, S. D. (2001). The class C Vps complex functions at multiple stages of the vacuolar transport pathway. *Traffic* 2, 476-486.

- Peterson, T. R., Laplante, M., Thoreen, C. C., Sancak, Y., Kang, S. A., Kuehl, W. M., Gray, N. S., and Sabatini, D. M. (2009). DEPTOR is an mTOR inhibitor frequently overexpressed in multiple myeloma cells and required for their survival. *Cell* 137, 873-886.
- Polekhina, G., Gupta, A., Michell, B. J., van Denderen, B., Murthy, S., Feil, S. C., Jennings, I. G., Campbell, D. J., Witters, L. A., Parker, M. W., Kemp, B. E., and Stapleton, D. (2003). AMPK beta subunit targets metabolic stress sensing to glycogen. *Curr Biol* 13, 867-871.
- Polson, H. E., de Lartigue, J., Rigden, D. J., Reedijk, M., Urbe, S., Clague, M. J., and Tooze, S. A. (2010). Mammalian Atg18 (WIPI2) localizes to omegasome-anchored phagophores and positively regulates LC3 lipidation. *Autophagy* 6.
- Potter, C. J., Pedraza, L. G., and Xu, T. (2002). Akt regulates growth by directly phosphorylating Tsc2. *Nat Cell Biol* 4, 658-665.
- Proikas-Cezanne, T., Waddell, S., Gaugel, A., Frickey, T., Lupas, A., and Nordheim, A. (2004). WIPI-1alpha (WIPI49), a member of the novel 7-bladed WIPI protein family, is aberrantly expressed in human cancer and is linked to starvation-induced autophagy. *Oncogene* 23, 9314-9325.
- Ptacek, J., Devgan, G., Michaud, G., Zhu, H., Zhu, X., Fasolo, J., Guo, H., Jona, G., Bretkreutz, A., Sopko, R., McCartney, R. R., Schmidt, M. C., Rachidi, N., Lee, S. J., Mah, A. S., Meng, L., Stark, M. J., Stern, D. F., De Virgilio, C., Tyers, M., Andrews, B., Gerstein, M., Schweitzer, B., Predki, P. F., and Snyder, M. (2005). Global analysis of protein phosphorylation in yeast. *Nature* 438, 679-684.
- Puissant, A., Robert, G., Fenouille, N., Luciano, F., Cassuto, J. P., Raynaud, S., and Auberger, P. (2010). Resveratrol promotes autophagic cell death in chronic myelogenous leukemia cells via JNK-mediated p62/SQSTM1 expression and AMPK activation. *Cancer Res* 70, 1042-1052.
- Ravikumar, B., Moreau, K., Jahreiss, L., Puri, C., and Rubinsztein, D. C. (2010). Plasma membrane contributes to the formation of pre-autophagosomal structures. *Nat Cell Biol* 12, 747-757.
- Reggiori, F., Tucker, K. A., Stromhaug, P. E., and Klionsky, D. J. (2004). The Atg1-Atg13 complex regulates Atg9 and Atg23 retrieval transport from the pre-autophagosomal structure. *Dev Cell* 6, 79-90.
- Roth, M. B., Zahler, A. M., and Stolk, J. A. (1991). A conserved family of nuclear phosphoproteins localized to sites of polymerase II transcription. *J Cell Biol* 115, 587-596.
- Roux, P. P., and Blenis, J. (2004). ERK and p38 MAPK-activated protein kinases: a family of protein kinases with diverse biological functions. *Microbiol Mol Biol Rev* 68, 320-344.
- Sakamoto, K., Goransson, O., Hardie, D. G., and Alessi, D. R. (2004). Activity of LKB1 and AMPK-related kinases in skeletal muscle: effects of contraction, phenformin, and AICAR. *Am J Physiol Endocrinol Metab* 287, E310-317.
- Sakamoto, K., McCarthy, A., Smith, D., Green, K. A., Grahame Hardie, D., Ashworth, A., and Alessi, D. R. (2005). Deficiency of LKB1 in skeletal muscle prevents AMPK activation and glucose uptake during contraction. *Embo J* 24, 1810-1820.
- Sakamoto, K., Zarrinpashneh, E., Budas, G. R., Pouleur, A. C., Dutta, A., Prescott, A. R., Vanoverschelde, J. L., Ashworth, A., Jovanovic, A., Alessi, D. R., and Bertrand, L. (2006). Deficiency of LKB1 in heart prevents ischemia-mediated activation of AMPKalpha2 but not AMPKalpha1. *Am J Physiol Endocrinol Metab* 290, E780-788.

- Sancak, Y., Bar-Peled, L., Zoncu, R., Markhard, A. L., Nada, S., and Sabatini, D. M. (2010). Ragulator-Rag complex targets mTORC1 to the lysosomal surface and is necessary for its activation by amino acids. *Cell* 141, 290-303.
- Sancak, Y., Peterson, T. R., Shaul, Y. D., Lindquist, R. A., Thoreen, C. C., Bar-Peled, L., and Sabatini, D. M. (2008). The Rag GTPases bind raptor and mediate amino acid signaling to mTORC1. *Science* 320, 1496-1501.
- Sancak, Y., Thoreen, C. C., Peterson, T. R., Lindquist, R. A., Kang, S. A., Spooner, E., Carr, S. A., and Sabatini, D. M. (2007). PRAS40 is an insulin-regulated inhibitor of the mTORC1 protein kinase. *Mol Cell* 25, 903-915.
- Sanders, M. J., Grondin, P. O., Hegarty, B. D., Snowden, M. A., and Carling, D. (2007). Investigating the mechanism for AMP activation of the AMP-activated protein kinase cascade. *Biochem J* 403, 139-148.
- Sano, H., Kane, S., Sano, E., Miinea, C. P., Asara, J. M., Lane, W. S., Garner, C. W., and Lienhard, G. E. (2003). Insulin-stimulated phosphorylation of a Rab GTPase-activating protein regulates GLUT4 translocation. *J Biol Chem* 278, 14599-14602.
- Sarbassov, D. D., Ali, S. M., and Sabatini, D. M. (2005). Growing roles for the mTOR pathway. *Curr Opin Cell Biol* 17, 596-603.
- Sarbassov, D. D., Ali, S. M., Kim, D. H., Guertin, D. A., Latek, R. R., Erdjument-Bromage, H., Tempst, P., and Sabatini, D. M. (2004). Rictor, a novel binding partner of mTOR, defines a rapamycin-insensitive and raptor-independent pathway that regulates the cytoskeleton. *Curr Biol* 14, 1296-1302.
- Schlumpberger, M., Schaeffeler, E., Straub, M., Bredschneider, M., Wolf, D. H., and Thumm, M. (1997). AUT1, a gene essential for autophagocytosis in the yeast *Saccharomyces cerevisiae*. *J Bacteriol* 179, 1068-1076.
- Scott, J. W., Hawley, S. A., Green, K. A., Anis, M., Stewart, G., Scullion, G. A., Norman, D. G., and Hardie, D. G. (2004). CBS domains form energy-sensing modules whose binding of adenosine ligands is disrupted by disease mutations. *J Clin Invest* 113, 274-284.
- Scott, R. C., Juhasz, G., and Neufeld, T. P. (2007). Direct induction of autophagy by Atg1 inhibits cell growth and induces apoptotic cell death. *Curr Biol* 17, 1-11.
- Scott, S. V., Guan, J., Hutchins, M. U., Kim, J., and Klionsky, D. J. (2001). Cvt19 is a receptor for the cytoplasm-to-vacuole targeting pathway. *Mol Cell* 7, 1131-1141.
- Seibenhener, M. L., Babu, J. R., Geetha, T., Wong, H. C., Krishna, N. R., and Wooten, M. W. (2004). Sequestosome 1/p62 is a polyubiquitin chain binding protein involved in ubiquitin proteasome degradation. *Mol Cell Biol* 24, 8055-8068.
- Sekito, T., Kawamata, T., Ichikawa, R., Suzuki, K., and Ohsumi, Y. (2009). Atg17 recruits Atg9 to organize the pre-autophagosomal structure. *Genes Cells* 14, 525-538.
- Shintani, T., Mizushima, N., Ogawa, Y., Matsuura, A., Noda, T., and Ohsumi, Y. (1999). Apg10p, a novel protein-conjugating enzyme essential for autophagy in yeast. *Embo J* 18, 5234-5241.
- Shintani, T., Suzuki, K., Kamada, Y., Noda, T., and Ohsumi, Y. (2001). Apg2p functions in autophagosome formation on the perivacuolar structure. *J Biol Chem* 276, 30452-30460.
- Stapleton, D., Mitchelhill, K. I., Gao, G., Widmer, J., Michell, B. J., Teh, T., House, C. M., Fernandez, C. S., Cox, T., Witters, L. A., and Kemp, B. E. (1996). Mammalian AMP-activated protein kinase subfamily. *J Biol Chem* 271, 611-614.

- Stasyk, O. V., Stasyk, O. G., Mathewson, R. D., Farre, J. C., Nazarko, V. Y., Krasovska, O. S., Subramani, S., Cregg, J. M., and Sibirny, A. A. (2006). Atg28, a novel coiled-coil protein involved in autophagic degradation of peroxisomes in the methylotrophic yeast *Pichia pastoris*. *Autophagy* 2, 30-38.
- Stephan, J. S., Yeh, Y. Y., Ramachandran, V., Deminoff, S. J., and Herman, P. K. (2009). The Tor and PKA signaling pathways independently target the Atg1/Atg13 protein kinase complex to control autophagy. *Proc Natl Acad Sci U S A* 106, 17049-17054.
- Straub, M., Bredschneider, M., and Thumm, M. (1997). AUT3, a serine/threonine kinase gene, is essential for autophagocytosis in *Saccharomyces cerevisiae*. *J Bacteriol* 179, 3875-3883.
- Stromhaug, P. E., Reggiori, F., Guan, J., Wang, C. W., and Klionsky, D. J. (2004). Atg21 is a phosphoinositide binding protein required for efficient lipidation and localization of Atg8 during uptake of aminopeptidase I by selective autophagy. *Mol Biol Cell* 15, 3553-3566.
- Studier, F. W., and Moffatt, B. A. (1986). Use of bacteriophage T7 RNA polymerase to direct selective high-level expression of cloned genes. *J Mol Biol* 189, 113-130.
- Sun, Q., Fan, W., Chen, K., Ding, X., Chen, S., and Zhong, Q. (2008). Identification of Barkor as a mammalian autophagy-specific factor for Beclin 1 and class III phosphatidylinositol 3-kinase. *Proc Natl Acad Sci U S A* 105, 19211-19216.
- Suter, M., Riek, U., Tuerk, R., Schlattner, U., Wallimann, T., and Neumann, D. (2006). Dissecting the role of 5'-AMP for allosteric stimulation, activation, and deactivation of AMP-activated protein kinase. *J Biol Chem* 281, 32207-32216.
- Suzuki, K., Kondo, C., Morimoto, M., and Ohsumi, Y. (2010). Selective transport of alpha-mannosidase by autophagic pathways: identification of a novel receptor, Atg34p. *J Biol Chem* 285, 30019-30025.
- Suzuki, K., Kubota, Y., Sekito, T., and Ohsumi, Y. (2007). Hierarchy of Atg proteins in pre-autophagosomal structure organization. *Genes Cells* 12, 209-218.
- Takahashi, Y., Coppola, D., Matsushita, N., Cuaing, H. D., Sun, M., Sato, Y., Liang, C., Jung, J. U., Cheng, J. Q., Mule, J. J., Pledger, W. J., and Wang, H. G. (2007). Bif-1 interacts with Beclin 1 through UVRAG and regulates autophagy and tumorigenesis. *Nat Cell Biol* 9, 1142-1151.
- Tan, J. M., Wong, E. S., Kirkpatrick, D. S., Pletnikova, O., Ko, H. S., Tay, S. P., Ho, M. W., Troncoso, J., Gygi, S. P., Lee, M. K., Dawson, V. L., Dawson, T. M., and Lim, K. L. (2008). Lysine 63-linked ubiquitination promotes the formation and autophagic clearance of protein inclusions associated with neurodegenerative diseases. *Hum Mol Genet* 17, 431-439.
- Tanida, I., Mizushima, N., Kiyooka, M., Ohsumi, M., Ueno, T., Ohsumi, Y., and Kominami, E. (1999). Apg7p/Cvt2p: A novel protein-activating enzyme essential for autophagy. *Mol Biol Cell* 10, 1367-1379.
- Tasdemir, E., Maiuri, M. C., Galluzzi, L., Vitale, I., Djavaheri-Mergny, M., D'Amelio, M., Criollo, A., Morselli, E., Zhu, C., Harper, F., Nannmark, U., Samara, C., Pinton, P., Vicencio, J. M., Carnuccio, R., Moll, U. M., Madeo, F., Paterlini-Brechot, P., Rizzuto, R., Szabadkai, G., Pierron, G., Blomgren, K., Tavernarakis, N., Codogno, P., Cecconi, F., and Kroemer, G. (2008). Regulation of autophagy by cytoplasmic p53. *Nat Cell Biol* 10, 676-687.

- Tasdemir, E., Maiuri, M. C., Tajeddine, N., Vitale, I., Criollo, A., Vicencio, J. M., Hickman, J. A., Geneste, O., and Kroemer, G. (2007). Cell cycle-dependent induction of autophagy, mitophagy and reticulophagy. *Cell Cycle* 6, 2263-2267.
- Tee, A. R., Manning, B. D., Roux, P. P., Cantley, L. C., and Blenis, J. (2003). Tuberous sclerosis complex gene products, Tuberin and Hamartin, control mTOR signaling by acting as a GTPase-activating protein complex toward Rheb. *Curr Biol* 13, 1259-1268.
- Teter, S. A., Eggerton, K. P., Scott, S. V., Kim, J., Fischer, A. M., and Klionsky, D. J. (2001). Degradation of lipid vesicles in the yeast vacuole requires function of Cvt17, a putative lipase. *J Biol Chem* 276, 2083-2087.
- Thomas, S. M., Hagel, M., and Turner, C. E. (1999). Characterization of a focal adhesion protein, Hic-5, that shares extensive homology with paxillin. *J Cell Sci* 112 (Pt 2), 181-190.
- Tian, E., Wang, F., Han, J., and Zhang, H. (2009). epg-1 functions in autophagy-regulated processes and may encode a highly divergent Atg13 homolog in *C. elegans*. *Autophagy* 5, 608-615.
- Toda, H., Mochizuki, H., Flores, R., 3rd, Josowitz, R., Krasieva, T. B., Lamorte, V. J., Suzuki, E., Gindhart, J. G., Furukubo-Tokunaga, K., and Tomoda, T. (2008). UNC-51/ATG1 kinase regulates axonal transport by mediating motor-cargo assembly. *Genes Dev* 22, 3292-3307.
- Toda, T., Cameron, S., Sass, P., Zoller, M., and Wigler, M. (1987). Three different genes in *S. cerevisiae* encode the catalytic subunits of the cAMP-dependent protein kinase. *Cell* 50, 277-287.
- Tomoda, T., Bhatt, R. S., Kuroyanagi, H., Shirasawa, T., and Hatten, M. E. (1999). A mouse serine/threonine kinase homologous to *C. elegans* UNC51 functions in parallel fiber formation of cerebellar granule neurons. *Neuron* 24, 833-846.
- Tomoda, T., Kim, J. H., Zhan, C., and Hatten, M. E. (2004). Role of Unc51.1 and its binding partners in CNS axon outgrowth. *Genes Dev* 18, 541-558.
- Toth, M. L., Sigmond, T., Borsos, E., Barna, J., Erdelyi, P., Takacs-Vellai, K., Orosz, L., Kovacs, A. L., Csikos, G., Sass, M., and Vellai, T. (2008). Longevity pathways converge on autophagy genes to regulate life span in *Caenorhabditis elegans*. *Autophagy* 4, 330-338.
- Tsukada, M., and Ohsumi, Y. (1993). Isolation and characterization of autophagy-defective mutants of *Saccharomyces cerevisiae*. *FEBS Lett* 333, 169-174.
- Tucker, K. A., Reggiori, F., Dunn, W. A., Jr., and Klionsky, D. J. (2003). Atg23 is essential for the cytoplasm to vacuole targeting pathway and efficient autophagy but not pexophagy. *J Biol Chem* 278, 48445-48452.
- Turnley, A. M., Stapleton, D., Mann, R. J., Witters, L. A., Kemp, B. E., and Bartlett, P. F. (1999). Cellular distribution and developmental expression of AMP-activated protein kinase isoforms in mouse central nervous system. *J Neurochem* 72, 1707-1716.
- van den Bout, I., and Divecha, N. (2009). PIP5K-driven PtdIns(4,5)P2 synthesis: regulation and cellular functions. *J Cell Sci* 122, 3837-3850.
- Vander Haar, E., Lee, S. I., Bandhakavi, S., Griffin, T. J., and Kim, D. H. (2007). Insulin signalling to mTOR mediated by the Akt/PKB substrate PRAS40. *Nat Cell Biol* 9, 316-323.
- Viollet, B., Andreelli, F., Jorgensen, S. B., Perrin, C., Geloën, A., Flamez, D., Mu, J., Lenzner, C., Baud, O., Bennoun, M., Gomas, E., Nicolas, G., Wojtaszewski, J. F., Kahn, B. M., and Alessi, M. C. (2007). The mTORC1 inhibitor rapamycin (sirolimus) improves insulin sensitivity in obese mice. *Diabetes* 56, 103-111.

- A., Carling, D., Schuit, F. C., Birnbaum, M. J., Richter, E. A., Burcelin, R., and Vaulont, S. (2003). The AMP-activated protein kinase alpha2 catalytic subunit controls whole-body insulin sensitivity. *J Clin Invest* 111, 91-98.
- Viollet, B., Athea, Y., Mounier, R., Guigas, B., Zarrinpashneh, E., Horman, S., Lantier, L., Hebrard, S., Devin-Leclerc, J., Beauloye, C., Foretz, M., Andreelli, F., Ventura-Clapier, R., and Bertrand, L. (2009). AMPK: Lessons from transgenic and knockout animals. *Front Biosci* 14, 19-44.
- Wakil, S. J., and Abu-Elheiga, L. A. (2009). Fatty acid metabolism: target for metabolic syndrome. *J Lipid Res* 50 Suppl, S138-143.
- Wang, Z., Wilson, W. A., Fujino, M. A., and Roach, P. J. (2001). Antagonistic controls of autophagy and glycogen accumulation by Snf1p, the yeast homolog of AMP-activated protein kinase, and the cyclin-dependent kinase Pho85p. *Mol Cell Biol* 21, 5742-5752.
- Warden, S. M., Richardson, C., O'Donnell, J., Jr., Stapleton, D., Kemp, B. E., and Witters, L. A. (2001). Post-translational modifications of the beta-1 subunit of AMP-activated protein kinase affect enzyme activity and cellular localization. *Biochem J* 354, 275-283.
- Warnecke, D., Erdmann, R., Fahl, A., Hube, B., Muller, F., Zank, T., Zahringer, U., and Heinz, E. (1999). Cloning and functional expression of UGT genes encoding sterol glucosyltransferases from *Saccharomyces cerevisiae*, *Candida albicans*, *Pichia pastoris*, and *Dictyostelium discoideum*. *J Biol Chem* 274, 13048-13059.
- Wei, Y., Pattingre, S., Sinha, S., Bassik, M., and Levine, B. (2008). JNK1-mediated phosphorylation of Bcl-2 regulates starvation-induced autophagy. *Mol Cell* 30, 678-688.
- Williams, T., Forsberg, L. J., Viollet, B., and Brenman, J. E. (2009). Basal autophagy induction without AMP-activated protein kinase under low glucose conditions. *Autophagy* 5, 1155-1165.
- Winder, W. W., and Hardie, D. G. (1999). AMP-activated protein kinase, a metabolic master switch: possible roles in type 2 diabetes. *Am J Physiol* 277, E1-10.
- Winder, W. W., Wilson, H. A., Hardie, D. G., Rasmussen, B. B., Hutber, C. A., Call, G. B., Clayton, R. D., Conley, L. M., Yoon, S., and Zhou, B. (1997). Phosphorylation of rat muscle acetyl-CoA carboxylase by AMP-activated protein kinase and protein kinase A. *J Appl Physiol* 82, 219-225.
- Woo, S. Y., Kim, D. H., Jun, C. B., Kim, Y. M., Haar, E. V., Lee, S. I., Hegg, J. W., Bandhakavi, S., Griffin, T. J., and Kim, D. H. (2007). PRR5, a novel component of mTOR complex 2, regulates platelet-derived growth factor receptor beta expression and signaling. *J Biol Chem* 282, 25604-25612.
- Woods, A., Dickerson, K., Heath, R., Hong, S. P., Momcilovic, M., Johnstone, S. R., Carlson, M., and Carling, D. (2005). Ca²⁺/calmodulin-dependent protein kinase kinase-beta acts upstream of AMP-activated protein kinase in mammalian cells. *Cell Metab* 2, 21-33.
- Woods, A., Johnstone, S. R., Dickerson, K., Leiper, F. C., Fryer, L. G., Neumann, D., Schlattner, U., Wallimann, T., Carlson, M., and Carling, D. (2003). LKB1 is the upstream kinase in the AMP-activated protein kinase cascade. *Curr Biol* 13, 2004-2008.
- Wullschleger, S., Loewith, R., and Hall, M. N. (2006). TOR signaling in growth and metabolism. *Cell* 124, 471-484.
- Yaffe, M. B., Rittinger, K., Volinia, S., Caron, P. R., Aitken, A., Leffers, H., Gamblin, S. J., Smerdon, S. J., and Cantley, L. C. (1997). The structural basis for 14-3-3:phosphopeptide binding specificity. *Cell* 91, 961-971.

- Yan, J., Kuroyanagi, H., Kuroiwa, A., Matsuda, Y., Tokumitsu, H., Tomoda, T., Shirasawa, T., and Muramatsu, M. (1998). Identification of mouse ULK1, a novel protein kinase structurally related to *C. elegans* UNC-51. *Biochem Biophys Res Commun* 246, 222-227.
- Yan, J., Kuroyanagi, H., Tomemori, T., Okazaki, N., Asato, K., Matsuda, Y., Suzuki, Y., Ohshima, Y., Mitani, S., Masuho, Y., Shirasawa, T., and Muramatsu, M. (1999). Mouse ULK2, a novel member of the UNC-51-like protein kinases: unique features of functional domains. *Oncogene* 18, 5850-5859.
- Yang, Q., Inoki, K., Ikenoue, T., and Guan, K. L. (2006a). Identification of Sin1 as an essential TORC2 component required for complex formation and kinase activity. *Genes Dev* 20, 2820-2832.
- Yang, Z., and Klionsky, D. J. (2010). Mammalian autophagy: core molecular machinery and signaling regulation. *Curr Opin Cell Biol* 22, 124-131.
- Yang, Z., Huang, J., Geng, J., Nair, U., and Klionsky, D. J. (2006b). Atg22 recycles amino acids to link the degradative and recycling functions of autophagy. *Mol Biol Cell* 17, 5094-5104.
- Yeh, Y. Y., Wrasman, K., and Herman, P. K. (2010). Autophosphorylation within the Atg1 activation loop is required for both kinase activity and the induction of autophagy in *Saccharomyces cerevisiae*. *Genetics* 185, 871-882.
- Yen, W. L., and Klionsky, D. J. (2007). Atg27 is a second transmembrane cycling protein. *Autophagy* 3, 254-256.
- Yen, W. L., Legakis, J. E., Nair, U., and Klionsky, D. J. (2007). Atg27 is required for autophagy-dependent cycling of Atg9. *Mol Biol Cell* 18, 581-593.
- Yla-Anttila, P., Vihinen, H., Jokitalo, E., and Eskelinen, E. L. (2009). 3D tomography reveals connections between the phagophore and endoplasmic reticulum. *Autophagy* 5, 1180-1185.
- Yorimitsu, T., and Klionsky, D. J. (2005). Atg11 links cargo to the vesicle-forming machinery in the cytoplasm to vacuole targeting pathway. *Mol Biol Cell* 16, 1593-1605.
- Yorimitsu, T., He, C., Wang, K., and Klionsky, D. J. (2009). Tap42-associated protein phosphatase type 2A negatively regulates induction of autophagy. *Autophagy* 5, 616-624.
- Yorimitsu, T., Zaman, S., Broach, J. R., and Klionsky, D. J. (2007). Protein kinase A and Sch9 cooperatively regulate induction of autophagy in *Saccharomyces cerevisiae*. *Mol Biol Cell* 18, 4180-4189.
- Young, A. R., Chan, E. Y., Hu, X. W., Kochl, R., Crawshaw, S. G., High, S., Hailey, D. W., Lippincott-Schwartz, J., and Tooze, S. A. (2006). Starvation and ULK1-dependent cycling of mammalian Atg9 between the TGN and endosomes. *J Cell Sci* 119, 3888-3900.
- Young, A. R., Narita, M., Ferreira, M., Kirschner, K., Sadaie, M., Darot, J. F., Tavares, S., Arakawa, S., Shimizu, S., Watt, F. M., and Narita, M. (2009). Autophagy mediates the mitotic senescence transition. *Genes Dev* 23, 798-803.
- Yu, L., Alva, A., Su, H., Dutt, P., Freundt, E., Welsh, S., Baehrecke, E. H., and Lenardo, M. J. (2004). Regulation of an ATG7-beclin 1 program of autophagic cell death by caspase-8. *Science* 304, 1500-1502.
- Yu, L., McPhee, C. K., Zheng, L., Mardones, G. A., Rong, Y., Peng, J., Mi, N., Zhao, Y., Liu, Z., Wan, F., Hailey, D. W., Oorschot, V., Klumperman, J., Baehrecke, E. H., and Lenardo, M. J. (2010). Termination of autophagy and reformation of lysosomes regulated by mTOR. *Nature* 465, 942-946.

- Yue, Z., Jin, S., Yang, C., Levine, A. J., and Heintz, N. (2003). Beclin 1, an autophagy gene essential for early embryonic development, is a haploinsufficient tumor suppressor. *Proc Natl Acad Sci U S A* 100, 15077-15082.
- Zalckvar, E., Berissi, H., Mizrachy, L., Idelchuk, Y., Koren, I., Eisenstein, M., Sabanay, H., Pinkas-Kramarski, R., and Kimchi, A. (2009). DAP-kinase-mediated phosphorylation on the BH3 domain of beclin 1 promotes dissociation of beclin 1 from Bcl-XL and induction of autophagy. *EMBO Rep* 10, 285-292.
- Zhang, L., Li, J., Young, L. H., and Caplan, M. J. (2006). AMP-activated protein kinase regulates the assembly of epithelial tight junctions. *Proc Natl Acad Sci U S A* 103, 17272-17277.
- Zhang, Y., Gao, X., Saucedo, L. J., Ru, B., Edgar, B. A., and Pan, D. (2003). Rheb is a direct target of the tuberous sclerosis tumour suppressor proteins. *Nat Cell Biol* 5, 578-581.
- Zhao, J., Brault, J. J., Schild, A., Cao, P., Sandri, M., Schiaffino, S., Lecker, S. H., and Goldberg, A. L. (2007). FoxO3 coordinately activates protein degradation by the autophagic/lysosomal and proteasomal pathways in atrophying muscle cells. *Cell Metab* 6, 472-483.
- Zheng, B., and Cantley, L. C. (2007). Regulation of epithelial tight junction assembly and disassembly by AMP-activated protein kinase. *Proc Natl Acad Sci U S A* 104, 819-822.
- Zhong, Y., Wang, Q. J., Li, X., Yan, Y., Backer, J. M., Chait, B. T., Heintz, N., and Yue, Z. (2009). Distinct regulation of autophagic activity by Atg14L and Rubicon associated with Beclin 1-phosphatidylinositol-3-kinase complex. *Nat Cell Biol* 11, 468-476.
- Zhou, X., Babu, J. R., da Silva, S., Shu, Q., Graef, I. A., Oliver, T., Tomoda, T., Tani, T., Wooten, M. W., and Wang, F. (2007). Unc-51-like kinase 1/2-mediated endocytic processes regulate filopodia extension and branching of sensory axons. *Proc Natl Acad Sci U S A* 104, 5842-5847.

7 Appendix

7.1 Abbreviations

2DG	2-Deoxyglucose
³² P	Radioactive phosphorus isotope, atomic mass 32 units
α-	Anti-
aa	Amino acid
ACC1/2	Acetyl-CoA (coenzyme A) carboxylase 1/2
ADP	Adenosine diphosphate
AICAR	5-aminoimidazole-4-carboxamide-1-β-D-ribofuranoside
AKT	Murine retrovirus Akt-8 homolog
Ambra 1	Activating molecule in Beclin 1 mediated autophagy
Amp	Ampicillin
AMP	Adenosine monophosphate
AMPK	Adenosine monophosphate activated protein kinase
APS	Ammonium persulfate
AS160	AKT substrate of 160 kDa
Atg1/2/etc	Autophagy-related protein 1/2/etc
ATP	Adenosine triphosphate
Bcl-2	B-cell lymphoma 2
Beclin 1	Coiled-coil myosin-like BCL2-interacting protein
Bif 1	Bax-interacting factor 1
BMAL1	Brain and muscle ARNT (Aryl hydrocarbon receptor nuclear translocator)-like 1
BSA	Bovine serum albumin
ca	Constitutively active
CamK2	Calcium/calmodulin dependent protein kinase 2
CamKKα/β	Calcium/calmodulin dependent protein kinase kinase α/β
cAMP	Cyclic adenosine monophosphate
CBS	Cystathionine β-synthase
CDC2	Cell division cycle 2-related protein kinase
CDK5	Cyclin-dependent kinase 5
ce	<i>Caenorhabditis elegans</i> (roundworm)
CHAPS	3-[(3-Cholamidopropyl)dimethylammonio] -1-propanesulfonate
CK1	Casein kinase 1
CLIP-170	Cytoplasmic linker protein of 170 kDa
CLOCK	Circadian locomotor output cycles protein kaput
COS7	Cells being CV-1 (simian) in Origin and SV40-transformed
Cry1	Cryptochrome 1
Cvt	Cytoplasm to vacuole targeting pathway
DAPK	Death receptor associated protein kinase
Deptor	DEP (dishevelled, egl-10, pleckstrin)-domain containing mTOR-interacting protein

DKO	Double knockout
DLC1	Dynein light chain 1
dm	<i>Drosophila melanogaster</i> (fruit fly)
DMEM	Dulbecco's modification of Eagle's medium
DMSO	Dimethyl sulfoxide
DNA	Deoxyribonucleic acid
dNTP	Deoxyribonucleotide
DTT	Dithiothreitol
EBSS	Earle's Balanced Salt Solution
ECL	Enhanced chemiluminescence
EDTA	Ethylenediamine tetraacetic acid
eEF2K	Eukaryotic elongation factor 2 kinase
EGFR	Epidermal growth factor receptor
epg-1	Ectopic PGL (P granule abnormality protein) granules 1
ER	Endoplasmic reticulum
ERK1	Extracellular signal-regulated kinase 1
FBS	Fetal bovine serum
FIP200	Focal adhesion kinase family interacting protein of 200 kDa
FOXO3	Forkhead box O3
GAP	GTPase activating protein
GβL	G protein β subunit-like
GFP	Green fluorescent protein
GPCR	G-protein coupled receptor
GS	Glycogen synthase
GSK3β	Glycogen synthase kinase 3 beta
GST	Glutathione S-transferase
H2B	Histone 2B
HBSS	Hank's buffered salt solution
HEK293T	Human embryonic kidney cells, clone 293, transformed
HEPES	4-(2-hydroxyethyl)-1-piperazineethanesulfonic acid
hs	<i>Homo sapiens</i> (human)
hVps34	human vacuolar protein sorting defective 34 homolog
IGFR	Insulin-like growth factor receptor
IgG	Immunoglobulin G
INPP4A/B	Inositol polyphosphate 4-phosphatase type I/ II
IPTG	Isopropyl β-D-1-thiogalactopyranoside
IRS1	Insulin receptor substrate 1
JNK	c-Jun amino terminal kinase
Kan	Kanamycin
kd	Kinase defective
kDa	Kilodalton
KO	Knockout

LB	Luri-Bertani (media)
LC/MS/MS	Liquid chromatography/tandem mass spectrometry
LC3	Microtubule-associated light chain 3
LKB1	Liver kinase B1
mAb	Monoclonal antibody
MAPK	Mitogen-activated protein kinases
mAtg9/13	Mammalian autophagy-related protein 9/13
MEF	Mouse embryonic fibroblast
MEKK	MAPK/ERK kinase kinase 1
MKK	MAP kinase kinase 4
mLST8	Mammalian lethal with SEC13 protein 8
mm	<i>Mus musculus</i> (house mouse)
MRLC	Non-muscle myosin regulatory light chain
mSIN1	Mammalian stress-activated MAP-kinase-interacting protein 1
Msn2/4	Multicopy suppressor of SNF1 mutation
mTOR	Mammalian target of rapamycin
mTORC1/2	mTOR complex 1/2
NAD ⁺	Nicotinamide adenine dinucleotide
NBR1	Neighbor of BRCA1 (Breast cancer type 1 susceptibility protein
NP-40	Nonidet TM P-40 (octylphenoxypolyethoxyethanol; IGEPAL® CA-630)
OD ₆₀₀	Optical density at 600 nanometers
p38	Mitogen-activated protein kinase p38
pAb	Polyclonal antibody
PAGE	Polyacrylamide gel electrophoresis
PAS	Preautophagosomal structure
PBS	Phosphate buffered saline
PCR	Polymerase chain reaction
PEI	Polyethyleneimine
PGC1 α	Peroxisome proliferator-activated receptor gamma coactivator 1 α
PI	Phosphatidylinositol
PI(3,4,5)P ₃	Phosphatidylinositol-3,4,5-trisphosphate
PI(3,4)P ₂	Phosphatidylinositol-3,4-bisphosphate
PI(3)P	Phosphatidylinositol-3-phosphate
PI(4,5)P ₂	Phosphatidylinositol-4,5-bisphosphate
PI(4)P	Phosphatidylinositol-4-phosphate
PI3K	Phosphatidylinositol 3-kinase/Phosphoinositide 3-kinase
PKA	Protein kinase A
PKC $\alpha/\beta/\gamma/\delta/\epsilon/\mu$	Protein kinase C $\alpha/\beta/\gamma/\delta/\epsilon/\mu$
PMSF	Phenylmethanesulfonylfluoride
PP2A/C	Protein phosphatase 2A/C
PRAS40	Proline-rich AKT substrate of 40 kDa
Protor	Protein observed with Rictor

PRR5	Proline-rich protein 5
PTEN	Phosphatase and tensin homolog deleted on chromosome 10
PVDF	Polyvinylidene difluoride
RaM	Rabbit anti mouse antibody
Raptor	Regulatory associated protein of mTOR
Rheb	Ras homolog enriched in brain
Rictor	Rapamycin insensitive companion of mTOR
Rim15	Regulator of IME2 (inducer of meiosis) 15
RIPA	Radio-immunoprecipitation assay buffer
rn	<i>Rattus norvegicus</i> (rat)
rpm	Rotations per minute
RT	Room temperature
Rubicon	RUN (RPIP8, UNC-14, NESCA) domain and cysteine-rich domain containing Beclin 1 interacting protein
SAP	Shrimp alkaline phosphatase
sc	<i>Saccharomyces cerevisiae</i> (budding/baker's yeast)
SD	Standard deviation
SDS	Sodium dodecyl sulfate
SEM	Standard error of the mean
Ser	Serine
SHIP1/2	SH2 (Src homology 2) domain-containing inositol-5'-phosphatase 1/2
SIRT1	SIR2 (Silent information regulator 2)-like protein 1
SNF1/4	Sucrose non fermenting 1/4
sp	<i>Schizosaccharomyces pombe</i> (fission yeast)
STAT3	signal transducer and activator of transcription 3
STK36	Serine/threonine kinase 36
TAK1	TGF β (transforming growth factor β) -activated kinase 1
TBE	Tris-borate-EDTA (buffer)
TBS	Tris buffered saline
TBST	Tris buffered saline with addition of Tween [®] -20
TEMED	N, N, N', N'-tetramethylethylenediamine
Thr	Threonine
Tpk1/2/3	Takashi's Protein Kinase 1/2/3
TRAIL	Tumor necrosis factor-related apoptosis-inducing ligand
Tris	Tris(hydroxymethyl)aminomethane
TSC1/2	Tuberous sclerosis protein 1/2
ULK1/2/etc	Unc-51-like kinase 1/2/etc
Unc-51	Uncoordinated protein 51
UVRAG	UV irradiation resistance-associated gene
Vps15/34/38	Vacuolar protein sorting defective 15/34/38
WT/wt	Wild type
YFP	Yellow fluorescent protein

7.2 Supplementary data

7.2.1 Sequence alignment of ULK1-homologs from various species

1	-----MEFGRGGVETVGKFEFSRKDLIGHGAFAVVFKGRHREKHDLEVAVKCINKKNL	mmULK1
1	-----MEVVDGFEYCKRDLVGHGAFAVVFRGRHRQKTDWEVAIKSINKKNL	mmULK2
1	-----MNVGEYEYSSKMDLGHGAFAVVYKGRHRKKH-MPVAIKCITKKGQ	dmULK
1	-----MEQFDGFEYSKRDLIGHGAFIVYRGRYVDRTDVPVAIKAIKKNI	ceUNC51
1	MGDIKNKDHTTSVNHNLMSAGNYTAEKEIGKGSFATVYRGHLTSDKSQHVAIKEVSRKLL	scATG1
54	A--KSQTLGKEIKILKEL---KHENIVALYDFQEMANSVYLVMEYCNGGDLADYLHTMRT	mmULK1
47	S--KSQILLGKEIKILKEL---QHENIVALYDVQELPNSVFLVMEYCNGGDLADYLQAKGT	mmULK2
47	L--KTQNLGKEIKILKELTELHHENVVALLDCKESQDCVSLVMEYCNGGDLADYLSVKGT	dmULK
47	S--KSKNLLTKEIKILKELSSLKHENLVGLLKCTETPTHVYLVMEFCNGGDLADYLQOKTT	ceUNC51
61	KNKKLLENLEIEIAILKKI---KHPHIVGLDCERTSTDFYLTMEYCALGDLTFLLKRRKE	scATG1
110	LSEDT-----VRLFLQOIAGAMRLLHSGKITHRDLKPQNILL	mmULK1
103	LSEDT-----IRVFLHQIAAAMRLLHSGKITHRDLKPQNILL	mmULK2
105	LSEDT-----VRLFLVQLAGAMKALYTKGIVHRDLKPQNILL	dmULK
106	LNEDT-----IQHFVVOIAHALEAINKKGIVHRDLKPQNILL	ceUNC51
120	LMENHPLLRVTFEKYPPPSENHNGLHRAFVLSYLLQQLASALKFLRSKNLVHRDLKPQNILL	scATG1
147	SN-----PGRRANPSNIR-----VKIADFGFARYLQSNMMAATLCGSPMYMAPEVIMS	mmULK1
140	SY-----ANRRKSNVSGIR-----IKIADFGFARYLHSNTMAATLCGSPMYMAPEVIMS	mmULK2
142	SH-----NYGKTLPAISKIT-----LKIADFGFARFLNEGMAATLCGSPMYMAPEVIMS	dmULK
143	CN-----NSRTQNPHTDIV-----IKLADFGFARFLNDGVMAATLCGSPMYMAPEVIMS	ceUNC51
181	STPLIGYHDSKSFHELGFVGIYNLPILKIADFGFARFLPNTSLAETLCGSPMYMAPEILNY	scATG1
196	QHYDGKADLWSIGTIVYQCLTGKAPFQASSPQDLRFLYEKNKTLVPAIP-RETSAPLRQLL	mmULK1
189	QHYDAKADLWSIGTVIYQCLVGKPPFQANSQDLRMFYEKNRSLMPSIP-RETSFYLANLL	mmULK2
192	LQYDSKADLWSIGTIVYQCLTGKAPFYAQTPNELKSYEQNANLAPKIP-SGVSPDLRDL	dmULK
193	MQYDAKADLWSIGTILFQCLTGKAPFVAQTPPQLKAYYEKTRRLRNIP-EWCSPNLRDL	ceUNC51
242	QKYNADLWSVGTIVFEMCCGTPPFRASNHLELFKKIKRANVITFPSYCNIEPELKELI	scATG1
256	LALLQRNHKDRMDFEFFHHPFLDASTPIKKSPPVPVPSYSSSGSSSSSSSSASHLASPP	mmULK1
249	LGLLQRNQKDRMDFEAFSSHFPLEQ-VPVKKSCVPVPVYSGVPVPGSSSSSSPSCRFAFSP	mmULK2
254	LCLLRNSKDRISYSEFFVHRFLQG----KKAAVSPGEPSONANLRRRVSKSGVLPVDMPP	dmULK
253	LRLKRNADKDRISFEDFFNHFLTS-----ELLSPSKRILESARSPLLANRRIITPQS	ceUNC51
303	CSLLTFDPAQRIGFEEFFANKVNE-----DLSSYELEDDLPELESKSKGIVESNM	scATG1
317	SLGEMPQLQK-TLTS-ADAAAGFLQGSRDSSG-SKDS-CTDDFVMVPAQFPGDLVAEAA	mmULK1
309	SLPDMQHIQEENLSSPPLGPPNYLQVSKDSASNSKNSSCDTDDFVLVPHNLSDDHSYDMP	mmULK2
309	LGGTPPAKAKSPLQQLEQLKLVKLAEQQQK-EREQEAQEDENTVSVANPAICATITN	dmULK
307	SLPVPKRAGSTKLDSP--TPVRRIGESPRVQ--RVITPGMPSFVPGAPMQESTDFTELPP	ceUNC51
354	FVSEYLSKQPKSPNSN-----LAGHQSMADN-PAELSDALKNSNILTAPAVKTDHTQAVD	scATG1
373	SAKPPDSSLCSGSSLVASAGLESHGRTPSPSPTCSSSPSPSRGPPGFSSNRYGASVPIPV	mmULK1
370	MG-----TTAR-RASNEFFMCGGQCQPTVSP-----HSETAPIPV	mmULK2
369	VG-----VLCDSENNSGSCSS-----HED-----S-	dmULK
364	RQE-----SSPVKQVQVHTNVSPS-----LTCKPVPV	ceUNC51
408	KK-----ASNKYNHNSLVSDRS-----FER-----	scATG1
435	PTQVHNYQRIEQNLQSPPTQQQT-----ARSSAIRRSGSTSPPLGFGRASPPSPSHTDGAMLA	mmULK1
404	PTQVRNYQRIEQNLISTASSGTINPHGSPRSVVRRS-NTSPMGFLRVGSCSPVPGDTVQTC	mmULK2
389	----DDEFVLVFKNLPEDQRQ-----G-----LAQVQAQPAS-----	dmULK
390	PSQRLTYQKMEERLAAARKT-----AVPSSSSP-----	ceUNC51
428	----EYVVVEKKSVEVNSLAD-----EVAQAGFNP-----	scATG1
491	-RKLGLGGGRPYTPSPQVGTIPERPSWSRVPSPQADVRVGRSPRPGSSVP-EHSPRTTGL	mmULK1
464	GRRLSTGSSRPYSPSPLVGTIPEQFSQCCGHFQGHARSRS--GSPVPTQAPQSLLL	mmULK2
416	----GGQRFQ--QQNQSEPRPSSLPITSEPK-----P-----VP-----	dmULK
420	----TGSVSAQHQQHQQQQEPASSPVQRIE-----RE--DQLPRR--TTLQ-	ceUNC51
454	----NPKHFTSTQNNVLLNEQFSPNQYFQ-----	scATG1
550	GCRLHSAPNLSDFHVVRPKLPKPPTDPLGATFSPP-QTSAPQPCP---GLQSCRPLRGSP	mmULK1
523	GARLQSAPTLTDIYQNKQKLRKQHSDPVCPSHAGAGYSYSPQSRPGSLGTSPTKHTGSSP	mmULK2
445	----AP-----ARRQVARE--GPLTVATLGGQQIPRSQPIIS-----VKQPREDDQ-R-	dmULK
461	----DP-----NAHDIERTMPNPTFVVCSSSTKPSNNAN-----RVRRSTITSP	ceUNC51
483	----NQG-----ENPRLLRATSSSSGSGDGRRPSLVDRRLS-----LSSLNPSNALS	scATG1

606	KLPDFLQRSPLPPIILGSPKAGPSFDFPKTPSSQNLTLTLARQGVVMTPPRNRILP-DLSE	mmULK1
584	RNSDWFFKTPLPITIIIGSPKTKTAPFKIPKIQASSNLLALVTRHGPAESQSKDGNPRECSH	mmULK2
484	-----KSSVSSDINSISPPAVQFAIGTPPR-----MRSASGGSLSETPPPHAP-----	dmULK
503	--ADTQDMVAADQMLSNLDPTTTTTIIPKSAITAN--IQGIPRGARDRSVTSPPQP-----	ceUNC51
527	R-----ALGIASRLFLFGGANQQQQQQITSSPPYS-----QTLNLSQLFHELTEN-----	scATG1
666	ASPFHGQQLGSGLRPAEDTRGPFGRSFSSTSRITDLLLKAAGFTQASDSGSTDSLQ-EKPMK	mmULK1
645	CLSVQGSERHR--SEQQQSKAVFGRSVSTGKLEQQVKAPLG---GHQGSTDSLINTERPMD	mmULK2
528	-----STWQVSPGHSSQSPLR-----RSGNS-S-----P	dmULK
555	-----TIHENEPLDNAKYQ-----QTDVNNNS-----	ceUNC51
573	-----IILRIDHLQHPETLK---LDNTNIVS-----	scATG1
726	IAPSAGFGGTLHPGARGGGASSPAPVVFTVGSPPSGATPPQST----RTRMFVSGSSSSSLG	mmULK1
701	VAPAGACG--VMLALPAGTAAASARAVLFTVGSPPHSATAPTCTHMLVLRTRTTVSGSSSSGG	mmULK2
550	VLPSAALT-----K-----LPTLGSPTMLVAPGSLG-----SIGSAGS-G	mmULK
576	--PTAPTEP-----FIILKNQTTCSSTSS-----SVVEEEEAM	ceUNC51
595	ILLESIAAK-----AFVVYSYAEVKFSQIVP-----LSTTLKG	scATG1
783	STGSSSARHLVPGACGEAPELSAPGHCCSLAD---PLAAN---LEGAVTFEAPDLPEETLM	mmULK1
760	SLCSASGRVCVGSPPGPGGLGSSPPGAEGAPSLRYVPYGASPPSLEGLITFEAPELPEETLM	mmULK2
584	SE-NNNQHHMLGPRAFTLPELGATGGLHSLD----TGAG--GGGEPHAFQAPELSEETLM	dmULK
608	SLPFASGSHLAAG-FKKTPAEVPMDHGALP-----PALDQEIVL	ceUNC51
627	MANFENRRSMDSNLAEEQDSDDAEEDETLKRYKEDCLSTKTFGKGRTLSATSQLSATFN	scATG1
838	EQEHTETLHSLRFTLFAFAQQVLEIAALKGS--ASEAAGGPE--YQLQESVVADQIS-QLSR	mmULK1
821	EREHTDTLRLHNMMLMFTCEVLDLTAVRGG--NPELCTSAVSLYQIQESVVADQIS-QLSK	mmULK2
638	DREHNETLSKLNFLVALTDCIQEVADSRCAPLSTFMVAGSQS-AAQAASADAQQIPPHAPE	dmULK
646	GEEHKQILAKLRFVAELVDTLIHVAEQKDNPLASAMASRRQ---LLTTGTSTNTS----S	ceUNC51
688	KLPRSEMIILLCNEAIVLYMKALSILSKSMQVTSNWWYESQEKSCSLRVNVLVQWLR----E	scATG1
894	EWGFAEQVLVLYLKVAEELLSSGLQTAIDQIRAGKLCSSSTVKQVVRRLNELYKASVVSQGL	mmULK1
879	DWGRVEQLVLYMKAAQLLAASLHLAKAQVKSGLSPSMVAVKQVVKNLNERYKFCITMCKKL	mmULK2
697	HCKRAERLVLLVRLGLQLSSGMNLASQQLSNGQLKPSNVKNALLTMNAKYRSMLEFESKRL	dmULK
700	PYRRAEQLVVYVRALHMLSSALLLAQTNVANRVLHPSVAVQVVLNQLNDKYHQCLVRSQEL	ceUNC51
745	KFNECLEKADFLR-LKINDLRFKHASEVAENQTLLEKGSSEEPVYLEKLLYDRALEISKMA	scATG1
955	SLRLQRFLLDKQRLLDGIHGVTAERLILSHAVQMVQSAALDEMFOHREGCVPRYHKALLLL	mmULK1
940	TEKLNRFSDKQRFIDEINSVTAEKLIYNCAVEMVQSAALDEMFOQTEDIYRYHKAALLL	mmULK2
759	NGSG---LLQKANAFN---ITADKILYDYALDMQAAALDELKNTKNCFERYNHTAHILL	dmULK
761	ASLG---LPGQDPAMA---VISAERIMYRHATELCQAAALDELFGNPQLCSQRYQTAYMML	ceUNC51
805	AHME----LKGENLYN-----CELAYATSLWMLETSLDDDEFTNAYGDYFPFKTNIHLKS	scATG1
1016	EGLQ-----HTLTDQADIENIAKCKLCIERRLSALLSGVYA-----	mmULK1
1001	EGLS-----KILQDPTDVENVHKYKCSIERRLSALCCSTATV-----	mmULK2
813	HSLV-----QKNHPQDKMMLNKYRDAVEKRLSILQQHGYTYMTDENA	dmULK
816	HTLA-----EQVNCQDKTVLTRYKVAVEKRLRILERQGFVAAVNT--	ceUNC51
855	NDVEDKEKYHSLVDENDRIIRKYIDSIANRLKILRQKMNHQN-----	scATG1

Figure S1. ClusatIW-alignment of ULK1-homologs from various model organisms. Predicted AMPK-sites, phosphorylation of which was not detected by mass spectrometry in our studies are highlighted in yellow, AMPK- and/or 14-3-3-binding sites detected to be phosphorylated in our studies are highlighted in green. Additional phosphorylated residues detected in our mass spectrometry experiments that do not match the AMPK and 14-3-3 binding motifs are highlighted in blue. Ce - *Caenorhabditis elegans*; dm - *Drosophila melanogaster*; mm - *Mus musculus*; sc - *Saccharomyces cerevisiae*.

7.2.2 ULK1-phosphorylation pattern and predicted upstream kinases

Table S1. Phosphorylation sites on ULK1 predicted by Scansite, but not identified by LC/MS/MS in this study.

Site	Sequence	Predicted kinase	Reference
T109	DYLHTRtLSEDTVR	PKC ϵ	
T114	MRTLSEdtVRLFLQQ	CK1, PKC δ	
T209	ADLWSIGtIVYQCLT	PKC μ	
S248	PAIPRETsAPLRQLL	14-3-3	
T282	HPFLDAsTPIKKSPP	CDC2, CDK5	
S294	SPPVPVPSYPSSGSG	GSK3β	
S298	PVPSYPSsGSGSSSS	GSK3β	
S300	PSYPSSGSGSSSSSS	CK1	
S302	YPSSGSGSSSSSSSA	GSK3 β	
S303	PSSGSGSSSSSSSAS	GSK3 β	
S304	SSGSGSSsSSSSASH	GSK3 β	
S307	SGSSSSsSASHLAS	CK1	
S308	GSSSSsASHLASP	CK1	
S310	SSSSSAsHLASPPS	CK1	
T327	EMPQLQKtLTSPADA	CamK2	
T329	PQLQKTLtSPADAAG	(14-3-3)	
S330	QLQKTLtSPADAAGF	p38	
S341	AAGFLQGsRDSGGSS	PKC δ	Dorsey <i>et al.</i> , 2009
S347	GSRDSGGsSKDSCDT	CK1	
T401	GLESHGRtPSPSPTC	ERK1, GSK3β	
S405	HGRTPSPsPTCSSSP	GSK3β	
T407	RTPSPStCSSSPSP	GSK3β	
S409	PSPSPTCsSSPSPSG	GSK3β	
S413	PTCSSSPsPSGRPGP	CDC2, CDK5, ERK1	
S415	CSSSPSPsGRPGPFS	ERK1, GSK3β	
S429	SSNRYGAsVPIPVPT	CK1	
S467	SAIRRGStSPPLGFG	AMPK, PKCδ (14-3-3)	Beausoleil <i>et al.</i> , 2006 ; Dephoure <i>et al.</i> , 2008 ; Dorsey <i>et al.</i> , 2009; CS 3882, 2008
S469	IRRGStsPLGFGRA	ERK1	Beausoleil <i>et al.</i> , 2006 ; Brill <i>et al.</i> , 2009 ; Dephoure <i>et al.</i> , 2008 ; Dorsey <i>et al.</i> , 2009: CS 3882, 2008
T502	LGGRPYtPSPQVGT	CDC2, CDK5, ERK1	
S517	IPERPSWsrVPSPQG	GSK3 β	
S543	GSSVPEHsPRTTGLG	CDC2, CDK5	
S582	DPLGATFsPPQTSAP	CDC2	
T586	ATFSPPQtSAPQPCP	GSK3β	
S604	SCRPLRGsPKLPDFL	CDK5	
S653	ARQGVVMtPPRNRTL	CDC2, CDK5	
S667	LPDLSEAsPFHGQQL	CK1	
S711	AAFGTQAsDSGSTDS	PKC δ	
T716	QASDSGStDSLQEKP	CK1	
S783	GSSSLGStGSSSAR	CK1	
T835	APDLPEEtLMEQEHT	PKC ϵ	
S847	EHTETLHsLRFTLAF	CK1	
T851	TLHSLRFtLAFQQV	PKC ϵ	
T784	SSSLGStGSSSARH	GSK3 β	
S869	AALKGSAsEAAGGPE	PKCδ	
T932	GKLCLSStVKQVRR	PKC $\alpha/\beta/\gamma/\mu$	

The sequences surrounding the Scansite-predicted sites are shown, with the phosphorylated serine or threonine indicated in bold, lower case letters. Kinases potentially phosphorylating ULK1 were predicted by searching the protein sequence of murine ULK1 with Scansite using the function “Search protein by input sequence” at low stringency. Sites also detected at medium or high stringency are shown in bold and bold italic font, respectively. The regulatory protein 14-3-3 is put in brackets since it is not a kinase. For phosphorylation sites predicted by Scansite and detected by mass spectrometry in this study, see table 4.1. CS 2333 2007 and CS 3882 2008 refer to studies performed at Cell Signaling Technology; the results are available in the Phosphosite database (www.phosphosite.org).

Table S2. Phosphorylation sites on ULK1 detected by other groups and not predicted by Scansite.

Site	Sequence	Reference
S87	DFQEMAN s VYLVMEY	Dorsey <i>et al.</i> , 2009
S195	MAPEVIM s QHYDGKA	Dorsey <i>et al.</i> , 2009
S224	GKAPFQA s SPQDLRL	Dorsey <i>et al.</i> , 2009
T456	QSPTQQQ t ARSSAIR	Dephoure <i>et al.</i> , 2008 ; CS 2333, 2007 ; CS 3882, 2008
S465	RSSAIRR s GSTTPLG	Beausoleil <i>et al.</i> , 2006
T468	AIRRS g s t TPLGFGR	Brill <i>et al.</i> , 2009
S482	RASPSP s HTDGAML	Dorsey <i>et al.</i> , 2009
S760	FTVGSPP s GATPPQS	Beausoleil <i>et al.</i> , 2006
S867	EIAALKG s ASEAAGG	Dorsey <i>et al.</i> , 2009
S913	KVAELLS s GLQTAID	Dorsey <i>et al.</i> , 2009
S1047	RRLSALL s GVYA	Dorsey <i>et al.</i> , 2009

Listed are additional phosphorylation sites in ULK1 that were detected in mass-spectrometry studies by other groups while this work was in progress. These sites do not match any currently known kinase target motif and thus were not predicted by Scansite to be phosphorylated. For additional details, see section 4.1.1 and Tables 4.1 and S1. CS 2333 2007 and CS 3882 2008 refer to studies performed at Cell Signaling Technology; the results are available in the Phosphosite database (www.phosphosite.org).

Table S3. Phosphorylation sites on ULK1 detected in this work.

Site	Phosphorylated at								Other studies identifying this site																
	Exp I EBSS			Exp II EBSS			Exp II 2DG		Exp III 2DG		Beausoleil et al., 2006	Wissing et al., 2007	Cantin et al., 2008	Daub et al., 2008	Dephourse et al., 2008	Pan et al., 2008	Trinidad et al., 2008	Brill et al., 2009	Chen et al., 2009	Oppermann et al., 2009	Dorsey et al., 2009	(CS 2333, 2007)	(CS 3882, 2008)	(CS 3885, 2008)	
	0 h	0.5 h	2 h	0 min	2.5 min	30 min	0 min	15 min	0 min	15 min															
S317	x		x																						
S403		x																							
S411			x																						
S450		x	x	x		x		x					x	x			x		x	x	x				x
S460									x																
S477	x	x											x												
S479		x											x							x					
S494		x						x	x	x															
S521	x	x	x																	x					
S532	x							x		x															
S537					x																				
S543	x	x		x				x		x															
S555	x	x													x										
S614	x	x	x																						
S622	x	x	x										x	x		x	x	x		x					x
T624	x																x								
T635			x																						
S637	x	x	x							x			x	x				x							
S638									x	x				x											x
T653						x																			
T659			x						x																
S693		x	x																						
T694		x	x																						
S695	x																								
S715	x	x	x																						
S718		x	x																						
S747	x								x																
T754	x																								
S757	x	x	x	x	x	x	x	x	x	x										x					
T763	x								x	x	x														
S774			x																						
S777		x																							
S780	x	x	x																						
S1043	x	x																		x					

Listed are all sites in murine ULK1 that were detected to be phosphorylated by mass-spectrometry in the present study (three experiments, Exp I – Exp III). Other studies that also identified this sites, and the conditions under which a particular site was detected are given as well. With regard to the experiments performed in this thesis: for Exp I, see section 4.1.1 and table 4.1, for Exp II and Exp III, see section 4.4.4.1. Exp II included nutrient-deprivation by EBSS- and 2DG-treatment. CS 2333 2007, CS 3882 2008 and CS 3885 2008 refer to studies performed at Cell Signaling Technology; the results are available in the Phosphosite database (www.phosphosite.org).

7.2.3 Full names of predicted ULK1-substrates

Table S4. Recommended names for putative ULK1-substrates.

YEAST PROTEIN		HUMAN HOMOLOG	
Short name	Recommended/alternative name	Short name	Recommended/alternative name
Abp140	Uncharacterised methyltransferase ABP140/140 kD actin-binding protein	METL2B	Methyltransferase-like protein 2B
Apm2	Adaptin medium chain homolog APM2 (Adaptin- μ 1-II)	AP1M1	AP-1 complex subunit μ -1/Clathrin coat-associated protein AP47
App1	Actin patch protein 1	Cam-PDE 1C	Calcium/calmodulin-dependent 3',5'-cyclic nucleotide phosphodiesterase 1C
Aut7/Atg8	Autophagy-related protein 8 precursor /Autophagy-related ubiquitin-like modifier ATG8	LC3	Microtubule-associated proteins 1A/1B, light chain 3C
Aut10/Atg18	Autophagy-related protein 18	WIPI3	WD repeat domain phosphoinositide-interacting protein 3
Atg21/Mai1	Autophagy-related protein 21/Maturation of proaminopeptidase I-protein	WIPI2	WD repeat domain phosphoinositide-interacting protein 2
Avo1	Target of rapamycin complex 2 subunit AVO1/Adheres voraciously to TOR2 protein 1	mSIN1	Target of rapamycin complex 2 subunit MAPKAP1/ Stress-activated map kinase-interacting protein 1
Bmh2	Protein BMH2 (<i>Brain Modulosignalin Homologue</i>)	14-3-3 ϵ	14-3-3 protein ϵ
Cdc55	Protein phosphatase PP2A regulatory subunit B/Cell division control protein 55	PP2AB $\alpha/\beta/\gamma/\delta$	Serine/threonine-protein phosphatase 2A 55 kDa regulatory subunit B $\alpha/\beta/\gamma/\delta$ isoform
Cns1	Cyclophilin seven suppressor 1	TTC4	Tetratricopeptide repeat protein 4
Crn1	Coronin-like protein	CORO6/2B	Coronin-6/2B
Elm1	Serine/threonine-protein kinase ELM1 (<i>Elongated Morphology</i>)	CamKK α/β	Calcium/calmodulin-dependent protein kinase kinase α/β
Ent5	Epsin-5 (<i>involved in clathrin-coated vesicle formation</i>)	EPN2	Epsin-2/EPS15-interacting protein 2
Glo3	ADP-ribosylation factor GTPase-activating protein GLO3 (<i>Glyoxalase</i>)	ARFGAP2	ADP-ribosylation factor GTPase-activating protein 2
Mig2	Regulatory protein MIG2 (<i>Multicopy /Inhibitor of GAL gene expression</i>)	EGR3	Early growth response protein 3 (<i>a transcription factor</i>)
Msb3	GTPase-activating protein GYP3/ Multicopy suppressor of bud emergence 3	GRTP1	Growth hormone-regulated TBC protein 1 (<i>a Rab-GAP</i>)
Mss4	Probable phosphatidylinositol-4-phosphate 5-kinase MSS4 (<i>Multicopy Suppressor of Stt4 mutation</i>)	PIP5K1 $\gamma/\alpha/\beta$	Phosphatidylinositol-4-phosphate 5-kinase type-1 $\gamma/\alpha/\beta$
Osh3	Oxysterol-binding protein homolog 3	OSBL3	Oxysterol-binding protein-related protein 3
Pde1	3',5'-cyclic-nucleotide phosphodiesterase 1	- - -	
Pfk26	6-phosphofructo-2-kinase 1	PFKFB1	6-phosphofructo-2-kinase/fructose-2,6-biphosphatase 1 (liver isoenzyme)
		PFKFB3	6-phosphofructo-2-kinase/fructose-2,6-biphosphatase 3 (brain/placenta-type isoenzyme)
Prc1	Carboxypeptidase Y precursor/ Proteinase C1	PPGB	Lysosomal protective protein/ Cathepsin A/ Carboxypeptidase C
Rio1	Serine/threonine-protein kinase RIO1 (<i>Right Open reading frame</i>)	RIOK1/2/3	Serine/threonine-protein kinase RIO1/2/3
Sec2	Rab guanine nucleotide exchange factor SEC2 (<i>Secretory</i>)	Rabin-3	Rab-3A-interacting protein

Table S4, continued.

Sip2	SNF1 protein kinase subunit beta-2/SNF1-interacting protein 2	AMPK β 1/2	5'-AMP-activated protein kinase subunit β -1/2
Sip5	SNF1-interacting protein 5	- - -	
Srp40	Suppressor protein SRP40 (Serine Rich Protein)	- - -	
Vip1	Inositol hexakisphosphate and diphosphoinositol-pentakisphosphate kinase	VIP1	Inositol hexakisphosphate and diphosphoinositol-pentakisphosphate kinase 1
Vps55	Vacuolar protein sorting-associated protein 55	VPS8	Vacuolar protein sorting-associated protein 8 homolog
YDL025C	Probable serine/threonine-protein kinase YDL025C	CHK1	Serine/threonine-protein kinase Chk1 (Checkpoint kinase)
Ypt11	GTP-binding protein YPT11/Rab GTPase YPT11 (Yeast Protein Two)	Rab12	Putative Ras-related protein Rab-12

Alternative names are given only if they explain the abbreviation that is used as the protein's name or if they contain information on the protein's function. For further details, see section 4.1.2 and table 4.2.

7.2.4 Influence of AMPK-activation on ULK1-AMPK-complex stability

Table S5. Summary of results obtained in experiments to clarify the influence of AMPK-activity on ULK-AMPK complex stability.

Cell line	Treatment	time	AMPK	N	10 %			20 %		
					+	-	0	+	-	0
COS7	AICAR	0.5 h	α 1	8	1	4	3	1	3	4
	AICAR	4 h	α 1	8	6	2	0	5	2	1
	Phenformin	0.5 h	α 2	2	2	0	0	2	0	0
	Phenformin	4 h	α 2	3	1	2	0	1	2	0
	2DG	15 min	α 2	9	3	6	0	3	6	0
	2DG	1 h	α 2	9	2	6	1	2	6	1
	A-769662	0.5 h	α 2	3	0	2	1	0	2	1
	A-769662	2 h	α 2	3	0	3	0	0	1	2
	EBSS	2.5 min	α 2	8	5	3	0	4	3	1
	EBSS	0.5 h	α 2	5	3	2	0	2	1	2
EBSS	4 h	α 2	5	1	3	1	1	2	2	
HEK293T	EBSS	2.5 min	α 2	2	1	1	0	0	1	1
	EBSS	0.5 h	α 2	2	0	1	1	0	1	1
	EBSS	4 h*	α 2	2	0	2	0	0	2	0

COS7- or HEK293T-cells stably overexpressing myc-ULK1 were treated with the compounds and for the times indicated and endogenous AMPK α 1 or $-\alpha$ 2 were immunoprecipitated using isoform-specific antibodies. Only experiments in which AMPK activation could be verified by Western blot for phospho-AMPK α (Thr172) or phospho-ACC (Ser79) in case of A-769662 were considered in this table. An exception to this were experiments in which cells had been treated with EBSS for more than 2.5 min, since under these conditions, no strong AMPK activation occurred. Western blot signals were quantitated on the LI-COR® Odyssey® system. The amount of myc-tagged ULK1 coprecipitated with endogenous AMPK α was calculated as (ULK1^{IP}/ULK1^{TCL})/(AMPK^{IP}/AMPK^{TCL}) and values were normalized to the untreated state. Listed are the total numbers (N) of independent experiments performed using a given treatment and the frequencies with which a particular result was obtained, i.e. at least 10 % increase (“+”) or decrease (“-“; in the alternative analysis: 20 % increase or decrease) or no change (“0”). For experiments that were repeated at least 3 times, results that were obtained in more than 50 % of the experiments are highlighted in bold font, results that were obtained in more than 2/3 of experiments are highlighted in bold italic font. For additional details, see section 4.3.4.3.

* Five additional experiments were performed using enhanced chemiluminescence detection. The blots were not scanned and quantitated but clearly show decreased myc-ULK1-coprecipitation at 4 h.

7.2.5 Determination of AMPK-dependent 14-3-3-binding sites in ULK1

Phosphorylatable site	wt (all)	S467	S494	S555	T659
<i>Primary data: relative 14-3-3-binding</i>	2.91	0.88	1.13	2.13	1.47
Exp1	3.18	0.95	1.16	1.9	1.81
Exp2	2.04	0.54	0.88	2.56	1.01
Exp3	3.64	0.48	1.33	2.18	1.86
Exp4	2.22	1.35	0.73	2.69	0.94
Exp5	3.47	1.07	1.57	1.32	1.71
<i>Column analysis</i>					
Mean	2.91	0.88	1.13	2.13	1.47
SD	0.734	0.367	0.338	0.550	0.452
SEM	0.328	0.164	0.151	0.246	0.202
<i>T-test with wt</i>					
P-value	N/A	0.0005	0.0012	0.0936	0.0056
<i>T-test with S555</i>					
P-value	N/A	0.0029	0.0087	N/A	0.0705

Table S6. Quantitative Western blot data and statistical analysis to determine AMPK-dependent 14-3-3-binding sites in ULK1. Five independent GST-14-3-3-pulldown experiments were performed as described in section 4.4.4.2 on myc-ULK1-mutants with only one predicted AMPK/14-3-3-binding site available for phosphorylation. Western blot signals were detected by scanning the membranes on the LI-COR® Odyssey® Infrared Imaging System. Signals were quantified using the corresponding software and 14-3-3-binding was calculated from the values obtained for myc-ULK1 (detected with α -myc-tag antibody) pulled down with GST-14-3-3 (ULK1^{GST-14-3-3}), myc-ULK1 in the total cell lysate (ULK1^{TCL}) and AMPK in the total cell lysate serving as a loading control (AMPK^{TCL}) for each time point and mutant as [ULK1^{GST-14-3-3}/(ULK1^{TCL}/AMPK^{TCL})]. Relative 14-3-3-binding was defined by dividing the 14-3-3-binding at 15 min 2DG treatment by 14-3-3-binding at 0 min 2DG treatment for each ULK1-construct. Statistical significance was assessed by unpaired T-tests comparing the wild type to each mutant and the S555-intact mutant to each of the other mutants. P-values given are nominal P-values. Note: AMPK-activation-inducible 14-3-3-binding of the T659-intact mutant is significantly different from that of the wild type, but not from that of the S555A-mutant, implying that it is a minor 14-3-3-binding.